

**Function and regulation of the axon guidance
molecules Sidestep and Beaten path Ia in
*Drosophila melanogaster***

Inaugural-Dissertation

zur Erlangung des Doktorgrades
der Mathematisch-Naturwissenschaftlichen Fakultät
der Heinrich-Heine-Universität Düsseldorf

vorgelegt von

Jaqueline Carolin Kinold
aus Bad Arolsen

Düsseldorf, Mai 2016

aus dem Institut für funktionelle Zellmorphologie
der Heinrich-Heine-Universität Düsseldorf

Gedruckt mit der Genehmigung der
Mathematisch-Naturwissenschaftlichen Fakultät der
Heinrich-Heine-Universität Düsseldorf

Referent: Prof. Dr. Hermann Aberle

Korreferent: Prof. Dr. Eckhard Lammert

Tag der mündlichen Prüfung:

Meiner Familie

Summary

For humans and all animals it is essential to be able to execute coordinated movements. At the basis of this ability is the correct wiring of the neuromuscular system during development. This thesis focussed on the regulation and function of the axon guidance molecule Sidestep (Side) and its receptor Beaten path 1a (Beat). Side shows during the embryogenesis of *Drosophila melanogaster* a spatio-temporal pattern to guide the Beat expressing motor axons to their target muscles. Thereby, Side is expressed in intermediate targets on some glia cells in the CNS and sensory neurons of the PNS. After contact with motor axons, Side expression is quickly down-regulated. Lack of *side* leads to persisting mis-innervation of larval somatic muscles that results in locomotion defects.

Different enhancer fragments, which exhibit highly conserved regions in the clade of *Drosophilidae*, reflect the dynamic Side expression during embryogenesis. Expression of *side* cDNA simultaneously by two enhancer Gal4-lines in sensory neurons and muscles leads to an almost complete rescue of the *side* larval phenotype.

Side expression in sensory neurons is down-regulated during embryogenesis at stage 14. Down-regulation depends on Beat and the metalloprotease Tolloid-related. Lack of *beat* and/or *tolloid-related* causes a constitutive expression of Side in sensory neurons in late embryos (stage 15 to 17) and to similar innervation defects in third instar larvae as detectable in *side* mutants.

Expression of Beat in motoneurons is reflected by one enhancer element, which exhibits one highly conserved region in the phylogenetical family of *Drosophilidae*. Driving expression of *beat* cDNA with the enhancer Gal4-line results in a complete rescue of the *beat* phenotype in third instar larvae.

Lack of Side causes also innervation defects of muscles in adult flies resulting, similar to larvae, in locomotion defects. In contrast to the embryogenesis, the interaction partner for Side during metamorphosis does not seem to be Beat, accounted for by a much milder locomotion phenotype of *beat* mutant flies.

Taken together, Sidestep is a key-regulator of motor axon guidance during both embryogenesis and metamorphosis. Innervation defects based on the lack of this axon guidance molecule causes locomotion defects in larval crawling and adult flying and walking.

Zusammenfassung

Für alle Tiere einschließlich dem Menschen ist es lebenswichtig in der Lage zu sein, koordinierte Bewegungen auszuführen. Grundlage hierfür stellt die korrekte Ausbildung eines neuromuskulären Systems während der Entwicklung des Organismus dar. In dieser Arbeit ist die Funktion und die Genregulation des axonalen Wegfindungsmoleküls *Sidestep* (*Side*) und seines Rezeptors, *Beaten path 1a* (*Beat*), untersucht worden. *Side* zeigt während der Embryogenese von *Drosophila melanogaster* ein räumlich-zeitlich veränderliches Expressionsmuster und dient den *Beat* exprimierenden Motoaxonen auf dem Weg zu ihren Zielmuskeln als Substrat. Hierbei wird *Side* im ZNS in einigen Gliazellen und im PNS in sensorischen Neuronen exprimiert. Ein Funktionsverlust von *Side* führt zu stabilen Fehlinnervierungen der larvalen somatischen Muskulatur, welche zu Bewegungsdefekten führen.

Das dynamische Expressionsmuster von *Side* während der embryonalen Entwicklung wird durch verschiedene Enhancer Fragmente widergespiegelt, welche hoch konservierte Bereiche in der phylogenetischen Familie der *Drosophilidae* besitzen. Werden zwei dieser Linien simultan genutzt, um eine *side* cDNA in sensorischen Neuronen und Muskeln zu exprimieren, so kann der larvale Phänotyp von *side* Mutanten beinahe komplett gerettet werden.

Die Expression von *Side* in den sensorischen Neuronen wird im Stadium 14 nach Interaktion mit den entgegen wachsenden Motoaxonen herunterreguliert. Diese Regulierung ist sowohl von *Beat* als auch der Metalloprotease *Tolloid-related* abhängig. Ein Funktionsverlust von *Beat* und/oder *Tolloid-related* führt zu einer konstitutiven Expression von *Side* in sensorischen Neuronen von Embryonen in späten Entwicklungsstadien (Stadium 15 bis 17).

Ähnlich zu *side* kann die Motoneuronen spezifische Expression von *beat* von einem Enhancer Element reflektiert werden, welches ebenfalls einen stark konservierten Bereich besitzt. Wird *Beat* durch dieses Element angetrieben, so gelingt eine vollständige Rettung des *beat* mutanten Phänotyps in Larven.

Der Verlust von *side* führt ebenfalls zu Fehlinnervierungen adulter Muskeln mit daraus resultierenden Bewegungsdefekten. Da *Beat* mutante adulte Fliegen einen wesentlich schwächeren Bewegungs-Phänotyp als *side* mutante Fliegen aufweisen, scheint *Side* im Gegensatz zur Embryogenese während der Metamorphose nicht mit *Beat* zu interagieren.

Zusammenfassend lässt sich somit sagen, dass Sidestep ein entscheidender Regulator der axonalen Wegfindung während der Embryogenese und Metamorphose von *Drosophila* ist. Fehl-Innervierungen bedingt durch einen Funktionsverlust von *side* führen zu Bewegungsdefekten beim larvalen Krabbeln und dem adulten Fliegen und Laufen.

Table of contents

| | |
|---|-----|
| 1. Introduction | 1 |
| 1.1 Development of the neuromuscular system | 1 |
| 1.1.1 Development of motoneurons..... | 1 |
| 1.1.2 Projections of motoneurons | 3 |
| 1.1.3 Sensory neurons and their projections | 5 |
| 1.2 Axon guidance..... | 6 |
| 1.2.1 The axon guidance molecule <i>Sidestep</i> | 8 |
| 1.2.2 The axon guidance receptor <i>Beaten path la</i> | 9 |
| 1.2.3 Axon guidance via <i>Side</i> and <i>Beat</i> | 10 |
| 1.4 Target muscles of motor axons | 10 |
| 1.4.1 Development of embryonic muscles..... | 11 |
| 1.5 The larval neuromuscular system | 12 |
| 1.6 Metamorphosis..... | 14 |
| 1.7 The adult fly..... | 15 |
| 1.7.1 The adult leg..... | 15 |
| 1.7.3 The indirect flight musculature..... | 16 |
| 1.8 Aims of the thesis | 19 |
| 2. Results | 20 |
| 2.1 Gene regulation of <i>sidestep</i> and <i>beaten path</i> | 20 |
| 2.1.1 Gene regulation of the axon guidance molecule <i>Side</i> | 20 |
| 2.1.2 Gene regulation of the axon guidance receptor <i>beaten path la</i> | 56 |
| 2.2 Larval phenotype..... | 61 |
| 2.2.1 Loss of <i>side</i> function leads to innervation defects in larvae..... | 61 |
| 2.2.2 Muscle specific overexpression of <i>side</i> leads to innervation defects in larvae..... | 67 |
| 2.2.3 <i>Side</i> loss- and gain of function larvae show locomotion defects | 72 |
| 2.3 Adult phenotypes of <i>Side</i> loss- and gain function flies | 78 |
| 2.3.1 <i>Side</i> mutant and overexpression flies exhibit locomotion defects | 79 |
| 2.3.2 <i>Side</i> loss- and gain of function flies are not able to groom themselves..... | 94 |
| 2.3.3 <i>Side</i> homozygous males are sterile..... | 95 |
| 3. Discussion..... | 97 |
| 3.1 Gene regulation of <i>sidestep</i> | 97 |
| 3.1.1 <i>Side</i> guides motor axons via two intermediate targets | 97 |
| 3.1.2 <i>Side</i> phenotype can be partly rescued by two enhancer fragments | 98 |
| 3.1.3 <i>Side</i> expression is not regulated by Hox-genes | 99 |
| 3.1.4 Lack of <i>Tolloid</i> -related causes a constitutive <i>Side</i> expression | 101 |
| 3.2 Gene regulation of <i>Beaten path la</i> | 104 |
| 3.3 Larval Phenotype | 105 |
| 3.3.1 Lack and gain of <i>Side</i> cause larval wiring errors | 105 |
| 3.3.2 Mis-innervation of larval somatic muscles results in locomotion defects..... | 107 |
| 3.4 <i>Sidestep</i> is also functional during metamorphosis | 108 |
| 4. Materials and Methods..... | 114 |
| 4.1 Materials..... | 114 |
| 4.2 Methods..... | 123 |
| 4.2.1 <i>Drosophila</i> culture..... | 123 |
| 4.2.2 Fixation of <i>Drosophila</i> embryos | 123 |
| 4.2.3 Antibody staining of <i>Drosophila</i> embryos | 123 |
| 4.2.4 <i>In situ</i> hybridisation | 124 |
| 4.2.5 Western Blot | 126 |
| 4.2.6 Quantitative PCR (qPCR)..... | 128 |

| | | |
|--------|--|-----|
| 4.2.7 | Characterisation of larval innervation | 129 |
| 4.2.8 | Larval locomotion assays | 130 |
| 4.2.9 | Adult locomotion assays | 131 |
| 4.2.10 | High-speed movies | 132 |
| 4.2.11 | Preparation and staining of adult flight musculature | 133 |
| 4.2.12 | Preparation of adult legs | 134 |
| 4.2.13 | Microscopy | 134 |
| 4.2.14 | Contributions | 134 |

1. Introduction

- *Every motion is a process in time and comes to an intended end.* -

(Aristoteles)

Coordinated movements are essential for all animals and humans. Regardless of searching for food or fleeing from an enemy or just a smile - each movement, even small, has to be coordinated and controlled. For this coordination the precise communication between the nervous system and muscles is fundamental. Wiring of the neuromuscular system occurs during embryogenesis in all higher organisms. In a process called axon guidance axons of motoneurons in the central nervous system (CNS) grow out in the periphery in order to find their target muscles. The model organism *Drosophila melanogaster* is well suited for studying these processes based on the stereotypic structure of the neuromuscular system. Further, *Drosophila* belongs to the holometabolic organisms and thus has to establish a functional neuromuscular system twice – during embryogenesis and metamorphosis. Thereby, structure of the neuromuscular system and the kind of movements are adapted to the environment of different developmental stages.

1.1 Development of the neuromuscular system

The basic locomotory system in *Drosophila* larvae comprises four different components – interneurons, motoneurons, body wall muscles and the cuticle (Landgraf and Thor, 2006). The development of this neuromuscular system starts in embryos during stage 12 with the outgrowth of the first motor axons from the CNS to the growing somatic muscles (Campos-Ortega and Hartenstein, 1997a).

1.1.1 Development of motoneurons

In each hemisegment of a *Drosophila* embryo there are approximately 35 motoneurons, which are mostly located in the ventral nerve cord anterior to the segment of muscles they innervate (Campos-Ortega and Hartenstein, 1997a). Motoneurons can be divided into two principle classes - intersegmental neurons,

Introduction

which innervate internal muscles and segmental neurons, which innervate external muscles except muscle 18 (Fig 1.1) (Landgraf and Thor, 2006).

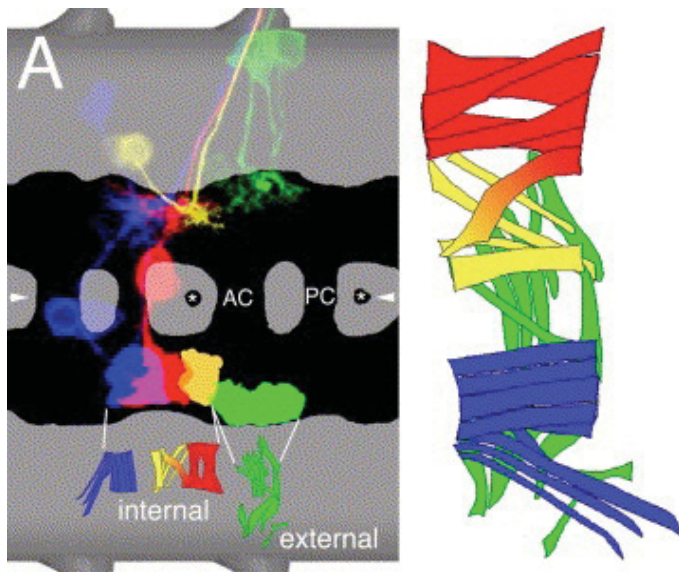


Fig 1. 1: Location of motoneuron dendrites in the ventral nerve cord and their target muscles.

Internal muscles are innervated by motoneurons with dendrites located anterior to the segment boundary, while dendrites of motoneurons with external target muscles are located posterior to the segment boundary. Blue, yellow, red: internal muscles. Green: external muscles. Black: neuropil. Grey: cortex. Asterisks: dorso-ventral channels. AC: anterior commissure. PC: posterior commissure. Triangles: ventral midline. Muscles and motoneurons are not to scale. Taken from Landgraf et al., 2003.

Motoneurons can be subdivided into dorsal and ventral motoneurons based on their projections and can be classified more detailed by their expression of different transcription factors. Projections of dorsal motoneurons appears to be under control of the Even-skipped (*Eve*) homeobox transcription factor, while projections of ventral neurons appears to be controlled by the combinatorial action of the *Nkx6* and *HB9* homeogenes (Fig 1.2) (Landgraf and Thor, 2006).

Eve in turn controls the transcription of other axon guidance molecules such as *Beaten path Ia*, *Uncordinated-5*, *Fasciclin II* and *Neuroglian*, at least in aCC and RP2 neurons based on *in situ* hybridisations with specific probes for the different CAMs and receptors in *eve* mutant embryos (Zarin et al., 2014a). Lack of one of these guidance genes leads to a mild phenotype, but a combined loss of several of these molecules results in stronger, *eve*-similar phenotypes (Zarin et al., 2014a). Therefore, the cumulative downregulation of these guidance factors is likely the reason for the disturbed growth of dorsal motoneurons in *eve* mutants.

The dorsal motoneurons are further specified by the GATA transcription factor *Grain* whose expression is limited to these motoneurons (Garces and Thor, 2006; Landgraf

and Thor, 2006). Together with the Zinc finger homeodomain factor 1 (Zfh1), which is present in all motoneurons, Grain is regulated by Eve (Fig 1.2) (Garces and Thor, 2006; Layden et al., 2006). Both transcription factors, Grain and Zfh1, control an overlapping subset of Eve-regulated genes in dorsal motoneurons. Thereby, Zfh1 is required for the regulation of a broader range of Eve-regulated genes than Grain (Zarin et al., 2014a).

Similar to Eve, *HB9* and *Nkx6* control several growth and guidance factors in ventral motoneurons such as the LIM-homeodomain factors *Islet* and *Lim3* (Fig 1.2) (Landgraf and Thor, 2006).

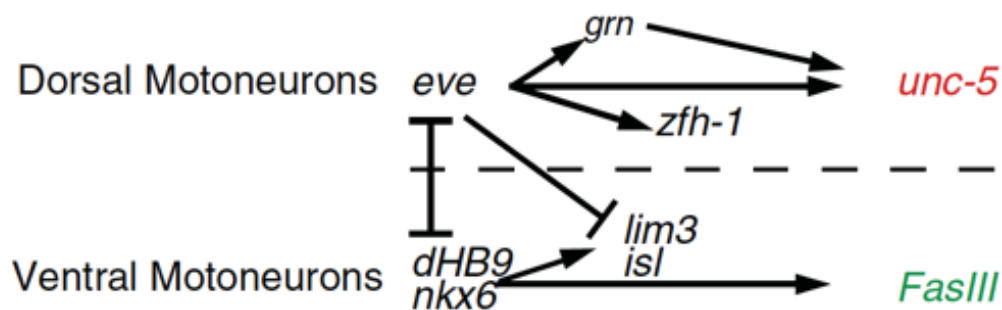


Fig 1. 2: Transcriptional regulation of dorsal and ventral motoneurons.

Eve stimulates the transcription of *grain* (*grn*), *zinc finger homeodomain-1* (*zfh-1*) and *uncoordinated-5* (*unc-5*) in dorsal motoneurons. In ventral motoneurons *lim3* and *islet* (*isl*) are stimulated by *HB9* and *Nkx6*. Further, negative cross-reactions between dorsal and ventral fate determinants exist. Arrows: positive regulation. Bars: negative regulation. Taken from Zarin et al., 2014b.

1.1.2 Projections of motoneurons

Motor axons leave the CNS in two main nerve bundles – the intersegmental nerve (ISN) and the segmental nerve (SN). In the periphery these nerves defasciculate in five bundles, ISN, ISNb, ISNd, SNa and SNc, each innervating a specific region of the embryonic and larval somatic musculature (Johansen et al., 1989a; Van Vactor et al., 1993).

At first, the axon of the anterior corner cell (aCC) leave the CNS and pioneers the anterior root of the ISN (Campos-Ortega and Hartenstein, 1997a; Sink and Whittington, 1991a). Further intersegmental motoneurons, the U neurons, follow. During outgrowth, axons of the aCC and U neurons fasciculate with the first ingrowing sensory axons (Fig 1.3 stage 14). Subsequently, the posterior root of the ISN is pioneered by the axons of two ventral unpaired median neurons (VUMs) and the RP2 neurons (Fig 1.3 stage 13). Axons of RP1, RP3, RP4 and RP5 neurons

Introduction

project contralaterally and consequently cross the midline in the anterior commissure to project posteriorly into the ISN (Fig 1.3 stage 17). Before they innervate their target muscles, they branch off the ISN (Campos-Ortega and Hartenstein, 1997a).

The segmental nerve consists of two pairs of axons of the VUMs and the lateral segmental neurons (LSN). Axons using the segmental nerve root and the posterior root of the ISN fasciculate with sensory axons of ventral sensilla shortly after leaving the CNS (Fig 1.3 stage 14) (Campos-Ortega and Hartenstein, 1997a).

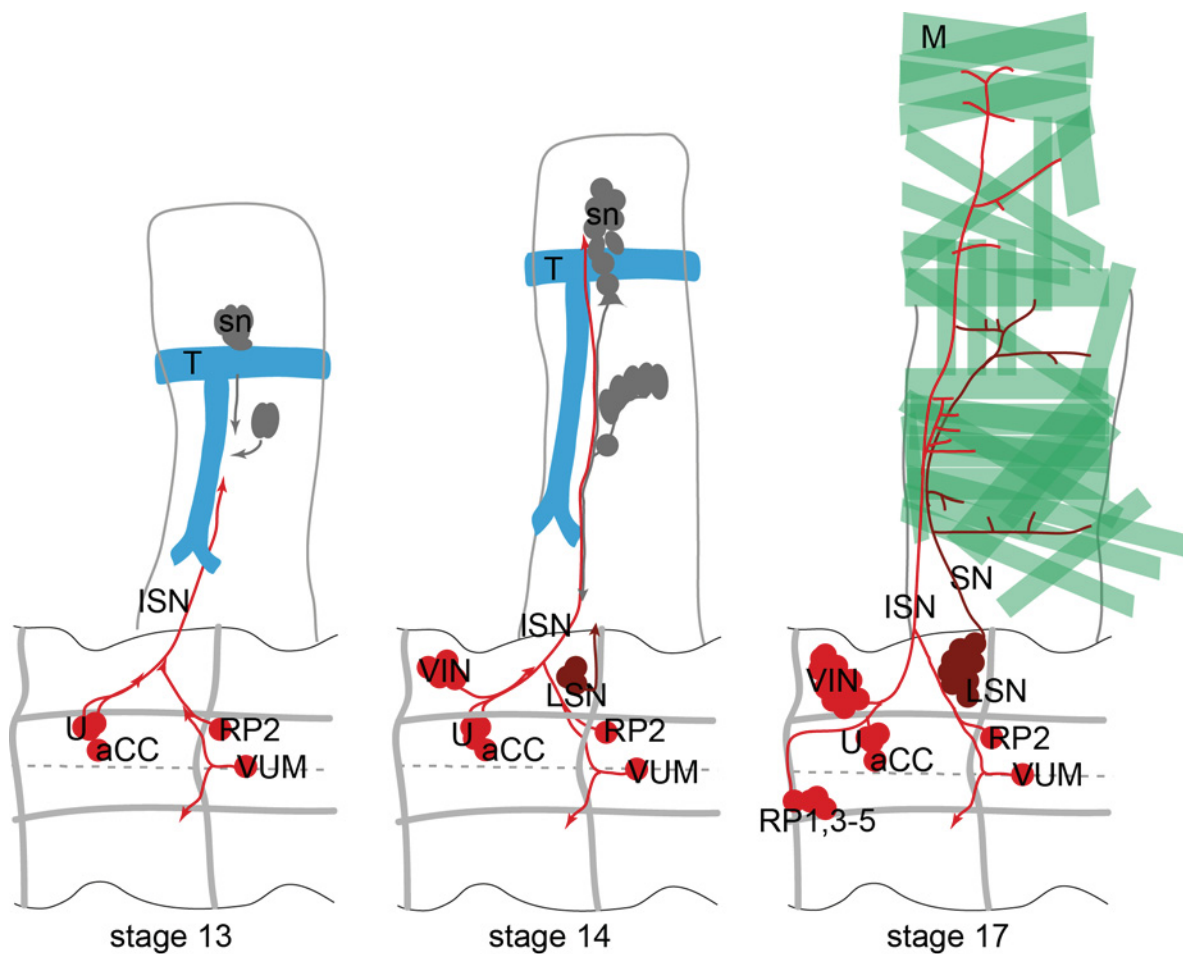


Fig 1. 3: Outgrowing of motor axons from the CNS to their target muscles.

During stage 13 the first axons of aCC, RP2, VUM and U motoneurons (light red) grow out of the CNS and pioneer in the anterior and posterior root of the intersegmental nerve (ISN) using the transverse branch of trachea (T) as substrate. At stage 14, axons of VIN neurons follow and the ISN fasciculates with the first ingrowing sensory neurons (sn). Additionally, axons of LSN neurons (dark red) pioneer the segmental nerve (SN). In late stage embryos (stage 17), motor axons reach their respective muscle field and innervate their target muscles (M). Modified from Campos-Ortega and Hartenstein, 1997a.

1.1.3 Sensory neurons and their projections

A mature *Drosophila* embryo exhibits approximately 45 sensory organs in each thoracic and abdominal hemisegment, which could be divided in three different types - external sensilla, chordotonal organs and multidendritic neurons. Firstly, external sensory (es) organs are mostly mechano- and chemo-sensory receptors including bristles. Secondly, the internal chordotonal (ch) organs are stretched receptors (Campos-Ortega and Hartenstein, 1997b; Ghysen and Dambly-Chaudiere, 1989). Thirdly, multidendritic neurons can be found in clusters composed of up to five cells attached to the inner surface of the epidermis or internal organs, such as trachea, peripheral nerves or muscles (Campos-Ortega and Hartenstein, 1997b). They can be further subdivided into three different types – neurons with extensive subepidermal dendritic arbors (da), neurons that innervate the trachea (td) and neurons with two opposing or bipolar dendrites (bd) (Bodmer and Jan, 1987). Da neurons can be further distinguished in four classes (class I to IV) based on their branching pattern (Grueber et al., 2002). Thereby, class I da neurons exhibit the simplest dendrites and the class IV neurons show the highest branching complexity (Grueber et al., 2002).

Sensory organs of each embryonic segment could be arranged into three different groups – a dorsal, lateral and ventral group. The ventral group exhibits 7 external and 2 chordotonal organs and 10 multidendritic neurons (Orgogozo and Grueber, 2005). Axons of these sensilla join the SNa, SNb or SNc of outgrowing motor axons (Campos-Ortega and Hartenstein, 1997b; Merritt and Whitington, 1995). The lateral group is composed of 3 external sensilla, 6 chordotonal organs and 4 multidendritic neurons and their axons, except for lateral chordotonal organ 1, project into the ISN (Campos-Ortega and Hartenstein, 1997b; Orgogozo and Grueber, 2005). The dorsal group consist of in total 13 sensory neurons - 5 external sensilla organs and 8 multidendritic neurons (Fig 1.4). Axons of sensilla of this group also join the ISN (Campos-Ortega and Hartenstein, 1997b; Orgogozo and Grueber, 2005).

Introduction

been identified in *Drosophila* as proteins secreted by midline glia and are the principal ligands for Robos (Kidd et al., 1999; Rothberg et al., 1988, 1990). Slits function as a repellent and thus, lack of Slits results in the extension of all CNS axons toward the midline (Araújo and Tear, 2003; Kidd et al., 1999). In contrast, mutations in *robo* causes axons to cross the midline, which normally not do so (Seeger et al., 1993). Robos were identified in a genetic screen for mutations that affect the formation of axon pathways in the developing CNS of *Drosophila* embryos and belong to the immunoglobulin superfamily of cell adhesion molecules (Seeger et al., 1993; Ypsilanti et al., 2010).

Before motor axons innervate their target muscles, they have to defasciculate from the nerve bundle. Different axon guidance molecules such as the transmembrane phosphatase LAR, the secreted metalloprotease Tolloid-related and the axon guidance receptor Beat play key-regulatory roles during this process (Desai et al., 1996; Krueger et al., 1996; Meyer and Aberle, 2006). Function of Tolloid-related in defasciculation process was discovered in a large-scale mutagenesis screen for genes that effect the maintenance and structure of neuromuscular junctions. Lack of this secreted protease causes stable innervation defects with missing and misguided neuromuscular junctions (NMJs) based on defasciculation errors (Meyer and Aberle, 2006). Similar bypass defects show mutants of the tyrosine phosphatase LAR (leukocyte antigen-related), which is expressed by neurons and their developing axons (Krueger et al., 1996; Tian et al., 1991). In *lar* mutants, axons, which normally innervate ventral muscles, fail to defasciculate from the main nerve bundle and grow further at the main motor pathway (Krueger et al., 1996).

Furthermore, muscles themselves play an important role for the defasciculation of motor axons (Landgraf et al., 1999). In mutant embryos lacking muscles, the SN and the ISN grow out of the CNS, but axons fail to defasciculate and remain unbranched (Landgraf et al., 1999). This fact suggests that muscles express cues that induce defasciculation and branching of motor axons in their target fields. One of these cues is Sidestep, which is expressed on muscle surface in late embryos and interacts with the axon guidance receptor Beaten path (Fambrough and Goodman, 1996; Siebert et al., 2009; Sink et al., 2001). Lack of each molecule leads to severe bypass defects suggesting that Side and Beat are key-regulators of motor axon guidance in *Drosophila* (Fambrough and Goodman, 1996; Sink et al., 2001).

1.2.1 The axon guidance molecule Sidestep

The gene *sidestep* (*side*) codes for an 939 amino acid long transmembrane protein and was identified in a genetic screen for recessive mutations affecting the structure of NMJs (Aberle et al., 2002; Sink et al., 2001; Van Vactor et al., 1993). The *Drosophila* genome encodes seven closely related proteins of Side (Zinn, 2009). Side consist of a signal-peptide at the N-terminus, five immunoglobulin domains, one transmembrane domain and a short cytoplasmic tail without an identifiable protein motive (Fig 1.5) (Sink et al., 2001).

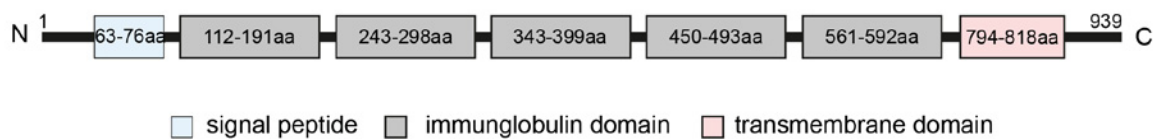


Fig 1. 5: Structure of the Side protein

Side is a transmembrane protein composed of a signal peptide and five immunoglobulin domains.

Side is expressed in a dynamic pattern during embryogenesis. During stage 9, *side* transcript can be first detected in cellclusters near the midline, which are presumably neuroblasts (Sink et al., 2001). During stage 12, Side protein is expressed in a belt-like pattern near the midline and changed at stage 13 into a segmentally repeated triangular structure with the tip pointing towards the periphery (Siebert et al., 2009). At stage 14 Side is no longer detectable in the CNS, but accumulates in a punctate pattern along longitudinal connectives at stage 17 (Sink et al., 2001). In addition to the CNS-specific expression, *side* can be detected during stage 13 and 14 in clusters of probably sensory neurons and developing muscles. The expression in these neurons is down-regulated in the end of stage 14, but the muscle specific expression is weakly detectable until stage 16-17 (Sink et al., 2001). Remarkably, identification of Side positive cells has mostly relied on their morphology and position. In addition, almost nothing is known about the regulation of the dynamic expression of Side.

In *side* mutant embryos, motor axons exit the CNS but fail to defasciculate from major nerve bundles at a high penetrance leading to phenotypes of the ISN and SNa. ISN often does not reach the final branch point in the dorsal muscle field, misses to innervate the dorsal muscles and sometimes crosses the anterior segment boundary independent of the hemisegment. In addition, SNa shows defasciculation defects or truncation of branches. In many hemisegments, motor axons only project in two main fascicles, the ISN and SNa, compared to five main nerves in wild-type embryos (Sink

et al., 2001). However, Side mediates axon defasciculation together with its receptor Beaten path.

1.2.2 The axon guidance receptor Beaten path Ia

Beaten path Ia (Beat) was discovered in a genetic screen for genes affecting the neuromuscular connectivity as essential for entering of motor axons in their respective muscle target field (Van Vactor et al., 1993). The *Drosophila* genome encodes fourteen different Beat proteins in total. Four of them (Beat Ib, Beat Ic, Beat IIa and Beat VI) are membrane-bound in comparison to Beat Ia which is predicted to be a secreted protein (Pipes et al., 2001; Van Vactor et al., 1993). A complementary function of Beat Ia and Beat Ic is revealed by genetic interactions with Beat Ia as an anti-adhesive and Beat Ic as a pro-adhesive molecule (Pipes et al., 2001). Probably, most members of the Beat family act as cell adhesion molecules and Beat Ia regulates them negatively to control axon defasciculation (Pipes et al., 2001).

Beat Ia is composed of 427 amino acids and belongs to the immunoglobulin superfamily. Beat Ia consists of two immunoglobulin domains and a Cys-rich carboxy-terminal domain separated by an unstructured linker (Fig 1.6) (Bazan and Goodman, 1997; Mushegian, 1997). The first 26 amino acids of Beat Ia present a cleaved signal peptide (Fig 1.6) (Fambrough and Goodman, 1996).

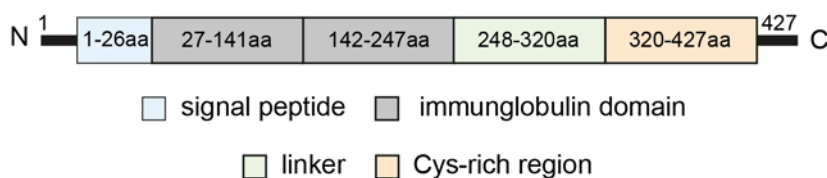


Fig 1. 6: Protein structure of Beat Ia.

The guidance receptor Beat consists of a signal peptide, two immunoglobulin domains, a linker and a Cys-rich region.

Expression of *beat Ia* mRNA can be first detected during stage 12 in a subset of CNS cells that are early born motoneurons based on their positions. Number of *beat* positive motoneurons increases and at early stage 13 the expression level reaches its maximum (Fambrough and Goodman, 1996). High level of *beat* expression can be detected up to stage 17. Expression level of *beat* is varied between the different motoneurons. Accordingly, RP1 and RP3 neurons express *beat* in a higher level than the aCC motoneuron (Fambrough and Goodman, 1996).

In *beat* mutants motor axon guidance phenotype and pattern of NMJs strongly phenocopy those observed in *side* mutants indicating that both molecules might function in a common pathway (Siebert et al., 2009).

1.2.3 Axon guidance via Side and Beat

Cell aggregation assays of our laboratory suggest that Side and Beat interact. Based on these experiments it was proposed that Beat expressing motor axon growth cones recognize and follow Side-labelled cell surfaces such that sensory axons guide motor axons to their target fields. Side disappears from the surface of migratory substrates once motor axons have passed by (Fig 1.7) (Siebert et al., 2009). This way motor axons migrate from the CNS along sensory axons to their respective target muscles guided by the developmentally controlled up-regulation of Side in different tissues.

In *side* mutants, the attractive pathway is no longer labelled resulting in motor axons projecting along aberrant trajectories and staying fasciculated (Fig 1.7, A vs B) (Siebert et al., 2009). In *beat* mutants, however, the intermediate targets still express Side, but motor axons fail to recognise the labelling causing a highly similar phenotype. Additionally, missing contact between motor axons and Side-expressing cells leads to constitutive expression of Side (Fig 1.7 B) (Siebert et al., 2009).

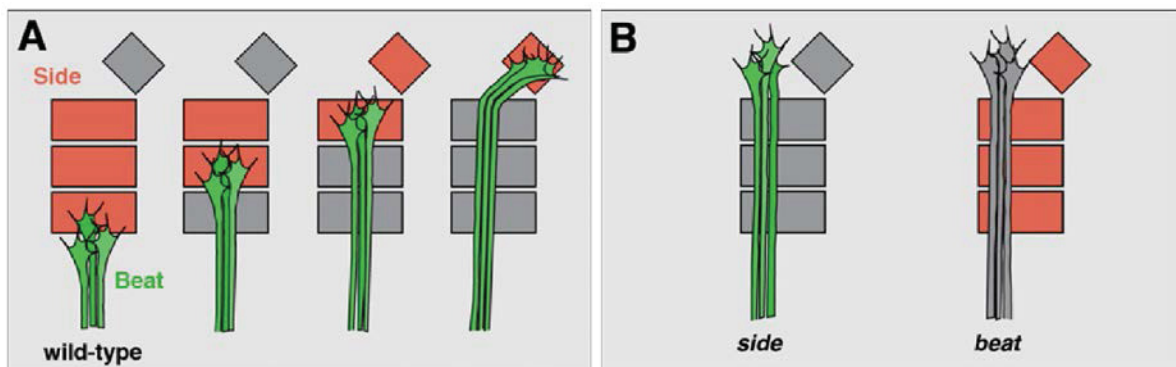


Fig 1. 7: Beat expressing motor axons migrate along Side-labelled substrate.

A: In wild-type embryos motor axons expressing Beat (green) recognize and follow Side-labelled pathway (red) to their respective target fields. Contact with motor axons induces down-regulation of Side (grey). Up-regulation of Side in other tissues induces growth cone turning. B: In *side* mutants, substrates are not labelled and motor axons fail to turn. In *beat* mutants, pathway is constitutively labelled by Side, but cannot be recognized. Taken from Siebert et al., 2009.

1.4 Target muscles of motor axons

Motor axons reach their target muscles at embryonic stage 16 and establish NMJs during stage 17. The somatic musculature of each hemisegment can be divided into a dorsal muscle field, a lateral muscle field and a ventral muscle field. The nerves of

Introduction

the ISN project to internal muscles of the dorsal muscle field and lateral muscle field, while the ISNb and the ISNd innervate muscles of the ventral field. The SNa projects to external muscles of the lateral muscle field and the SNc innervates three muscles of the ventral muscle field (Fig 1.8) (Johansen et al., 1989a; Landgraf et al., 1997; Sink and Whitington, 1991b).

Recently, Hoang and Chiba could assign specific motoneurons to specific muscles by retrograde labelling in larvae (Hoang and Chiba, 2001). They have shown that almost all neurons (83%) projecting in the ISN innervate only one muscle, while the majority of motoneurons projecting in the SN innervate one or two muscles (72%). All other neurons of both nerve bundles project to 3, 5, 6, 7, 8, 9 or 10 different muscles resulting in a multiple innervation of almost all muscles (Hoang and Chiba, 2001).

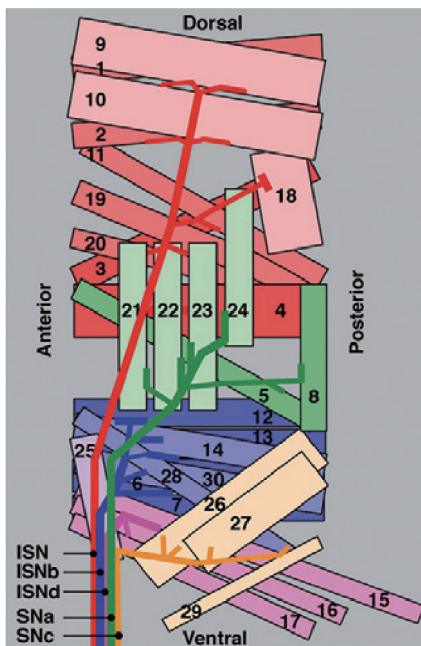


Fig 1. 8: Schematic scheme of innervation pattern of somatic muscles of an abdominal hemisegment (viewed from exterior).

Approximate branching pattern of the five main nerves and their innervation sites onto the muscle pattern. Main nerves and their respective target muscle fields are marked in similar colours. Bright colours: internal muscles. Dark colours: external muscles. Taken from Beuchle et al., 2007.

1.4.1 Development of embryonic muscles

The somatic muscles, heart muscles and visceral muscles of a *Drosophila* embryo derives from different domains of the mesodermal monolayer, which is formed by the ventral most cells of the blastoderm (Bate, 1990; Paululat et al., 1999). Differentiation and invagination is regulated by the transcription factor Dorsal that activates the transcription of the gene *twist* (Paululat et al., 1999). Cells expressing high levels of

Introduction

Twist segregate muscle precursors, myoblasts, characterised by the gene *lethal of scute* (Paululat et al., 1999; Schnorrer and Dickson, 2004). One cell per Lethal of scute expressing cell group is singled out by lateral inhibition mediated by the transcription factor Notch and its ligand Delta and becomes the progenitor or so called founder cell (FCs) (Paululat et al., 1999; Schnorrer and Dickson, 2004). At first, FCs of ventral muscles are detectable and the progenitors of dorsal muscles and lateral muscles follow (Bate, 1990).

Muscle precursors grow by fusion with adjacent cells of the mesoderm, the fusion competent myoblasts (FCMs), with no nuclear division or DNA replication (Fig 1.9) (Bate, 1990). This fusion of the FCs with the FCMs is highly selective – founder cells fuse with myoblasts, but myoblasts do not fuse with each other (Taylor, 2002). Thus, muscle fibre growth is achieved by progenitor cells fusing into a syncytium, the myotube, with a direct correlation between the muscle size and the nuclear number – bigger myotubes exhibit more nuclei than smaller ones (Fig 1.9) (Bate, 1990).

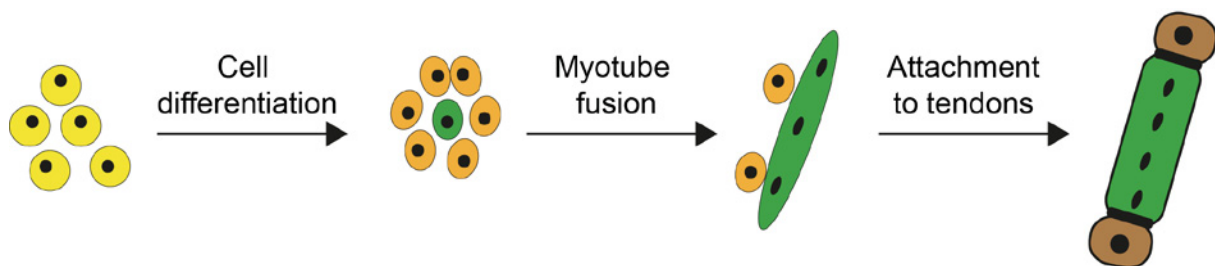


Fig 1. 9: Development of muscles during *Drosophila* embryogenesis.

Undifferentiated myoblasts (yellow circles) differentiate into founder cells (green circle) and fusion competent myoblasts (FCMs) (orange circles). Based on fusion of founder cells with FCMs a syncytial cell, the myotube (green ellipse), develops and attaches to tendon cells (brown squares). Modified from Abmayr and Pavlath, 2012 and Schweitzer et al., 2010.

Myotubes are connected to specialised muscles attachment cells, called tendon cells, which emerge in parallel to the founder cells (Fig 1.9) (Schweitzer et al., 2010). They are part of the epidermal cell layer and form - together with the cuticle - the exoskeleton of *Drosophila* (Schweitzer et al., 2010).

1.5 The larval neuromuscular system

The number, size and location of larval muscles are similar as in stage 16 embryos (13 hours after egg laying). Each hemisegment exhibits approximately 30 muscles. While the abdominal segments A2 to A7 show the same stereotypic pattern of

Introduction

muscles, the thoracic segments and the first and last abdominal segments exhibit a slightly different architecture (Fig 1.10).

Muscle fibres grow enormously during development from first instar larvae (L1) to third instar larvae (L3) from an approximate length of 50µm to more than 500µm per segment. This growth is independent of fusion with further myoblasts (Weitkunat and Schnorrer, 2014).

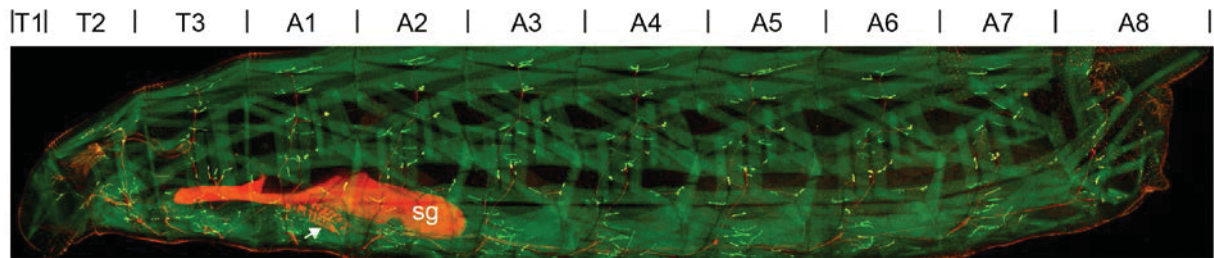


Fig 1. 10: Larval neuromuscular system of a third instar larva (lateral view).

30 muscles of each abdominal hemisegment (A2-A7) (dark green, based on ShGFP) are innervated by around 35 motor axons (red, based on OK371>dsRED). NMJs: bright green/yellow. sg: salivary gland. Arrow: CNS.

The pattern of neuromuscular connectivity is settled in the middle of embryonic stage 16 and appears to be maintained throughout larval life (Landgraf and Thor, 2006). Development of NMJs starts at stage 16 with the first contact of growth cones with the muscles (Keshishian et al., 1996; Marqués, 2005). Different components of the later synapse are expressed in motor axons and muscles before the synapse is formed such as the transcripts for glutamate receptors, which can be detected in the developing muscles several hours before motor axons innervate them (Keshishian et al., 1996). One hour after the first contact between motor axons and muscles synapses are active. After an additional hour muscles contract coordinately (Broadie et al., 1993; Marqués, 2005).

Typical *Drosophila* NMJs consist of presynaptic sites build by motor axons and postsynaptic sites build by muscles separated by a synaptic cleft. NMJs exhibit boutons with active zones, the T-bars. Two classes of boutons can be distinguished between – type I boutons are large boutons with a diameter up to 8µm, while type II boutons are smaller with a mean diameter of only approximately 1.5µm and often spread over the entire length of the muscle (Johansen et al., 1989b). NMJs grow during larval stages by an increase of boutons per synapse (Schuster et al., 1996). Newly build boutons develop in three different ways. Firstly, they can emerge by symmetric division from one old bouton dividing into two new boutons. Secondly,

they can develop via an asymmetric division where a small bouton butts of a larger bouton (budding). Thirdly, boutons can emerge “de novo” (Zito et al., 1999). The newly build boutons localise between previously existing boutons, but also at the edge of NMJs (Zito et al., 1999).

1.6 Metamorphosis

Since *Drosophila* belongs to the holometabolic insects, larvae have to pass through a metamorphosis to get their adult habitus. Thereby, larvae transform in an immobile pupal phase meanwhile the larval organisation is changed dramatically including amongst others histolysis of almost all muscles (Tissot and Stocker, 2000). Therefore, most of the adult muscles are newly build during metamorphosis by fusion of adult muscle precursors (AMPs) (Weitkunat and Schnorrer, 2014). AMPs develop during embryogenesis together with the progenitors of the embryonic and larval somatic musculature. In contrast to these progenitors, the AMPs are positive for *twist* expression after embryonic stage 12 (Bate et al., 1991; Thisse et al., 1988). In each abdominal hemisegment of a late embryo there are six AMPs located at three stereotypic positions (Figeac et al., 2010). In contrast, in the thoracic segments the AMPs are associated with the imaginal discs (Bate et al., 1991). During the larval stages AMPs proliferate and build during the pupal stages the adult muscles by fusion of founder cells with fusion competent myoblasts similar to the embryonic muscle development (see 1.4.1) (Bate et al., 1991; Dutta et al., 2004).

Motoneurons pass through two different fates during metamorphosis. Most of them survive up to the adult stage despite the lysis of their larval target muscles (Tissot and Stocker, 2000; Truman, 1990). Larval NMJs retract during this process and after a transition motor axons grow out again and innervate the adult muscles (Fernandes and Vijayraghavan, 1993). The remaining motoneurons degenerate in two waves. The first wave starts shortly after pupation, while the second one begins within 24 hours after hatching of the adult fly (Tissot and Stocker, 2000; Truman, 1990).

Most of the sensory neurons of the *Drosophila* embryo and larva die during metamorphosis. Thus, most adult PNS neurons develop during the pupal stage de novo in specific imaginal discs (Tissot and Stocker, 2000; Truman, 1990).

1.7 The adult fly

Pupation ends after 96 hours and adult flies hatch consisting of three different parts - the head with the dominant compounded eyes, the thorax with three leg pairs, one wing pair and one halter pair and the abdomen with the external genital apparatus.

1.7.1 The adult leg

Drosophila legs, and of insects in general, composed of five different segments – coxa, trochanter, femur, tibia, tarsus (from proximal to distal). Legs are moved by muscles, which develop *de novo* from leg imaginal discs during metamorphosis. They emerge from a subpopulation of AMPs, which proliferate during the second instar and produce approximately 500 myoblasts. These myoblasts fuse during metamorphosis in two waves – the first wave occurs between 20 and 25 hours after pupae formation, while the second one begins 35 hours after pupae formation (Soler et al., 2004). In contrast to all other muscles of the adult fly, the leg muscles develop in association with internal tendons, which emerge synchronously with the muscles. The muscles of the mature legs are positioned around their internal tendons (Soler et al., 2004).

Leg muscles are innervated by approximately 50 motoneurons, which develop from 11 neuroblasts during embryogenesis, whose cell bodies are located anterior to the neuropil (Baek and Mann, 2009). Two of these 11 neuroblast lines (A and B) produce the main amount of motoneurons. Thereby, motoneurons emerging from lineage A innervate the muscles of the femur and tibia, while motor axons of neurons from lineage B project to muscles of the coxa, trochanter and femur (Baek and Mann, 2009).

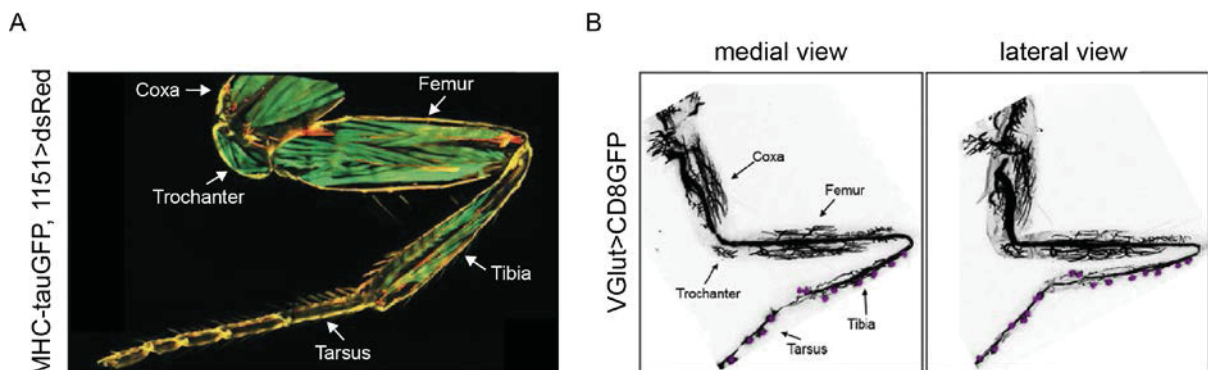


Fig 1. 11: Muscles and innervation pattern of a *Drosophila* leg.

A: Musculature (green) visualised by MHC-tauGFP and myoblasts and tendons marked by 1151>dsRED (red). B: Motor axons of a leg marked by VGlut>CD8GFP. Purple dots: sensory neurons. Modified from Baek and Mann, 2009; Soler et al., 2004.

Introduction

Walking and the associated coordinated movements performed by the leg apparatus, consists of muscles, tendons and motoneurons, are essential amongst others for food searching in the nearby area and male courtship behaviour. During walking flies show a tripod gait, moving simultaneously the fore (prothoracic) - and hindlegs (metathoracic) of one body half together with the contralateral middle (mesothoracic) leg (Strauss and Heisenberg, 1990). This gait is independent from the walking speed of the fly in contrast to, for example, horses, which use different gaits for different walking speeds (Mendes et al., 2013). However, during slower walks walking pattern is altered with a delayed metathoracic leg in comparison to the pro- and mesothoracic legs. When walking, flies show six different footprints with a specific arrangement. The second legs produce thereby the outermost prints and first legs the innermost prints. Prints of metathoracic legs are positioned between the two others (Strauss and Heisenberg, 1990). This pattern is often altered on one body side with close together footprints of the fore- and hindlegs. Asymmetry correlates with a shifting of 2-3° of the longitudinal body axis in relation to walking direction toward the side where leg prints fall together (Strauss and Heisenberg, 1990).

Analysing gait parameters using high-resolution tracking, Mendes and colleagues suggest that *Drosophila* and flies in general use different neural programs for slow, medium and fast walking. Genetic manipulations to disrupt sensory feedback from the legs demonstrate further that blocking proprioception causes a reduced walking precision especially at slower speeds, but the ability to walk in a tripod gait is not effected (Mendes et al., 2013). Therefore, additional to the muscles, tendons and motoneurons, sensory neurons are also regulators of the coordinated walking of flies.

1.7.3 The indirect flight musculature

Another essential locomotion behaviour of flies to survive is the ability to fly. The flight musculature of *Drosophila* consists of two different types of muscles – direct flight muscles (DFMs) and indirect flight muscles (IFMs) (Fig 1.12). Direct flight muscles adjust the orientation of wings based on their insertion directly on (direct control muscles) or near (indirect control muscles) the wing hinge. They are able to reconfigure the wing hinge rapidly and are controlled neuronally. Thereby, almost all muscles are innervated by a single neuron (Dickinson and Tu, 1997).

IFMs, also called power muscles, can be divided into three dorsal-ventral muscle bundles (DVMs) and six dorsal longitudinal muscles (DLMs) (Dutta et al., 2004;

Introduction

Fernandes et al., 1991; Jährling et al., 2010). As mediated by figure 1.12, the six DLMs are located in an anterior-posterior position in the interior of the adult thorax and run along the full length of the thorax. The seven DVMs have a more dorso-ventral position located lateral to the DLMs (Fig 1.12) (Dickinson and Tu, 1997; Jährling et al., 2010).

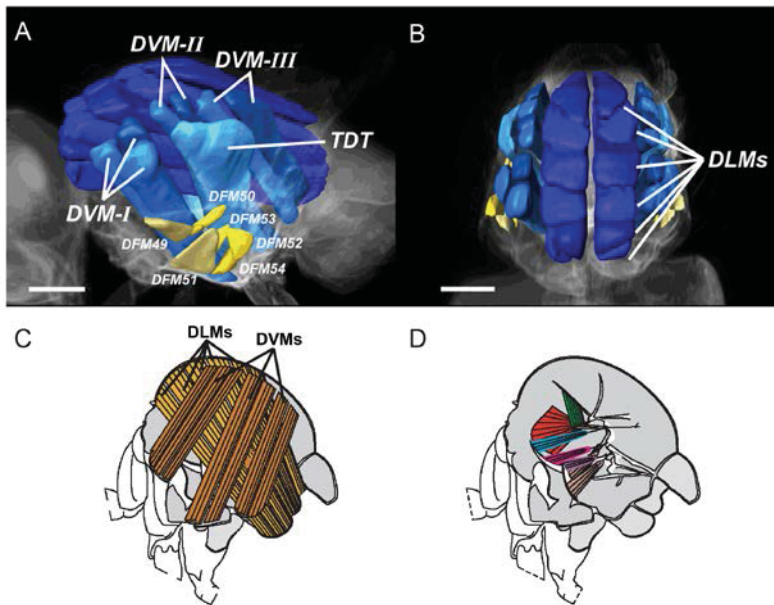


Fig 1. 12: Flight musculature of adult *Drosophila* flies.

A+B: 3D reconstruction of flight muscles. Dark-blue: dorsal longitudinal muscles (DLMs). Blue: dorsal ventral muscles (DVMs). Light-blue: tergal repressor of the trochanter (TDT). Yellow: direct flight muscles (DFMs). Modified from Jährling et al., 2010. C+D: Power (C) and control (D) muscles. Modified from Frye and Dickinson, 2004.

The two types of indirect flight muscles develop at the same time, but in two different ways. While the DVMs emerge from AMPs, the DLMs develop from larval muscles, which were not histolysed. The larval meso-thoracic oblique muscles 9, 10 and 19 survive the histolysis during metamorphosis and build the template for the DLMs. Each template muscle splits into two muscles and grows by fusion with AMPs (Fernandes et al., 1991). The innervation of the indirect flight musculature emerges simultaneously with the muscles by remodelling the larval intersegmental and segmental nerve of the meso-thoracic segment (Fernandes and Vijayraghavan, 1993). All six DLMs and two DVMs (I and III) are innervated by the ISN, while the third DVM (II) is innervated by the SN (Fig 1.13) (Fernandes and Vijayraghavan, 1993).

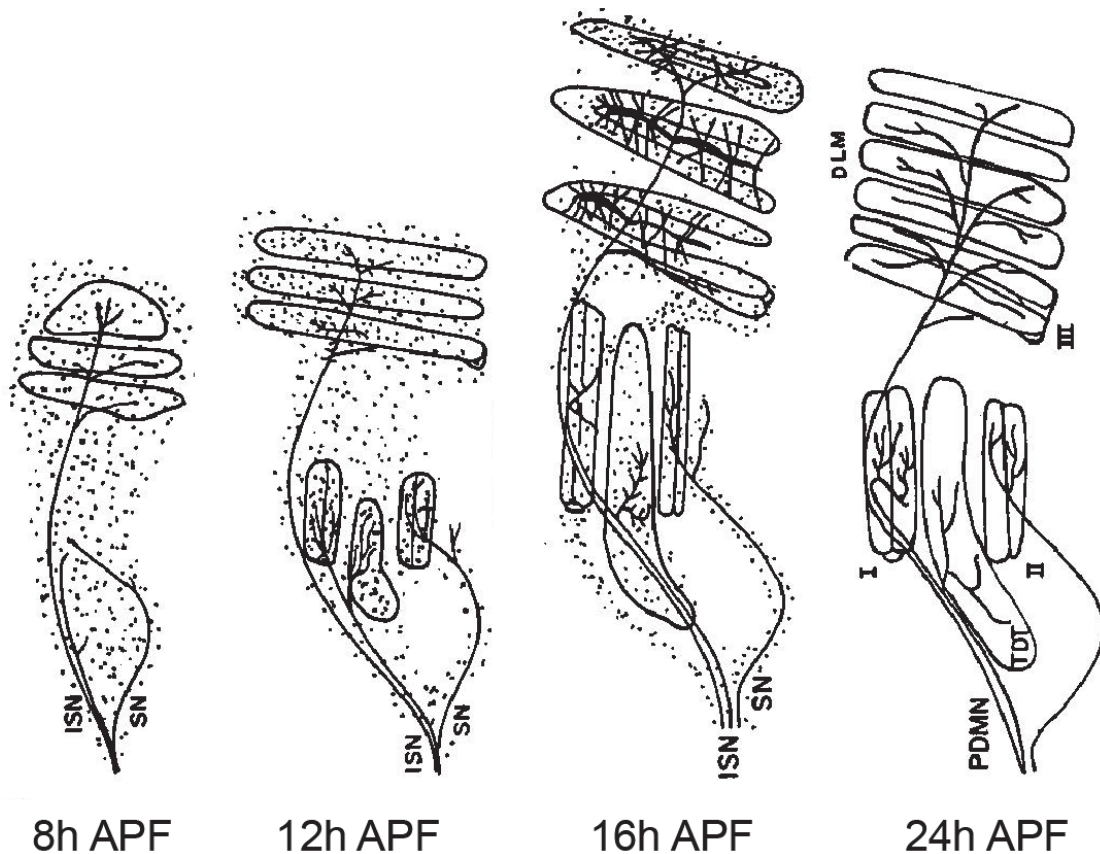


Fig 1. 13: Temporal progress of innervation of indirect flight musculature during pupation.

ISN innervates all six DLMs and two DVMs (I+III), while the SN projects only to one DVM (II). APF = after pupae formation. ISN = intersegmental nerve. SN = segmental nerve. PDMN = posterior dorsal mesothoracic nerve. TDT = tergal repressor of the trochanter. DLM = dorsal longitudinal muscle. I-III = dorsal-ventral muscle (DVM) I-III. Modified from Fernandes and Vijayraghavan, 1993.

The indirect flight musculature is responsible to generate the power for the wing beat. Thereby, ventral and longitudinal muscles act antagonistically. Contraction of the DLMs leads to a decreased length and an increased width and height of the thorax. In contrast, DVM contraction decreases the width and height and increases the length of the thorax (Dickinson and Tu, 1997). Therefore, contraction of DLMs, responsible for moving the wing downward, stretches the DVMs and vice versa, whereby the wings are moved upward. Based on this stretch activation each action potential mediated by the motoneurons innervating the indirect flight muscles results in many wing beats and not only in one wing beat per action potential (Dickinson and Tu, 1997).

1.8 Aims of the thesis

The aim of the present thesis is to elucidate the regulation and functional consequences of mutations of the two members of the immunoglobulin superfamily *sidestep* (*side*) and *beaten path la* (*beat*). Both are key-regulators of motor axons guidance during embryogenesis in *Drosophila melanogaster*. While motor axons in wild-type embryos defasciculate into their respective muscle fields, they fail to do so in *beat* and *side* mutants and bypass muscle fields resulting in non- or mis-innervated muscle fibres.

In an approach to better understand the dynamic expression pattern of *side* during embryogenesis of *Drosophila*, the exact cell types expressing Side in the CNS and PNS and potential transcription factors of *side* shall be identified. Furthermore, the potential promoter of *side* and its interaction partner *beat* is planned to be determined analysing genomic enhancer fragments. It is intended to investigate the potential degradation mechanism of Side in order to reveal how the potential down-regulation of Side in intermediate targets after contact with Beat expressing motor axons is regulated. Thereby, prevention of Side degradation should lead to constitutive Side expression.

Since *Drosophila* is a holometabolic insect, the neuromuscular system has to be established a second time during metamorphosis. Here, the question shall be addressed if Side is also functional in axon guidance during this process. Therefore, innervation pattern of adult flight and leg musculature shall be analysed.

Furthermore, it shall be elucidated if mis-innervation leads to behavioural consequences. It is generally being estimated that the performance of coordinated movements is based on the correct wiring of a neuromuscular system. Therefore, mis-innervation of muscles would lead to locomotion defects. Remarkably, a direct correlation between mis-innervation and behavioural defects has not been shown previously in *Drosophila*. To address this question, locomotion assays of *side* mutant larvae and adult flies shall be performed.

2. Results

2.1 Gene regulation of *sidestep* and *beaten path*

The axon guidance molecule Sidestep and its interaction partner Beaten path play an important role during migration of motor axons from the CNS to their target muscles. While the loss of function phenotypes and the interaction of both molecules are well described (Fambrough and Goodman, 1996; Siebert et al., 2009; Sink et al., 2001), almost nothing is known about their regulation. Therefore, this thesis focussed amongst others on the cell-specific expression of Side, the regulation by transcription factors and the identification of enhancer elements of *beat* and *side*.

2.1.1 Gene regulation of the axon guidance molecule Side

2.1.1.1 Side is expressed in glia and sensory neurons

To better understand the spatiotemporal regulation of *side* it was attempted to determine Side-expressing cell types. Side is expressed dynamically during embryogenesis (Fig 2.1). In early stages (stage 9-12) Side can be detected in the CNS in cells near the midline and during stages 12 to 14 in clusters of sensory neurons in the PNS. So far, cells were specified due to their morphology and location of expressing cells, due to antibody incompatibilities (Siebert et al., 2009; Sink et al., 2001). To unequivocally identify Side expressing cells antibody co-stainings with anti-Side and cell-specific markers as well as transgenic embryos were performed. Table 2.1 gives an overview of the used markers and their specificity. For detailed information about references or resources see chapter 4 Material and Methods.

Results

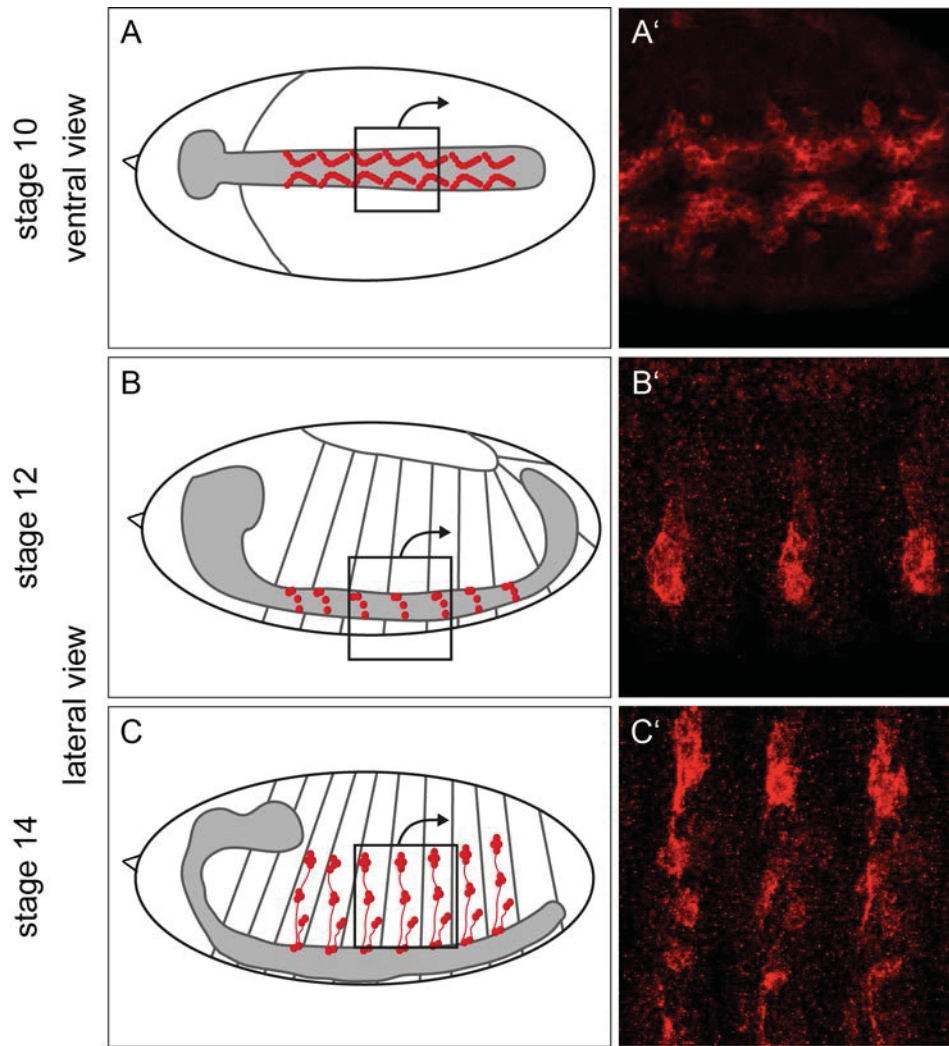


Fig 2. 1: Side is expressed dynamically during embryogenesis.

A+A': In early embryos (stage 10) Side (red) is expressed in the CNS. B-C': In mid-stage embryos (stage 12-14) sensory neurons of the PNS express Side. A-C: Schemes of Side expression during embryogenesis. A'-C': Confocal images of wild-type embryos stained with anti-Side.

Tab 2. 1: Markers employed to identify Side expressing cells.

| tissue | marker | cell type |
|--------|---------------------------------|--|
| CNS | (anti-) BarH1/2 | SNa neurons and ventral unpaired midline dopaminergic neurons (VUMs) (Garces et al., 2006) |
| | reversed polarity (repo) (-Gal) | almost all glia cells except midline glia (Xiong et al, 1994) |
| PNS | 21-7 (-Gal4) | multidendritic neurons (Song et al., 2007) |
| | (anti-) BarH1/2 | external sensory organs (Higashijima et al., 1992) |
| | repo (-Gal4) | almost all glia cells (Xiong et al, 1994) |
| | breathless (-Gal4) | trachea (Klambt et al., 1992) |

Results

To investigate if Side is expressed in glia cells of the CNS, UAS-mCD8GFP driven by repo-Gal4, which reflect the expression of the Repo protein, was used (Sepp et al., 2000). mCD8-GFP is a fusion protein composed of the mouse transmembrane protein CD8 and the coding sequence of GFP protein (Lee and Luo, 1999). Embryos were stained with anti-GFP and anti-Side. At stage 11, Side co-localise with four longitudinal glia (Fig 2.2 A-C). In later stages (stages 12 and 13), Side overlaps with centrally-born peripheral glia cells - the intersegmental glia 1 and 2 along the ISN and segmental glia along the SN (Fig 2.2 D-I) based on the position of the cells (Kläämbt and Goodman, 1991). This co-localisation is also visible in single section images (not shown).

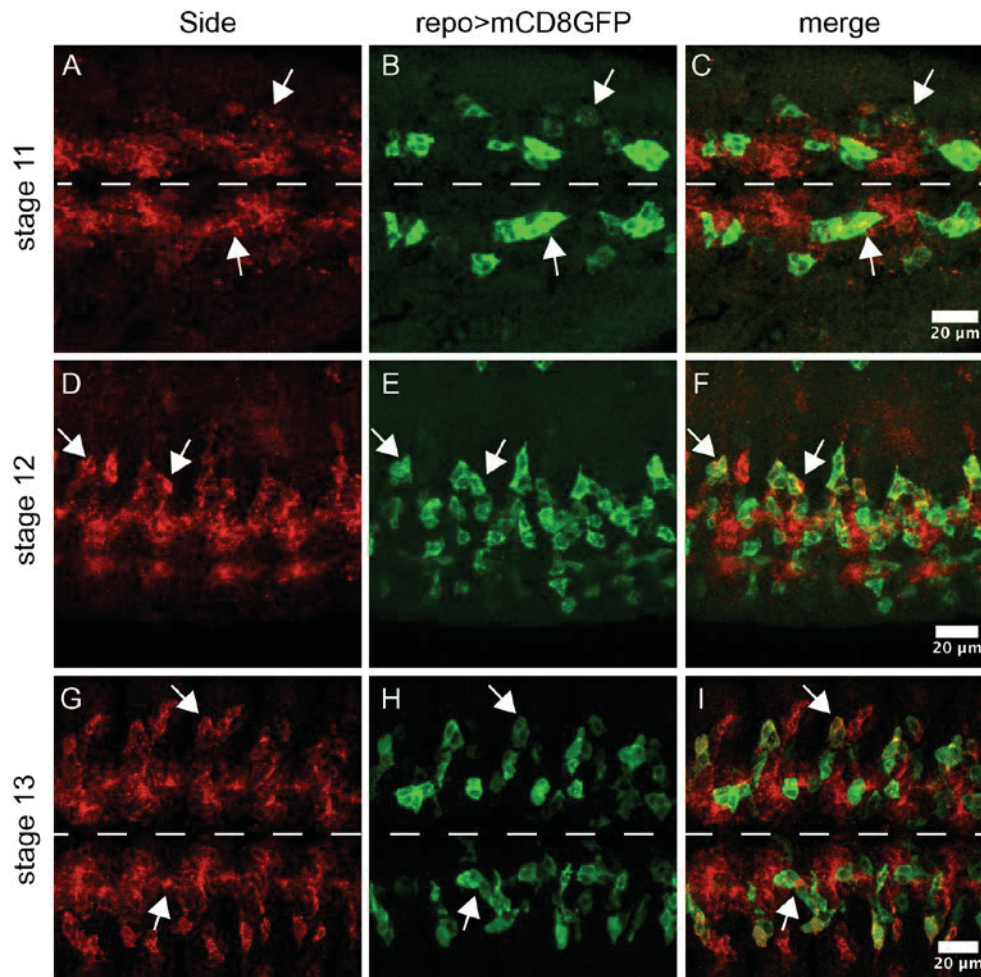


Fig 2. 2: Side is expressed in a subset of glia cells in the CNS.

Antibody co-stainings of repo>mCD8GFP embryos with anti-Side (red) and anti-GFP (green). A-C: Side is expressed in longitudinal glia (arrows). D-I: Segmental and intersegmental glia show also Side expression (arrows). A-C + G-I: ventral view. D-F: ventro-lateral view. Broken line: midline. All images in this figure and all following confocal images are maximum intensity projections with an anterior -> posterior orientation.

Results

To confirm that Side is not expressed in motoneurons anti-BarH1/2 antibody was used. Side co-localise with BarH1/2 in two of the three unpaired ventral midline neurons (VUMs) (arrows Fig 2.3 A-C + D-F), but in single sections this co-localisation is not visible (arrows Fig 2.3 A'-C'). Further, SNa neurons do not show any signal overlap (Fig 2.3) (Garces et al., 2006). This observation is consistent with results of former members of our working group using a Fasciclin II exon-trap line (FasII^{GFP^{Mue397}}), which is expressed in a cluster of motoneurons including the aCC and pCC neurons (Siebert et al., 2009).

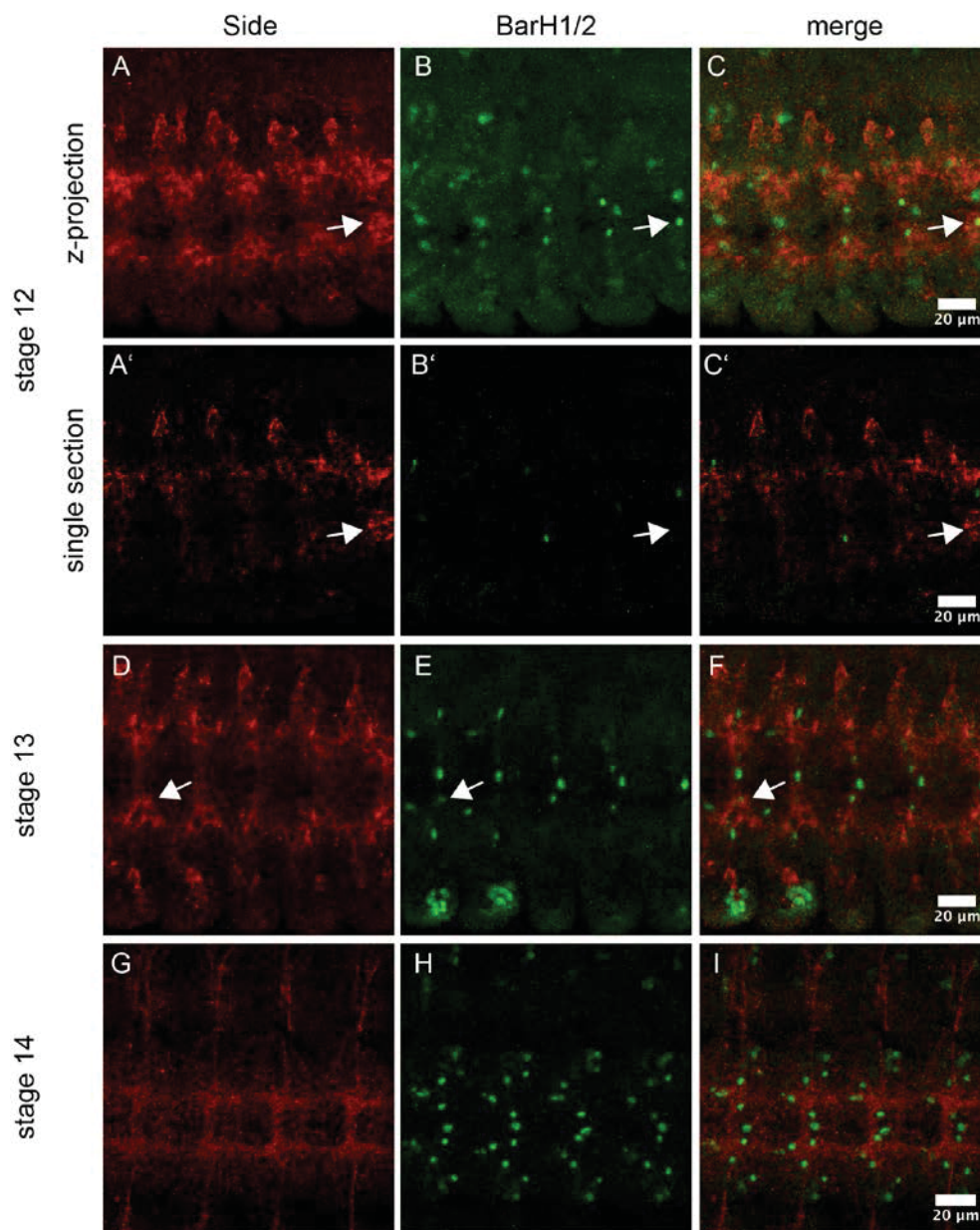


Fig 2. 3: Side is not expressed in motoneurons in the CNS.

Confocal images of antibody stainings of wild-type embryos with anti-Side (red) and anti-BarH1/2 (green). A-F: Early stages (12+13) show signal overlaps in ventral midline neurons (arrows), which are visible in maximum projections. A'-C': Single sections show no co-localisation. G-I: Mid-stage embryos (stage 14) show no co-localisation of Side-expressing cells and motoneurons. A-I: ventral view.

Results

In summary, in the CNS Side is expressed in some glia cells, but not in motoneurons.

To investigate if the Side-positive structures in the PNS indeed belong to sensory neurons, again anti-BarH1/2 antibody is used. In the PNS, BarH1/2 are expressed in external sensory organs and their associated cells as well as in intersegmental dorsal epidermis cells (Higashijima et al., 1992). Based on their function as transcription factors, signal of anti-BarH1/2 antibody is localised in the nucleus of cells, while the anti-Side antibody binds to the extra-cellular domain of Side.

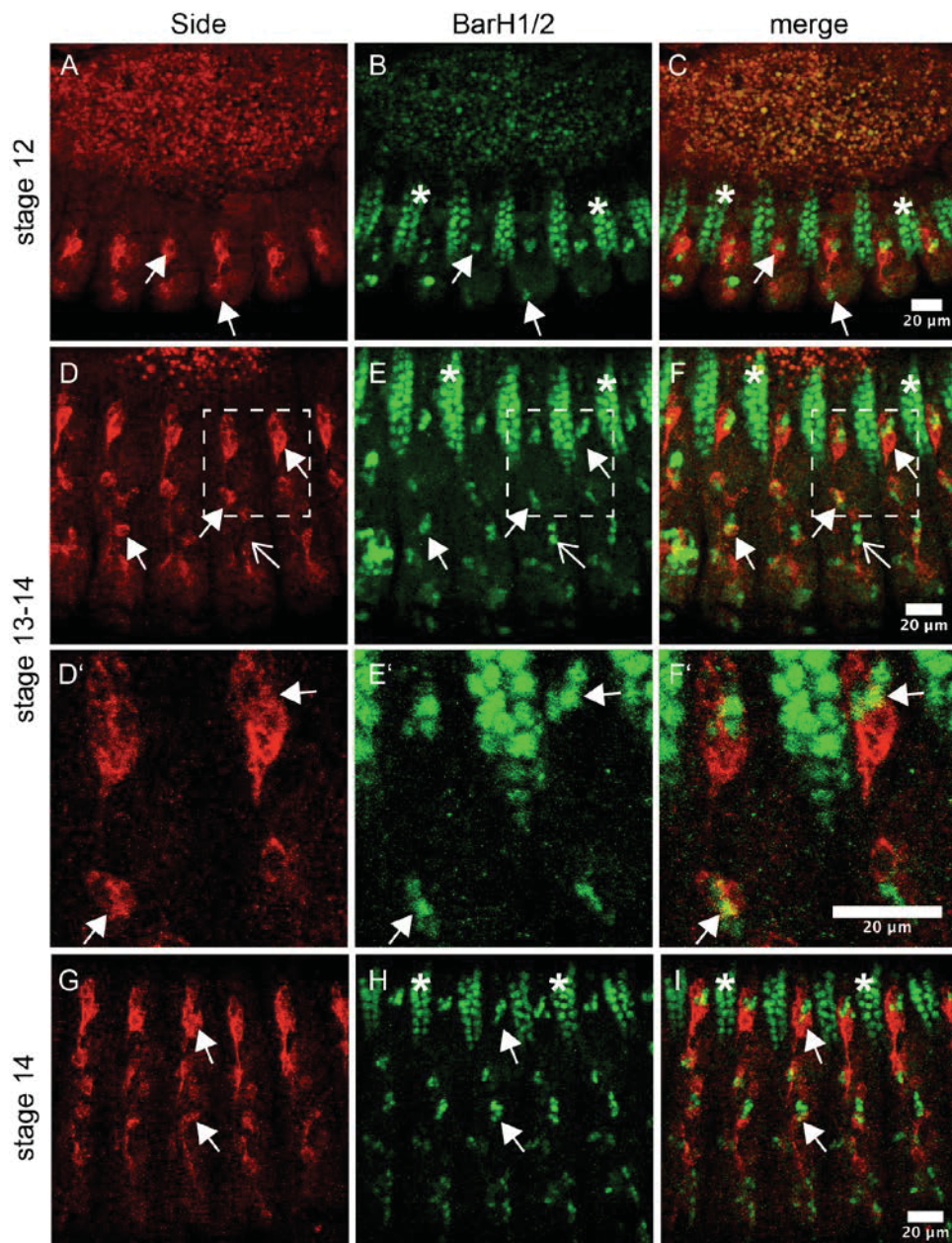


Fig 2. 4: Side is expressed in a subset of external sensory organs.

Anti-Side (red) and anti-BarH1/2 (green) stainings of wild-type embryos. A-I: Subset of external sensilla express Side during stages 12 to 14 (arrows). Asterisks mark dorsal epidermal cells (ventral view). D-F: Empty arrows mark external sensory organs negative for Side expression. D'-F': Close-up.

Results

Side is localised around the BarH1/2 signal in the dorsal group and ventral group of external sensory organs (arrows Fig 2.4 A-I). However, in the lateral group some external sensilla without a surrounding by Side exist (empty arrows Fig 2.4 D-E).

To test if Side is expressed in another type of sensory neurons the driver line 21-7 - Gal4 was used, which drives the expression of effector lines specific in all multidendritic (md) sensory neurons (Song et al., 2007). This fact makes it possible to mark md neurons and their axons using UAS-mCD8GFP. Side is expressed in early stages in cell bodies of md neurons of the dorsal group (filled arrows Fig 2.5 A-I) and in later stages also in their axons (asterisks Fig 2.5 G-I). Side does not overlap with multidendritic neurons of the ventral group (empty arrows Fig 2.5 A-C and G-I).

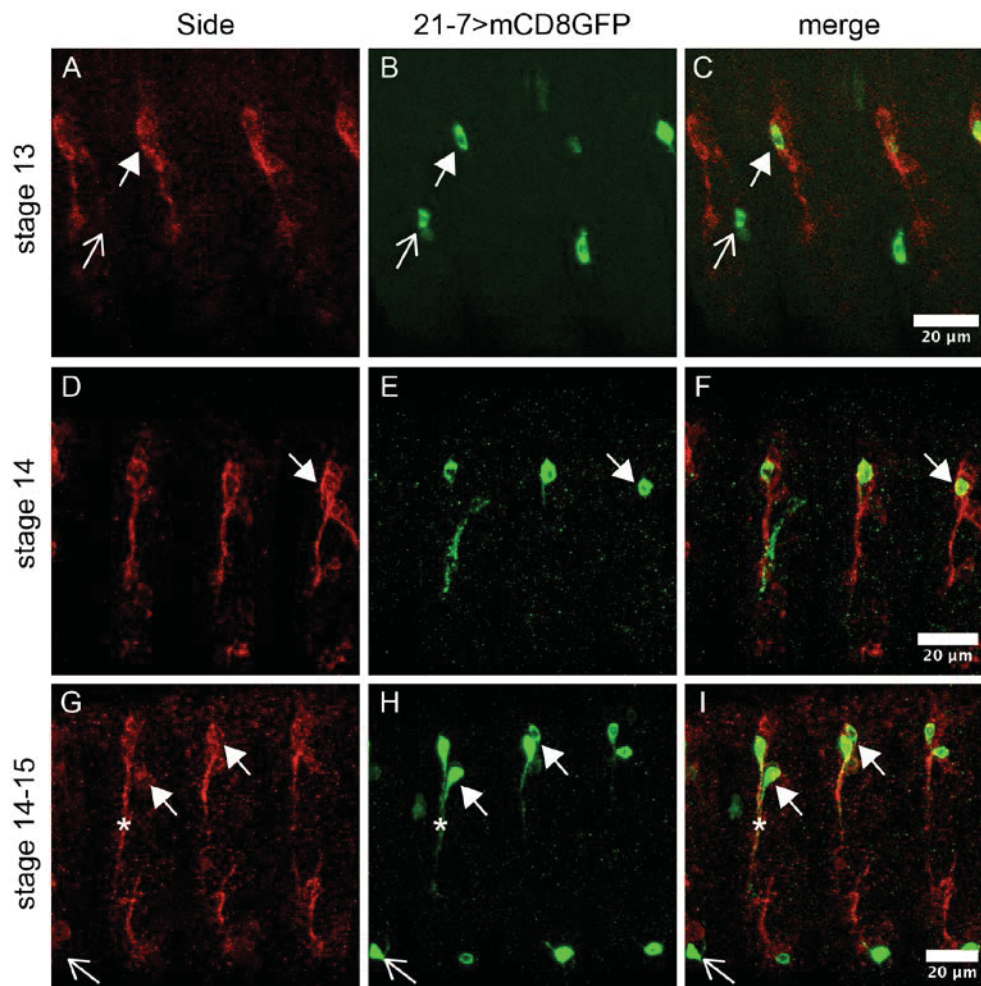


Fig 2. 5: Dorsal multidendritic neurons express Side in the PNS.

Antibody staining of 21-7>mCD8GFP embryos with anti-Side (red) and anti-GFP (green). A-I: Side expression can be localised in dorsal multidendritic neurons (arrows) (lateral view). G-I: In mid-stage embryos (stage 14-15) Side is additionally expressed in the axons of dorsal multidendritic neurons (asterisks). A-C and G-I: Ventral multidendritic neurons show no Side expression (empty arrows).

Results

The localisation of Side to md neurons is not as distinct as the localisation in external sensory neurons, since the driver line 21-7-Gal4 drives the effector line UAS-mCD8GFP too late in comparison to the Side expression. The strongest GFP expression driven by 21-7-Gal4 is visible during the embryogenesis in stage 15 to 16 embryos, but at this time, Side is no longer expressed in sensory neurons.

To investigate if Side is also expressed in peripheral glia cells, the driver line repo-Gal4 was used again to overexpress UAS-mCD8GFP. In stage 13 to 14 old embryos, Side does not co-localise with peripheral glia cells (Fig 2.6 A-C). At stage 14, Side overlaps with one glia cell per hemisegment (arrows Fig 2.6 D-F). Based on the position, this cell is probably the external glia cell 9 (von Hilchen et al., 2008). Later, a second cell, probably the external glia cell 10, is also positive for Side (arrows Fig 2.6 G-J) (von Hilchen et al., 2008).

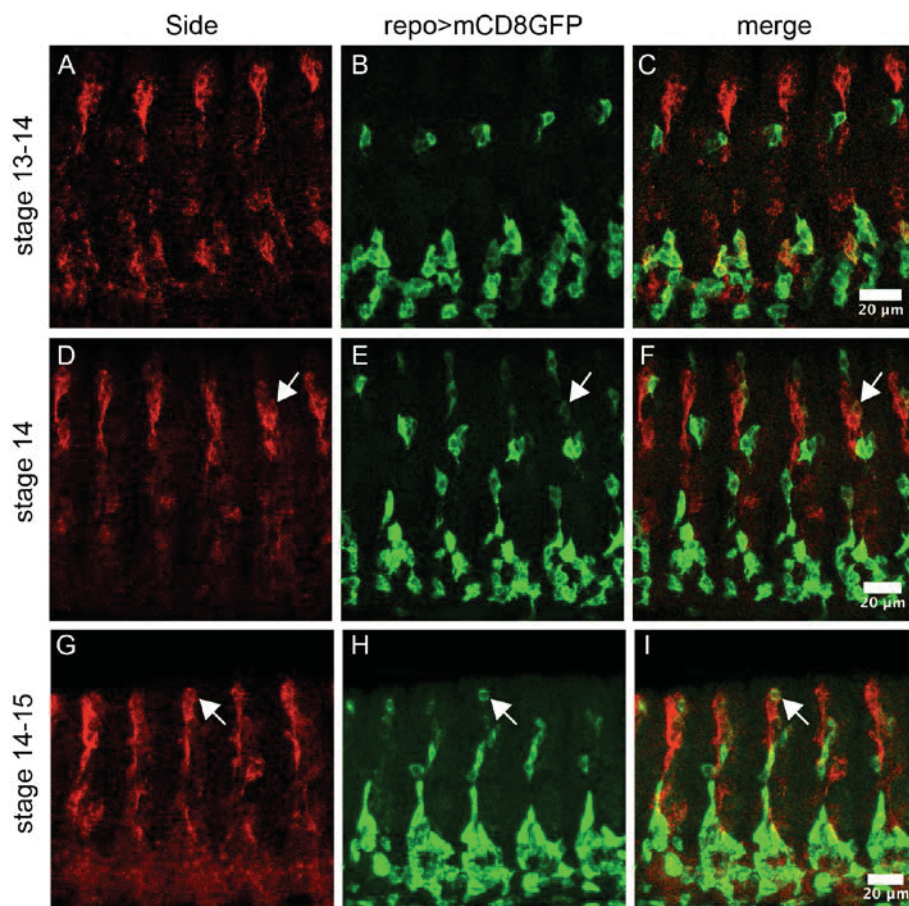


Fig 2. 6: In the PNS, Side is expressed in two glia cells per hemisegment.

Confocal images of repo>mCD8GFP embryos stained with anti-GFP (green) and anti-Side (red). A-C: At stage 13-14 Side is not expressed in peripheral glia. D-F: At stage 14, Side overlaps with the external glia cell 9 (arrows). G-I: At stage 14-15, the external glia cell 10 also expresses Side. A-I: ventral view.

Results

The embryonic trachea serves as an intermediate target for motor axons during their migration from the CNS to their final muscle targets. Thus, trachea might also express Side to guide motor axons. However, Side expression could not be found in trachea (data not shown).

Taken together, Side is expressed during stage 12 to stage 14 in multidendritic and external sensory neurons and some glia cells, but not in trachea.

2.1.1.2 Side expression is reflected by two different enhancer Gal4-lines

Since Sidestep is expressed in a coordinated, spatio-temporal manner during embryonic development of *Drosophila*, various promoter-fragment-Gal4-lines were analysed to identify possible key-regulatory elements. During the last years collections with non-coding genomic DNA-fragments with a length of around 2.5kb, cloned in front of the transcription factor Gal4, were established (Kvon et al., 2014; Pfeiffer et al., 2008). For the potential promoter region of *sidestep*, there are five different lines available from VDRC (Fig 2.7) (Kvon et al., 2014). The genomic fragments are named based on the VDRC stock number and the expression pattern of the fragments can be analysed by crossing to a UAS-line combined with a fluorescent protein. Three of the fragments (204347, 204220 and 213798) are localised in front of the start codon of *side*. One fragment (206961) ends 81bp after the ATG.

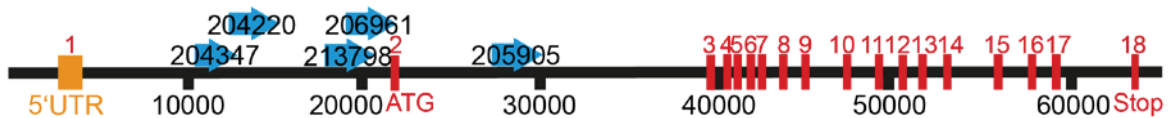


Fig 2. 7: Side promoter-fragment-Gal4-lines.

Blue arrows represent the position and length of the genomic fragments in relation to the *side* gene. Exons are marked in red. The genomic fragments are named based on the VDRC stock number and cover predominantly intronic regions.

The different lines were crossed to UAS-mCD8GFP and expression pattern of GFP driven by the particular promoter-fragment during the embryogenesis and in larval stages were analysed (Figs 2.8 and 2.9). It has to be considered that conditioned by the size of UAS-mCD8GFP protein like most, if not all, GFP-fusion proteins and the duration for the protein folding, a time displacement occurs resulting in a later detectable GFP-signal as the enhancer fragment is active.

Results

Line 204347-Gal4 drives GFP expression in early embryos probably in muscle precursor cells, since in late embryonic stages as well as in first and second instar larvae a green staining of the muscles is visible. In stage 16 embryos muscles 3, 4, 6, 7, 8, 11, 12, 13, 28, 16 and 17 are stained (Fig 2.8 B+B'). In L1 and L2 larvae muscles 21 to 24 and 18 in the lateral muscle field predominantly express GFP (Fig 2.8 C-D'). In L3 larvae, muscle specific expression of GFP is no longer detectable (Fig 2.8 E+E'). However, two ventral chordotonal organs per hemisegment express GFP (Fig 2.8 E+E' arrows).

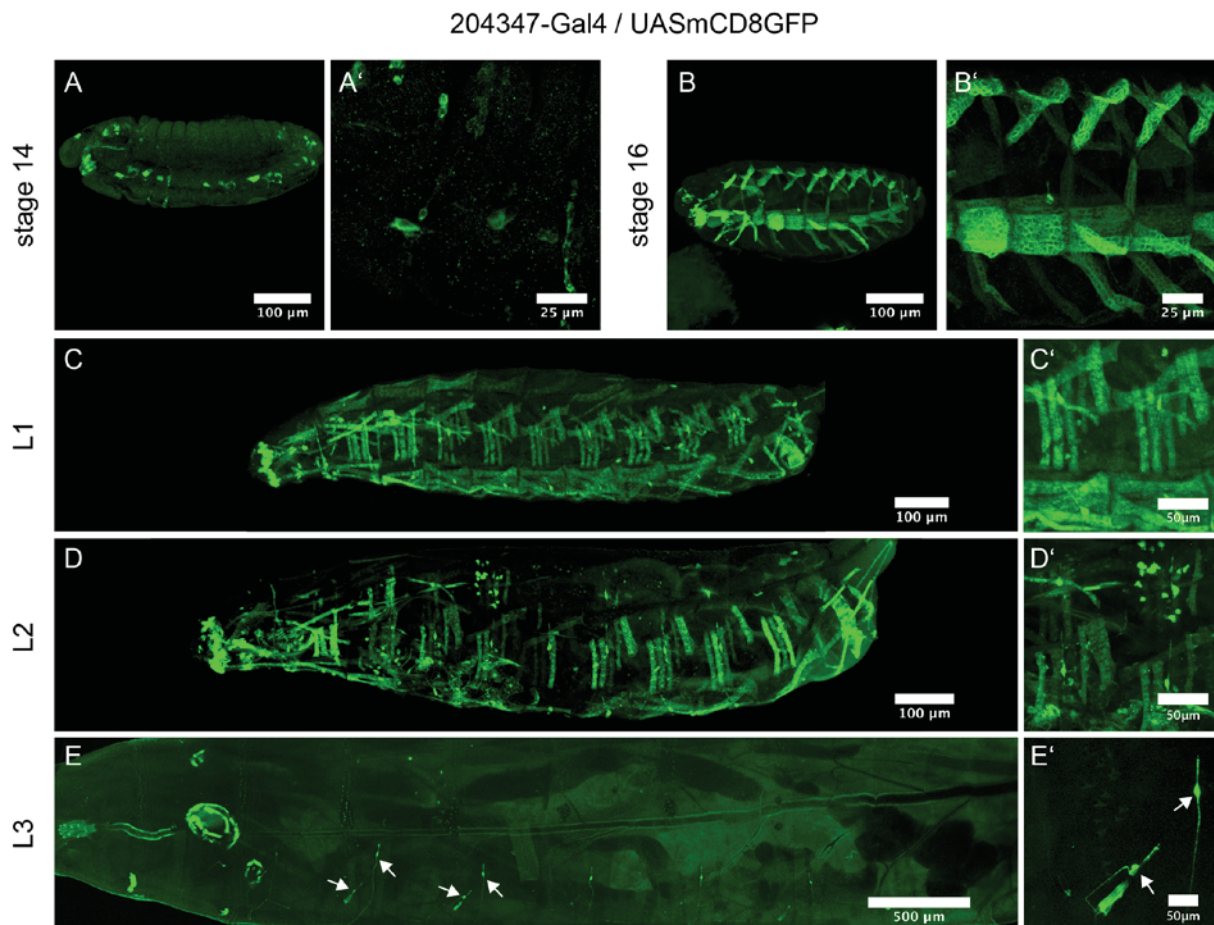


Fig 2. 8: GFP driven by 204347-Gal4 is expressed in muscles and chordotonal organs.

Anti-GFP stainings of 204347>mCD8GFP embryos and endogenous GFP expression in 204347>mCD8GFP whole mount larvae. A+A': GFP is expressed in muscle precursors in mid-stage embryos. B+B': At stage 16, muscle specific GFP expression is detectable. C-D': In first and second instar larvae 204347 activates GFP expression most prominent in muscles 21 to 24. E+E': In third instar larvae, GFP expression is visible in two chordotonal organs per hemisegment (arrows). A-E': Lateral view.

The enhancer fragment 206961 activates GFP expression during embryogenesis in sensory neurons based on localisation and morphology of GFP positive cells (Fig 2.9 A-B'). In first and second instar larvae, the CNS and various sensory neurons such

Results

as the dorsal bidendritic neuron, dorsal multidendritic neuron, lateral da neurons A and B and the ventral anterior da neuron express GFP (Fig 2.9 C-D'). Remarkably, in third instar larvae GFP expression is only visible in five unidentifiable cells (Fig 2.9 E+E').

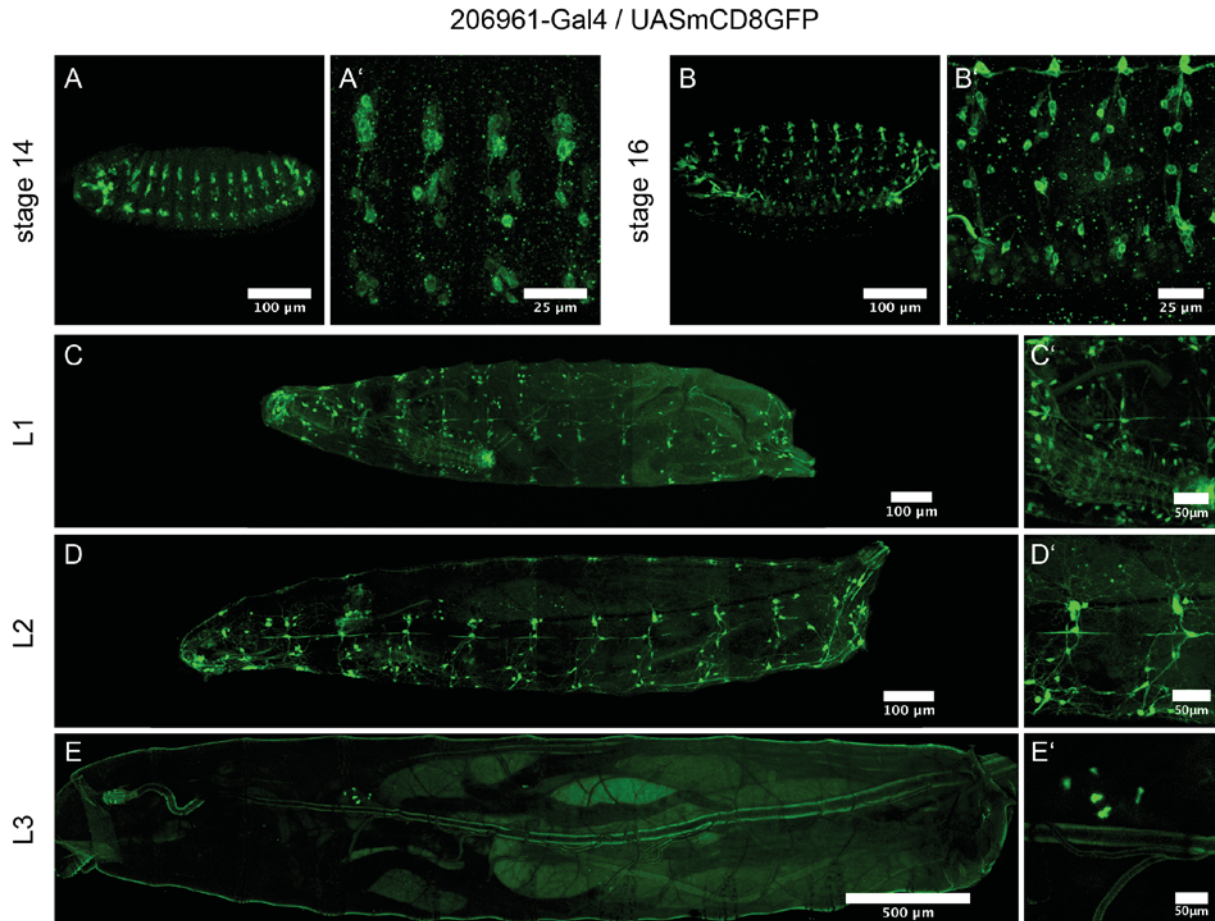


Fig 2. 9: 206961-Gal4 activates GFP expression in sensory neurons.

Confocal images of 206961>mCD8GFP embryos stained with anti-GFP and endogenous GFP expression in whole mount larvae. A-B': In mid-stage and late embryos GFP is expressed in sensory neurons. C-D': Sensory neuron specific GFP expression persists in first and second instar larvae. Further, GFP is visible in the CNS. E+E': In third instar larvae 206961-Gal4 drives GFP expression only in five unidentifiable cells. A-E': Lateral view.

The other three tested lines generate some sort of enhancer activity, but, in contrast to the fragments 204347 and 206961, GFP expression does not fit the expected Side expression (data not shown).

To confirm GFP expression activates by the lines 204347-Gal4 and 206961-Gal4 in sensory neurons and muscles, respectively, antibody co-staining's with markers for these cell types were carried out (Figs 2.10 and 2.11). For the promoter fragment 204347, co-stainings anti-MHC, present in all muscles, were performed (Bernstein et

Results

al., 1983). In stage 16 embryos, GFP overlaps with ventral muscles and lateral muscles (6, 7, 12, 13) clarified by co-staining with anti-MHC (Fig 2.10 A-C').

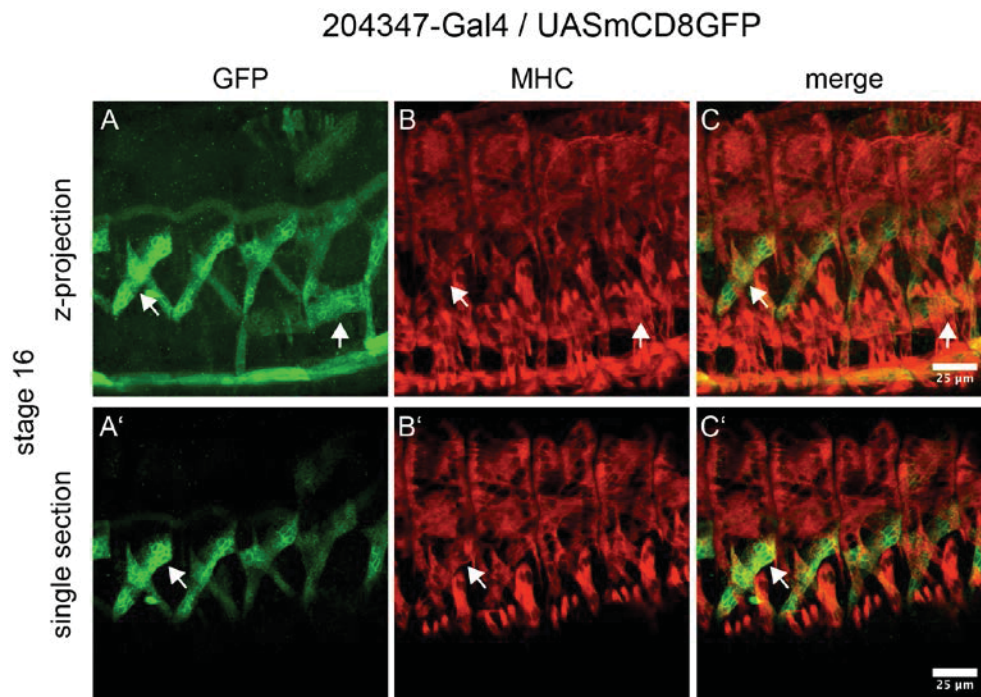


Fig 2. 10: 204347-Gal4 activates GFP expression in muscle cells.

Antibody co-stainings of 204347>mCD8GFP embryos with anti-GFP (green) and anti-MHC (red). A-C': In late embryos, GFP expression is localised in muscles (arrows) (lateral view). A-C: Maximum projection. A'-C': Single section.

To investigate if the promoter fragment *206961* drives GFP in sensory neurons three different co-stainings with the antibodies anti-Futsch, anti-Repo and anti-Side were performed. At stage 14, GFP co-localises almost completely with Futsch-positive cells in the CNS and the PNS as well (Fig 2.11 A-C). However, it is striking that the GFP-signal is limited to cell bodies in contrast to the Futsch-signal, which is also detectable in the axons. In stage 16 embryos, the overlap between both signals is still prominent and GFP expression is predominantly confined to cell bodies (Fig 2.11 D-F). In addition, GFP overlaps with a subset of glia cells marked by anti-Repo in the CNS as well as in the PNS (Fig 2.11 G-I), but in a much lesser intensity in comparison to the strong localisation of GFP in sensory neurons.

If the genomic fragment *206961* includes the promoter of *sidestep* it should be expressed in a similar subset of cells. A possibility to proof that is a co-staining with anti-Side antibody. Endogenous Side protein and GFP driven by the promoter fragment are localised in the same cells in CNS and particular in the PNS (arrows Fig

Results

2.11 J-O). Signals do not overlap completely, but this can be explained might with the fact that the mCD8GFP protein leads to a temporal shift of the signal.

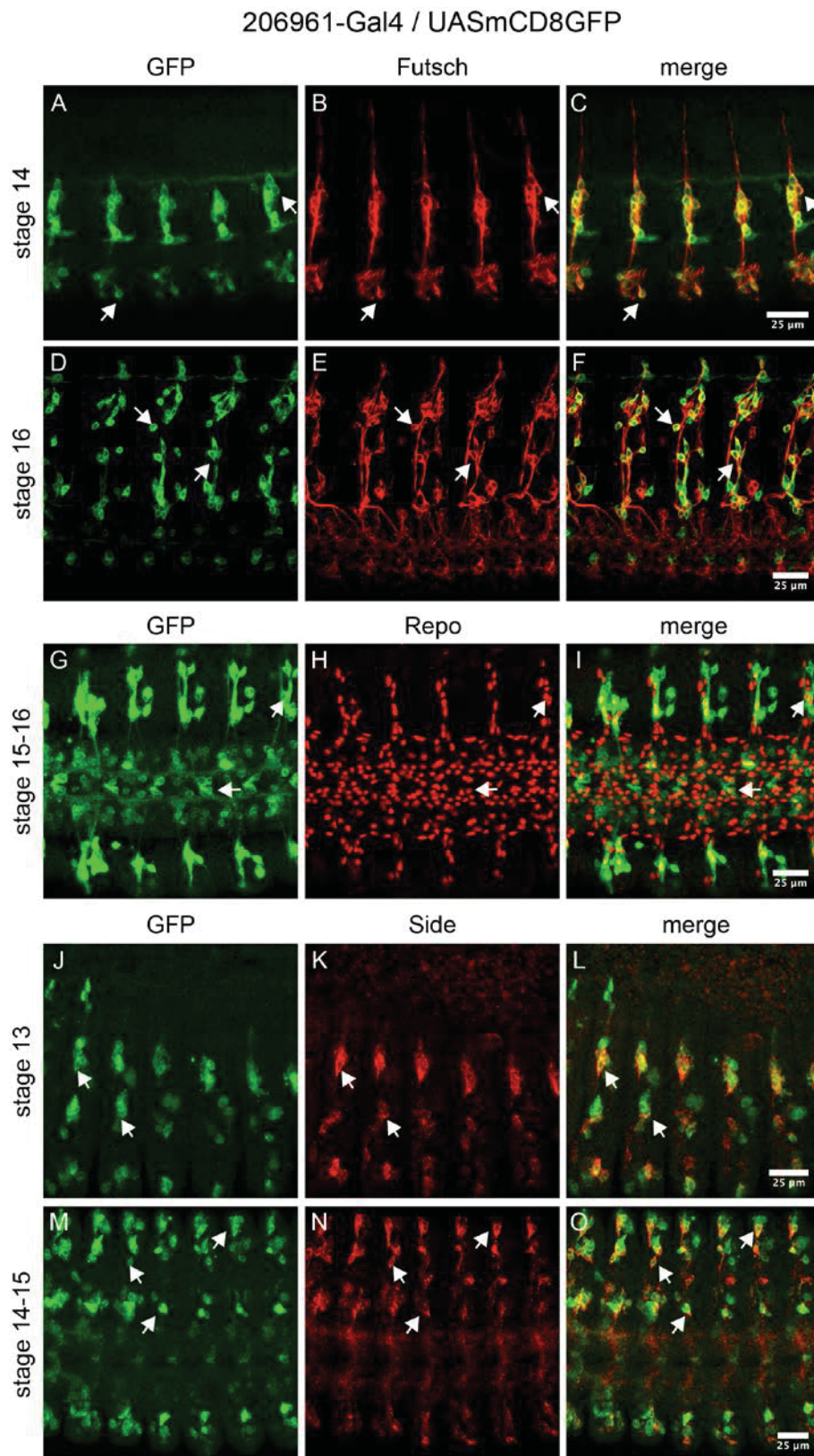


Fig 2. 11: UAS-mCD8GFP expression driven by 206961-Gal4 is localised in Side-positive cells. Confocal images of 206961>embryos stained with anti-GFP (green) and anti-Futsch (red, A-F) or anti-Repo (red, G-I) or anti-Side (red, J-O). A-F: GFP is expressed in the PNS in sensory neurons (arrows)

Results

(lateral view). G-I: In late embryos, glia cells of the CNS and PNS are positive for GFP (arrows) (ventral view). J-O: In the PNS of mid-stage embryos, 206961-Gal4 activates GFP expression in Side-expressing cells (arrows) (J-L: lateral view, M-O: ventro-lateral view).

In summary, the enhancer fragment *206961* drives expression in sensory neurons and Side expressing cells and the line 204347-Gal4 activates expression in muscles. Thus, the fragment *206961* displays Side expression in mid-stage embryos (stage 12-14), while the fragment *204347* represents Side expression in late embryos (stage 15-17).

To test if both lines are functional in *side* expressing cells and thus are able to rescue the *sidestep* phenotype, rescue experiments with wild-type *side* cDNA cloned beyond a UAS (UAS-Side46;+;+ and w;+;UAS-Side29A (Sink et al., 2001)) were performed. Using the line 204347-Gal4 for the rescue experiment, the strong mis-innervation of the ventral muscle field typical for *side* mutant larvae in contrast to wild-type is no longer detectable (arrows Fig 2.12 A'-C'), but the larvae exhibit missing NMJs in the dorsal muscle field in comparison to the wild-type (arrows Fig 2.12 A+C). Larvae with *side* cDNA driven by 206961-Gal4 show an opposite result. Mis-innervation of ventral muscle field compared to wild-type is still present (arrows Fig 2.12 A'+D'), but the dorsal muscle field show wild-type innervation (arrows Fig 2.12 A+D). A combined expression of both enhancer fragments leads to an almost complete rescue of the *side* phenotype (arrows Fig 2.12 E+E'). However, some innervation defects in all muscle fields are still visible.

Results

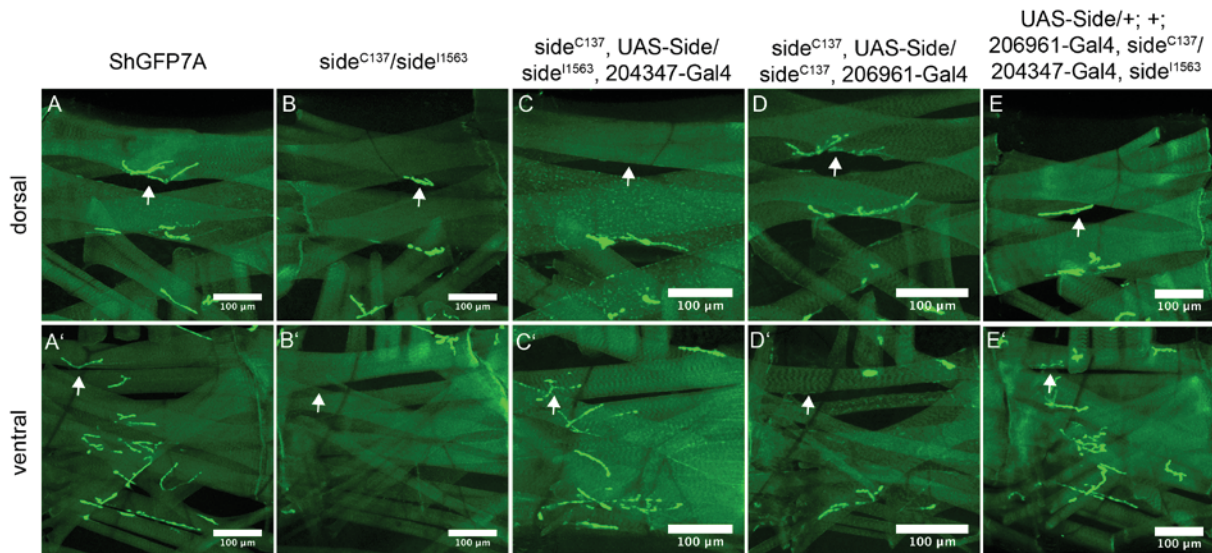


Fig 2. 12: *Sidestep* phenotype can be rescued partially.

Dorsal and ventral muscle fields of wild-type larvae, *side* mutant larvae and larvae driving a *side* cDNA using the enhancer fragment driver lines 204347-Gal4 and 206961-Gal4 in a *side* mutant background. A+A': Innervation pattern of wild-type larvae. B+B': Compared to wild-type, *side* mutant larvae show strong mis-innervation in the ventral and dorsal muscle fields (arrows). C+C': Line 204347-Gal4 rescues the ventral phenotype, but show dorsal innervation defects in comparison to the wild-type (arrows). D+D': Rescue experiments with the enhancer fragment 206961 show no rescue of ventral muscle innervation (arrow D'). E+E': Combination of both promoter lines rescues best the phenotype (arrows).

2.1.1.3 Promoter fragments of *sidestep* exhibit various conserved regions

The analysed genomic fragments exhibit, with a length of around 2.5kb, large sizes for a promoter. To potentially narrow down the active sequence of promoter lines, an analysis for conserved regions in all *Drosophila* species was carried out. Species are listed based on their phylogenetical relationship to *Drosophila melanogaster*. Thereby, species closely related to *Drosophila melanogaster* exhibit bigger conserved regions in comparison to the more distant species. Nevertheless, in eleven different species the promoter fragment of the muscle specific line 204347-Gal4 has three conserved regions with 43, 51 and 53 nucleotides (Fig 2.13). They are localised close to each other on the 3'-end of the enhancer fragment (Fig 2.14).

Results

```

D.melanogaster  TTATTATGCAAATTAATTATTGTGTGAATGAAATGTAAATTTTAAATTGATTT
D.simulans      TTATTATGCAAATTAATTATTGTGTGAATGAAATGTAAATTTTATTGATTT
D.sechellia     TTATTATGCAAATTAATTATCGTGTGAATGAAATGTAAATTTTAAATTGATTT
D.yakuba        TTATTATGCAAATTAATTATTGTGTGAATGAAATGTAAATTTTAAATTGATTT
D.erecta        TTATTATGCAAATTAATTATTGTGTGAATGAAATGTAAATTTTAAATTGATTT
D.ananassae     TTATTATGCAAATTAATTATTGTGTGAATGAAATGTAAATTTTAAATTGATTT
D.pseudoobscura TTATTATGCAAATTAATTATTGTGTGAATGAAATGTAAATTTTAAATTGATTT
D.persimilis    TTATTATGCAAATTAATTATTGTGTGAATGAAATGTAAATTTTAAATTGATTT
D.wilistoni     -TATTACGCAAATTAATTCATTGTGTGAATGAAATGTAAATTTTAAATTGATTT
D.mojavensis   --ATTATGCAAATTAATTATTGTGTGAATGAAATGTAAATTTTAAATTGATTT
D.virilllis     --ATTATGCAAATAAATTATTGTGTGAATGAAATGTAAATTTTAAATTGATTT
D.grimshawi     ---TTATGTAAATTAATTATTGTGCGAATGAAATGTAAATTTTAAATTGATTT
                *** * **** * * * * * **** * * * * *

```



```

D.melanogaster  CTGCACC-GAAACTGTTGACATTCACGCACAAATGGATTTACTAACGAGTTG
D.simulans      CTGCACC-GAAACTGTTGACATTCACGCACAAATGGATTTACTAACGAGTTG
D.sechellia     CTGCACC-GAAACTGTTGACATTCACGCACAAATGGATTTACTAACGAGTTG
D.yakuba        CTGCACC-GAAACTGTTGACATTCACGCACAAATGGATTTACTAACGAGTTG
D.erecta        CTGCACC-GAAACTGTTGACATTCACGCACAAATGGATTTACTAACGAGTTG
D.ananassae     CTGCACC-GAAACTGTTGACATTCACGCACAAATGGATTTACTAACGAGTTG
D.pseudoobscura CTGCACC-GAAACTGTTGACATTCACGCACAAATGGATTTACTAACGAGTTG
D.persimilis    CTGCACC-GAAACTGTTGACATTCACGCACAAATGGATTTACTAACGAGTTG
D.wilistoni     CTGCACC-GAAACTGTTGACATTCACGCACAAATGGATTTACTAACGAGTTG
D.mojavensis   CTGCACC-GAAACTGTTGACATTCACGCACAAATGGATTTACTAACGAGTTG
D.virilllis     CTGCACC-GAAACTGTTGACATTCACGCACAAATGGATTTACTAACGAGTTG
D.grimshawi     CTGCACC-GAAACTGTTGACATTCACGCACAAATGGATTTACTAACGAGTTG
                ***** * **** * * * * * ***** * * * * *

```



```

D.melanogaster  TTTTCGCGCCTGTTATTTATGGCTTCGATTATCCCGGCACACAATGGGCCAACA
D.simulans      TTTTCGCGCCTGTTATTTATGGCTTCGATTATCCCGGCACACAATGGGCCAACA
D.sechellia     TTTTCGCGCCTGTTATTTATGGCTTCGATTATCCCGGCACACAATGGGCCAACA
D.yakuba        TTTTCGCGCCTGTTATTTATGGCTTCGATTATCCCGGCACACAATGGGCCAACA
D.erecta        TTTTCGCGCCTGTTATTTATGGCTTCGATTATCCCGGCACACAATGGGCCAACA
D.ananassae     TTTTCGCGCCTGTTATTTATGGCTTCGATTATCCCGGCACACAATGGGCTAACA
D.pseudoobscura TTTTCGCGCCTGTTATTTATGGCTTCGATTATCCCGGCACACAATGG-CCAACA
D.persimilis    TTTTCGCGCCTGTTATTTATGGCTTCGATTATCCCGGCACACAATGG-CCAACA
D.wilistoni     -TTTCGCGCCTGTTATTTATGGCTTCGATTATCCCT--CACACAATGG-CCAACA
D.mojavensis   -TTTCGCGCCTGTTATTTATGGCTTCGATTATCCCT--ACACAATGGGCC----
D.virilllis     -TTTCGCGCCTGTTATTTATGGCTTCGATTATCCCTG---GCAATAA---AACA
D.grimshawi     -TTTCGCGCCTGTTATTTATGGCTTCGATTATCCCTG---ACACAATGGGCC----
                ***** * **** * * * * * ***** * * * * *

```

Fig 2. 13: The promoter fragment 204347 exhibits three conserved regions.

3 different regions of the enhancer fragment 204347 are highly conserved in 11 other members of the clade of *Drosophilidae*. Two of these regions have predicted binding sites for the Hox genes *antennapedia* and *ultrabithorax* (frames).

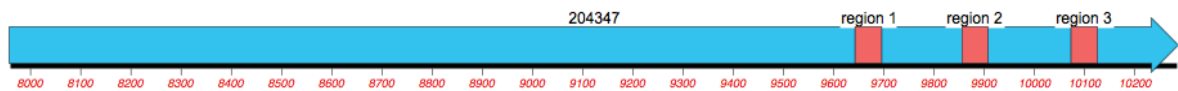


Fig 2. 14: Position of the conserved regions within the promoter fragment 204347.

All three conserved regions are localised close to each other on the 3'-end of the fragment.

The sensory neuron specific enhancer fragment 206961 exhibits four conserved regions in 10 members of the clade *Drosophilidae* with a length between 24 and 36 nucleotides shown in figure 2.15. The localisation of these four regions is distributed over the complete length of the promoter fragment (Fig 2.16).

Results

```

D.melanogaster  GCTTGTGCGAAATTTACTAATGAGSCAAAGTTTGACTGTCAATAGCCTCAGTTCTCACCCC
D.simulans      GCTTGTGCGAAATTTACTAATGAGSCAAAGTTTGACTGTCAATAGCCTCAGTTCTCACCCC
D.sechellia     GCTTGTGCGAAATTTACTAATGAGSCAAAGTTTGACTGTCAATAGCCTCAGTTCTCACCCC
D.yakuba        GCTTGTGCGAAATTTACTAATGAGSCAAAGTTTGACTGTCAATAGCCTCAGTTCTCACCCC
D.erecta        GCTTGTGCGAAATTTACTAATGAGSCAAAGTTTGACTGTCAATAGCCTCAGTTCTCACCCC-
D.ananassae     -CTTGTCTGAAATTTACTAATGAGSCAAAGTTTGACTGTCAATAGCC-----
D.pseudoobscura GCTTGTCTGAAATTTACTAATGAGSCAAAGTTTGACTGGCAATAGCC-----
D.persimilis    GCTTGTCTGAAATTTACTAATGAGSCAAAGTTTGACTGGCAATAGCC-----
D.wilistoni     -----GAAATTTACTAATGAGSCAAAGTTTGACT-----
D.virilllis     -GCTAACTGAAATTTACTAATGAGSCAAAGTT-----
D.grimshawi     -----GAAATTTACTAATGAGSCAAAGTT-----
                *****
                *****
                *****
                *****

D.melanogaster  ATCTCGCATTGAAACGCGCCATTAAATCACACTTTCATCGATGCGCTGGCC---ACATAAAA
D.simulans      ATCTCACATTGAAACGCGCCATTAAATCACACTTTCATCGATGCGCTGGCC---ACATAAAA
D.sechellia     ATCTCACATTGAAACGCGCCATTAAATCACACTTTCATCGATGCGCTGGCC---ACATAAAA
D.yakuba        ATCTCACATTGAAACGCGCCATTAAATCACACTTTCATCGATGCGCTGGCC---ACATAAAA
D.erecta        ATCTCACATTGAAACGCGCCATTAAATCACACTTTCATCGATGCGCTGGCC---ACATAAAA
D.ananassae     GTCTCACATTGAAACGCGCCATTAAATCACACTTTCATCGATGCGCTGGCC---ACATAAAA
D.pseudoobscura GTCGCCCTCGAAACGCGCCATTAAATCACACTTTCATCGATGCGCTGGCC---ACATAAAA
D.persimilis    GTCGCCCTCGAAACGCGCCATTAAATCACACTTTCATCGATGCGCTGGCC---ACATAAAA
D.wilistoni     GTCTCACATTGAAACGCGCCATTAAATCACACTTTCATCGATGCGCTGGCC---ACATAAAA
D.virilllis     -----CATTGAAATGCGCCATTAAATCACACTTTCATCGATGCGCTGGCC---ACATAAAA
D.grimshawi     GACTCACATTGAAATGCGCCATTAAATCACACTTTCATCGATGC-----
                * * * * *
                *****
                *****
                *****

D.melanogaster  AAAAAAAAAACGAAAGGAATGTCCATAAAAAGGGCGAATAAACATGTAAAAGCACATTAAG
D.simulans      AAAAAA---GAAAGGAATGTCCATAAAAAGGGCGAATAAACATGTAAAAGCACATTAAG
D.sechellia     AAAAAA---GAAAGGAATGTCCATAAAAAGGGCGAATAAACATGTAAAAGCACATTAAG
D.yakuba        CAAAAAATACGGAACGGAATGTCCATAAAAAGGGCGAATGAACATGTAAAAGCACATTAAG
D.erecta        AAGGAAAG---GAATG---TCCATAAAAAGGGCGAATGAACATGTAAAAGCACATTAAG
D.ananassae     -----CCATAAAAAGTGCAAAATAAACATGTAAAAGCACATTAAG
D.pseudoobscura -----AATAAACATGTAAAAGCACATTAAG
D.persimilis    -----AATAAACATGTAAAAGCACATTAAG
D.wilistoni     AAAAAAAAAACGAAAG-----AAAAGTGCAAAATAAACATGTAAAAGCACATTAAG
D.virilllis     -----TAAAAGTGCAAAATAAACATGTAAAAGCACATTAAG
D.grimshawi     -----CATAAAAAGTGCAAAATAAACATGTAAAAGCACATTAAG
                * * * * *
                *****
                *****
                *****

```

Fig 2. 15: The enhancer fragment 206961 exhibits four short conserved regions.

The conserved regions have only a length of 24 to 36 nucleotides and three of them exhibit predicted binding sites for the Hox genes *antennapedia* and *ultrabithorax* (frames).

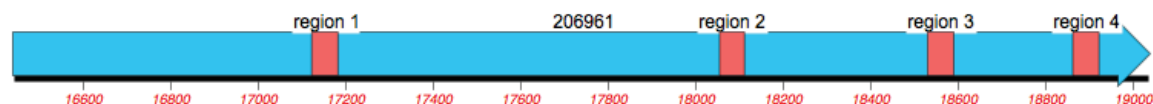


Fig 2. 16: Position of the conserved regions of line 206961.

The promoter fragment 206961 has four conserved regions distributed over the complete fragment.

The conserved regions of both promoter fragments were analysed using the website algen.lsi.upc.es to get information about potential transcription factor binding sites. The results are summarized in table 2.3. Interestingly, 3 conserved regions of enhancer fragment 206961 and 2 conserved regions of promoter fragment 204347 show predicted transcriptional binding sites for Ultrabithorax (*ubx*) and Antennapedia

Results

(Antp). These binding sites are also conserved in other *Drosophila* species (frames Figs 2.13 and 2.15).

Tab 2. 2: Predicted transcription factor binding sites of the conserved enhancer fragments.

| enhancer fragment | conserved region | binding site for: |
|-------------------|------------------|---|
| 204347 | 1 | •Ultrabithorax • BR-C Z2 •Tll •Antennapedia •Prd •dri •Zen-1 •Zen-2 •Eve •Ftz •En •Croc |
| | 2 | •E2F •BR-CZ2 |
| | 3 | •E2F •Ultrabithorax •BR-C Z2 •Tll •Antennapedia •Prd •Croc |
| 206961 | 1 | •E74A •BR-C Z2 •Tll •Antennapedia •Prd •Ultrabithorax |
| | 2 | •Ultrabithorax •Tll •Ftz •Antennapedia •BR-C Z2 •Prd •Dri •Glia cell missing |
| | 3 | •BR-C Z2 •Croc •Ultrabithorax •Tll •Antennapedia •Prd |
| | 4 | •BR-C Z2 • Ttk 69K |

2.1.1.4 Regulation of *side* expression by transcription factors

An important step for the understanding how the dynamic expression of *side* is regulated is the identification of the transcription factor(s) of *side*. Possibly, the dynamic expression of *side* is regulated in each *side*-expressing tissue by a different regulatory element.

2.1.1.4.1 Binding sites of promoter fragments

The two identified transcription factors, using binding site analyses of the conserved regions of the promoter fragments, Antennapedia (Antp) and Ultrabithorax (Ubx) belong to the Hox gene family, which are expressed along the anterior-posterior axis of *Drosophila* and are responsible for the segmentation of the embryo as well as of the adult fly (Hughes and Kaufman, 2002). *Antp* and *ubx* are expressed in thoracic segments. Since Side is expressed in all segments of an embryo, additional the transcription factors encoded by the Hox genes *abdominal A* and *B* were analysed, which are expressed in the abdomen of *Drosophila* embryos and adult flies (Hughes and Kaufman, 2002). Homozygous mutant embryos of each Hox gene were stained with anti-Side and the expression pattern of Side was compared to that in wild-type.

Results

Loss of one of these four Hox genes does not lead to a lack or strongly increase of Side expression in sensory neurons in stage 14 embryos (Fig 2.17). Remarkably, in homozygous embryos of *antennapedia* Side expression is altered compared to wild-type (Fig 2.17 B).

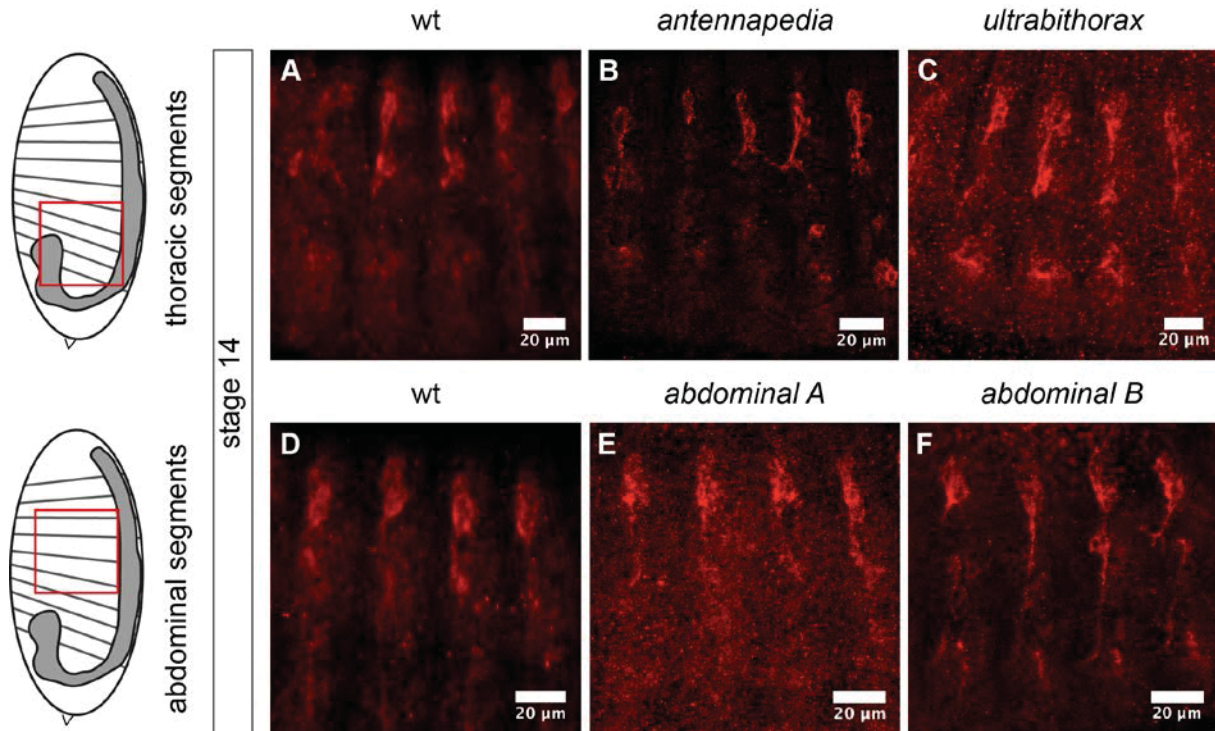


Fig 2. 17: Side expression is altered in *antennapedia* mutant embryos.

Anti-Side antibody stainings of wild-type and *antennapedia*, *ultrabithorax*, *abdominal A* and *abdominal B* mutant embryos. A: Side expression in thoracic segments of a wild-type embryo. B: In *antennapedia* mutant embryos Side expression is altered compared to wild-type. C: Thoracic segments of *ultrabithorax* mutant embryos show no difference. D: Side expression in abdominal segments of a wild-type embryo. E+F: In *abdominal A* and *B* mutant embryos Side is expressed in a wild-type pattern. A-F: Lateral view.

To examine if the loss of *antp* alters the expression of Side or influence the morphology of sensory neurons and therefore alters only passive the Side expression, *antp* loss of function embryos were stained against Futsch. Lack of *antp* causes morphology defects of sensory neurons based on an altered Futsch expression (arrows Fig 2.18 A+B). Therefore, the altered Side expression in *antp* loss of function embryos probably is based on the observed altered sensory neuron morphology.

Results

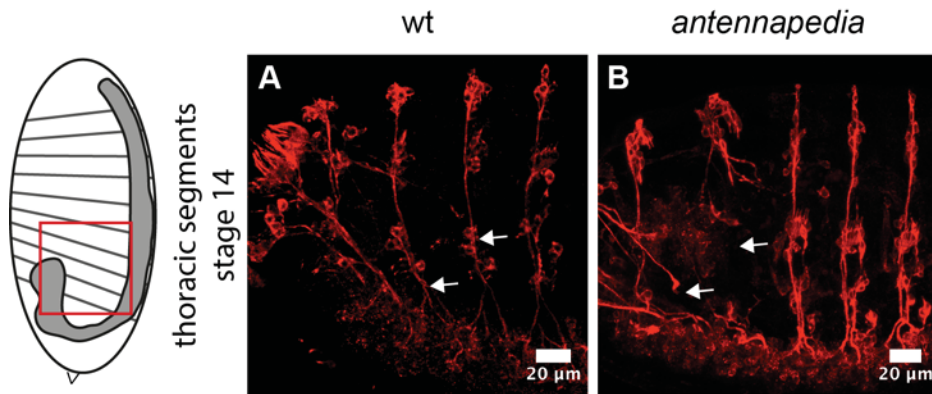


Fig 2. 18: Morphology of sensory neurons is altered in *antennapedia* mutant embryos.

Confocal images of anti-Futsch antibody stainings of wild-type and *antennapedia* mutant embryos. A: Sensory neurons of thoracic segments of a wild-type embryo. B: *Antennapedia* mutant embryos show an altered morphology of sensory neurons in thoracic segments compared to wild-type (arrows). A+B: Lateral view.

2.1.1.4.2 Notch regulates Side expression in sensory neurons

Since the analysis of transcription factors with predicted binding sites in the conserved regions of the enhancer fragments does not lead to the identification of the transcription factor of *side*, loss of function mutants of transcription factors or differentiation factors with known functions in the development of nervous system or axon guidance and/or known expression in one of the *side*-expressing tissue were ordered from different *Drosophila* stock centres. The selected factors are listed in table 2.3. For further information about the analysed alleles or stock numbers see chapter Material and Methods table 4.9. To test if Side expression is lacking or down-regulated in these fly-lines, again antibody stainings using anti-Side antibody of homozygous loss of function embryos were performed.

Homozygous mutant embryos of the transcription factors Hucklebein, Klumpfuss, Lola, Prospero and Sox neuro were analysed to test if the early expression of Side in the CNS is altered. In wild-type, Side is expressed at stage 10 in cellpairs near the midline and shows in stage 12 embryos a belt-like expression pattern (Fig 2.19 A+A'). In all tested homozygous mutant embryos Side expression is still present and not altered compared to wild-type (Fig 2.19).

Results

Tab 2. 3: Selected transcription and differentiation factors

| Transcription factor | Expression tissue | Process and reference | Reference |
|-----------------------------|--------------------------|--|---|
| Apontic | motor axons | synaptic transmission | Takasu-Ishikawa et al., 2001 |
| Cut | sensory neurons | external sensory identity, dendrite morphology of multidendritic neurons | Blochlinger et al., 1988; Bodmer et al., 1987; Grueber et al., 2003 |
| Deadpan | CNS, sensory neurons | dendrite morphology of multi-dendritic neurons | Bier et al., 1992; Parrish et al., 2006 |
| Grain | motoneurons | motor axon guidance | Garces and Thor, 2006 |
| Hb9 | motoneurons | motor axon guidance | Odden et al., 2002 |
| Huckebein | CNS | cell specification, regulation of <i>eve</i> | Bossing et al., 1996; Chu-LaGraff et al., 1995 |
| Klumpfuss | CNS | cell specification, regulation of <i>eve</i> | Klein and Campos-Ortega, 1997; Yang et al., 1997 |
| Knot/collier | sensory neurons | dendrite morphology | Crozatier and Vincent, 2008 |
| Lim3 | motoneurons | motor axon guidance | Thor et al., 1999 |
| Lola | CNS | axon growth and guidance, muscle innervation | Giniger et al., 1994; Madden et al., 1999; Seeger et al., 1993 |
| Notch | CNS | lateral inhibition | Goodman and Doe, 1993 |
| Prospero | CNS, Glia | axon growth and guidance | Doe et al., 1991 |
| Senseless | sensory neurons | sensory organ development | Nolo et al., 2000 |
| Sox neuro | CNS | axon growth and guidance | Buescher et al., 2002; Crémazy et al., 2000; Seeger et al., 1993 |
| Squeeze | CNS | dendrite morphology of multi-dendritic neurons | Allan et al., 2003; Parrish et al., 2006 |
| Zinc finger homeodomain 1 | motoneurons, muscles | motor axon guidance | Layden et al., 2006 |

Results

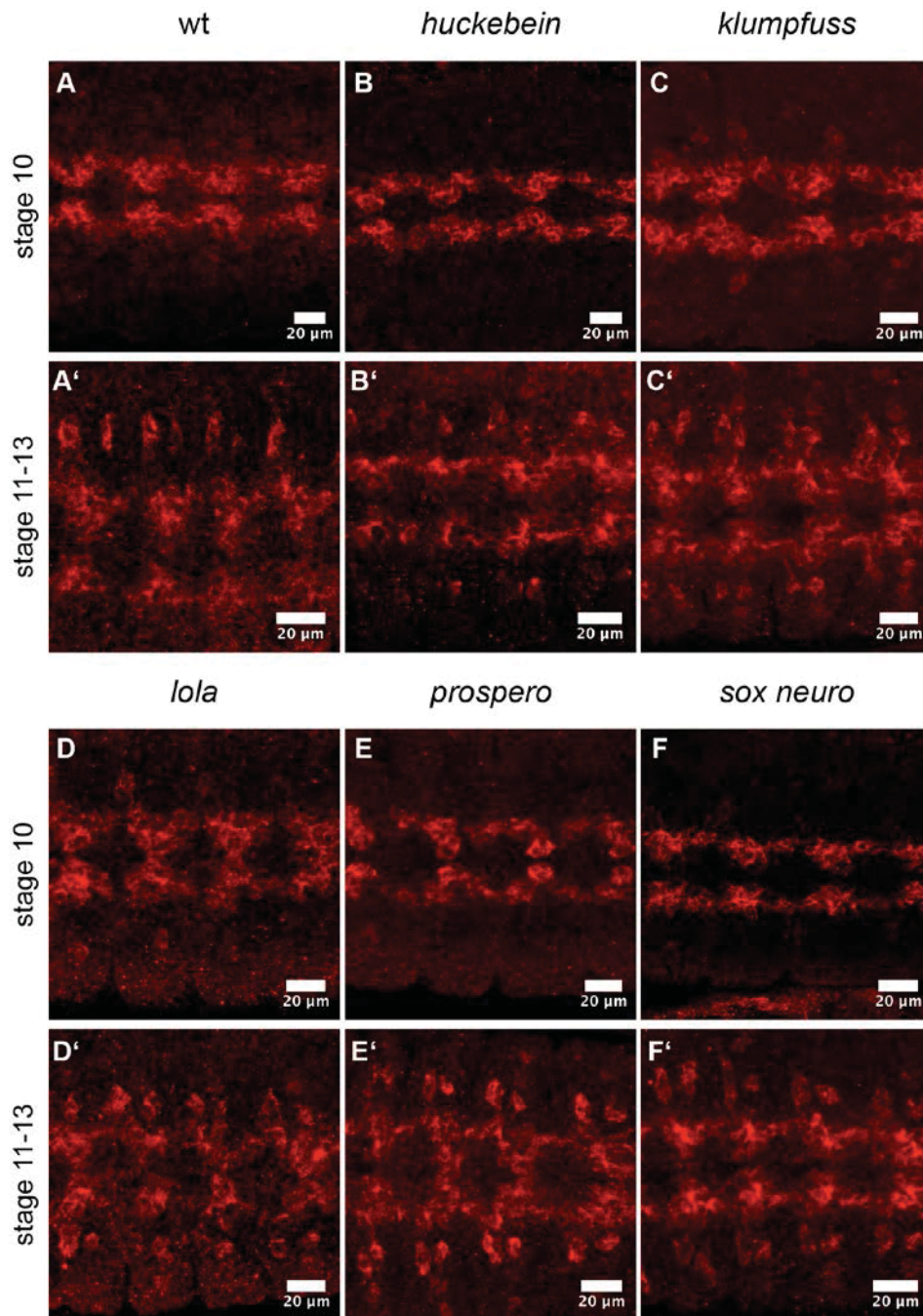


Fig 2. 19: Side expression is not altered in *huckebein*, *klumpfuss*, *lola*, *prospero* and *sox neuro* mutant embryos.

Confocal images of anti-Side antibody stainings of stage 10 and 12 old wild-type and mutant embryos. A+A': Side expression in wild-type. B-F': In all tested mutant embryos (mutant as depicted) Side expression show no difference in comparison to wild-type. A-F': Lateral view.

To determine, which transcription factor regulates Side expression in sensory neurons in mid-stage embryos (stage 14), homozygous mutant embryos of the transcription factors Apontic, Cut, Deadpan, Grain, Hb9, Knot, Lim3, Notch, Senseless, Squeeze and Zinc finger homeodomain-1 as well of the wild-type were stained with anti-Side. Again, none of the tested factors show a lack or down-regulation of Side expression compared to wild-type (Fig 2.20). Notably, in *notch*

Results

mutant embryos a strong overexpression of Side in comparison to wild-type is visible (Fig 2.20 I). In addition, in *senseless* homozygous embryos expression of Side is altered compared to wild-type (Fig 2.20 J).

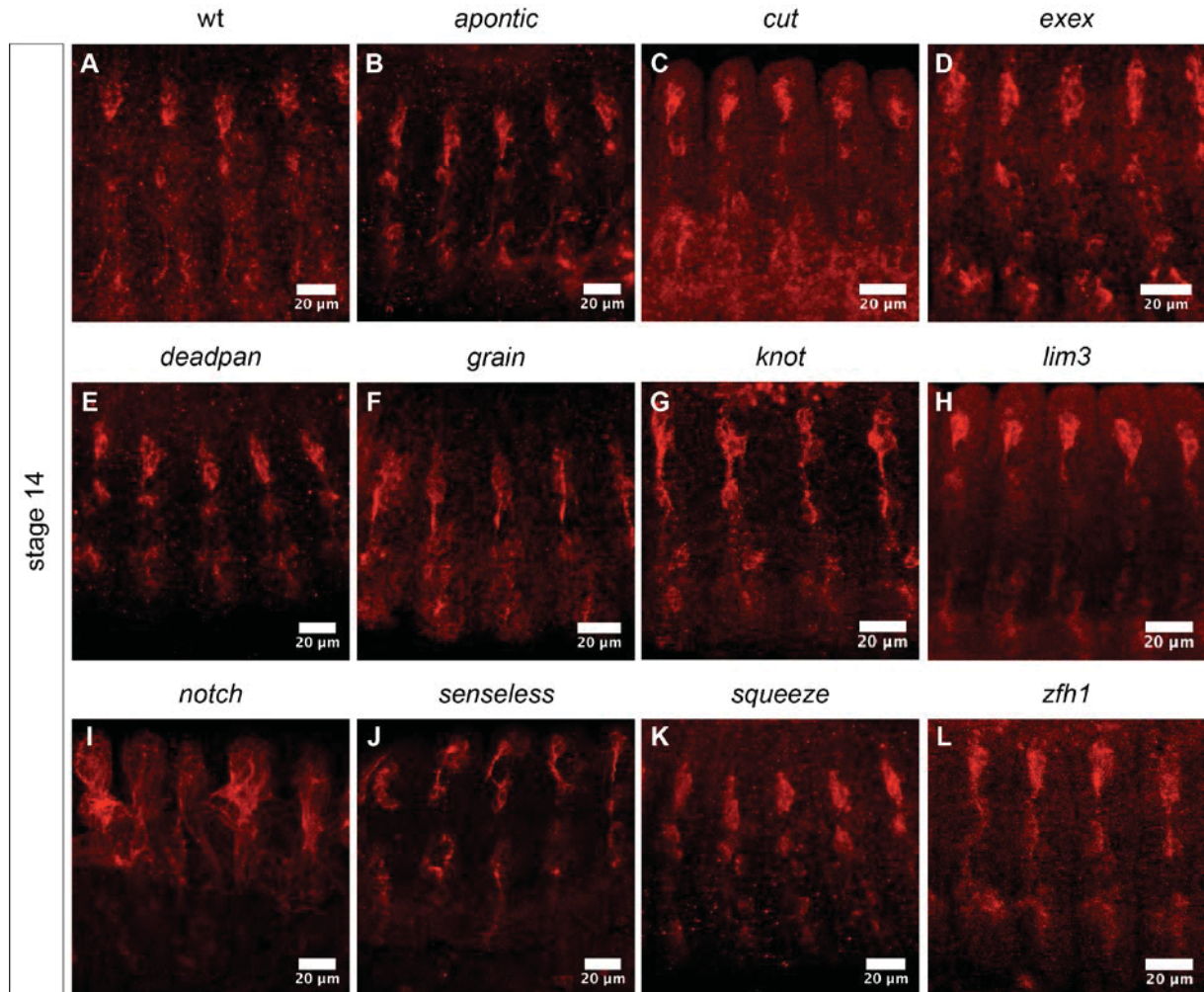


Fig 2. 20: Side expression is increased in *notch* mutant embryos.

Stage 14 embryos of wild-type and *apontic*, *cut*, *exex*, *deadpan*, *grain*, *knot*, *lim3*, *notch*, *senseless*, *squeeze* and *zinc finger homeodomain 1 (zfh 1)* mutant embryos stained with anti-Side. A: Side expression of wild-type embryo. I: Loss of *notch* leads to an increased Side expression. J: In *senseless* mutant embryos Side expression is altered compared to wild-type. B-H, K+L: All other tested mutants do not display obvious alterations in comparison to wild-type. A-L: Lateral view.

Based on these observations, *notch* and *senseless* mutant embryos were used for a more detailed analyses. First, it was tested if other stages of *notch* loss of function embryos also show an up-regulation of Side expression. Lack of *notch* causes a strong overexpression of Side in early (stage 10) and mid-stage (12 to 14) embryos. Interestingly, in late stages (17) Side expression is down-regulated in the PNS in *notch* mutant embryos similar to the wild-type (Fig 2.21 D+H). Additionally, no overexpression of Side in muscles in late embryos can be detected (Fig 2.21 H).

Results

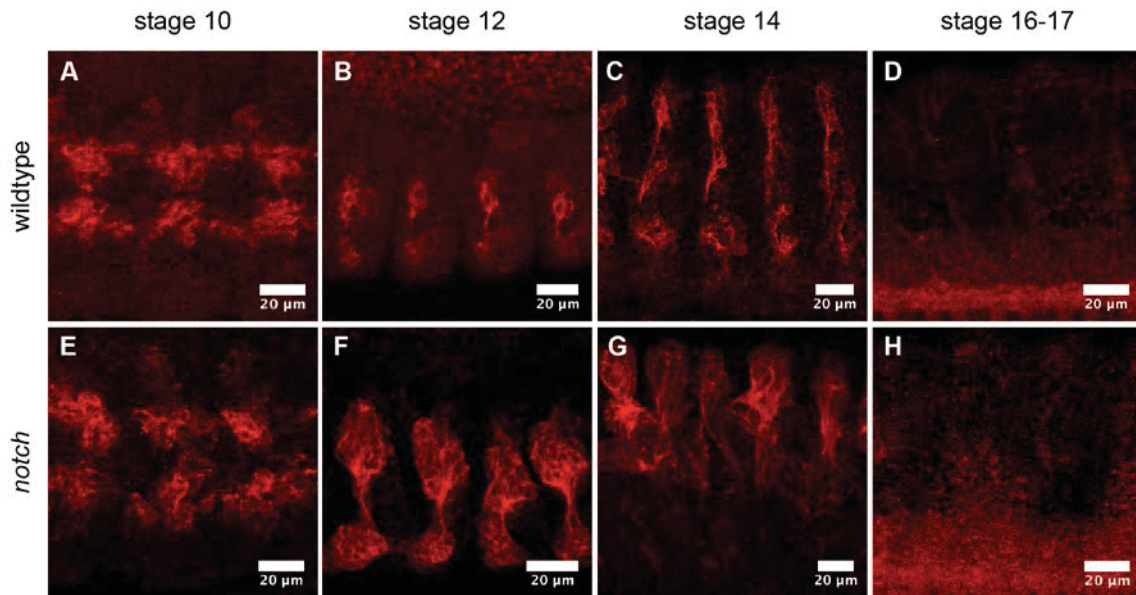


Fig 2. 21: Increased Side expression in *notch* mutant embryos is detectable from stage 10 to stage 14.

Anti-Side antibody staining of wild-type and *notch* loss of function embryos. A-D: Side expression in wild-type during embryogenesis. E-H: *Notch* mutant embryos. E-G: Side expression is increased in the CNS of early embryos as well as in the PNS of mid-stage embryos compared to wild-type. H: Late loss of function embryos show no difference to wild-type embryos. A+E: Ventral view. B-D, F-H: Lateral view.

To quantify the upregulation of Side in *notch* loss of function embryos, western blot analysis was carried out. Therefore, embryos were separated by age and thus, two lysates from wild-type and two lysates from *notch* mutant embryos were produced. The first one contains the lysate of early embryos up to stage 14 and the second one the lysate from old embryos between stages 15 to 17. As housekeeping gene serves α -tubulin.

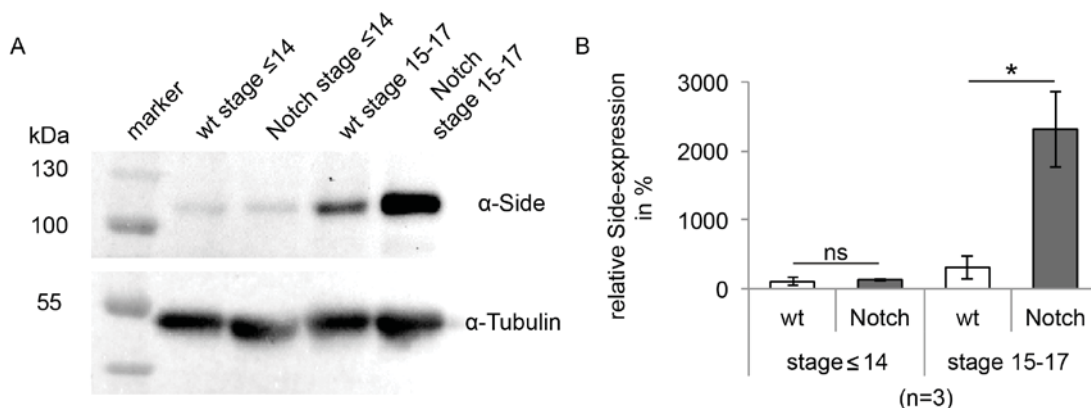


Fig 2. 22: Side expression is upregulated in late stage *notch* loss of function embryos.

Western blot analysis of wild-type (wt) and *notch* mutant embryos using lysates from embryos at indicated stages. A: Western blot. B: Statistical analysis. Amount of Side expression in wild-type embryos up to stage 14 were set on 100%. A+B: Early and mid-stage mutant embryos show no significant difference of relative Side expression in comparison to wild-type embryos (p -value = 0.41 using students T-test), but in late stage (15-17) mutant embryos Side expression is increased compared to wild-type (p -value = 0.02).

Results

Western blot analysis shows an opposite result as the antibody staining. In early embryos, Side protein is expressed in the same amount in wild-type (Fig 2.22 A lane 2) and *notch* mutant embryos (Fig 2.22 A lane 3). In contrast, lack of *notch* leads to a strong increase of relative Side expression in late embryos (stage 15-17) (Fig 2.22 A lane 5) compared to wild-type (Fig 2.22 A lane 4).

To address the question how the opposite results came about using western blot analysis and antibody stainings, *in situ* hybridisation using a *side* specific probe were performed. Similar to antibody staining, *notch* mutant embryos up to stage 14 show an increase of *side* mRNA expression in comparison to wild-type embryos (Fig 2.23). In late embryos, stage 17, no *side* mRNA is detectable in both *notch* loss of function and wild-type embryos (Fig 2.23 D+H).

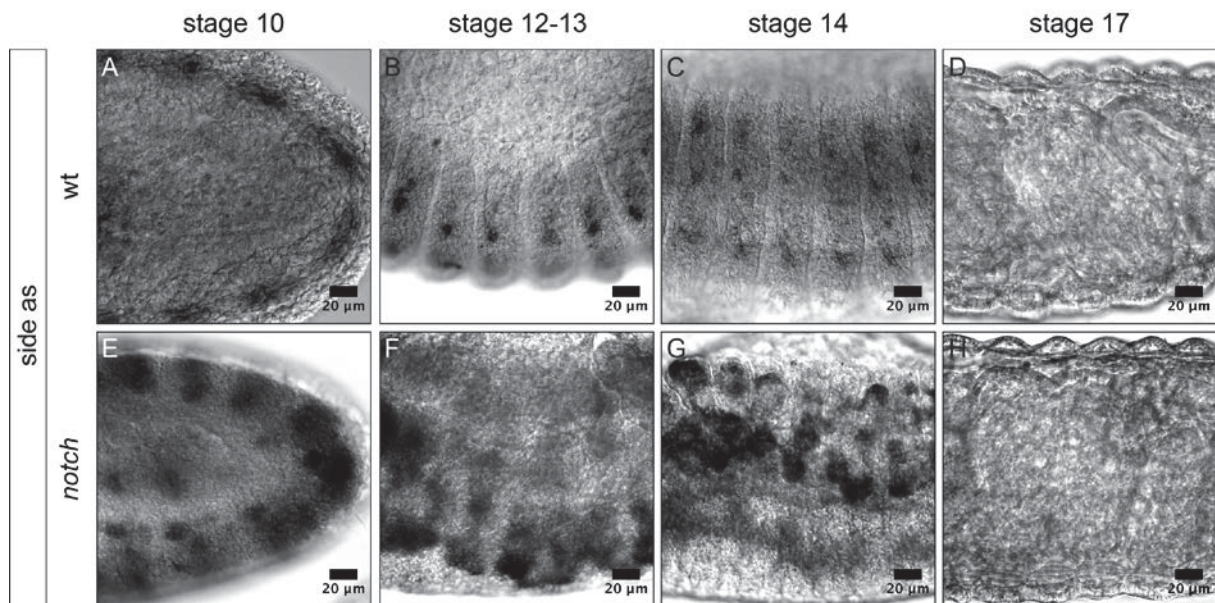


Fig 2. 23: In *notch* mutant embryos expression of *side* mRNA is also upregulated in early and mid-stage embryos compared to wild-type.

In situ hybridisation of wild-type and *notch* loss of function embryos with *side* anti-sense probe. A-D: *Side* mRNA expression in wild-type during embryogenesis. E-H: Expression of *side* in *notch* loss of function embryos. E-G: *Side* expression is increased in early and mid-stage mutant embryos compared to wild-type. H: In late stage loss of function embryos expression of *side* mRNA is no longer detectable similar to wild-type. A-H: Lateral view.

To quantify this upregulation of *side* expression on mRNA level in early and mid-stage embryos of *notch* mutants, qPCRs using *side* specific primer were carried out. Again embryos were collected and separated by age to isolate the RNA from early (≤ 14) and late stages (15-17). As housekeeping gene serves the ribosomal protein 32 (RpL32).

Results

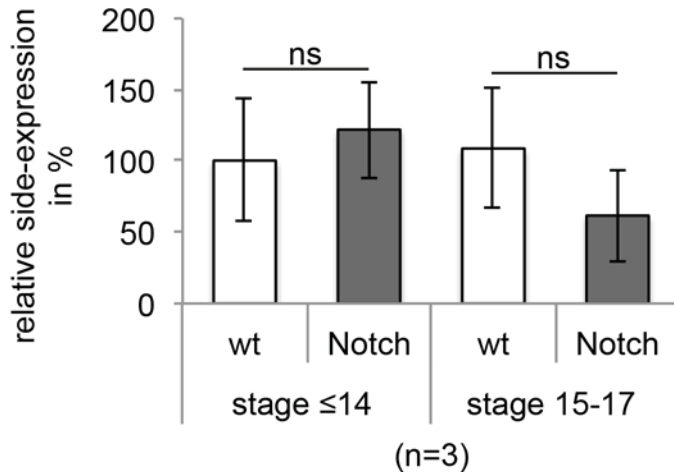


Fig 2. 24: qPCR shows no upregulation of *side* expression in *notch* mutant embryos.

Statistical analysis of qPCR of wild-type and *notch* loss of function embryos using *side* specific primer. Expression of *side* mRNA in wildtype embryos up to stage 14 was set to 100%. Early and late stage *notch* loss of function embryos show no significant difference of relative *side* mRNA expression compared to wild-type (p-value ≤14 = 0.53, 15-17 = 0.20 using students T-test).

Early as well as late *notch* loss of function embryos show no significant different relative expression of *side* mRNA compared to wild-type embryos. In early *notch* mutant embryos the amount of *side* mRNA is slightly but not significant increased, while late embryos exhibit less *side* mRNA in comparison to wild-type (Fig 2.24).

In summary, early and mid-stage (stage 9-14) *notch* mutant embryos show an increased *side* expression using *in situ* hybridisation to visualise *side* mRNA and antibody staining to visualise Side protein. Analysis of relative *side* expression on RNA level (qPCR) shows similar tendencies. In contrast, using western blot to analyse relative protein expression reveals an opposite result with an increased Side expression in old *notch* mutant embryos in comparison to wild-type.

As mentioned before, Side expression is altered *senseless* mutants compared to wild-type (Fig 2.20 A+J). Since the differentiation factor Senseless is required for the development of PNS (Nolo et al., 2000), it is possible that the observed mis-expression of Side in *senseless* mutant embryos based on morphological defects in the PNS. To address this, *senseless* homozygous embryos were stained with anti-Futsch and the expression pattern of Futsch in *senseless* mutant mid-stage and old embryos was compared with Futsch expression in wild-type embryos (Fig 2.25).

Results

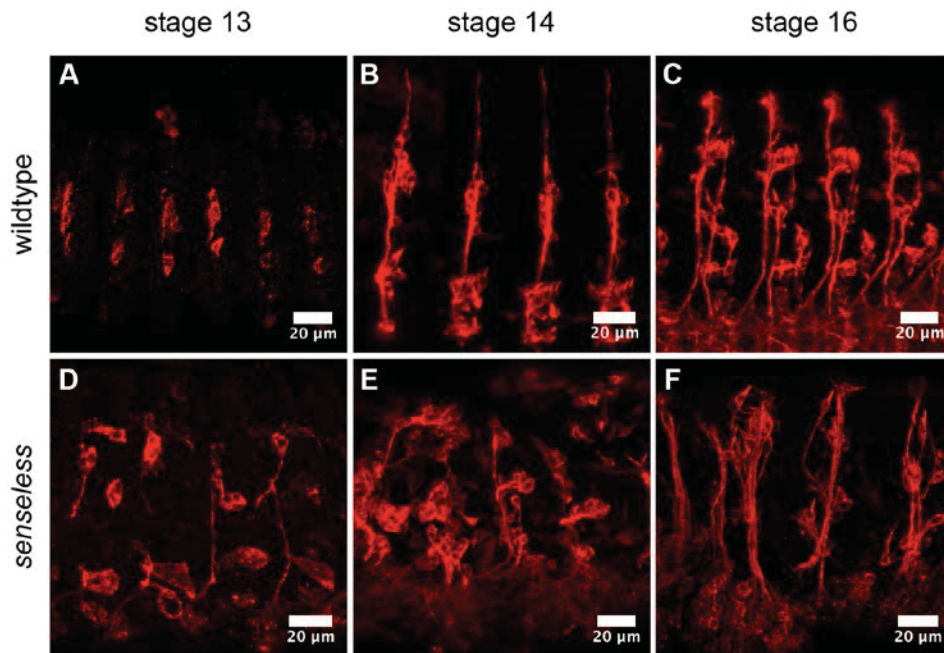


Fig 2. 25: Sensory neuron morphology is strongly altered in *senseless* mutant embryos.

Confocal images of anti-Futsch antibody stainings of wild-type and *senseless* mutant embryos. A-C: Sensory neurons marked by anti-Futsch in wild-type embryos. D-F: In *senseless* mutant embryos sensory organs show an altered morphology compared to wild-type. A-F: Lateral view.

Futsch expression is dramatically changed in *senseless* loss of function embryos in comparison to wild-type (Fig 2.25). In wild-type embryos Futsch is expressed in different sensory clusters per hemisegment (Fig 2.25 A-C). This clustering is no longer detectable and it is hard to distinguish the single hemisegments in embryos lacking *senseless*. Especially in later stages, the ingrowing axons of the sensory neurons are conspicuous thicker in *senseless* loss of function mutants compared to wild-type embryos (Fig 2.25 C and F).

Taken together, all tested mutants of the twenty selected transcription factors do not result in a down-regulation or lack of Side expression in the CNS or PNS. The observed altered expression of Side in *notch*, *senseless* and *antennapedia* mutant embryos seems to be based on indirect effects suggested by western blot analysis and immunofluorescence analysis using anti-Futsch antibody.

2.1.1.5 Side is constitutively expressed in *tolloid-related* mutants

Another question concerned the potential down-regulation of Side, which is important for the neutralisation of formerly attractive cell surfaces. During embryogenesis Sidestep is expressed in a dynamic manner with an early expression in the CNS, a temporary expression in the sensory neurons and a late expression on the muscle

Results

surface to guide the motor axons to their target muscles. Expression of Side in sensory neurons starts in embryonic stage 12 and is hardly detectable using immunohistochemical stainings from late stage 14 or early stage 15 onward. This down-regulation results in defasciculation and immigration of the motor axons into the muscle field (Sink et al., 2001). Down-regulation could occur by extracellular proteolysis, endocytosis or proteasome-mediated degradation. Previous studies of our working group demonstrate that lack of the axon guidance receptor Beat leads to a constitutive expression of Side in sensory neurons resulting in a still detectable Side expression in sensory neurons in late *beat* mutant embryos (stage 15 to 17) (Siebert et al., 2009).

Since Beat is an axon guidance molecule and no enzymatic activity is known, the down-regulation of Side has to be regulated by further proteins. To elucidate which type of mechanism is responsible for Side degradation, the expression level of Side in the background of various mutants that block proteolytic processes were examined and are summarized in table 2.4. For further information about the alleles and stock numbers see chapter Material and Methods table 4.9.

Tab 2. 4: Degradation ways of a protein and genes affecting these different ways

| Degradation way | Genes | Reference |
|-----------------|-----------------------------------|--|
| proteases | <i>tolloid</i> | Canty et al., 2006 |
| | <i>tolloid-related</i> | Meyer and Aberle, 2006; Serpe and O'Connor, 2006 |
| | <i>kuzbanian</i> | Fambrough et al., 1996 |
| | <i>presenilin</i> <i>aph-1</i> | Iwatsubo, 2004 |
| endocytosis | <i>Dmon-1</i> | Yousefian et al., 2013 |
| ubiquitination | <i>Uba1</i> | Watts et al., 2003 |
| | <i>UbcD10</i> | Aguilera et al., 2000 |

In a first step homozygous embryos of all mutants were stained with anti-Side antibody and expression pattern of Side in mid-stage (stage 13-14) and old (stage 16-17) embryos was compared to Side expression in wild-type and *beat* mutant embryos at same stages. In wild-type embryos Side is detectable at stage 14 in sensory neurons, but in late stage embryos only a weak staining of the neuropil is remaining (Fig 2.26 A+A'). In contrast, in *beat* homozygous embryos Side is still expressed in the PNS in late stages (Fig 2.26 B'). At stage 13 to 14, almost all homozygous mutant embryos reflect the Side expression in wild-type embryos.

Results

However, in *uba1* homozygous embryos an altered and increased expression of Side during stage 13 to 14 is visible (Fig 2.26 I). Among *beat*, one other mutant line exhibits a constitutive expression of Side in the periphery in late embryos. Lack of *tolloid-related* leads similar to *beat* to a constitutive Side expression in the PNS (Fig 2.26 D'). The remaining eight tested mutants show no difference compared to wild-type. Only a weak staining of the neuropil is visible.

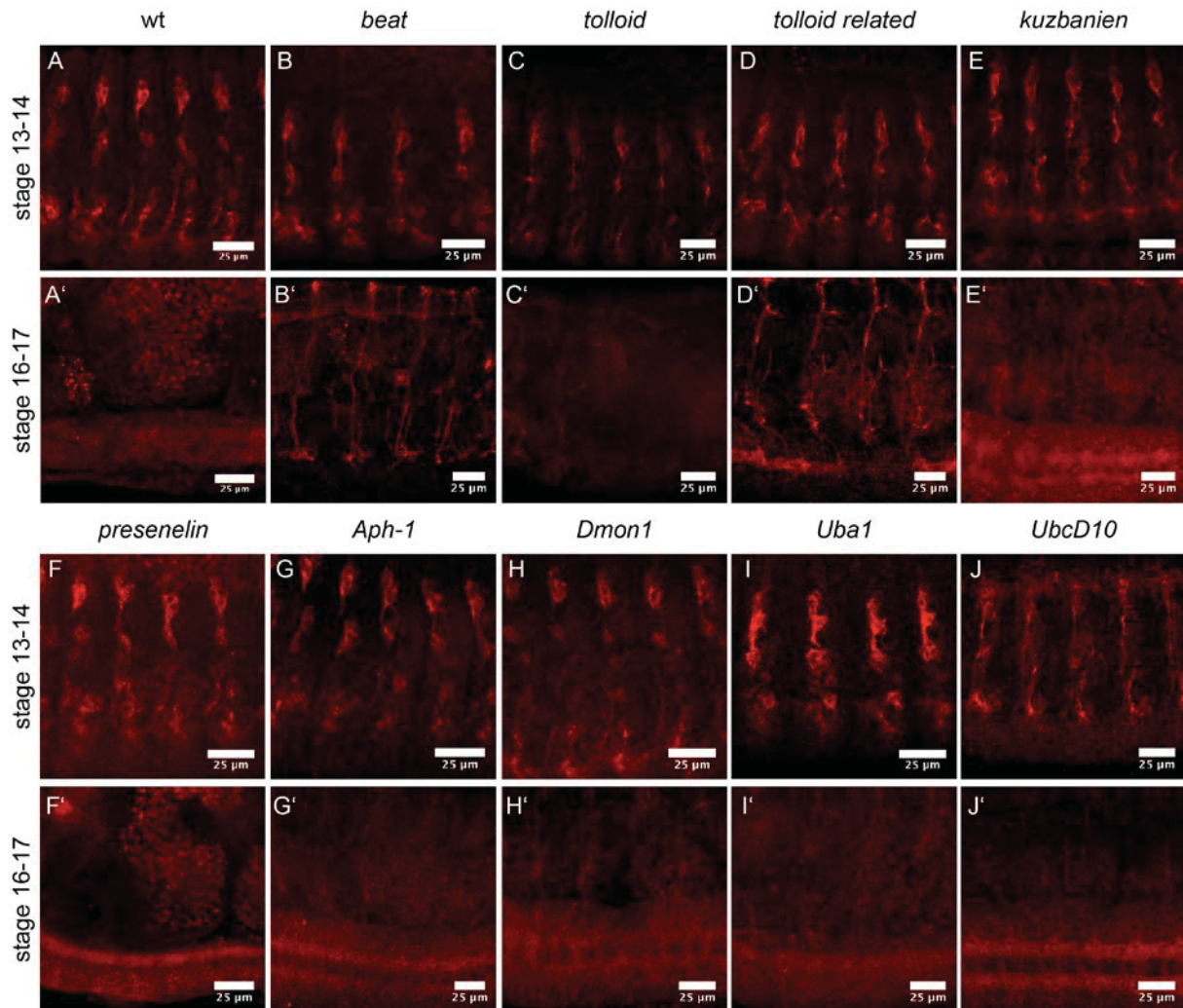


Fig 2. 26: In late *beat* and *tolloid-related* mutant embryos Side is constitutively expressed.

Confocal images of wild-type and *beat*, *tolloid*, *tolloid-related*, *kuzbanien*, *presenelin*, *anterior pharynx defective 1 (Aph-1)*, *Dmon1*, *Uba1* and *UbcD10* mutant embryos stained with anti-Side (red). A+A': Side expression in wild-type embryos. A: At stage 13-14 Side is expressed in sensory neurons. A': Only a weak expression of Side in the neuropile is detectable. B-J: Mid-stage Side expression is only altered in *Uba1* mutant embryos. B'+D': In late *beat* and *tolloid-related* loss of function embryos Side is still detectable in the PNS in contrast to wild-type. C', E'-J': All other tested mutant embryos show no constitutive Side expression. A-J': Ventro-lateral view.

To quantify Side expression in *beat* and *tolloid-related* mutants compared to the wild-type, western blot analyses were carried out. Therefore, embryos were separated again based on their age and as already mentioned two different lysates were

Results

produced. The expression level of Side in early wild-type embryos was set to 100% and α -tubulin serves as housekeeping gene.

In early embryos Side is expressed relatively in wild-type and also in *beat* and *tolloid-related* mutants on a similar level (Fig 2.27). As expected, late embryos show a different result. In *beat* mutant embryos, a 250% higher amount of Side protein is detectable compared to old wild-type embryos (Fig 2.27). A similar result shows *tolloid-related* mutants with a 320% increased Side expression (Fig 2.27). Interestingly, in stage 15-17 wild-type embryos significantly more relative Side protein is detectable than in early wild-type embryos (100% vs 481%).

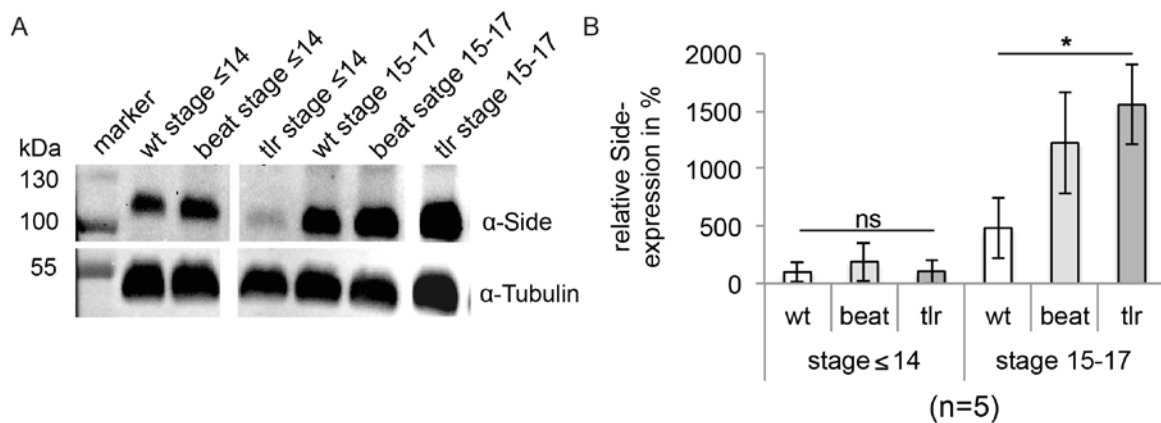


Fig 2. 27: Side expression is increased in late *beat* and *tolloid-related* mutant embryos.

Western blot analysis of wild-type, *beat* and *tolloid-related* loss of function embryos. A: Western blot. B: Statistical analysis. A+B: Early and mid-stage (≤ 14) *beat* and *tolloid-related* mutant embryos show the same amount of Side protein in comparison to wild-type (p-value: 0.33 or more using students T-test), but in late embryos (stage 15-17) Side expression is increased in *beat* and *tolloid-related* loss of function embryos compared to wild-type (p-value: 0.015 or less).

Analysing the expression of Side in *beat* and *tolloid-related* mutant embryos it is striking that the Side signal seems to be not localised in the same cells in late stage embryos based on the different morphology of the Side positive cells (Fig 2.26 B'+D'). In stage 16 to 17 *tolloid-related* mutant embryos Side appears to be in motor axons, as branches contact muscles fibres are visible. In contrast, in *beat* mutants these branches are cannot be seen. To address the question in which cell type Side is expressed in *beat* and *tolloid-related* mutant embryos, antibody co-stainings were performed. *Beat* mutant embryos were co-stained with anti-Side and anti-Ankyrin-2, a marker for sensory neurons, or DVGlut, a marker for glutamateric motoneurons and axons (Koch et al., 2008; Mahr and Aberle, 2006). Using anti-Side and anti-Ankyrin-2 for co-staining, both signals overlap partially. However, there are regions where only

Results

a Side signal or only an Ankyrin-2 signal is detectable (Fig 2.28 A-C). Using anti-DVGlut for co-staining, both signals are located next to each other, but no overlap is visible. Thus, Side and DVGlut are expressed probably in different cells, which are localised close to each other.

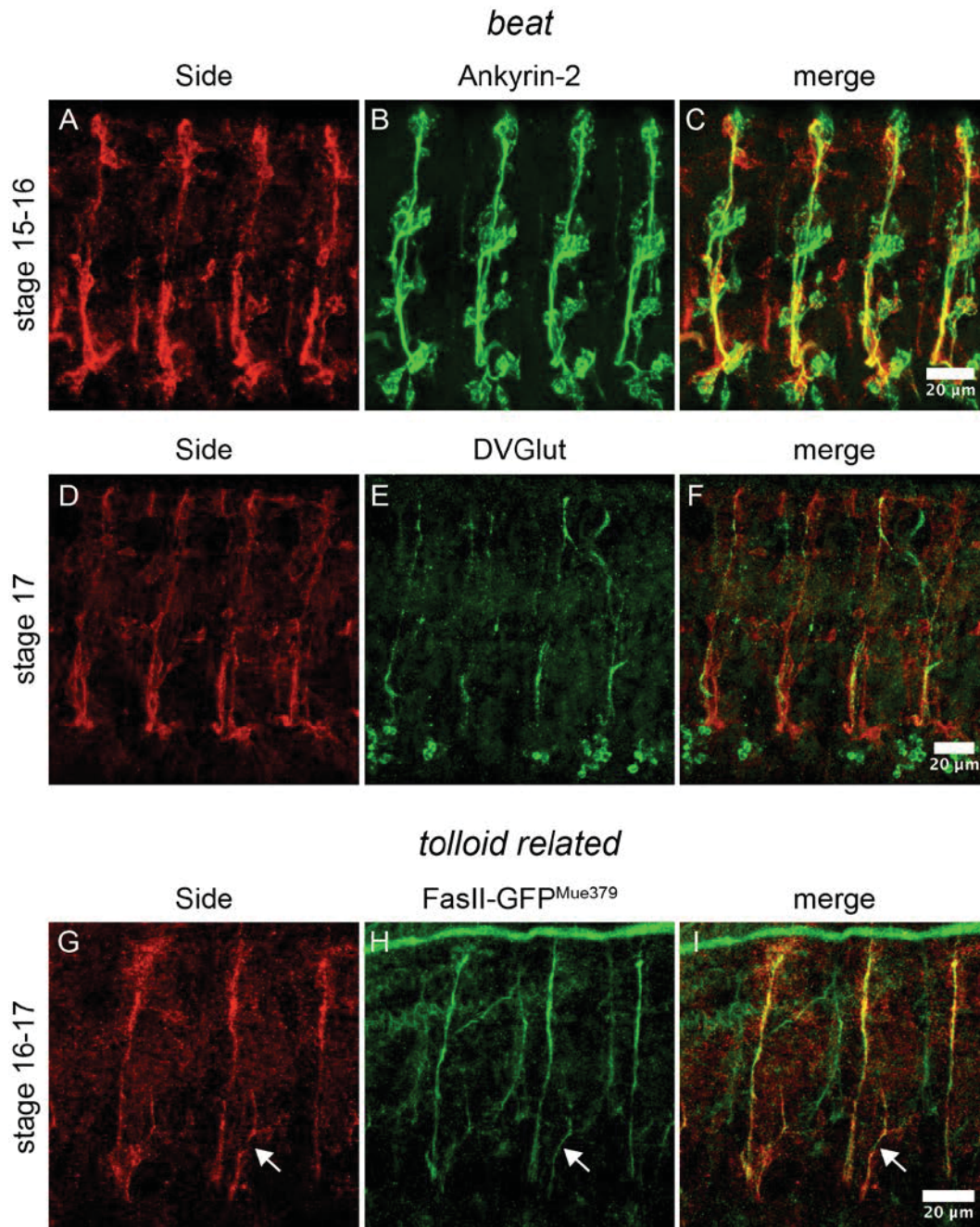


Fig 2. 28: In late *beat* and *tolloid-related* mutant embryos Side is expressed in sensory neurons and motor axons, respectively.

Antibody co-stainings of *beat* mutant embryos with anti-Side (red) and anti-Ankyrin (green, A-C) or anti-DVGlut (green, D-F), and of *tolloid-related* loss of function embryos with anti-Side (red) and anti-GFP (green, G-I) in a FasII-GFP exon trap background. A-F: In late *beat* mutant embryos Side is expressed in sensory neurons. G-I: In late *tolloid-related* loss of function embryos motor axons express Side. Arrows mark the SNa. A-I: Lateral view.

Results

In *tolloid-related* mutants co-stainings with anti-Side and anti-GFP in a FasII-GFP exon trap background were carried out. Side and Fasciclin II overlap in the ISN and SNa in late *tolloid-related* mutant embryos (Fig 2.28 G-I). These results suggest that in *beat* mutants Side is constitutive expressed in sensory neurons in late embryos, but in *tolloid-related* mutants constitutively expressed Side is localised in motor axons.

To elucidate at what time localisation of Side shifts from sensory neurons to motor axons in *tolloid-related* mutants, images of different embryonic stages of homozygous *tolloid-related* embryos with FasII-GFP exon trap background were acquired.

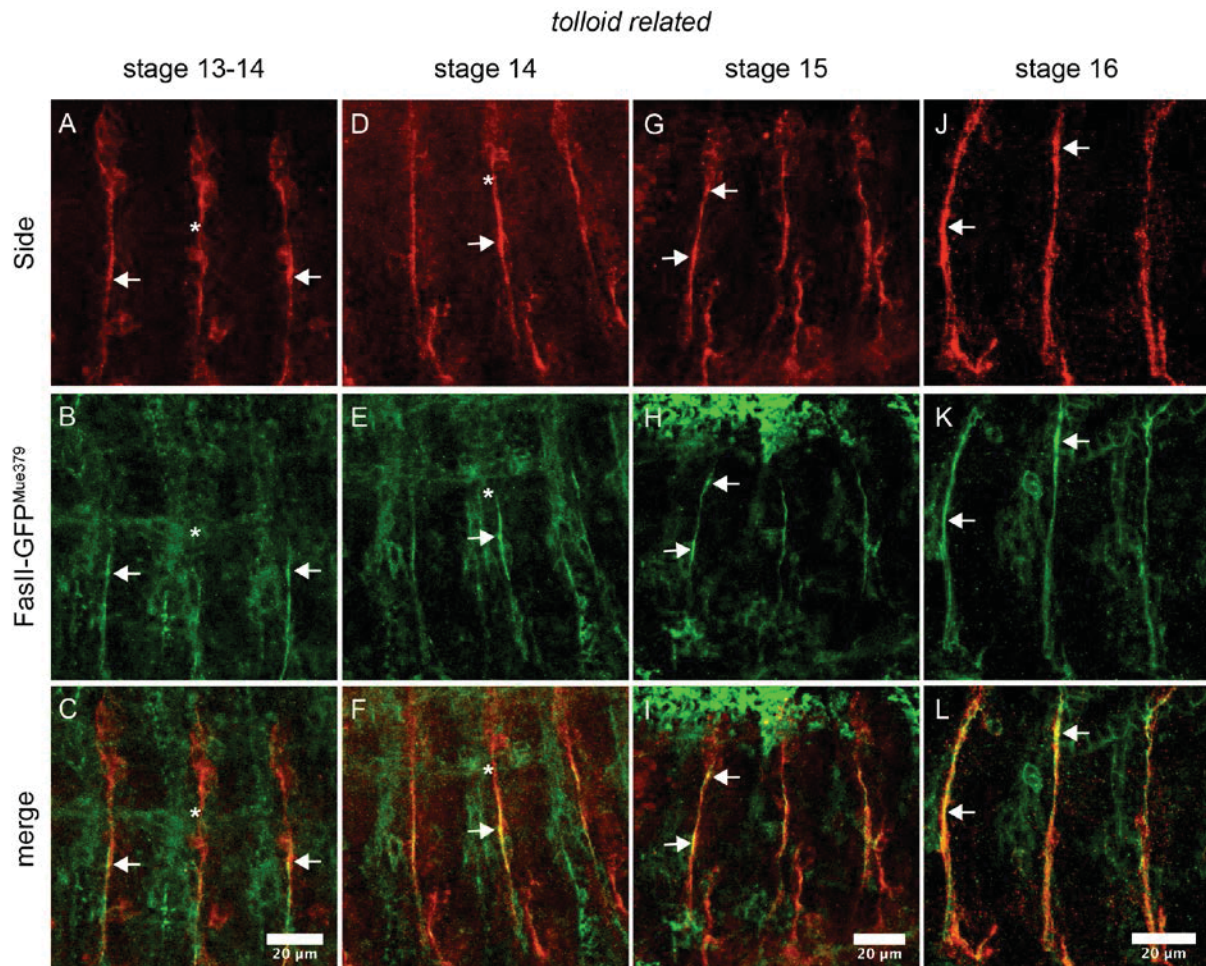


Fig 2. 29: Side-localisation shifts between stage 15 and 16 from sensory neurons to motor axons in *tolloid-related* mutants.

Confocal images of antibody co-stainings with anti-Side (red) and anti-GFP (green) of *tolloid-related* loss of function embryos with a FasII-GFP exon trap background. A-F: In early stages Side is expressed in ingrowing sensory axons (asterisks) partly fasciculating with outgrowing motor axons (arrows). G-L: In later stages Side is expressed in motor axons (arrows). A-L: Lateral view.

Results

In stage 13 and 14 old *tolloid-related* loss of function embryos Side is expressed in migrating axons of sensory neurons, which partly fasciculate with outgrowing motor axons marked with GFP. However, this localisation shifts between stage 15 and 16. At stage 15 Side is still localised predominantly in sensory neurons, but there are already some motor axons positive for Side. In stage 16 embryos, Side completely overlaps with motor axons.

To verify that the observed constitutive expression of Side protein in *beat* and *tolloid-related* mutants is not based on an alteration of mRNA expression, *in situ* hybridisation and quantitative PCR (qPCR) were carried out. Using a *side*-specific anti-sense probe for *in situ* hybridisation, expression pattern of *side* mRNA in wild-type embryos were compared with *beat* and *tolloid-related* mutant embryos. No difference of *side* expression pattern in wild-type and mutant embryos is visible (Fig 2.30). In early embryos (stage 10), *side* mRNA is localised in the CNS and in mid-stage embryos (stage 12-14) in sensory neurons in mutant as well as in wild-type embryos. Late embryos of all three genotypes show no *side* mRNA expression.

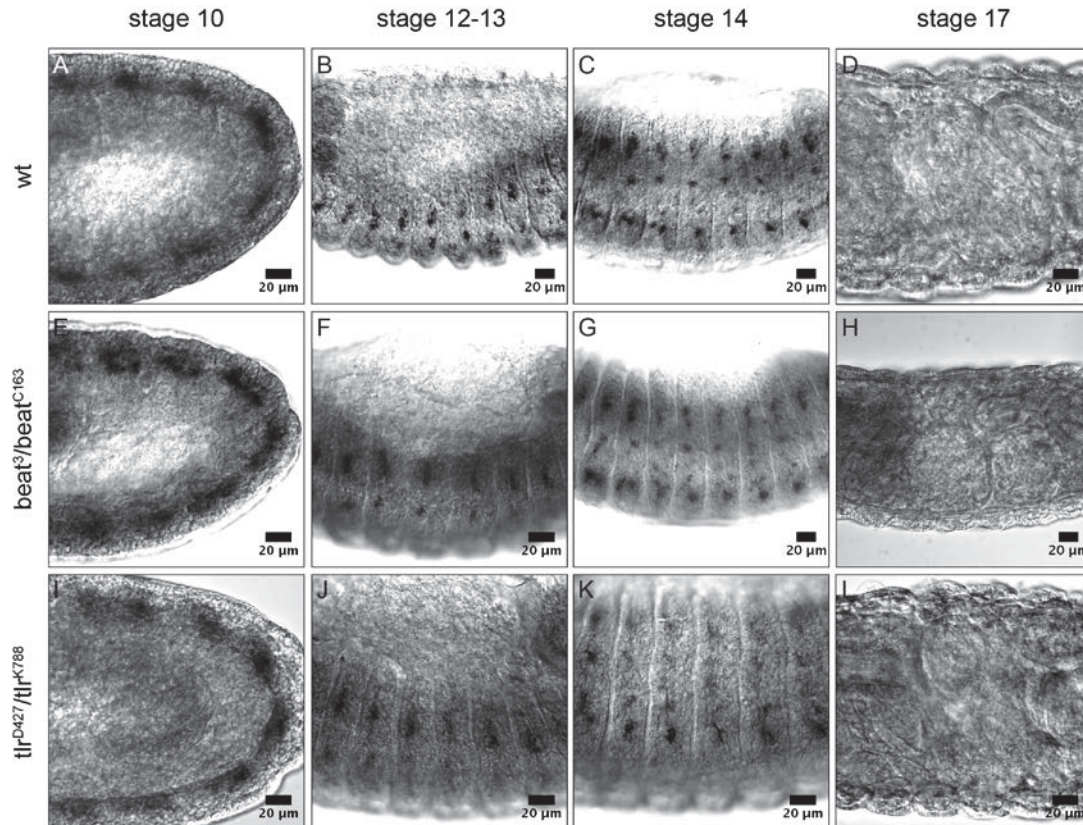


Fig 2. 30: Expression of *side* mRNA is not altered in *beat* and *tolloid-related* mutant embryos. *In situ* hybridisation with *side* specific probe of wild-type (wt), *beat* and *tolloid-related* (*tlr*) loss of function embryos. A-D: Expression of *side* mRNA in wild-type embryos during embryogenesis. E-L: *Beat* and *tolloid-related* mutant embryos show no altered *side* expression. A-L: Lateral view.

Results

Quantitative PCR provides a different result using *side* specific primer. Embryos were separated by age similar to western blot analyses and total RNA was isolated. The ribosomal protein 32 (*RpL32*) serves as housekeeping gene. In early *beat* and *tolloid-related* homozygous embryos, *side* mRNA expression is decreased compared to the wild-type. However, only in *beat* mutants the difference is significant using student's T-test. In old *beat* mutant embryos a similar tendency as in young embryos is detectable with a decreased *side* mRNA expression. In contrast, lack of *tolloid-related* leads in late embryos to a weak increased *side* expression.

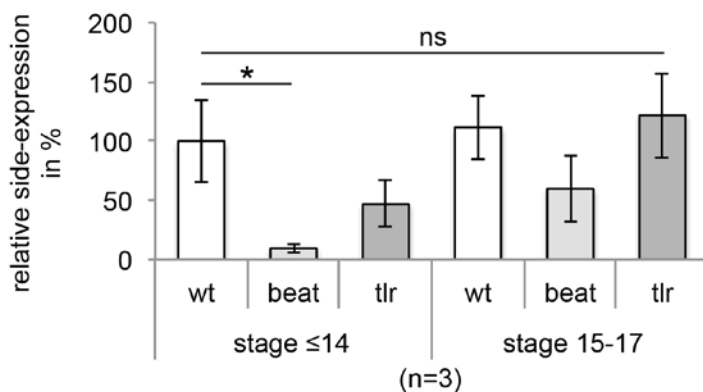


Fig 2. 31: In early *beat* mutant embryos *side* expression is decreased.

Statistical analysis of qPCR performed with wild-type (wt), *beat* and *tolloid-related* (*tlr*) loss of function embryos. Lack of *beat* leads to a significant decreased *side* expression in early and mid-stage embryos in comparison to wild-type (p-value: 0.04 using students T-test), but in late stage embryos no significant difference can be detected (p-value: 0.19). In *tolloid-related* mutants *side* expression is not significantly altered in early and late stage embryos compared to wild-type (p-value: 0.1 or more). However, early and mid-stage *tolloid-related* mutant embryos show a tendency of a decreased *side* expression and old embryos a tendency of an increased *side* expression.

To investigate further whether *beat* and *tolloid-related* regulate *Side* expression during embryogenesis and therefore influence possibly motor axon guidance, the innervation pattern of third instar larvae of *side*, *beat* and *tolloid-related* homozygous mutants were analysed and compared to innervation pattern of ShGFP L3 larvae. Innervation of whole mount larvae can be readily observed and analysed through the transparent cuticle of intact larvae using the fusion protein ShGFP, a postsynaptic marker composed of the extracellular and transmembrane domain of the human T-cell antigen CD8, the protein sequence of GFP and the C-terminus of the potassium channel Shaker (Zito et al., 1999). The MHC (myosin heavy chain) promoter drives the construct and leads to an expression in all somatic muscles. The bright staining of the NMJs is based on the interaction between the C-terminus of Shaker and the

Results

postsynaptic protein Discs large. This interaction causes an accumulation of the fusion protein at the post-synapses (Zito et al., 1999).

All three mutant larvae show missing NMJs especially in the ventral muscles field compared to wild-type. The strongest phenotype show *Side* loss of function larvae compared to *beat* and *tolloid-related* mutants. Lack of *tolloid-related* results in the mildest phenotype (Fig 2.32).

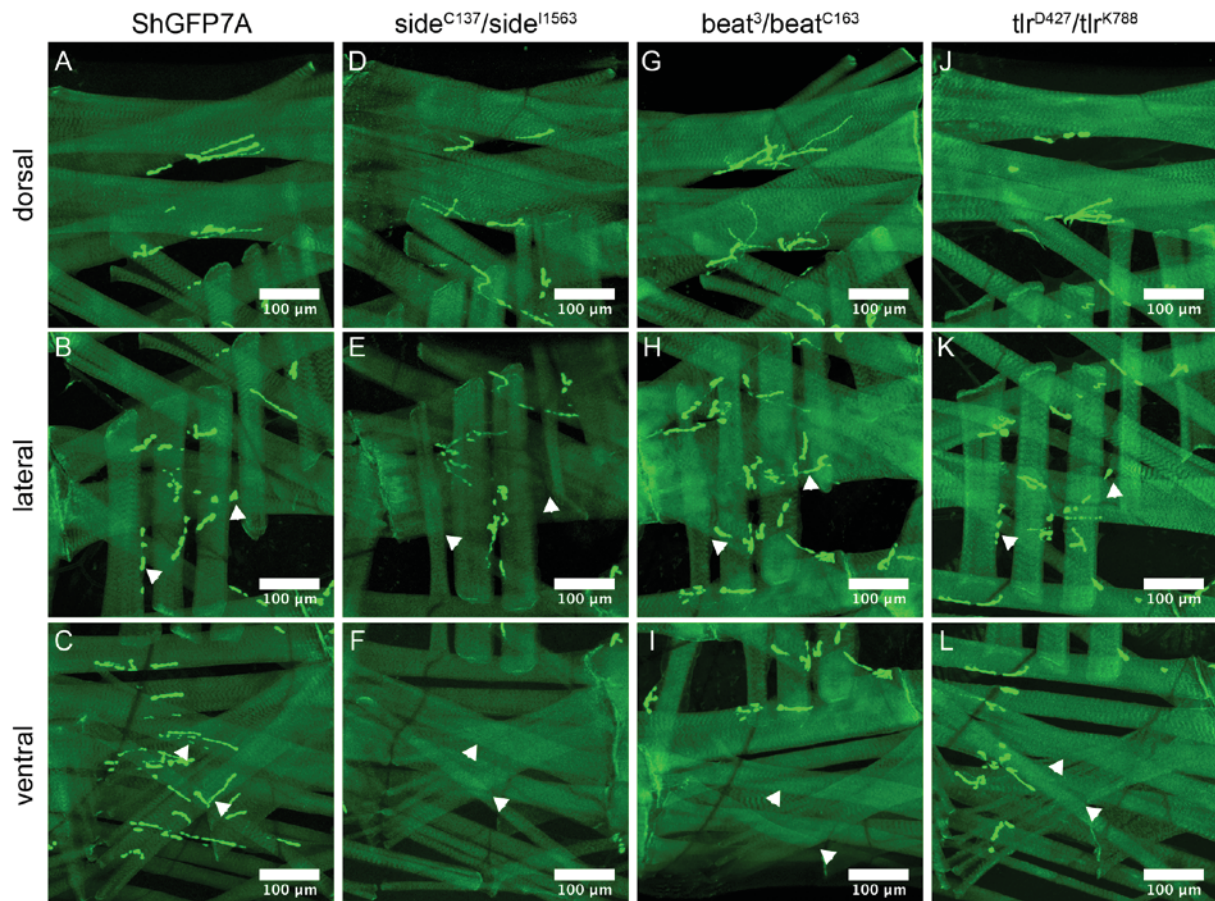


Fig 2. 32: The lateral muscle field of *side*, *beat* and *tolloid-related* mutants show strong mis-innervation.

Confocal images of innervation pattern of dorsal, lateral and ventral muscle fields of wild-type, *side*, *beat* and *tolloid-related* loss of function third instar larvae. A-C: Control larva. D-F: *Side* mutant larvae exhibit missing NMJs in the ventral and lateral muscle fields compared to wild-type (arrowheads). G-I: Loss of *beat* leads to mis-innervations predominantly in the ventral muscle field in comparison to wild-type (arrowheads, I). J-L: *Tolloid-related* mutant larvae show the weakest phenotypes with some missing NMJs in the ventral muscle field (arrowheads, L). A, D, G, J: Dorsal view. B, E, H, K: Lateral view. C, F, I, L: Ventral view.

The analysis of *beat* and *tolloid-related* double mutants is a possibility to illuminate if these two genes function in the same pathway controlling *Side* expression. Double mutant embryos were stained with anti-*Side* and the expression pattern was compared to that in wild-type. In mid-stage embryos (stage 14), *Side* expression is not altered in double mutants (Fig 2.33 A+B). In contrast, late double mutant

Results

embryos show a similar phenotype as single mutants with a still detectable Side signal in the periphery (Fig 2.33 A'+B').

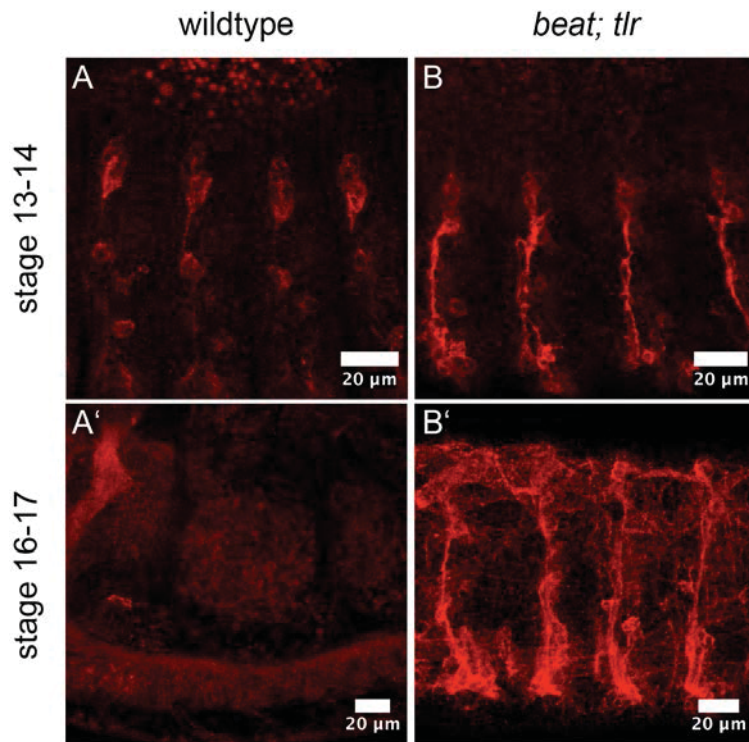


Fig 2. 33: Side is constitutively expressed in *beat; tolloid-related* double mutants.

Antibody staining of wild-type and *beat; tolloid-related* mutant embryos with anti-Side. A+A': Side expression in wild-type embryos (lateral view). A: Sensory neuron specific expression of Side in mid-stage wild-type embryo. A': In late stage wild-type embryos Side is no longer detectable in the PNS. B+B': Expression of Side in *beat; tolloid-related* loss of function embryos. B: In early stages *beat; tolloid-related* double mutant embryos show no difference in Side expression compared to wild-type (ventro-lateral view). B': In late mutant embryos Side is still expressed in the PNS in contrast to wild-type (lateral view).

The quantification using western blot proves the impression of a constitutive expression of Side in double mutants (Fig 2.34). Late mutant embryos express Side in a 180% higher amount compared to late wild-type embryos. Interestingly, early double mutant embryos show a significant decreased Side expression in comparison to wild-type (Fig 2.34).

Results

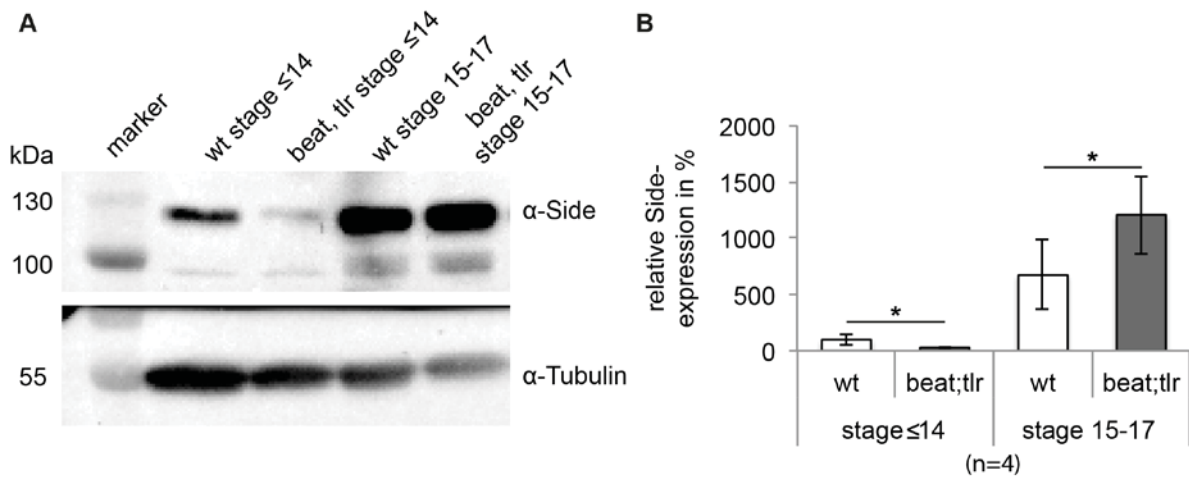


Fig 2. 34: Side expression is increased in late *beat; tolloid-related* mutant embryos.

Western blot analysis of double mutant embryos. A: Western blot. B: Statistical analysis. A+B: Expression of Side is decreased in early (lane 3) and increased in late (lane 5) double mutant embryos compared to wild-type (lane 2+4) (p-value: 0.04 or less using students T-test).

To identify the localisation of Side in late stage double mutant embryos, again antibody co-stainings with anti-Side and anti-DVGlut were performed. Side co-localises with motor axons of the ISN and SNa (arrows Fig 2.35) marked by anti-DVGlut suggesting a similar motor axon specific expression as visible in *tolloid-related* single mutants.

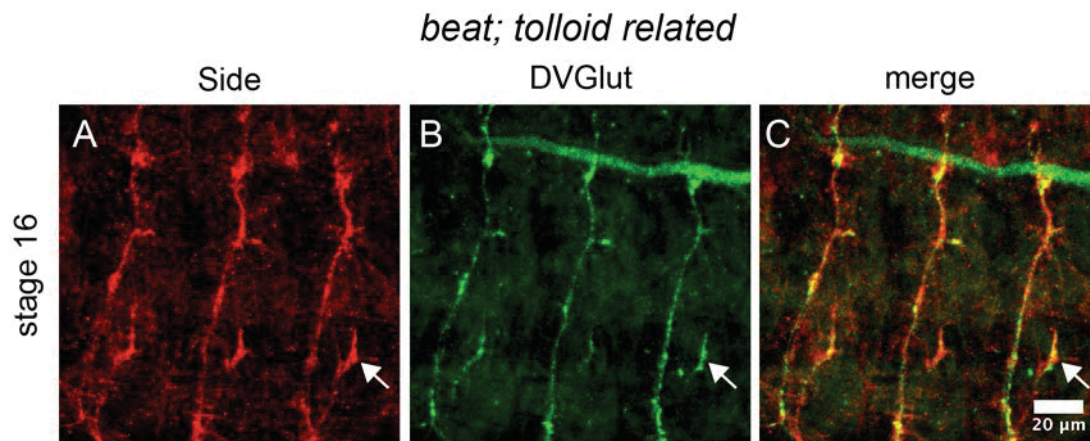


Fig 2. 35: In stage 16 *beat; tolloid-related* double mutant embryos Side is expressed in motor axons.

Confocal images of co-staining of *beat; tolloid-related* loss of function embryos with anti-Side (red) and DVGlut (green). A-C: In late double mutant embryos Side is expressed in motor axons. Arrows mark SNa. Lateral view.

2.1.2 Gene regulation of the axon guidance receptor *beaten path la*

Similar to *side*, almost nothing is known about the gene regulation of its receptor *Beaten path*. Therefore, during this thesis it was also tried to identify the promoter of *beat*.

2.1.2.1 The *beat* phenotype can be completely rescued by the enhancer fragment 40636

Beat is expressed during embryogenesis specifically in motoneurons (Fambrough and Goodman, 1996). To scan regulatory elements in the *beat* gene, the expression pattern of 11 different promoter-fragment-Gal4 lines were documented in the same manner as described before for the *sidestep* promoter. They cover large areas of the first intron and the complete second, third and fifth introns (Fig 2.36). The size of the fragments variants between around 1.4 and 4.2 kb and some of the lines overlap partially. Notably, the fragment 203094 is completely located in the region covered by line 48633 upstream of the start codon.

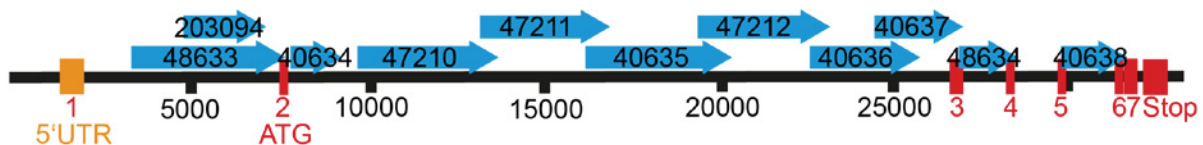


Fig 2. 36: *Beat* promoter-fragment-Gal4-lines.

Blue arrows represent the position and length of the analysed lines in relation to the *beat* gene and in red the exons are depicted. The genomic fragments are named based on the VDRC or Bloomington stock number and cover intronic regions.

The driver line UAS-mCD8-GFP was employed again as reporter and embryonic and larval expression patterns were analysed. The enhancer fragment 40636 drives GFP expression dominantly in cells of the CNS and shows an increase of the GFP signal from stage 14 (Fig 2.37 A+A') to stage 16 (Fig 2.37 B+B') during embryogenesis. Additionally, an unspecific GFP expression beyond the CNS is visible. In all three larval stages GFP is expressed in the CNS and in motor axons, predominantly in the SNa (Fig 2.37 C-E').

Results

40636-Gal4 / UASmCD8GFP

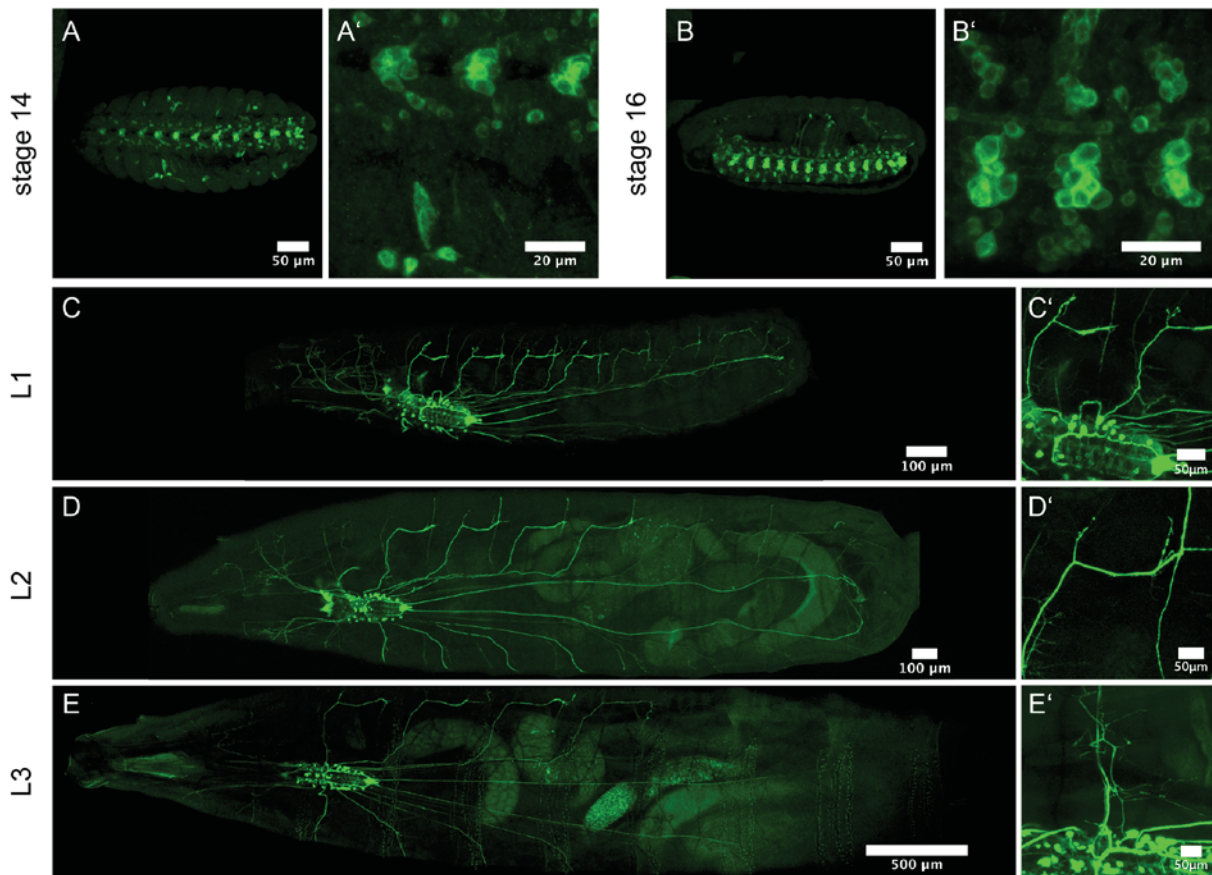


Fig 2. 37: 40636-Gal4 activates GFP expression in motoneurons and axons during embryogenesis and larval development.

Confocal images of anti-GFP stainings of 40636>mCD8GFP embryos and endogenous GFP expression driven by 40636-Gal4 in larvae. A-B': During embryogenesis GFP is driven in motoneurons. C-E': In larvae GFP expression is localised in motoneurons and axons. A+A', D-E': Ventral view. B-C': Ventro-lateral view.

To identify the GFP positive cells, three different antibodies were used for co-stainings - anti-Fasciclin II, anti-Eve and anti-BarH1/2. Eve is expressed in dorsal motoneurons including aCC and RP2 neurons (Doe et al., 1988). The enhancer activity of 40636 co-localises partly with the expression of all three markers. GFP overlaps with aCC, pCC, U/CQ and RP neurons marked by anti-Eve (Fig 2.38 D-F) as well as with SNa projecting neurons marked by anti-BarH1/2 (Fig 2.38 G-I). Therefore, 40636-Gal4 activates GFP expression in motoneurons projecting in the ISN and SNa (Fig 2.38).

Results

40636-Gal4 / UASmCD8GFP

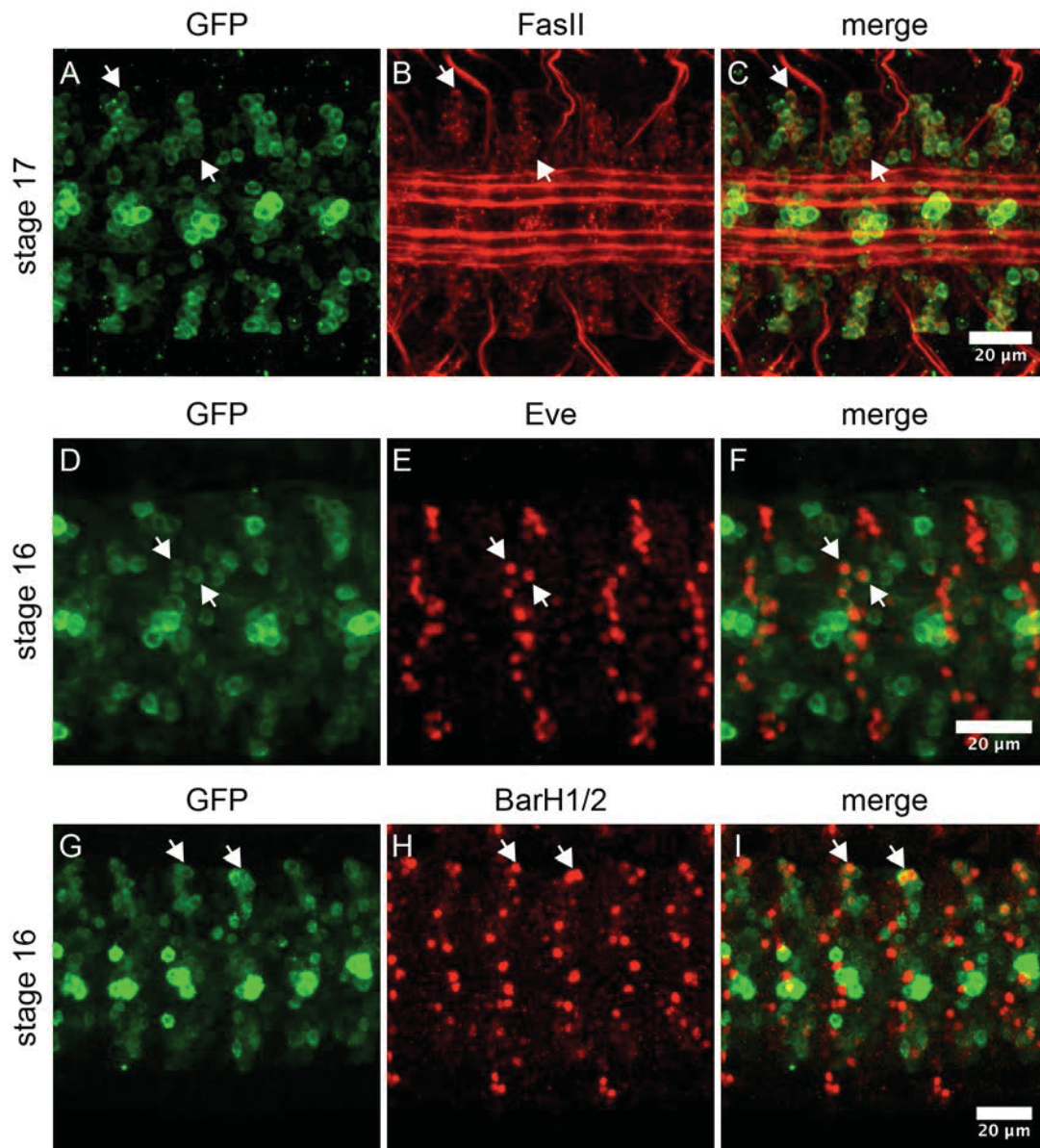


Fig 2. 38: GFP driven by 40636-Gal4 is expressed in motoneurons.

Confocal images of antibody stainings of 40636>mCD8GFP embryos with anti-GFP (green), anti-FasII (red, A-C), anti-Eve (red, D-F) or anti-BarH1/2 (red, G-I). A-C: GFP is expressed in motoneurons projecting in the ISN and SNa (arrows). D-F: aCC, pCC, U/CQ and RP neurons are positive for GFP (arrows). G-I: GFP is expressed in BarH1/2 positive SNa neurons (arrows). A-I: Ventral view.

All other fragments generate some sort of enhancer activity, but 7 fragments (48633, 203094, 40634, 47211 and 48634) drives GFP expression only in some unspecific cells. The GFP expression activated by two additional fragments does not fit to the expected expression for the *beat* promoter (40637 and 48638) (data not shown). The fragments 47210, 40635 and 47212 activate GFP expression similar to 40636 CNS specific. However, using antibody co-stainings to identify the GFP expressing cells only the expression pattern of line 40636 reflects the described expression pattern of

Results

beat by Fambrough and Goodman (data not shown) (Fambrough and Goodman, 1996).

If the *beat* fragment 40636 is functional in *beat* expressing tissues it should rescue the *beat* phenotype. To address this question, wild-type cDNA of *beat* (UAS-*beat*⁵ (Fambrough and Goodman, 1996; Siebert et al., 2009)) were driven in *beat* mutants by this fragment. In *beat* loss of function larvae the ventral muscles field show strong innervation errors in the ventral muscle field (arrows Fig 2.29 B) compared to wild-type (arrows Fig 2.39 A). Using the enhancer fragment 40636-Gal4 for the rescue experiment, it was possible to rescue the *beat* phenotype completely (arrows Fig 2.39 C).

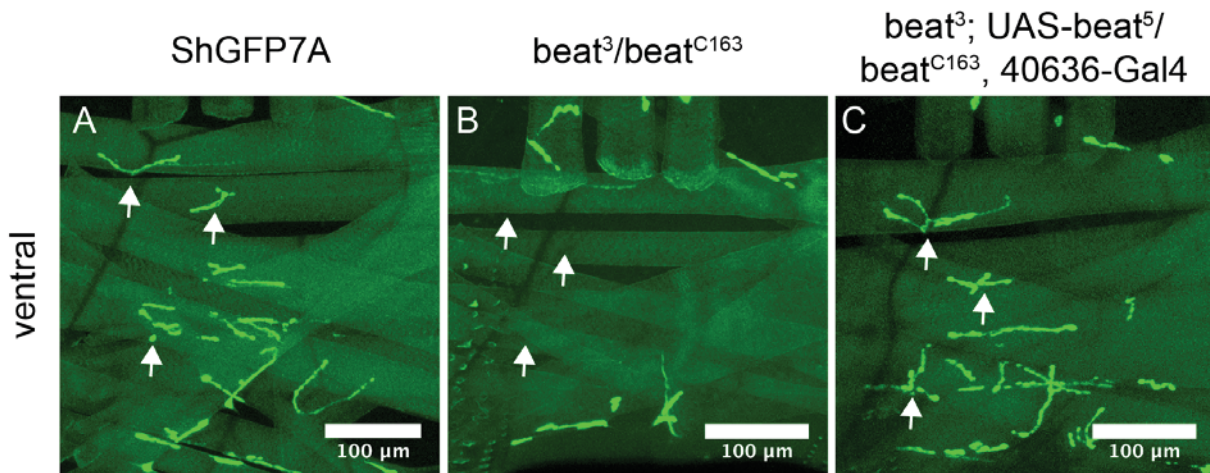


Fig 2. 39: Complete rescue of *beat* phenotype by the enhancer fragment 40636-Gal4.

Innervation of ventral muscle fields of a wild-type, *beat* mutant and rescue larvae. A: Control larva. B: Lack of *beat* leads to missing NMJs in the ventral muscle field (arrows). C: Driving *beat* cDNA expression with 40636-Gal4 in *beat* mutant background rescues the phenotype completely (arrows).

2.1.2.2 The *beat* promoter fragment 40636 exhibit one conserved region

Similar to *side* enhancer fragments, the *beat* enhancer fragment 40636 was analysed concerning conserved regions in other *Drosophila* species of the clade *Drosophilidae*. 40636 exhibit only one highly conserved region of 56 nucleotides localised at the 5'-end of the fragment (Figs 2.40 and 2.41).

Results

```

D.melanogaster  ATGAGCTTAGTTGGCGATTTAGCGATGCTTGTCTTATTTAGTTTAAATAAAATGG
D.simulans      ATGAGCTTAGTTGGCGATTTAGCGATGCTTGTCTTATTTAGTTTAAATAAAATGG
D.sechellia     ATGAGCTTAGTTGGCGATTTAGCGATGCTTGTCTTATTTAGTTTAAATAAAATGG
D.yakuba        ATGAGCTTAGTTGGCGATTTAGCGATGCTTGTCTTATTTAGTTTAAATAAAATGG
D.erecta        ATGAGCTTAGTTGGCGATTTAGCGATGCTTGTCTTATTTAGTTTAAATAAAATGG
D.ananassae     ATAAGCTTAGTTGGCGATTTAGCGATGCTTGTCTTATTTAGTTTAAATAAAATGG
D.pseudoobscura ATGAGCTTAGCCGGCGATTTAGCGATGCTTGTCTTATTTAGTTTAAATAAAATGG
D.persimilis    ATGAGCTTAGCCGGCGATTTAGCGATGCTTGTCTTATTTAGTTTAAATAAAATGG
D.wilistoni     ATGAGCTTAGTTGGCGATTTAGCGATGCTTGTCTTATTTAGTTTT-AAATAAAATGG
D.mojavensis   ATGAGCTTAGTTGGCGATTTAGCGATGCTTGTCTTATTTAGTCTT-ATATAAAATGG
D.virillilis    ATGAGCTTAGTTGGCGATTTAGCGATGCTTGTCTTATTTAGTTTTTAAATAAAATG-
D.grimshawi     ATGAGCTTAGTTGGCGACTTAGCGATGCTTGTCTTATTTAGTTTT-AAATAAAATGG
** *****  ***** *****

```

Fig 2. 40: The promoter fragment 40636 exhibits one conserved region.

The conserved region has two predicted binding sites for the transcription factor Eve (frames).

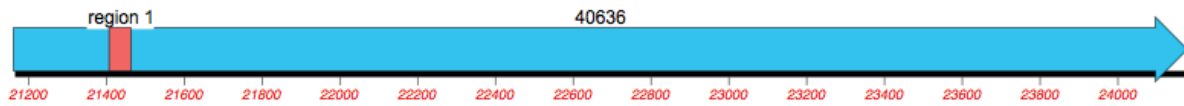


Fig 2. 41: Position of the conserved region within the *beat* promoter-fragment 40636.

The conserved region is localised at the 5'-end of the fragment 40636.

Analysis of the *beat* promoter fragment 40636 for transcription factor binding sites, using again the website alggen.lsi.upc.es, predicted amongst others two binding sites for the transcription factor Eve (frames Fig 2.40). This result fits with the observation of Zarin and colleagues, who have shown that Eve activates *beat* expression in aCC and RP2 neurons (Zarin et al., 2014a).

2.2 Larval phenotype

2.2.1 Loss of *side* function leads to innervation defects in larvae

Since *side* has been identified in a genetic screen for genes involved in motor axon guidance it is already known that the lack of Side causes innervation defects in *Drosophila* larvae using the post-synaptic marker ShGFP as read-out. Using OK371-Gal4 (Mahr and Aberle, 2006) and the effector-line UAS-DsRed, it is possible to analyse the projections of motor axons without an antibody-staining through the transparent cuticle additionally to NMJs marked by ShGFP (Fig 2.42). In Side loss of function larvae the nerves frequently fail to defasciculate from the ISN and SN and to predominantly innervate the ventral muscle field resulting in a decreased number of NMJs (Fig 2.42 J-R). Furthermore, mis-guidance of nerves and dislocated NMJs are detectable (Fig 2.42 J-R). Therefore, lack of Side affects the location and the total number of NMJs.

To better characterise the larval phenotype, different statistical analyses were carried out. As control for all analyses serves ShGFP. The number of neuromuscular junctions (NMJs) of around 50 hemisegments in total and also divided in the three muscle fields (ventral, lateral and dorsal) was counted (for details: chapter 4.2.7). On average, *side* mutant larvae exhibit 44% less NMJs per abdominal hemisegment than the control larvae (*side*= 14 NMJs, ShGFP= 26 NMJs) (Fig 2.43 A). In the ventral muscle field, the strongest percentage difference between both phenotypes is detectable with only 5 NMJs in mutant larvae compared to 10 NMJs in control larvae (Fig 2.43 B). During the analyses, it was striking that the different hemisegments do not show the same phenotype or the same number of NMJs. A histogram depicts this observation (Fig 2.43 C). Most of the control larvae have 25 to 28 NMJs (78%) per hemisegment. In contrast, *side* mutant larvae exhibit 8 to 27 NMJs per hemisegment. Additional to the number of NMJs, the area of NMJs was also quantified. As expected, *side* mutant larvae exhibit a lesser synaptic area than the control larvae (1959 μm^2 vs 4353 μm^2) (Fig 2.43 D). Interestingly, lack of Side leads therefore to a 55% decreased synaptic area, but the number of NMJs is only minus 44% compared to control larvae.

Results

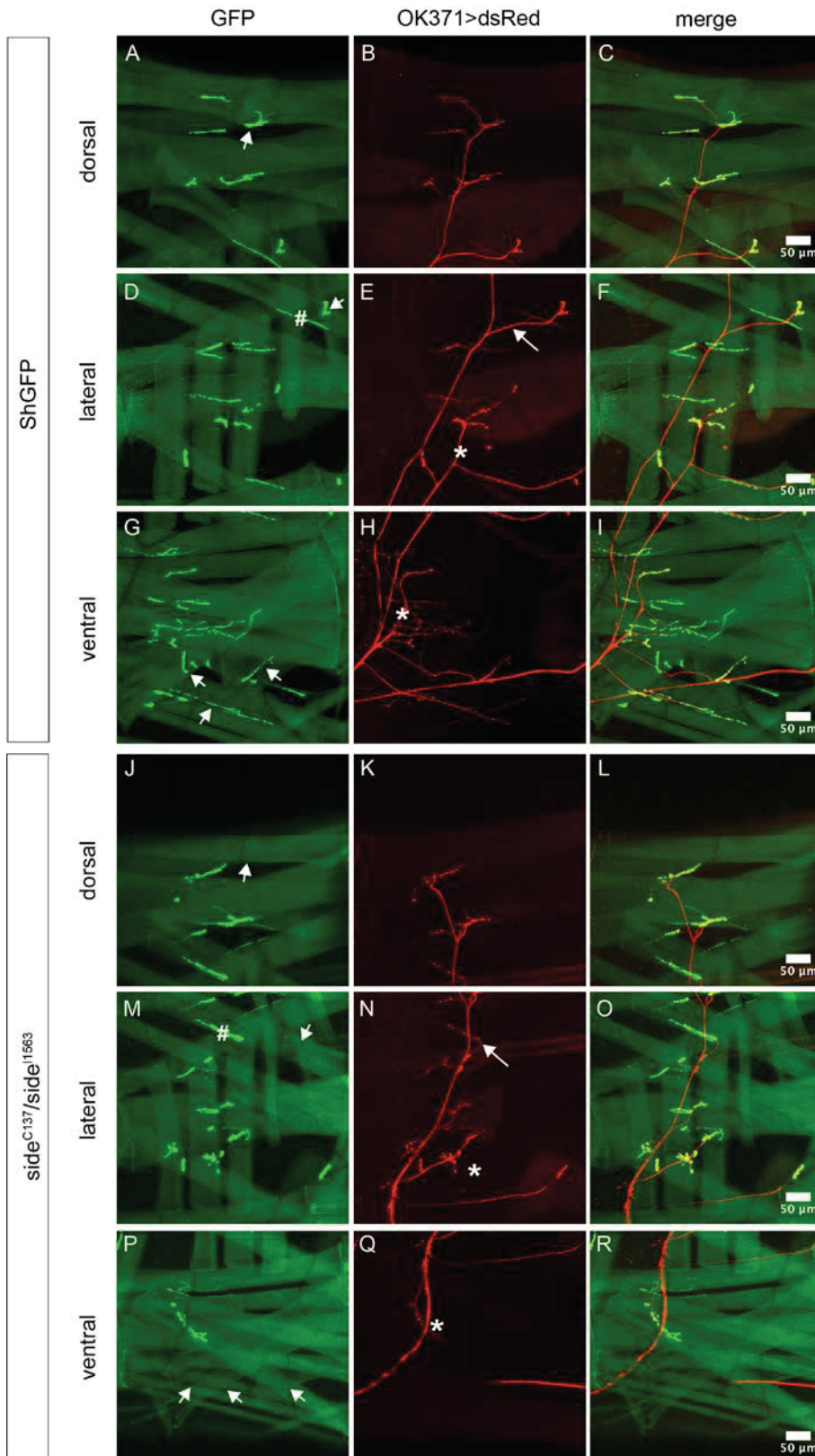


Fig 2. 42: *Side* mutant larvae exhibit mis-innervations in ventral, lateral and dorsal muscle fields.

NMJs (green) and motor axons (red) of wild-type ($w;OK371-Gal4,ShGFP1A/+;ShGFP7A,UAS-DsRed$) and *Side* loss of function ($w;OK371-Gal4/+;side^{C137},ShGFP/side^{I1563},ShGFP7A,UAS-DsRed$) third instar larvae. A-I: In wild-type, muscles are innervated by five main nerves. J-R: *Side* mutant larvae show several defects compared to wild-type marked by following symbols: * = missing nerves/branches, arrows = misguidance of nerves, small arrows = missing NMJs, # = incorrect positioned NMJs.

Results

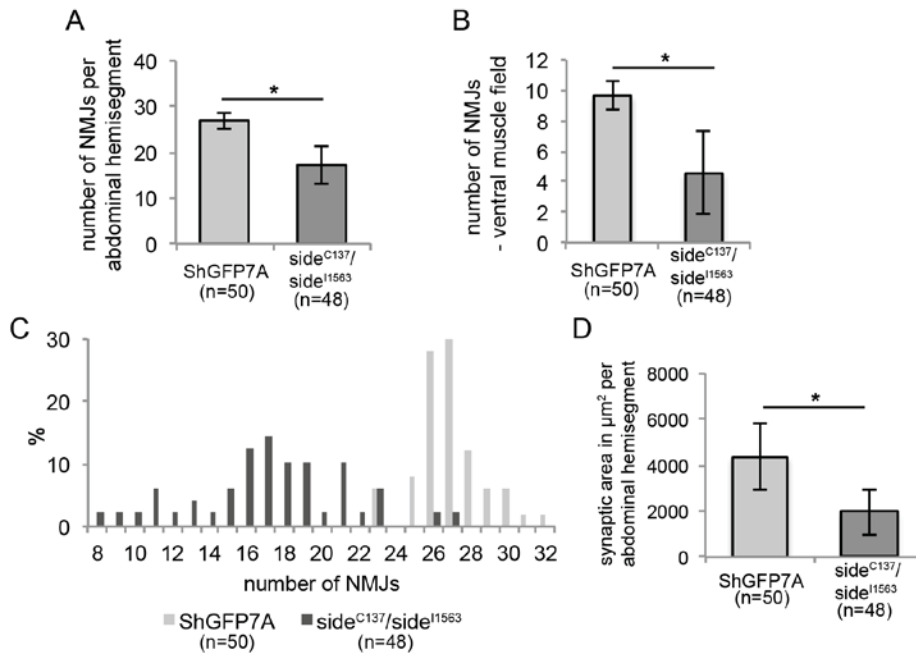


Fig 2. 43: Side loss of function larvae show a decreased number of NMJs.

Statistical analysis of innervation pattern of wild-type and *side* mutant larvae. A: Number of NMJs per abdominal hemisegment. B: Number of NMJs in the ventral muscle field. C: Distribution of NMJs per counted hemisegment. D: Area of all NMJs per hemisegment. A+B: *Side* mutant larvae exhibit less NMJs per abdominal hemisegment with the strongest decrease in the ventral muscle field in comparison to wild-type (p-values: less than 0.001 using students T-test). C+D: Additional, a decreased synaptic area (p-value: less than 0.001) and a wide distribution of NMJ number per hemisegment are detectable compared to wild-type.

Since the lack of muscle innervation induce muscular atrophy resulting in a reduction of muscle mass, strength and myofiber diameter in mammalian (Cisterna et al., 2014), the diameter of various non-innervated muscles was analysed. In *side* mutant larvae muscle 12 is not innervated to 38%. These 19 non-innervated muscles show a 14% lesser diameter compared to control muscles (Fig 2.44). Similar results were observed for muscles 9, 10, 18 and 8 (data not shown).

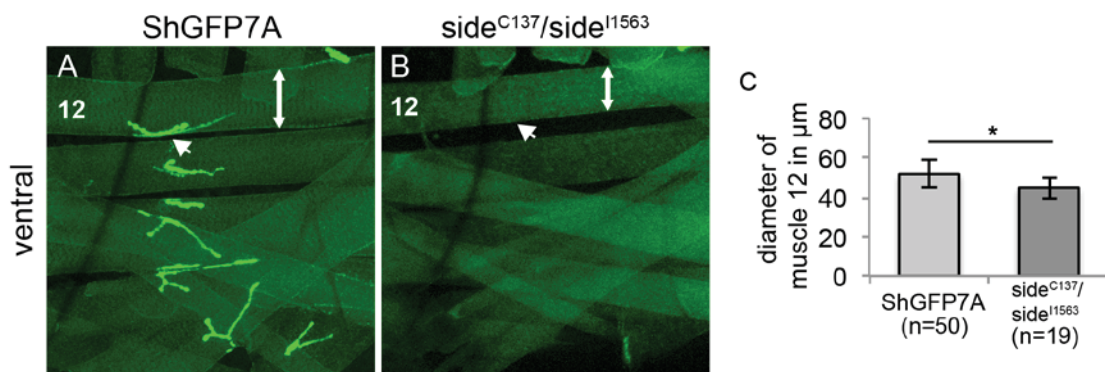


Fig 2. 44: Non-innervation leads to a smaller diameter of muscle 12.

Ventral muscle fields of ShGFP and *side* mutant third instar larvae and statistical analysis of muscle diameter. A: Ventral muscle field of a wild-type larva. B: Loss of *side* leads to non-innervation of amongst others muscle 12 in the ventral muscle field (arrow). C: Not innervated muscles exhibit a decreased muscle diameter (p-value: 0.008 using students T-test).

Results

For all analyses the post-synaptic marker ShGFP7A was used as read-out for mis-innervation. To ensure that the non-innervated muscles do also not exhibit pre-synapses, an antibody co-staining with anti-Synaptotagmin, a pre-synaptic marker (Littleton et al., 1993), and anti-GFP on larval filets was performed.

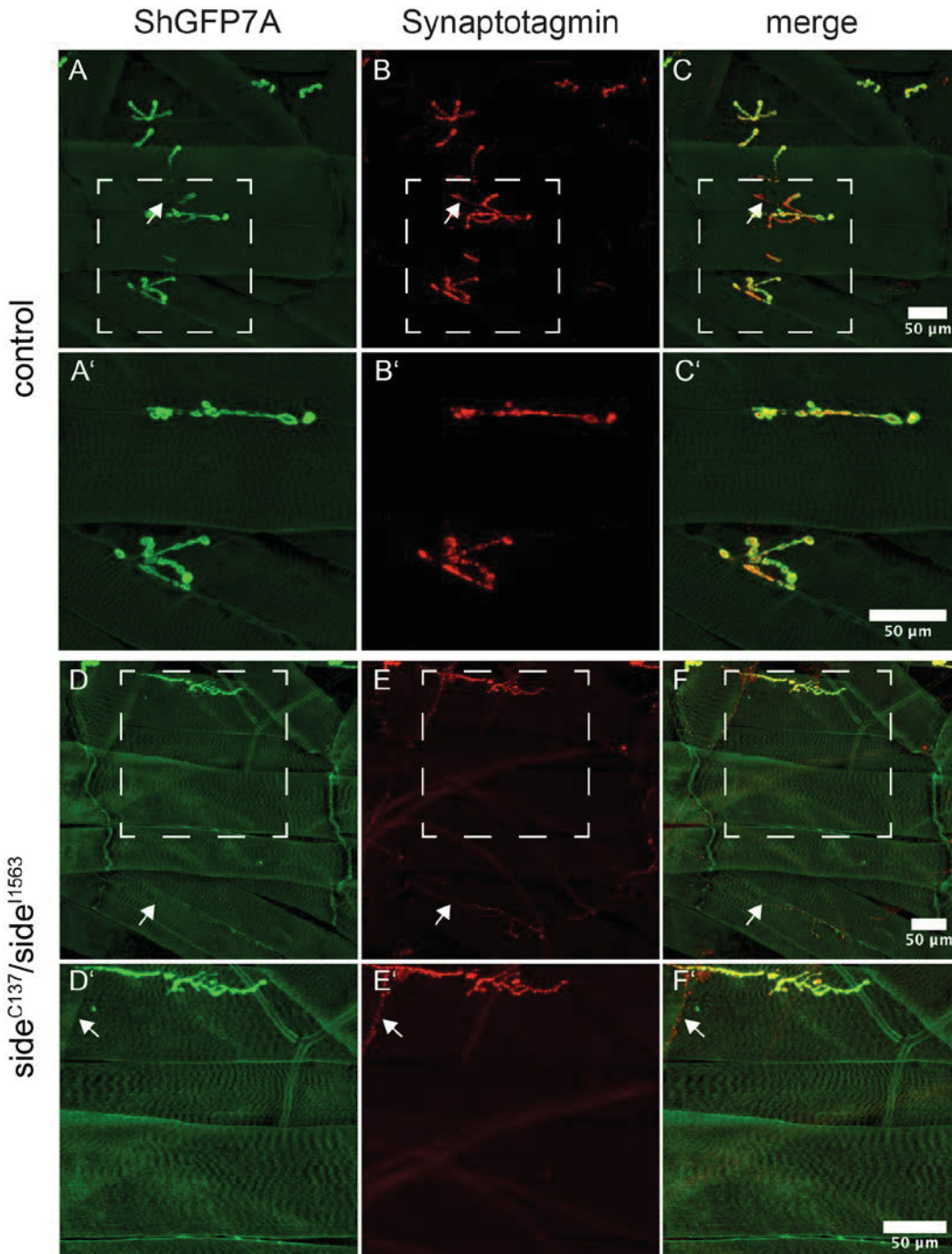


Fig 2. 45: Muscles without post-synapses exhibit also no type I pre-synaptic structures in *side* mutants.

Antibody stainings of wild-type and Side loss of function larval filets with anti-GFP (green) and anti-Synaptotagmin (red). A-F': In control and Side loss of function larva some mis-matches of pre-synaptic type II boutons and post-synaptic structures are visible (arrows). Ventral view.

Results

Control and mutant larvae show some mis-matches between the pre- and postsynaptic signals (arrows Fig 2.45). Interestingly, boutons without postsynaptic structure belong to the class of type II boutons based on their size. Bigger boutons, type I boutons, show no mis-matches between the GFP and Synaptotagmin signal.

To verify if the SN neurons are still present and therefore the observed innervation defects in *side* mutant larvae are indeed based on defasciculating defects with attached SN axons to ISN axons different analyses were carried out. First, *side* heterozygous and homozygous embryos were stained with anti-FasII and anti-BarH1/2 to mark all motor axons and the cell bodies of the SNa neurons, respectively. Homozygous embryos show no conspicuous different BarH1/2 expression pattern compared to heterozygous embryos (Fig 2.46). Therefore, the SNa neurons are still present in late embryos. In order to work out, if they survive up to the third instar, brains of L3 larvae were analysed.

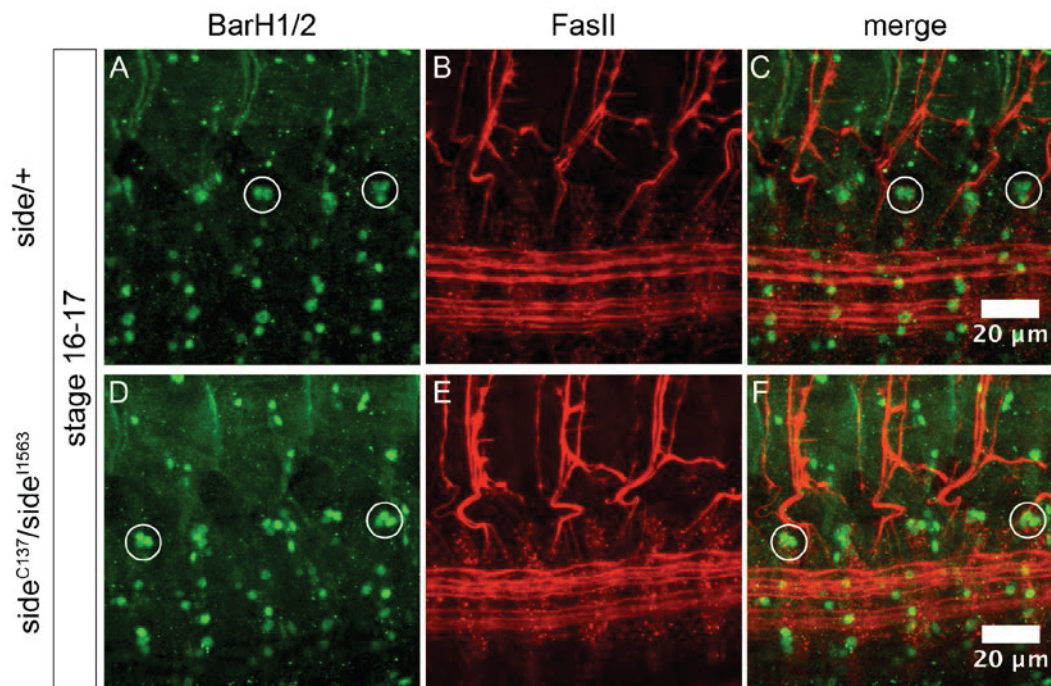


Fig 2. 46: In *side* homozygous embryos SNa neurons are still present.

Co-stainings of *side* heterozygous and homozygous embryos with anti-BarH1/2 (green) and anti-FasII (red). A-F: Heterozygous and homozygous embryos show a similar number of SNa neurons (circles). Ventro-lateral view.

Using again the effector line UAS-DsRed driven by OK371-Gal4 motoneurons and their axons are marked in larval CNS. The control and mutant brains show a regular staining in each neuromere (Fig 2.47 A+B) and the close up demonstrates again no

Results

conspicuous difference in number of motoneurons suggesting that motoneurons do not die during the larval stages in *side* mutants (Fig 2.47 A'+B').

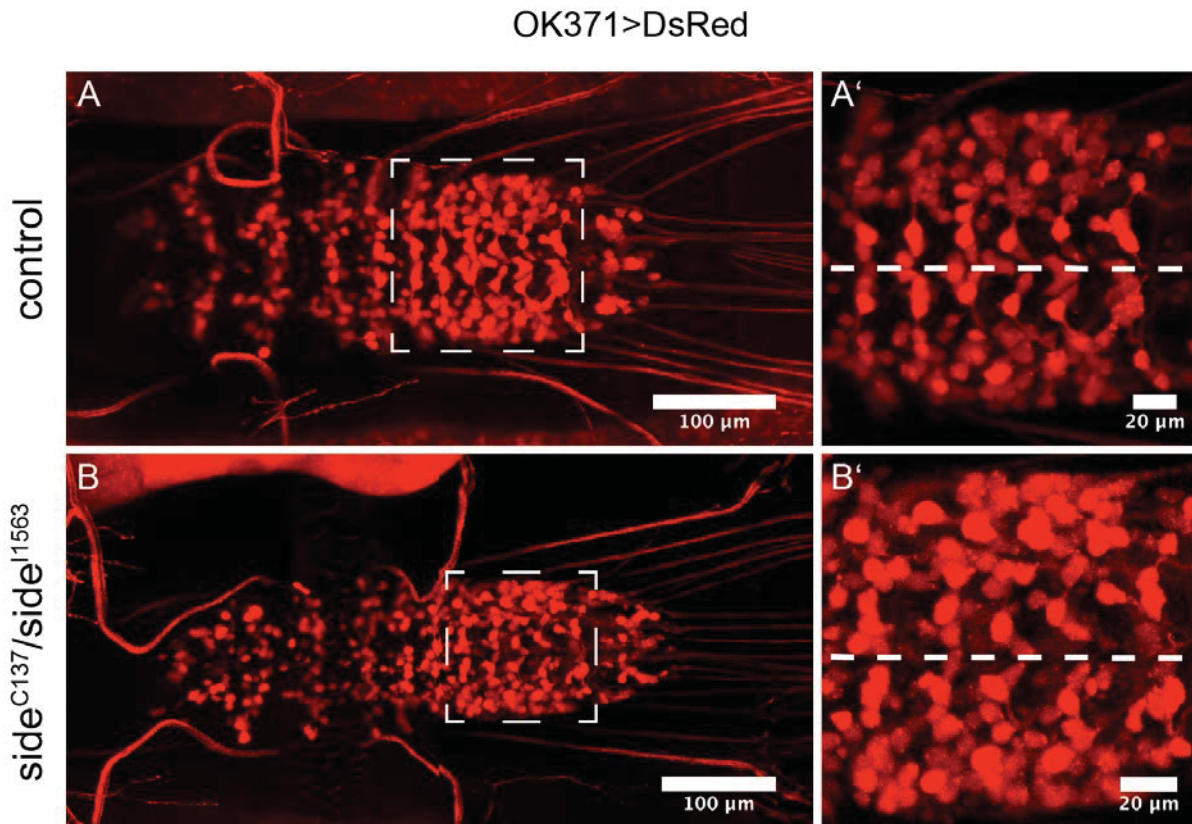


Fig 2. 47: Motoneurons survive up to third instar in *side* homozygous larva.

Confocal images of CNS of wild-type ($w;OK371-Gal4,ShGFP1A/+;ShGFP7A,UAS-DsRed$) and *Side* loss of function larvae ($w;OK371-Gal4/+;side^{C137},ShGFP7A/side^{11563},ShGFP7A,UAS-DsRed$) marked by $OK371>dsRed$. A+A': CNS of a control third instar larva. B+B': *Side* mutant larvae show the same number of motoneurons compared to wild-type larvae. Broken line: midline.

Figure 2.47 demonstrates that motor axons leave the brain to innervate the muscles in wild-type as well as in *side* mutant larvae. However, it cannot be ensured that the SN neurons also send out motor axons. To address this question, the diameter of the ISN at the level of muscle 12 was analysed. Remarkably, the ISN has an around 2.2-fold thicker diameter in *side* mutant larvae compared to control larvae (*side*= 7.4μm, ShGFP= 3.3μm) (Fig 2.48). Taken together, the SN neurons survive and send out axons, which are still attached to the ISN in third instar larvae.

Results

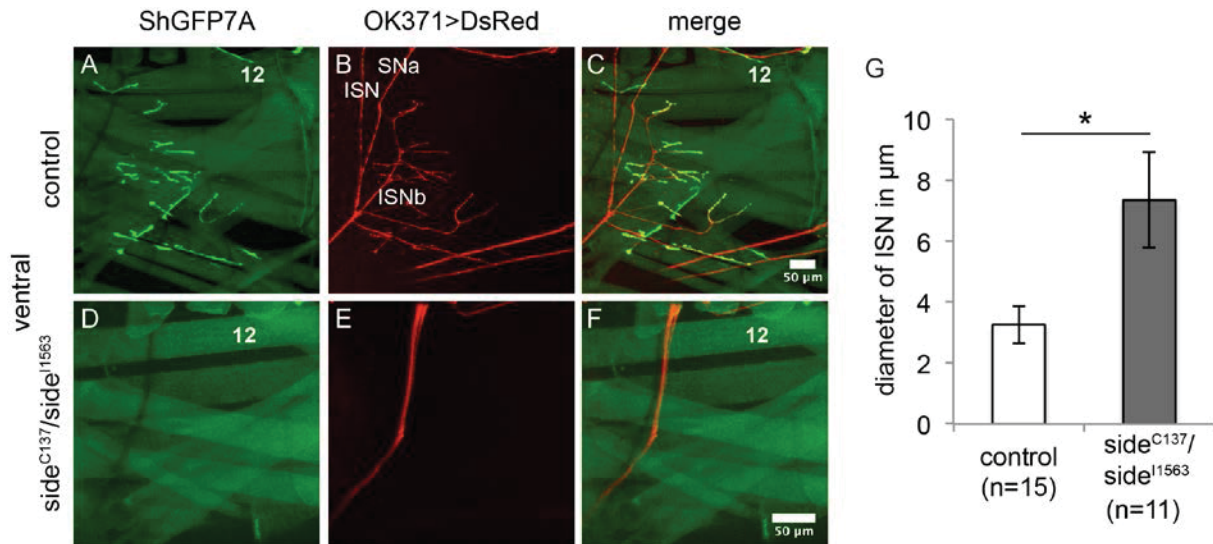


Fig 2. 48: ISN of Side loss of function larvae exhibit a thicker diameter.

NJMs (green) and motor axons (red) of ventral muscle fields of wild-type (w;OK371-Gal4,ShGFP1A/+;ShGFP7A,UAS-DsRed) and *side* mutant larvae (w;OK371-Gal4/+; *side*^{C137},ShGFP7A/*side*^{I1563},ShGFP7A,UAS-DsRed) and statistical analysis of ISN diameter. A-C: In wild-type larvae SNa and ISNb defasciculate from ISN to innervate the ventral muscle field and lateral muscle field. D-F: In *Side* loss of function larvae SNa and ISNb do not defasciculate from the ISN and miss to innervate ventral and lateral muscles. G: Defasciculation defects lead to a thicker diameter of the ISN in *side* mutants compared to wild-type (p-value: less than 0.001 using students T-test).

2.2.2 Muscle specific overexpression of *side* leads to innervation defects in larvae

Mis-expression of *Side* on a subset of muscles fibres during the targeting period could overturn targeting preferences of motor axons resulting in the formation of additional ectopic NMJs. However, mis-expression of *Side* at later stages show no effects (De Jong et al., 2005). Using the driver-line *mef2-Gal4,ShGFP7A* it is possible to overexpress *Side* on all muscles during targeting period causing mis-innervations and ectopic NMJs of the larval somatic musculature in comparison to wild-type larvae (Fig 2.49). In contrast to *side* mutant larvae, the dorsal muscle field shows the strongest defects (Fig 2.49 D). In *Side* gain of function larvae, the ventral and lateral muscle fields exhibit less obvious defects (Fig 2.49 E+F). To characterise the innervation defects, the same statistical analyses as for *side* mutant larvae were performed and again, ShGFP serves as control (Fig 2.50). Larvae overexpressing *Side* muscle-specifically have around 18 NMJs per hemi-segment instead of 26 for the controls (Fig 2.50 A). As expected, the dorsal muscle field shows the biggest percentage difference in the number of NMJs. The control larvae exhibit 5 dorsal NMJs, but the overexpression larvae have only on average 2.6 NMJs in the dorsal muscle field (Fig 2.50 B).

Results

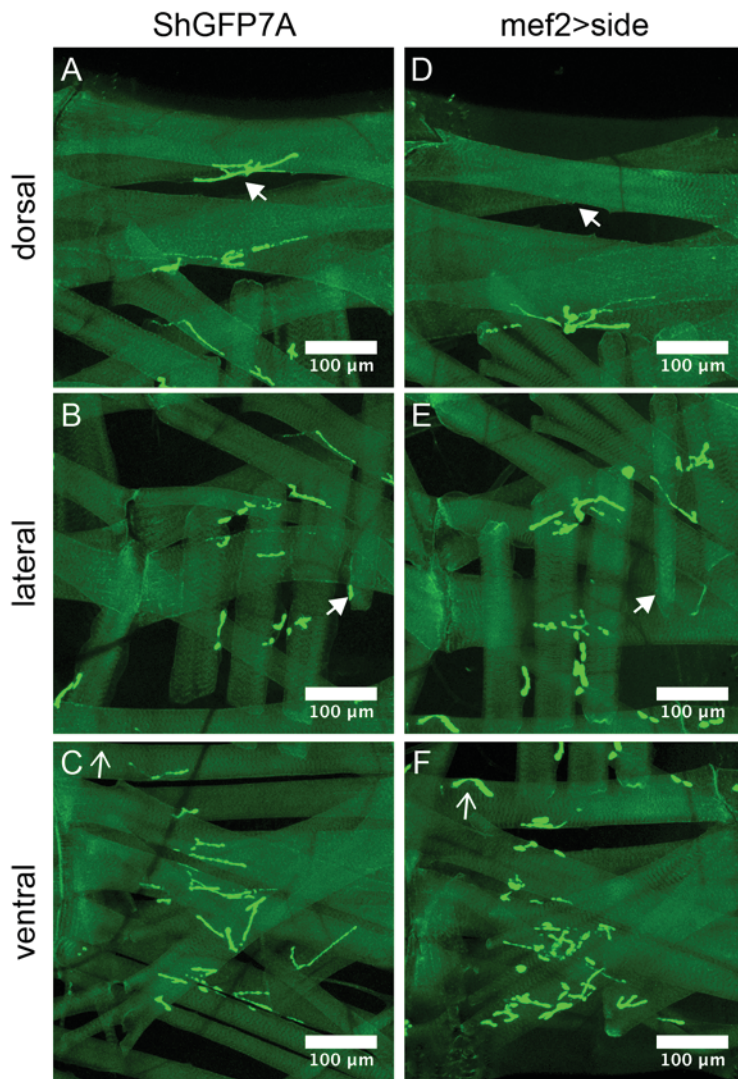


Fig 2. 49: Muscle specific overexpression of Side leads to innervation defects.

NMJs of ventral, lateral and dorsal muscle fields of a wild-type and Side gain of function ($w;+; mef2-Gal4/UAS-side$) larvae. A-C: Control larva. D+E: Overexpression of Side leads to missing NMJs on muscles 1, 9 and 24 compared to wild-type (arrows). F: Muscle 12 exhibits in the overexpression larva an ectopic synapse in comparison to wild-type (empty arrow).

Similar to *side* mutants, a strong variance in the number of NMJs in the 50 analysed hemi-segments are visible (Fig 2.50 C). Segments exhibit a number of NMJs between 14 and 23 (Fig 2.50 C). Additional, as expected, Side gain of function larvae show also a significant smaller synaptic area than the ShGFP larvae ($2676\mu m^2$ vs $4353\mu m^2$) (Fig 2.50 D).

Results

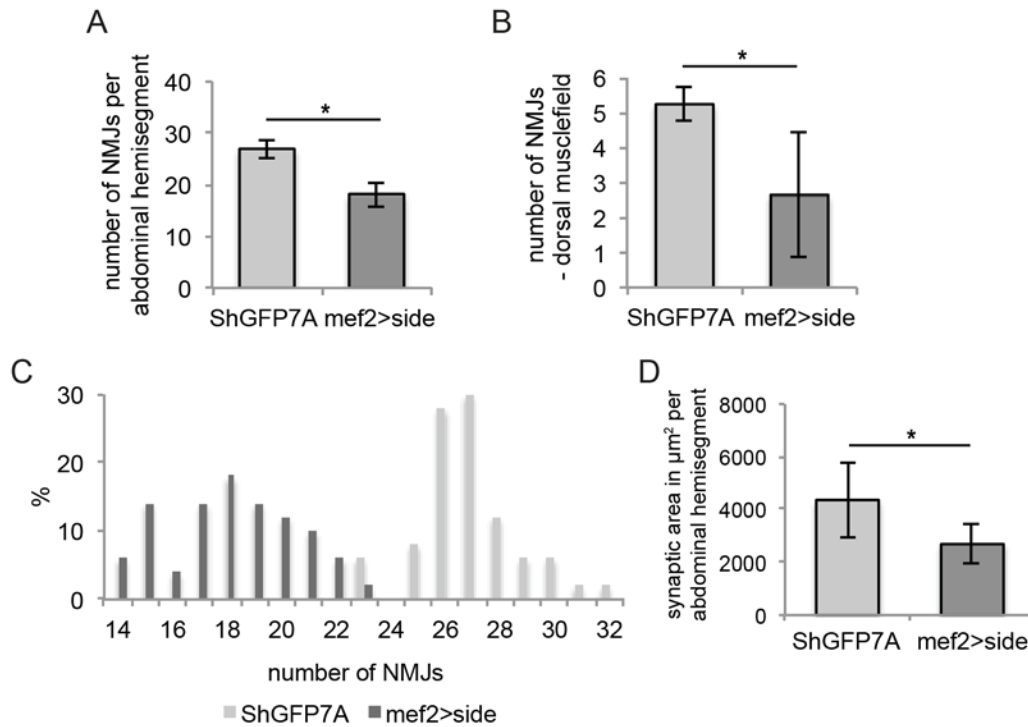


Fig 2. 50: Side overexpression larvae exhibit less NMJs.

Statistical analysis of innervation pattern in wild-type and Side gain of function larvae. A: Number of NMJs per abdominal hemisegment. B: Number of NMJs in the dorsal muscle field. C: Distribution of NMJs per counted abdominal hemisegment. D: Area of all NMJs per abdominal hemisegment. A-D: Muscle specific overexpression of Side results in a decreased number of NMJs per hemisegment (p-value: less than 0.001 using students T-test). Thereby, the dorsal muscle field show the strongest defects (p-value: less than 0.001). Additional, a decreased synaptic area (p-value: less than 0.001) and a wide distribution of NMJ number per hemisegment are detectable compared to wild-type.

Since it is not possible with the Gal4/UAS-system to independently express Side in muscles and DsRed in nerves, antibody-staining with embryos overexpressing Sidestep were used to analyse the projections of the axons and to find a possible reason for the innervation defects in larvae (Fig 2.51). In the control embryos (ShGFP), motor axons stained with Fasciclin II are grown out from the CNS to the periphery and the SNa and SNC defasciculate from the ISN to innervate the ventral and lateral muscle field. The ISN exhibits two branch points and reaches the dorsal muscles (Fig 2.51 A-C). In the overexpression embryos, motor axons also grow out of the CNS and defasciculate. However, gain of Side causes missing branch points of the ISN and results often in a truncation phenotype compared to wild-type (asterisks Fig 2.51). Axons stop to growth further on their stereotypic trajectories to the dorsal muscles and cross frequently the segmental boundary (arrows Fig 2.51 D-F).

Results

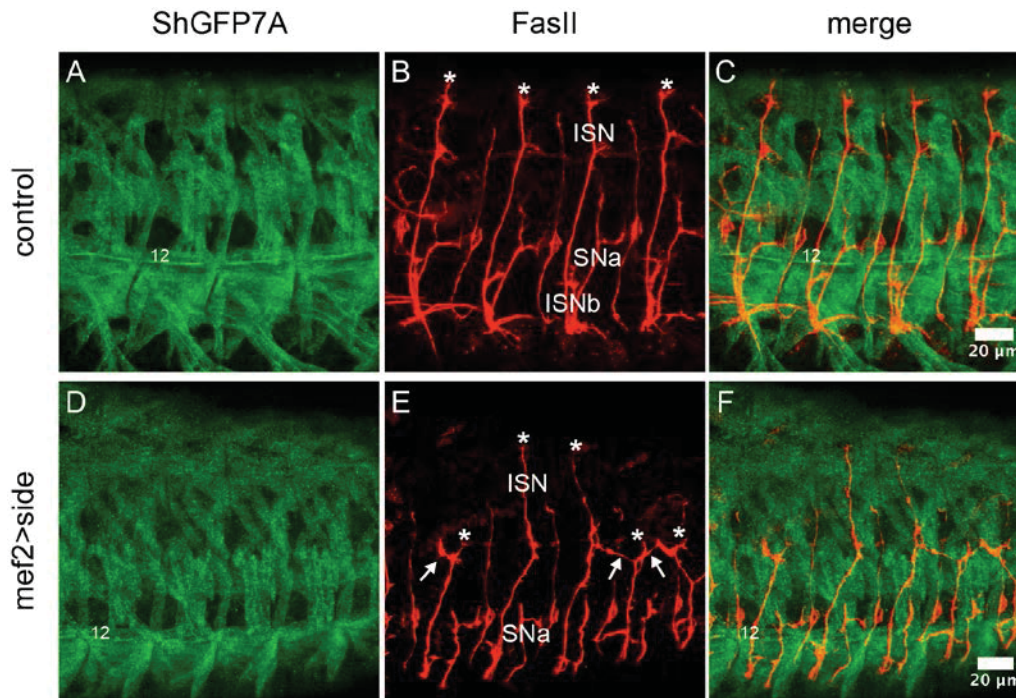


Fig 2. 51: In Side gain of function embryos motor axons are attracted too early.

Confocal images of antibody stainings of wild-type and Side overexpression embryos using anti-GFP (green) and anti-FasII (red). A-C: In control embryos ISN reaches the dorsal muscles field to innervate the muscles 1, 2, 9 and 10 (asterisks). D-F: In embryos overexpressing Side muscle specifically ISN is attracted to muscles left and right of the path (arrows) resulting in truncation of the ISN in some segments (asterisks). 12 = muscle 12. A-F: Lateral view.

Analysing the larval innervation pattern, it is again obvious that non-innervated muscles are thinner than innervated muscles. In gain of function larvae, the muscles pairs 1+9 and 2+10 are not innervated to 70% and 36%, respectively (Fig 2.52). The 35 non-innervated muscles 9 and the 18 non-innervated muscles 10 exhibit a significant smaller diameter compared to control muscles (Fig 2.52).

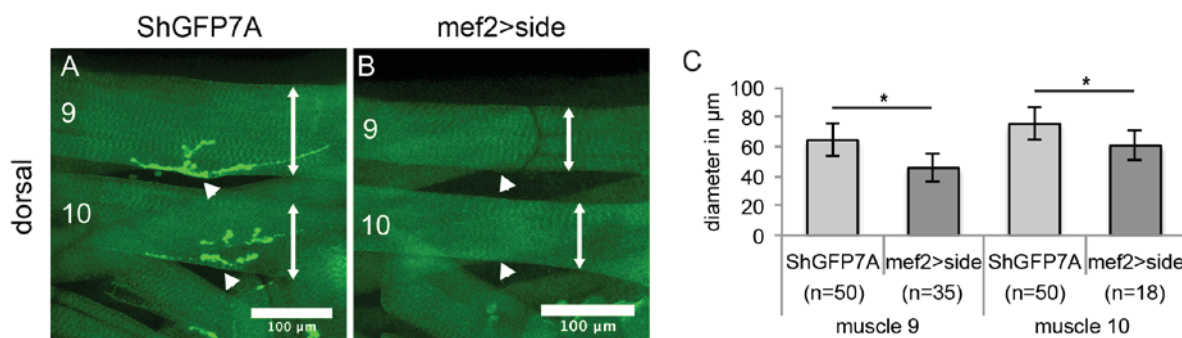


Fig 2. 52: Non-innervated muscles 9 and 10 exhibit a decreased diameter.

Dorsal muscle fields of ShGFP and Side gain of function larvae and statistical analysis of muscle diameter. A: Dorsal muscle field of a wild-type larva. B: Overexpression of Side causes non-innervation of amongst others muscles 9 and 10 (arrowheads). C: Non-innervated muscles exhibit a decreased muscle diameter compared to innervated control muscles (p-value: 0.003 or less using students T-Test).

Results

Additionally it was also examined, if non-innervated muscles exhibit pre-synaptic innervation using again anti-Synaptotagmin and anti-GFP for an antibody staining of larval filets. Control and Side gain of function larvae show again some mis-matches between pre-synaptic structures marked by anti-Synaptotagmin and post-synaptic structures marked by ShGFP (arrows Fig 2.53).

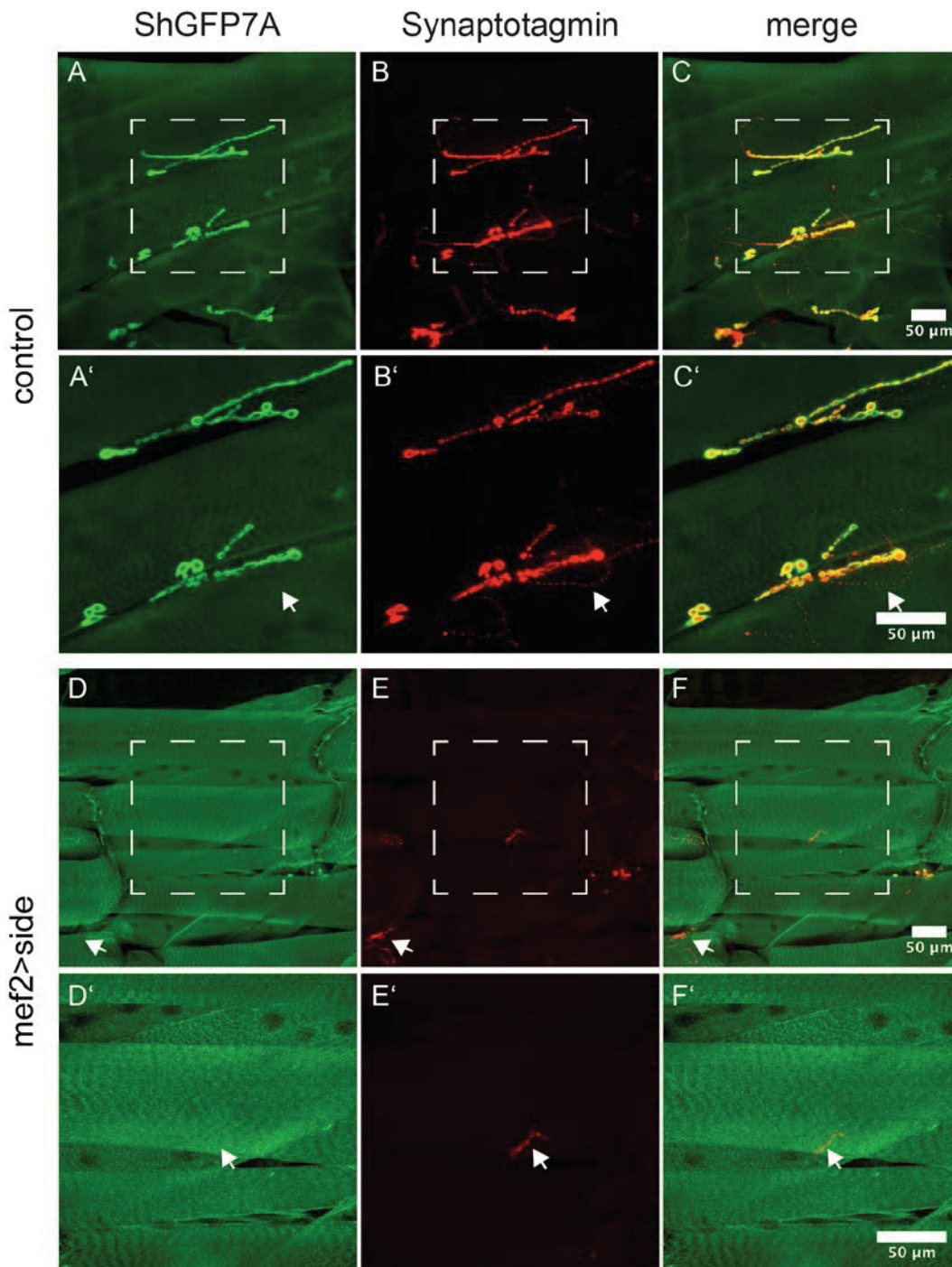


Fig 2. 53: Muscles without post-synapses exhibit also no pre-synaptic structures in Side gain of function larvae.

Antibody stainings of wild-type and Side overexpression larval filets with anti-GFP (green) and anti-Synaptotagmin (red). A-F': In control and Side gain of function larvae some mis-matches of pre-synaptic signal and post-synaptic structures are detectable (arrows).

Results

2.2.3 Side loss- and gain of function larvae show locomotion defects

Does the observed innervation defects of larval somatic muscles results in locomotion defects? To address this question, behaviour of larvae were analysed using locomotion assays comparing crawling speed and duration of peristaltic waves. To get more precise information about the motion, sequence video analysis with a high-speed camera were performed. As controls ShGFP larvae were used.

For the first locomotion assay the larvae were placed in the middle of an agar plate and the crawling larvae were record for one minute and three minutes. Movies were analysed with the software Tracker and Fiji to get the distance covered by the larvae during one minute. Control larvae crawl on average 5.9cm per minute. In contrast, mutant larvae cover only 2.7cm (Fig 2.54). A similar result is detectable for overexpression larvae with a covered distance of 3.6cm per minute. Comparing crawling tracks it becomes clear that the control larvae crawl more targeted than the mutant and overexpression larvae (Fig 2.54 A-C).

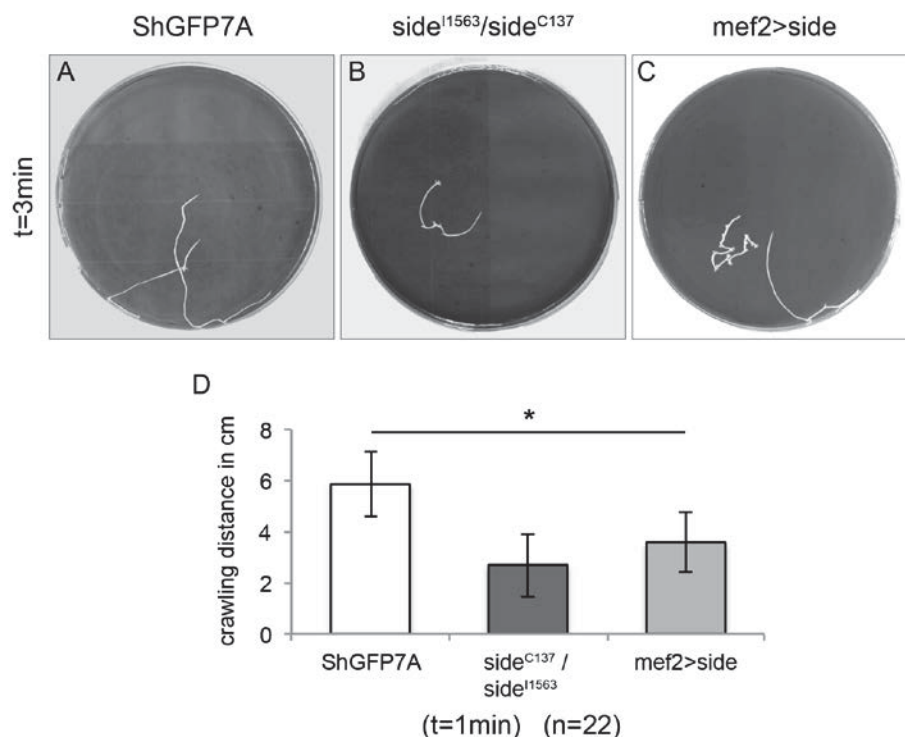


Fig 2. 54: Side loss- and gain of function larvae crawl slower.

Crawling tracks of wild-type and *side* mutant and overexpressing larvae and statistical analysis of crawling distances. A: Control larvae crawl purposefully forward. B+C: Side gain- and loss of function larvae perform circular crawls. D: Control larvae reach significant longer distances during one minute performing time compared to Side loss- and gain of function larvae (p-values: less than 0.001 using students T-test).

Results

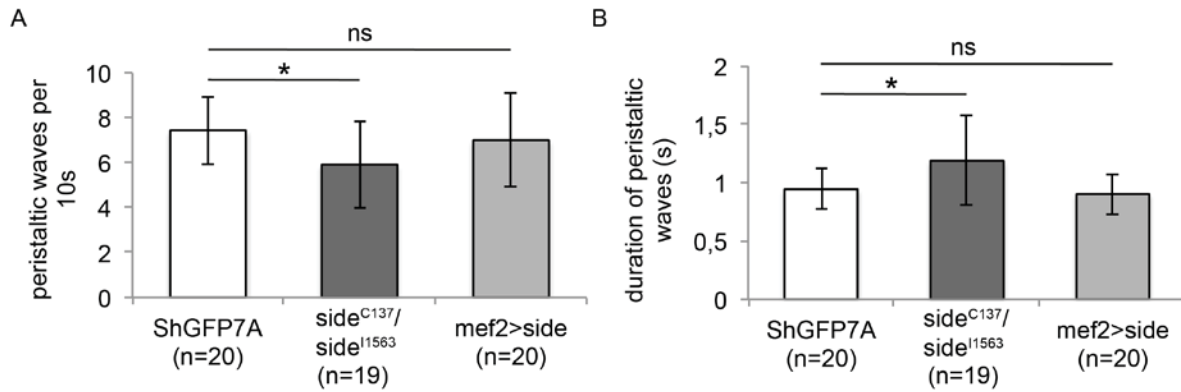


Fig 2. 55: Side loss of function larvae perform longer peristaltic waves.

Statistical analysis of number of peristaltic waves during 10 seconds and of duration per peristaltic wave. A: *Side* mutants perform significant fewer waves per 10 seconds compared to wild-type (p-value: 0.018 using students T-test). Side overexpression larvae show no difference (p-value: 0.46). B: Peristaltic waves of Side loss of function larvae take significant longer compared to wild-type (p-value: 0.018). Larvae overexpressing Side show again no significant difference in comparison to wild-type (p-value: 0.46).

To study the duration of the peristaltic waves, larvae were recorded in lateral view and analysed with the software Vcode and Vdata. On average, one single peristaltic wave of mutant larvae takes longer in comparison to controls (*side*= 1.2 seconds, ShGFP= 0.9 seconds) resulting in less peristaltic waves per 10 seconds compared to control larvae (*side*= 5.9, ShGFP= 7.44) (Fig 2.55). Gain of Side causes no significant differences compared to control larvae analysing the number of peristaltic waves per 10 seconds (*mef2>side*= 7, ShGFP= 7.44) and the duration of one wave (*mef2>side*= 0.9, ShGFP= 0.9) (Fig 2.55).

Analysing high-speed movies from lateral and dorsal views it is detectable that control larvae always have tight contact with the substrate and only the head and the rear were raised slightly during the movement (Fig 2.56). Peristaltic contraction begins with the elongation and subsequent downward hooking of the head (Fig 2.56 A-F). Simultaneously, the rear raises and the ventral part is pushed afterwards on the substrate (Fig 2.56 C-F) resulting in a wandering of the peristaltic contraction from posterior to anterior (Fig 2.56 F-L) (Berrigan and Pepin, 1995). Additional, from the dorsal perspective it is nicely to see that the larvae crawl forward in a straight line (Fig 2.56).

Results

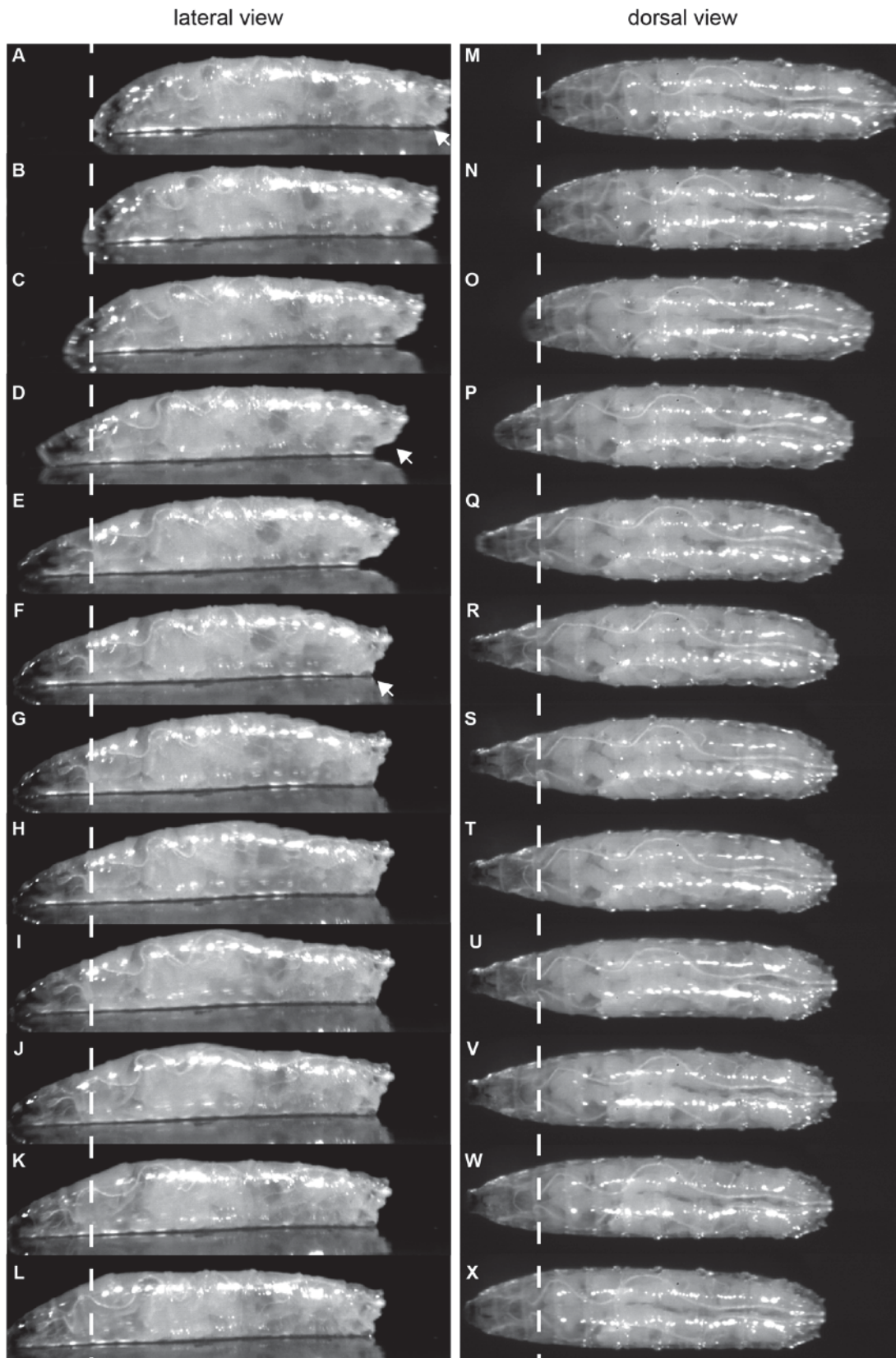


Fig 2. 56: Control larvae crawl straight forward with tight contact to the substrate.

Peristaltic waves of ShGFP control larvae recorded from lateral and dorsal view. A-F+M-R: In the beginning the larvae raise their rear and elongate their head (arrows). F: The peristaltic wave starts with pushing the ventral part of their rear on the substrate. G-L+S-X: Peristaltic wave wanders from posterior to anterior. At the same time, the larvae hook in the substrate with its mouth hooks resulting in straight forward crawling on the agarose.

Results

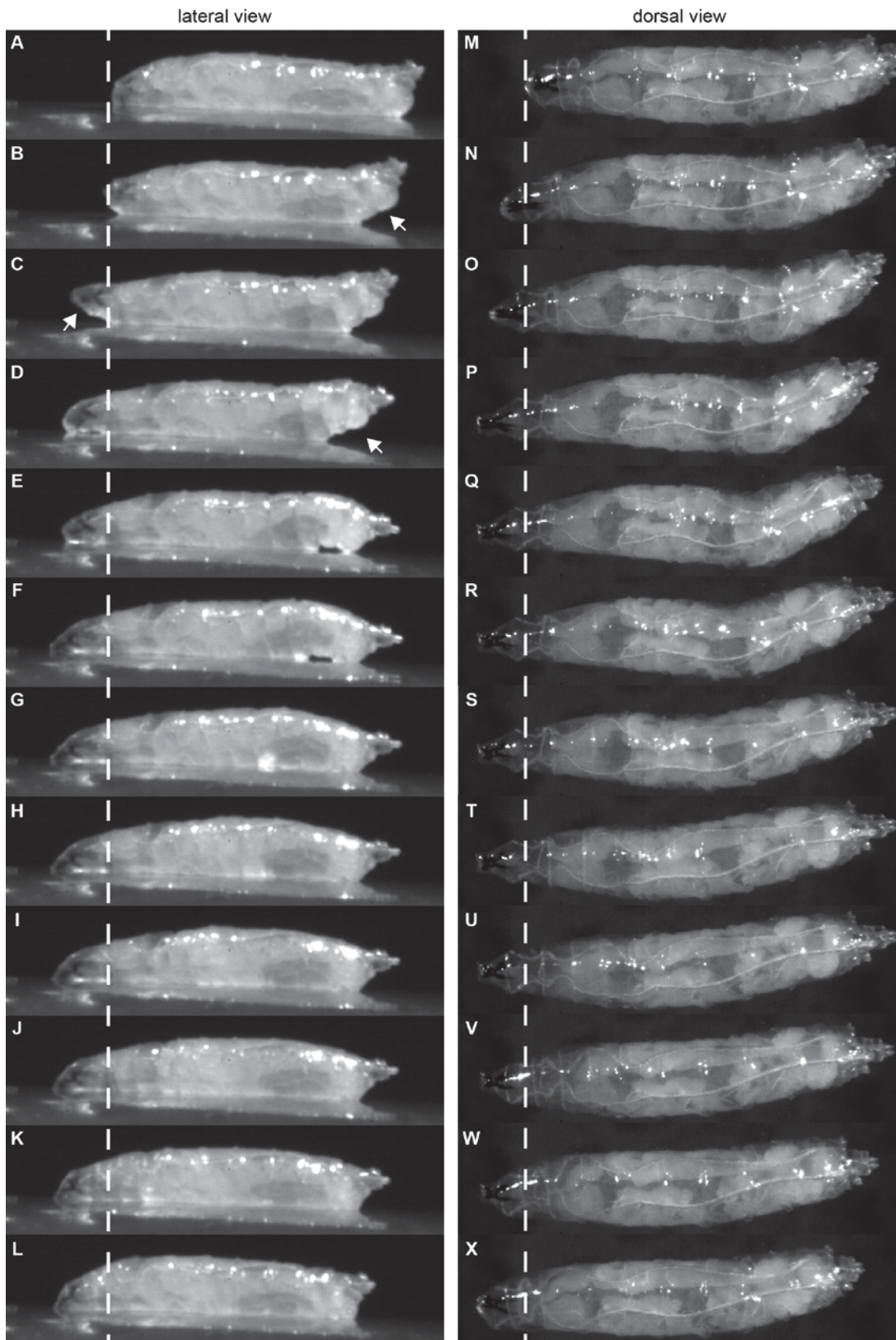


Fig 2. 57: Side loss of function larvae lose contact to the substrate during crawling.

Peristaltic waves of *side* mutant larvae recorded from lateral and dorsal. A-D: Side loss of function larvae ($w;+;side^{C137}/side^{I1563}$) raise their anterior and posterior end stronger than wild-type larvae (arrows). E-L: Peristaltic waves start also by pressing the ventral site of the rear on the substrate, but larvae lose contact to the substrate during the peristaltic waves wander from posterior to anterior. M-X: Form dorsal view, *side* mutant larvae show during crawling a rotation of the dorsal body part to ventral.

Results

Side loss of function larvae are also able to perform peristaltic waves, but recorded from lateral and dorsal view multiple phenotypes are visible (Fig. 2.57 and supplemental movies S3 and S4). Mutant larvae raise their rear higher than control larvae (55% (n=20)) resulting in a loss of contact between the ventral part of the abdominal segments and the substrate after pressing the ventral part of the rear on it (60% (n=20)) (arrows Fig 2.57 B+D). Additionally, half of the tested larvae lift their head conspicuous in contrast to control larvae (Fig 2.57 B, F and L). From dorsal view it is also notable that the whole posterior body part of some larvae rotate to ventral after pressing the posterior end onto the substrate (15% (n=20)) (Fig 2.57 O-R).

Analysing high-speed movies of Side gain of function larvae stronger phenotypes compared to the mutants are detectable (Fig 2.58 and supplemental movies S5 and S6). Peristaltic wave starts also by lifting the rear and pressing the ventral side of it on the substrate. Simultaneously, overexpression larvae elongate their head exuberantly in comparison to the control and the mutant larvae (84% (n=25) (Fig 2.58 B-H). Additional, Side gain of function larvae lose the contact to the substrate during crawling similar to the mutants (64% (n=25)). Movies recorded from dorsal demonstrate furthermore that the overexpression larvae rotate along the dorso-ventral axis during the peristaltic wave wanders from anterior to posterior resulting in a body shape like the letter "S" (52% (n=25) (Fig 2.58 Q-T).

Taken together, lack and gain of Side cause mis-innervation of larval somatic muscles resulting in locomotion phenotypes which are apparent both in the crawling assay and in the high-speed movies.

Results

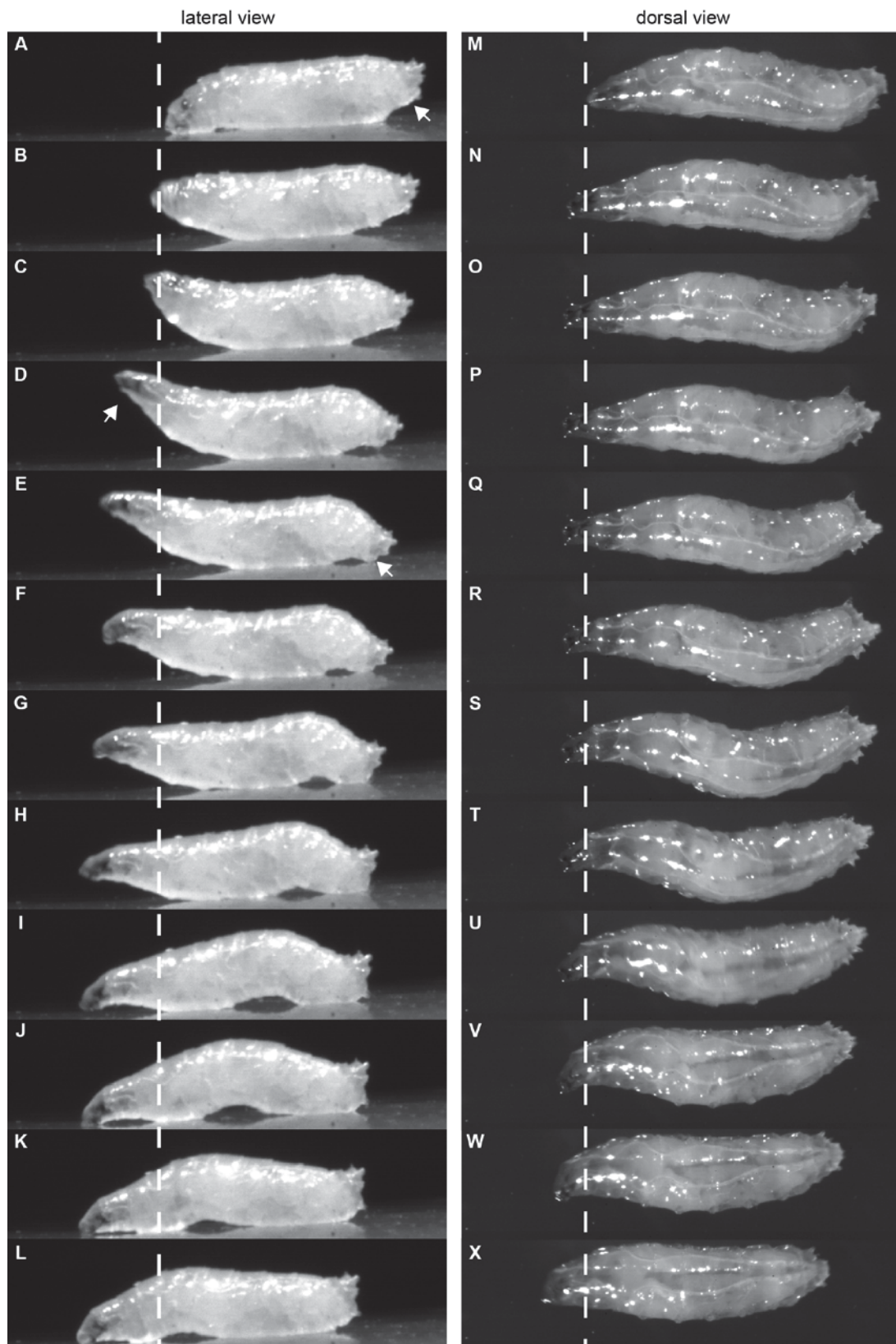


Fig 2. 58: Side gain of function larvae strongly elongate their anterior end during crawling.

Peristaltic waves of larvae overexpressing Side recorded from lateral and dorsal view. A-H: Overexpression larvae elongate and lift their anterior end exuberantly in comparison to wild-type. E-L: During wandering of the peristaltic wave from posterior to anterior larvae lose contact to the agarose substrate. M-X: Larvae rotate during crawling along the dorso-ventral axis and show a letter "S" like body shape.

Results

2.3 Adult phenotypes of Side loss- and gain function flies

Is Side a key-regulator of the neuromuscular system establishing during metamorphosis? To address this question, it was analysed if *side* mutant flies and flies overexpressing Side muscle specific exhibit an adult phenotype using four different locomotion assays in order to test if the flies are able to walk, to climb, to fly and to take off. Recording movies with a high-speed camera made it possible to get further information about the adult motion behaviour. Additionally, the innervation pattern of the adult legs and the indirect flight musculature were analysed. Lack of Side should result in innervation errors of adult muscles if it is required during metamorphosis.

In the beginning it was tested how many flies with a Side loss of function genotype reach the adult stage and thus are available for the locomotion assays. For this, number of mutant pupae and adult flies were counted and compared with the number of heterozygous flies. Only approximately 2.5% of the pupae and only around 1% of the hatched flies have the genotype $side^{C137}/side^{I1563}$. Consequently, 60% of *side* mutant flies are not able to hatch out of the pupae.

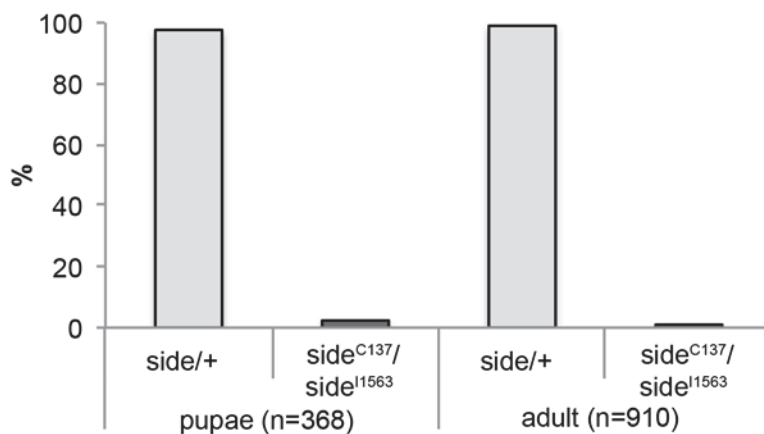


Fig 2. 59: Mutations in the *side* gene are lethal.

Statistical analysis of lethality and ability to hatch of Side loss of function flies. Only around 2.5% of pupae and 1% of adults exhibit the genotype $side^{C137}/side^{I1563}$.

In contrast to the Side loss of function flies, Side gain of function flies ($mef2>side$) are homozygous viable and therefore, all larvae and pupae reach the adulthood.

Results

2.3.1 *Side* mutant and overexpression flies exhibit locomotion defects

In all experiments, ShGFP serve as control for mutant and overexpression flies. Assays were performed as described in Materials and Methods (4.2.9 - 4.2.12). To investigate if *Side* loss of function and gain of function flies are able to fly, flies were dropped from an empty tube onto the lab bench (Fig 2.60 A) (Newquist et al., 2013). All control flies are able to fly, but only 8% of the *side* mutants and 23% overexpression flies can escape by flying (Fig 2.60 A).

Using the island assay it is possible to test if flies can take off from an island surrounded by water (Fig 2.60 B) (Schmidt et al., 2012). Control flies are able to take off to 82% after 30 seconds and 91% after 120 seconds. Not a single mutant fly is able to take off during the two minutes performing time and only 14% of the overexpression flies depart from the island (Fig 2.60 B). For more detailed analyses why flies are not able to vanish from the island movies with a high-speed camera were performed.

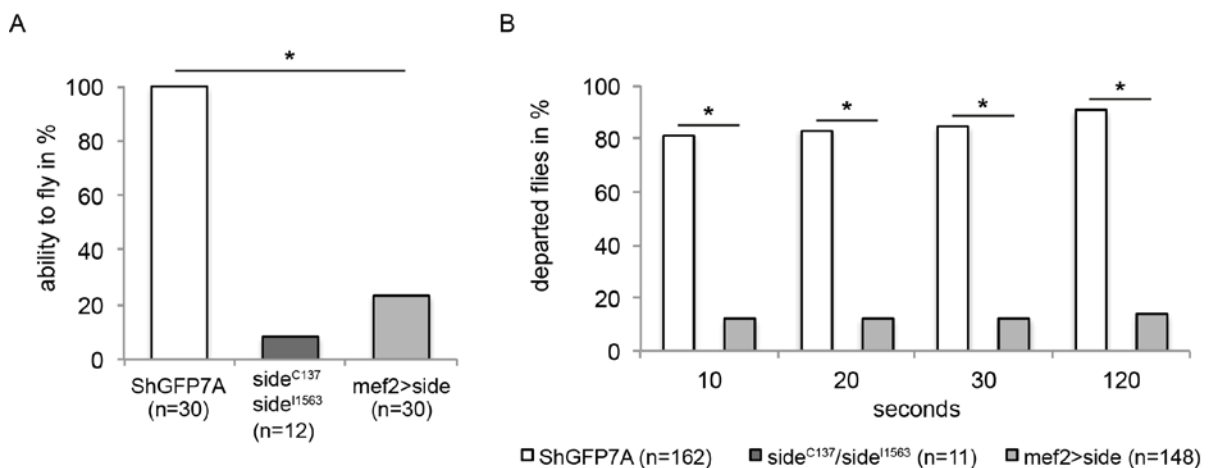


Fig 2. 60: Side gain- and loss of function flies are not able to fly and to take-off.

A: Dropping assay. Significant less mutant and overexpression flies are able to fly in comparison to the control flies (p-value: less than 0.001 using Fisher exact test). B: Island assay. No mutant fly is able to take off from the island within 120 seconds, while 14% of gain of function flies can vanish (p-value to each time point in comparison to control: less than 0.001 using Fisher exact test).

High-speed movies demonstrate that control flies start to take off from the island by lifting their wings (arrows Fig 2.61 A-B and supplemental movie S7). Subsequently, flies remove the prothoracic legs (1st leg pair) and metathoracic legs (3rd leg pair) from the ground (arrowhead Fig 2.61 D) and take off by jumping using the mesothoracic (2nd leg pair) legs (asterisks Fig 2.61 D-H). Simultaneously, flies move their wings downwards and start in this way the first wing beat (Fig 2.61 C-H). During the second wing beat, flies lose completely the contact to the island.

Results

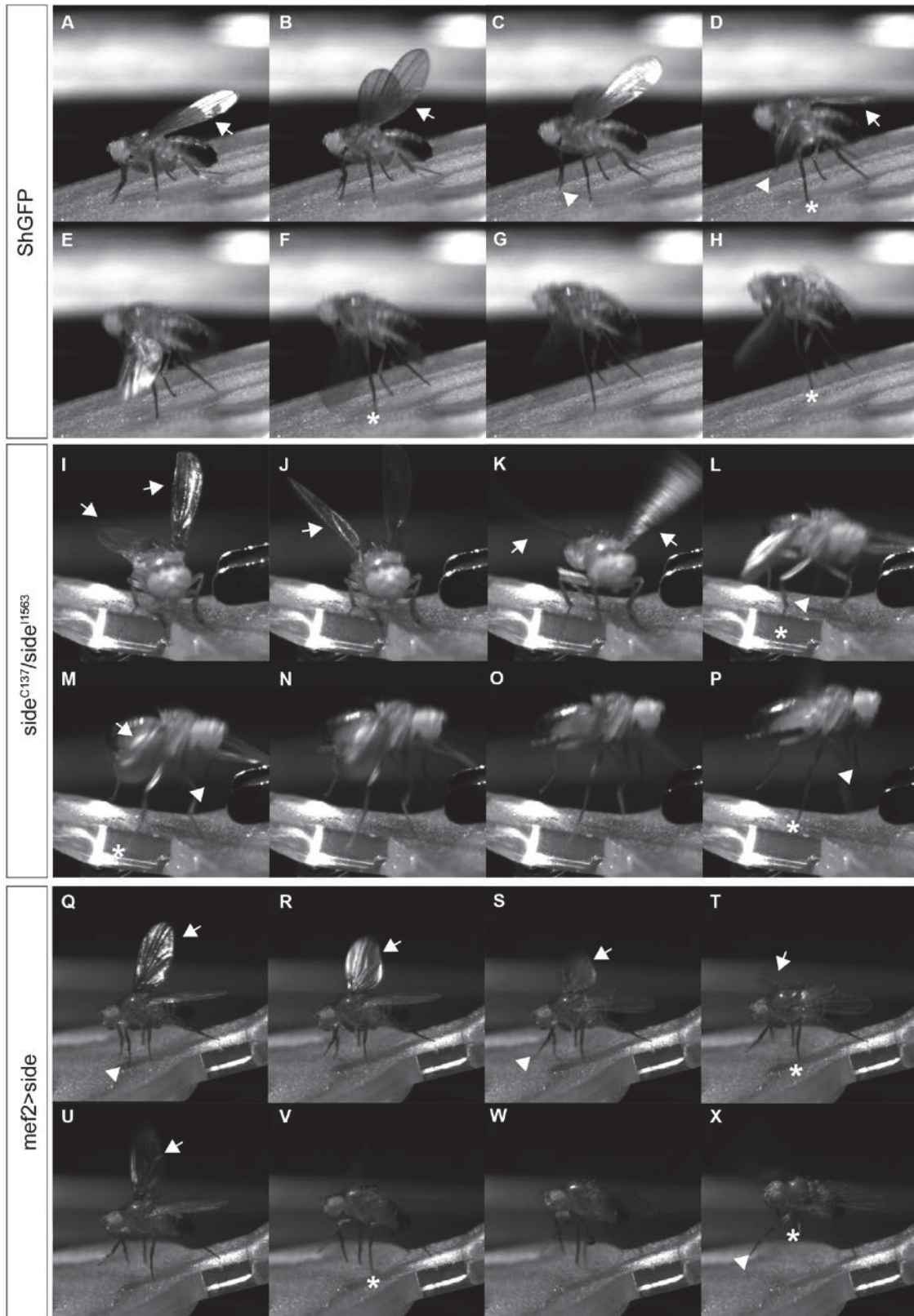


Fig 2. 61: *Side* mutant and overexpression flies show an altered take-off sequence.

Time series of high-speed movies of take-offs of wild-type (A-H), *Side* loss (I-P) and gain (Q-X) of function flies. A+B: Control flies start take-off with elevating their wings (arrows). C+D: Afterwards, flies lift synchronously their first and third legs and depress their wings (arrows and arrowheads). E-H: Flies take off by jumping using the second leg pair. I+J: *Side* loss of function fly also starts to take-off by lifting its wings, but moves them asynchronously. L+M: In contrast to wild-type, wings were already lowered down to the half of the body, when the fly starts lifting its pro- and metathoracic legs (arrowheads). Mesothoracic legs have still contact with the ground (asterisks). N-P: The asymmetric

Results

movement of the wings leads to a rotation around the anterior-posterior axis of the fly during the take-off. Q+R: Gain of function flies can only lift one of the two wings. S+T: During depressing the wings only pro-thoracic legs are elevated (arrows and arrowhead). Second (asterisk) and third legs have still contact to the island. U-X: Moving only one wing leads to a rotation around the ventro-dorsal axis of the gain of function flies during take-off.

High-speed movies of mutant flies support the observed inability to take off using the island assay. However, one fly departed from the island after nudging with a forceps (Fig 2.61 I-P and supplemental movie S8). The mutant fly starts to take off also by elevating its wings, but it is not able to move them synchronously (Fig 2.61 I+J). Additionally, first and third legs were raised later from the ground compared to control flies based on the wing position. The control flies starts to raise their pro- and metathoracic legs when the wings reach an approximately angle of 180° to each other (Fig 2.61 D). In contrast, the *side* mutant fly starts to lift their thirst legs and third legs when the wings reach nearly their lowest position (Fig 2.61 M). Furthermore, the fly rotates during the take-off around its anterior-posterior axis.

Most of the overexpression flies are also not able to move their wings normally. They often move only one wing, whereas the other one stays at the same position during the complete take-off sequence (arrows Fig 2.61 Q-X). Additionally, overexpression fly lifts only the pro-thoracic legs during the depressing of the moving wing in contrast to control flies (arrowhead Fig 2.61 S+T). Therefore, the second leg pair (asterisks Fig 2.61 T) and the third leg pair have still contact to the island. Furthermore, fly does not start to take off by jumping, but rather by starting a second wing beat resulting in a rotation around its dorso-ventral axis (Fig 2.61 U-X).

To further analyse the observed asynchronous wing movement of the *Side* loss- and gain of function flies, additional high-speed movies of flight behaviour were carried out. Therefor flies were fixed on their thorax with a needle and recorded from frontal view. Control flies beat their wings synchronously up and down and rotate them at the lowest position before lifting them again (Fig 2.62 A-H). Mutant and overexpression flies show various phenotypes. They are not able to elevate their wings as high as control flies based on the angle between both wings (Fig 2.62 I-X). Additional, *side* mutant and overexpression flies often move their wings non-simultaneously in contrast to control flies (Fig 2.62 I-X). Furthermore, they are only able to rotate one of the two wings. The other wings oscillate only up and down without rotation. In addition, it is obvious that the legs of the control flies (Fig 2.62 A-

Results

H) are not visible in contrast to the legs of the overexpression (Fig 2.62 Q-X) and mutant flies (Fig 2.62 I-P).

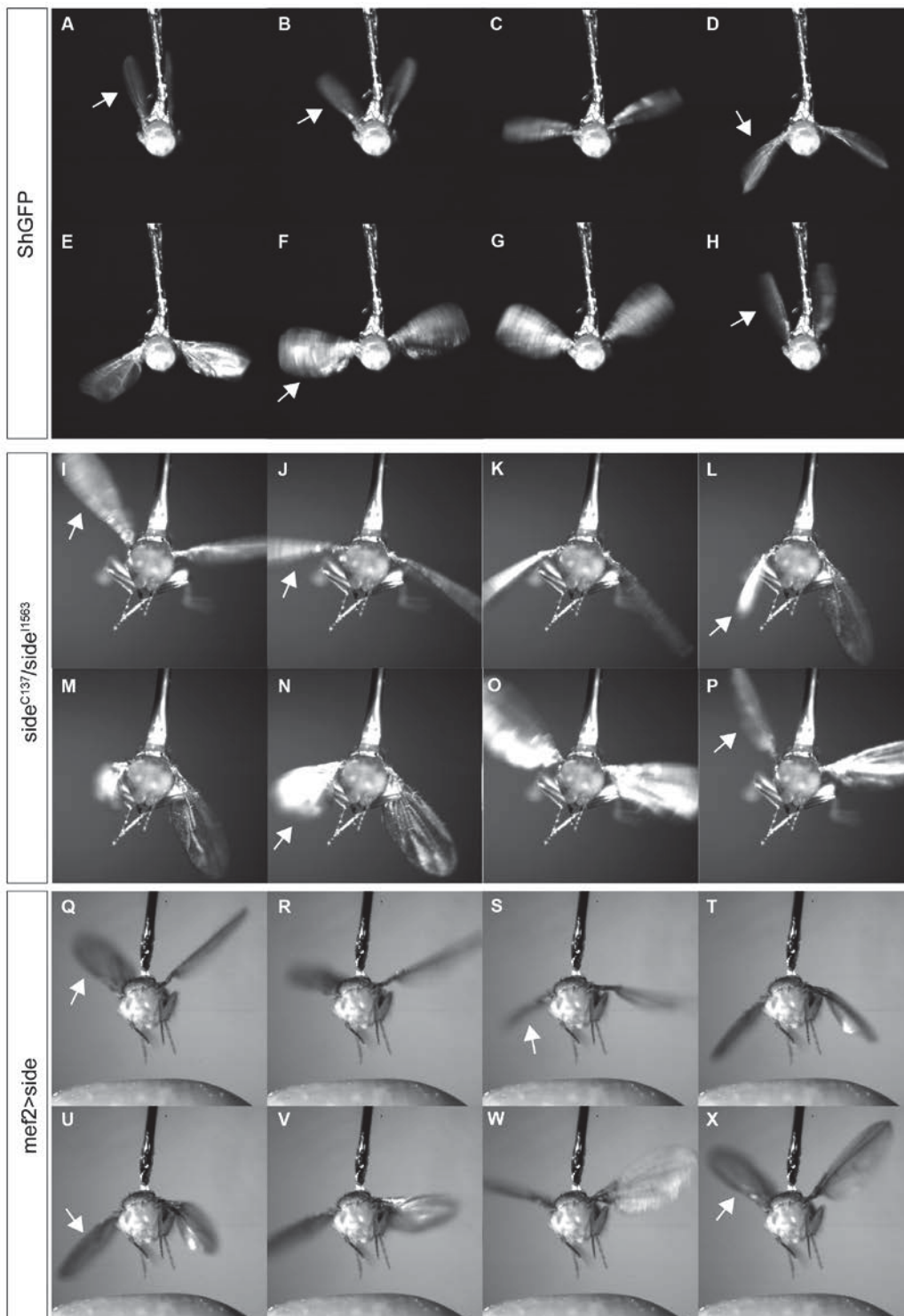


Fig 2. 62: Side loss- and gain of function flies are not able to oscillate their wings synchronously.

Time series of high-speed movies of wing beats of wild-type, *side* mutant and overexpressing flies. A-E: Control flies depress both wings synchronously (arrows). F: Rotation of both wings (arrow). G-H: Synchronous lifting of both wings (arrow). I-K: Side loss of function flies lower also both wings synchronously (arrows). L-N: Mutant flies are not able to rotate both wings (arrows). O+P: Loss of function flies elevate both wings asynchronously and are not able to lift them as high as the wild-type

Results

(arrow). Q-T: Side gain of function flies lower their wings not synchronously (arrows). U+V: Similar to side mutant, they are only able to rotate one wing. W-X: Flies overexpressing Side are not able to elevate their wings as high as controls.

Making the wing beat movies it strikes that the control, mutant and overexpression flies show different movements of halters. Therefore, further movies of all three genotypes from the lateral view were performed. The control flies move their halters always together with their wings, but in the opposite direction resulting in a lifting of the halters during the wings are depressed and vice versa (Fig 2.63 A-C). In contrast, Side gain- and loss of function flies are not able to move their halters or move them only slightly, respectively (Fig 2.63 D-I).

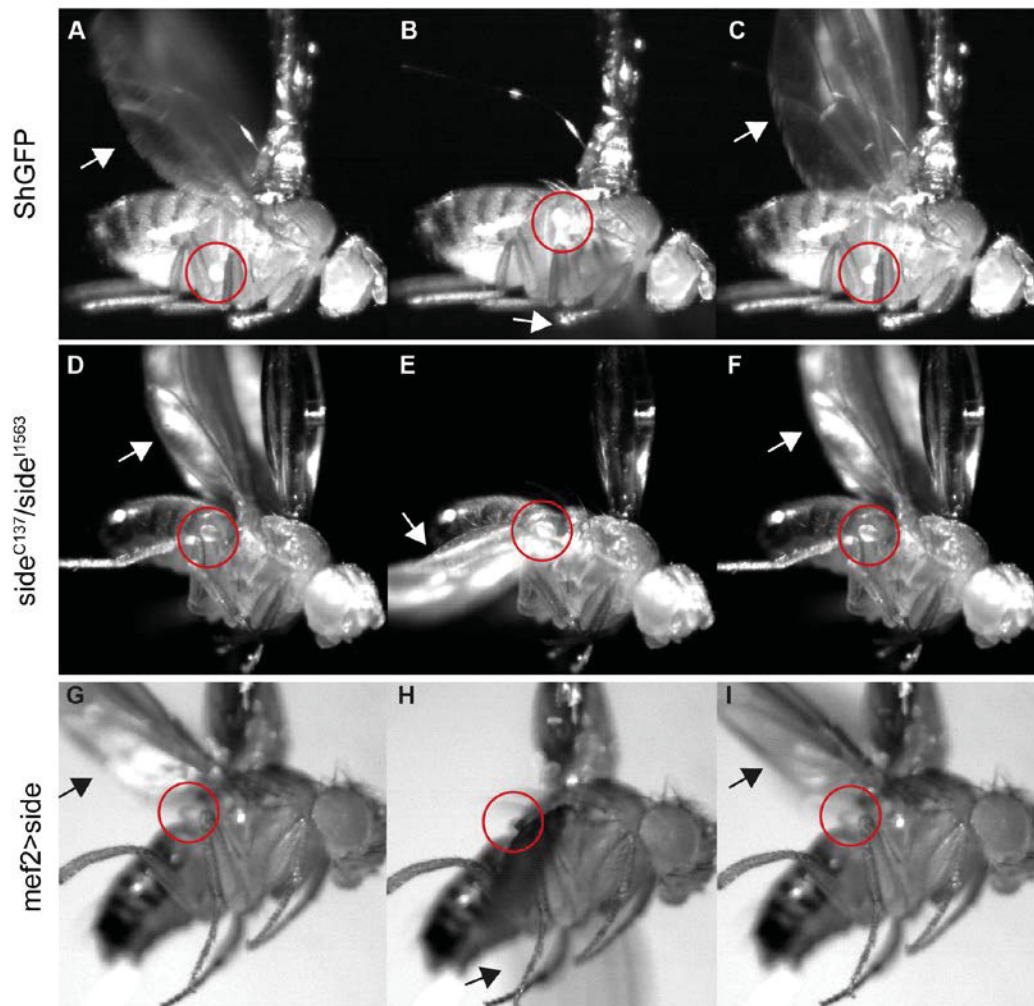


Fig 2. 63: Side gain- and loss of function flies are not able to move their halters.

Time series of high-speed movies of halter movement in comparison to the wing beat of wild-type and *side* mutant and overexpression flies. A-C: The halter of the control fly is moved into the opposite direction than the wings (arrows, red circles). When the fly lowers its wings, the halters are elevated and vice versa. D-F: The mutant fly lifts its halter less compared to wild-type (arrows, red circles). G-I: Overexpression flies are not able to move it at all (red circles).

Results

Movies from lateral view support also the observation of a different leg position during flight of control and loss- and gain of function flies. Control flies tuck their legs close to their body and therefore, legs are not visible from frontal view (Figs 2.62 A-H and 2.63 A-C). In contrast, mutant and overexpression flies are not able to tuck their legs as close as control flies (Fig 2.63 D-I).

Using the software Tracker it is possible to track the wing beats using the high-speed movies of fixed flies from frontal view. The tested control flies (ShGFP) beat their wings on average 210 times per second (Fig 2.64 A). This result fits to the data of Frye and Dickinson with more than 200 wing beats per second (Frye and Dickinson, 2004). Side loss- and gain of function flies show a decreased number of wing beats per minutes with 180 and 170 wing beats per second, respectively (Fig 2.64 A). Furthermore, the position of the left wing of one fly per genotype were analysed to investigate the impression that mutant and overexpression flies are not able to elevate the wings as high as the controls. Control fly oscillates its wings approximately 1.5mm up and down setting the position of the wings in a 180° angle to each other to zero (Fig 2.64 B). In contrast, *side* mutant fly is not able to lift its left wing higher as the 180° angle position. However, only a less difference is visible comparing the depth of wing beats of *side* mutant fly and control fly (Fig 2.64 B). Side gain of function fly is able to lift their wing approximately 1mm and depress it as deep as the controls (Fig 2.64 B).

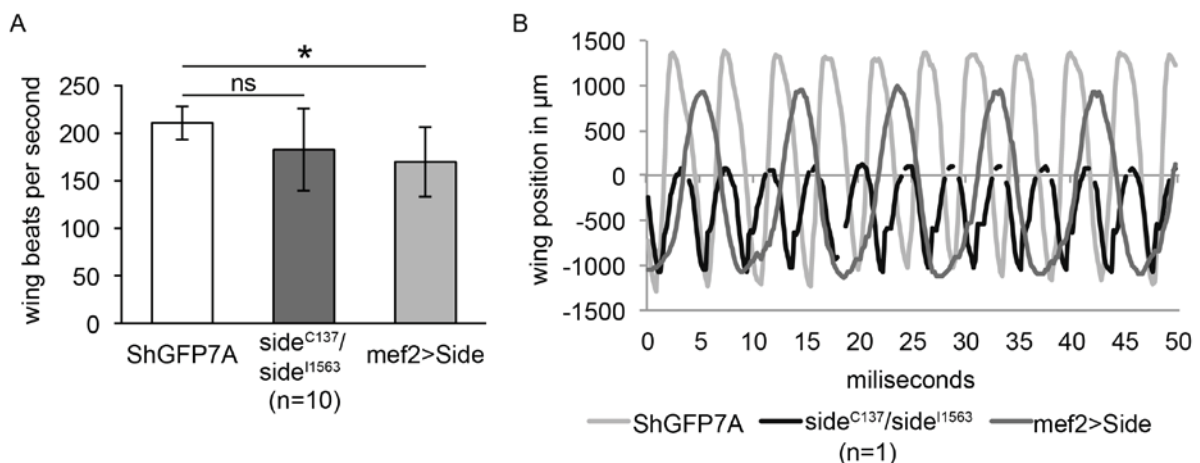


Fig 2. 64: Side gain of function flies exhibit a decreased number of wing beats compared to wild-type.

Statistical analysis of number of wing beats per second and amplitudes of wing beats of wild-type and Side gain- and loss of function flies. A: Side mutant flies show no difference compared to wild-type (p-value: 0.082 using students T-test), while Side gain of function flies perform significant less wing beats per second (p-value: 0.007). B: Loss- and gain of Side lead to a decreased amplitude in comparison to wild-type.

Results

Taken together, lack of Side does not alter the number of wing beats per seconds, but results in decreased amplitude. In contrast, gain of Side causes a decreased number of wing beats with similar amplitude compared to wild-type.

To investigate if the observed locomotion errors moving the wings are caused by a mis-innervation of the indirect flight muscles (IFMs), adult thoraxes of control flies and Side gain- and loss of function flies were prepared and stained with anti-Ankyrin-2. Control flies (ShGFP) show a uniform innervation of the surface of IFMs based on different main nerves which defasciculate in smaller axons to innervate the whole muscle surface (Fig 2.65 A). Some parts of the muscle surface of indirect flight musculature of mutant flies show no conspicuous difference to the control muscles (Fig 2.65 B). Other areas show a main nerve with a thicker diameter and more branches compared to the control (Fig 2.65 C). But it has been consider that thoraxes of Side loss of function flies are more difficult to prepare in comparison to the control flies. The muscles of these flies seem to be pulpier compared to control muscles. Therefore, only four thoraxes of *side* mutant flies could be analysed.

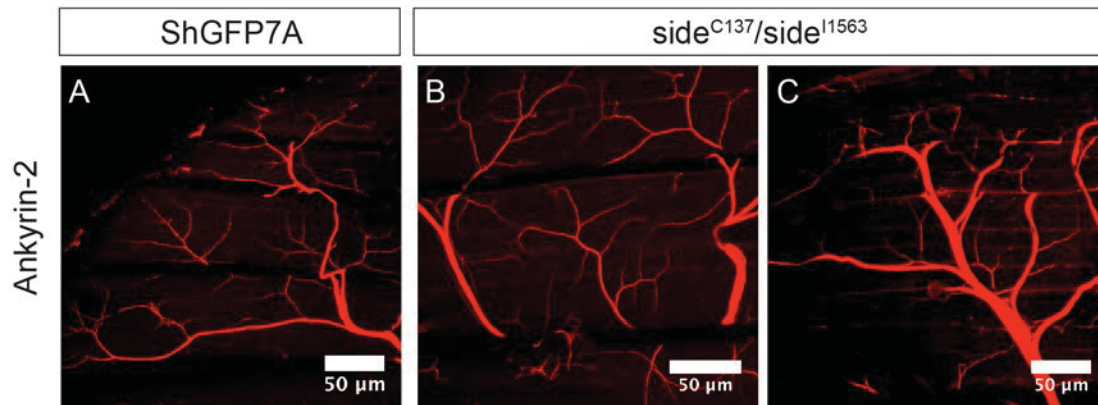


Fig 2. 65: *Side* mutant flies show minor differences of indirect flight muscles innervation.

Confocal images of indirect flight muscles of wild-type and *side* mutant flies stained with anti-Ankyrin-2. A: Wild-type flies show a regular innervation of indirect flight muscles. B+C: Indirect flight musculature of *side* mutant flies exhibit parts with wild-type pattern (B) and also parts with an increased branching of the main nerve (C) compared to the wild-type.

Analysing the innervation pattern of indirect flight muscles of flies overexpressing Side on the muscles surface, heterozygous flies serve as control. Three principle phenotypes are detectable for overexpression flies (Fig 2.66 B-D) compared to heterozygous controls (Fig 2.66 A). Motor axons innervate IFMs similar to controls and wild-type (Fig 2.66 B) or show excessive branching at the nerve entry side

Results

resulting in a tree-like structure of motor axons (arrow Fig 2.66 C) or miss to defasciculate resulting in non-innervated muscles parts Fig 2.66 D).

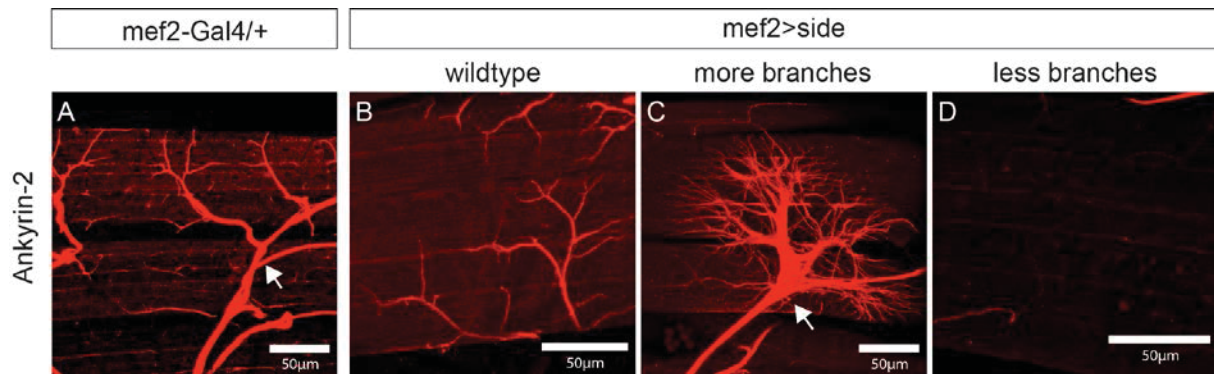


Fig 2. 66: Gain of Side causes irregular innervation of indirect flight muscles.

Antibody staining with anti-Ankyrin-2 of heterozygous controls and flies overexpressing Side. A: Regular innervation of control IFMs. B-D: Overexpression flies show three different phenotypes – similar innervation to the control (B), exuberant branching of motor axons (C) and areas with almost no innervation (D).

These detectable innervation defects of IFMs of overexpression flies causes a 38% lesser innervated muscle surface compared to controls (Fig 2.67 A). Analysing the number of branches for a specific size of muscle surface support the impression of three different phenotypes based on one genotype (*mef2>side*). Areas that seem to be innervated in a wild-type manner have no significant different number of nerve-branches. In contrast, areas with tree-like nerve structures have significant more branch points and areas with almost no innervation have significant less branch points (Fig 2.67 B).

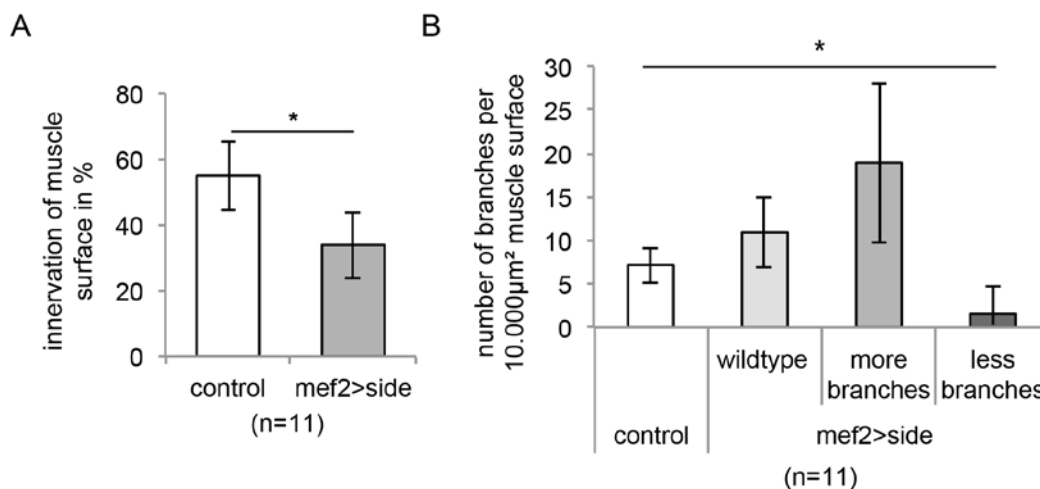


Fig 2. 67: IFMs of Side gain of function flies are less innervated.

Statistical analysis of indirect flight musculature innervation. A: Compare to controls, muscle surface of overexpression flies is significant less innervated (p-value = less than 0.001 using the students T-test). B: Muscle areas with a wild-type innervation pattern of flies overexpressing Side have no significant different amount of branches (p-value = 0.02), while other parts have significant more (p-value = 0.002) or less (p-value = less than 0.001) branches.

Results

Additionally, the six muscle fibres of indirect flight musculature in overexpression flies are predominantly innervated on the ventral side resulting in a ventral increased number of branch points and a dorsal decreased number of branch points compared to controls (Fig 2.68 A-F). Thereby, overexpression flies exhibit a big difference of branch points between ventral and dorsal side. On average, they have eleven branch points per $2500\mu\text{m}^2$ muscle surface in the ventral part, but dorsally only 1.5 branch points (Fig 2.68 G). In contrast, control flies exhibit on the ventral and dorsal side of muscle fibres the same number of branch points (Fig 2.68 G).

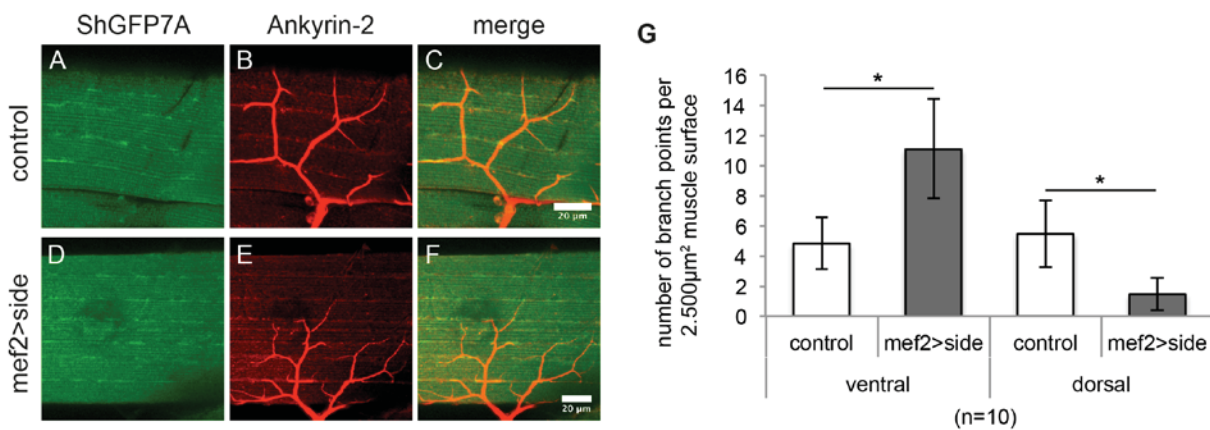


Fig 2. 68: Gain of Side causes irregular innervation of single muscle fibres of indirect flight musculature.

Antibody staining with anti-GFP (green) and anti-Ankyrin-2 (red) of single muscles of indirect flight musculature of wild-type and flies overexpressing Side and statistical analysis of number of branch points. A-C: In control flies nerves innervate the whole muscle surface. D-F: Muscles of Side gain of function flies are innervated predominantly at the ventral side. G: Muscles of wild-type flies show no difference of number of branch points between the ventral and dorsal muscle half. In overexpression flies the ventral part exhibit an increased number of branch points and the dorsal part is less innervated compared to wild-type (p-values = less than 0.001 using students T-test).

These results suggest that the irregular innervation of IFMs is the reason for the inability to fly and to take off of Side gain of function flies. Since *side* mutant flies show no conspicuous innervation phenotype analysing IFMs, the observed inability to take off might raise on innervation defects of leg muscles. As primarily described by Kaplan and Trout, mesothoracic legs are essential for take-off based on their association with the jump muscles (Fernandes et al., 1991; Kaplan and Trout, 1974). To proof this, innervation pattern of femurs of wild-type and *side* mutant flies was analysed.

Results

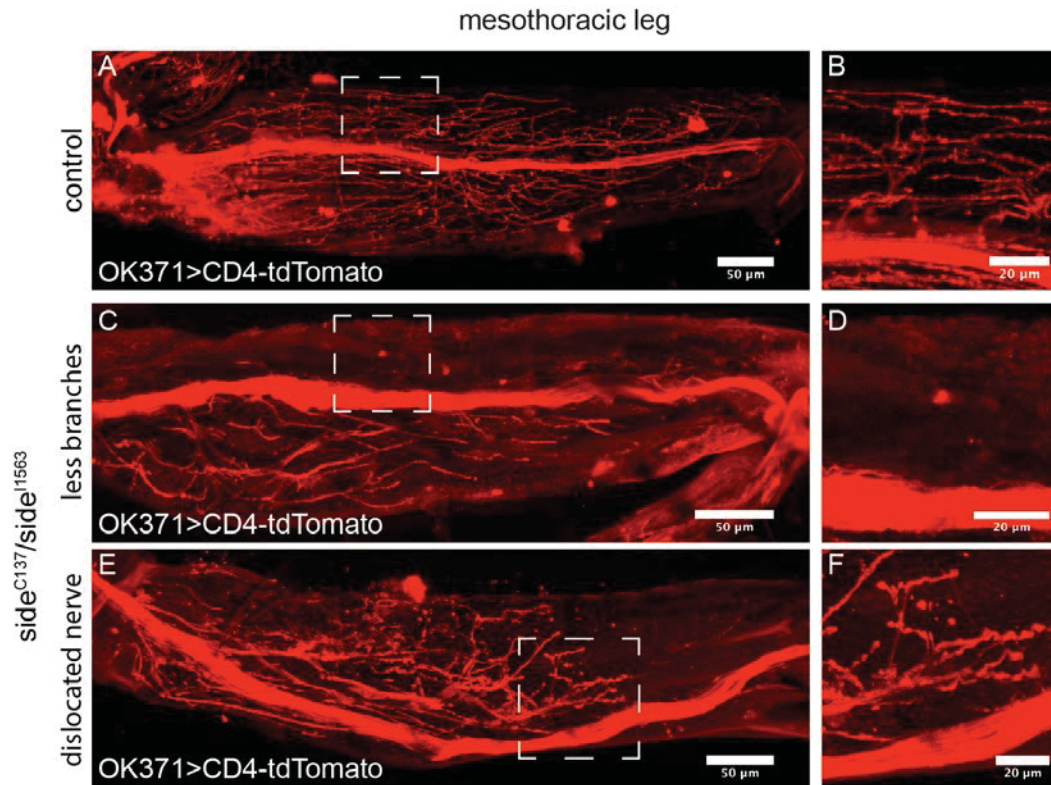


Fig 2. 69: Side loss of function flies show mis-innervation of femurs.

Femur innervation of wild-type ($w;OK371-Gal4,ShGFP1A/+;ShGFP7A,UAS-CD4-tdTomato$) and *side* mutants ($w;OK371-Gal4/+;side^{C137},ShGFP7A/side^{I1563},ShGFP7A,UAS-CD4tdTomato$) marked by $OK371>CD4-tdTomato$. A+B: Control legs exhibit one main nerve bundle in the middle of the femur and a lot of branches migrating in the periphery. C-F: Mutant legs show different phenotypes with fewer branches or a dislocated main nerve.

Leg nerves stained with tdTomato under control of $OK371-Gal4$ were imaged through the translucent cuticle of late pupae. Controls showed one main nerve bundle in the middle of the femur and many defasciculated nerves, which innervated the periphery. Lack of *Side* causes different phenotypes. The femurs of mutant flies contain substantially fewer nerves and nerve branches (Fig 2.69 B+D). Additionally, the main nerve bundle frequently migrate along ectopic pathways resulting in a lateral dislocation compared to wild-type (Fig 69 E). In 93% ($n=15$) of the control femurs the main nerve bundle migrate along a pathway with a distance between $60\mu m$ and $80\mu m$ from the cuticle. Lack of *Side* causes a projection along trajectories with smaller distances to the cuticle (54% ($n=26$)). Furthermore, femurs of loss of function flies are in average significantly thinner than control femurs. In contrast, the main nerve bundle exhibits a thicker diameter in the distal part of the femur of mutant flies in comparison to controls (Fig 2.70).

Results

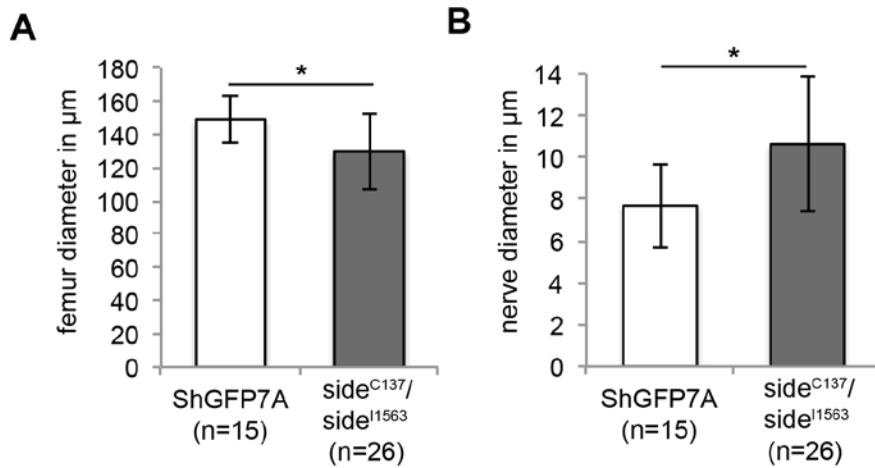


Fig 2. 70: Side loss of function flies exhibit a thicker leg main nerve bundle.

Statistical analysis of femur diameter and nerve diameter of wild-type and *side* mutant legs. A: Side mutant legs exhibit a significant smaller diameter of femurs (p-value = 0.002 using student T-test). B: Diameter of main nerve bundle is on average significant thicker at a distal position in Side loss of function femurs compared to wild-type (p-value = less than 0.001).

Due to the wiring defects in femurs, it was also assessed if this alters adult walking behaviour using the leg print assay and climbing assay (Chaudhuri et al., 2007; Maqbool et al., 2006). Performing the climbing assay it is possible to test if flies are able to climb on the wall of an empty plastic tube against the geotaxis. Lack and gain of Side result in an inability to climb (Fig 2.71). After 15 seconds performing time only around 15% of the mutant flies and 33% of the gain of function flies are able to climb while around 80% of the controls pass the mark (Fig 2.71).

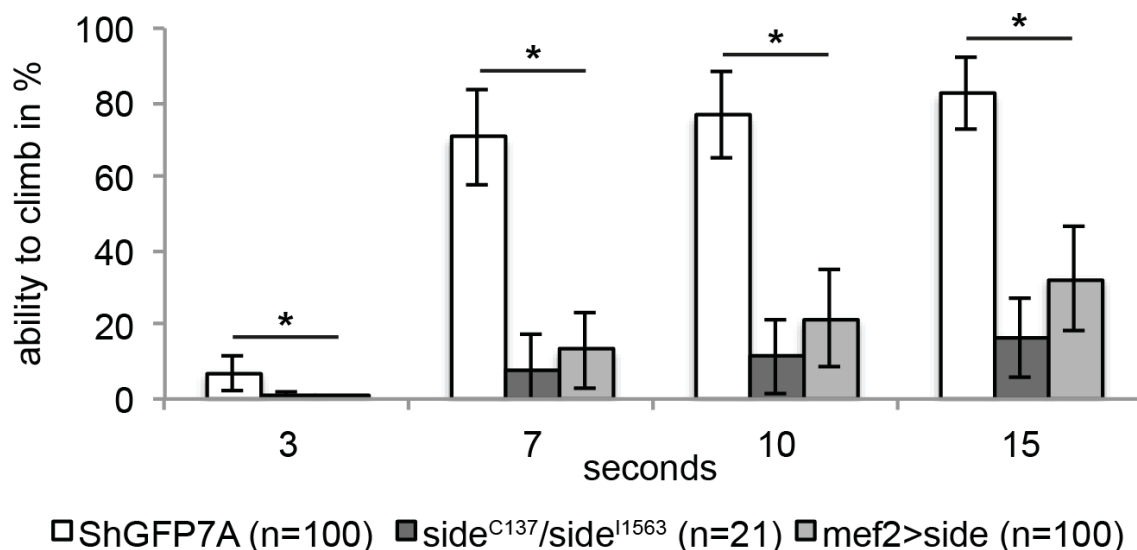


Fig 2. 71: Side loss- and gain of function flies are not able to climb.

Statistical analysis of climbing assay. Already after 3 seconds mutant and overexpression flies show a significant decreased number of flies able to climb compared to the ShGFP flies (p-value: 0.002 or less using student T-test).

Results

Using the leg print assay, various parameters can be analysed – among others the position of the tarsus prints, the step length and the length of tarsus print of the metathoracic leg (Fig 2.72). Leg prints of controls exhibit the expected stereotypic pattern. The prothoracic (first) tarsus print is the inner one and the print of the mesothoracic (third) tarsus is the outer one. In the middle between these two prints the print of the metathoracic (second) tarsus is located (Fig 2.72 A).

For mutant flies again three different phenotypes are detectable (Fig 2.72 D-F). Flies representing the weak phenotype drag their metathoracic leg causing an 87% longer tarsus print compared to control flies (Figs 2.72 D and 2.73 A). In addition, they position their third tarsus on the inner position resulting in an abnormal tarsus print pattern (Figs 2.72 D and 2.73 B). Furthermore, the step length of mutant flies is a little bit shorter in comparison to the controls (*side*= 1.8mm, *ShGFP*= 1.9mm) (Fig 2.73 A). Around 30% of the flies reflect the moderate and strong phenotype. For the statistical analyses, only the prints of flies with the weak phenotype could be used, since it is not possible to match the tarsus prints to a leg of flies representing the moderate phenotype and flies with the strong phenotype are not able to walk over the microscopy slides.

Gain of function flies show two different phenotypes compared to controls (Fig 2.72 B+C). Flies representing the moderate phenotype have thicker tarsus prints compared to control flies (Fig 2.72 B). The strong phenotype represents flies with a characteristic dragging of the metathoracic leg (Figs 2.72 C and 2.73 A) and a different position of the tarsus prints (Figs 2.72 C and 2.73 B). Additionally, they exhibit a decreased step length in comparison to controls (Fig 2.73 A). However, all overexpression flies are able to walk over the microscopy slides.

Results

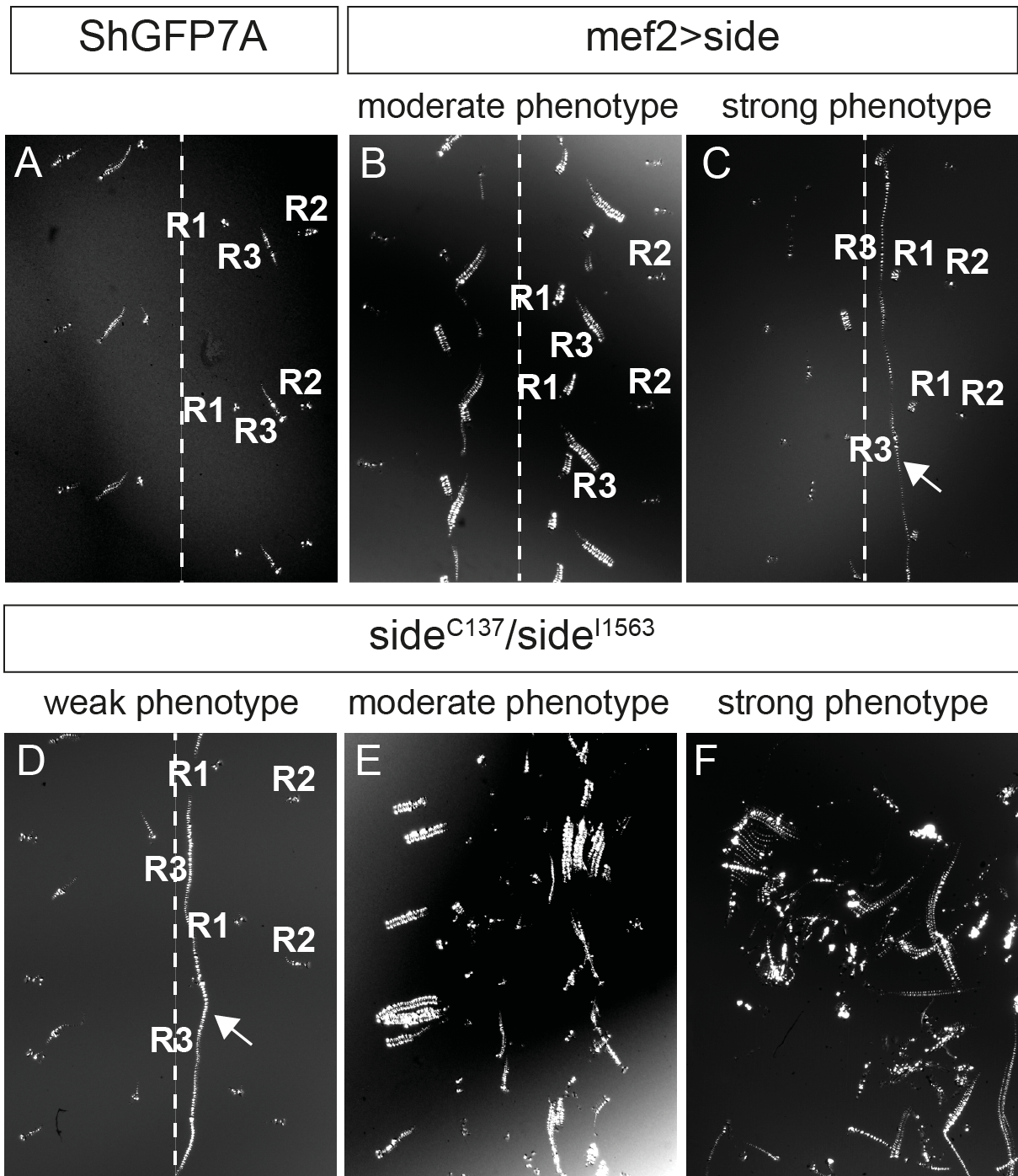


Fig 2. 72: Side loss- and gain of function flies exhibit altered leg prints.

Leg prints of wild-type, *side* mutant and overexpressing flies. A: Control flies show a regular pattern of leg prints with an axis of symmetry in the middle. Leg prints are always positioned in the following order from outside to inside: second print (R2), third print (R3) and first print (R1). B+C: Overexpressing flies exhibit two different phenotypes with thicker prints (B) and dragging the third leg (arrow C). D-F: Mutant flies show three different phenotypes with irregular print pattern (D+E) and inability to walk over the cover slides (F).

Results

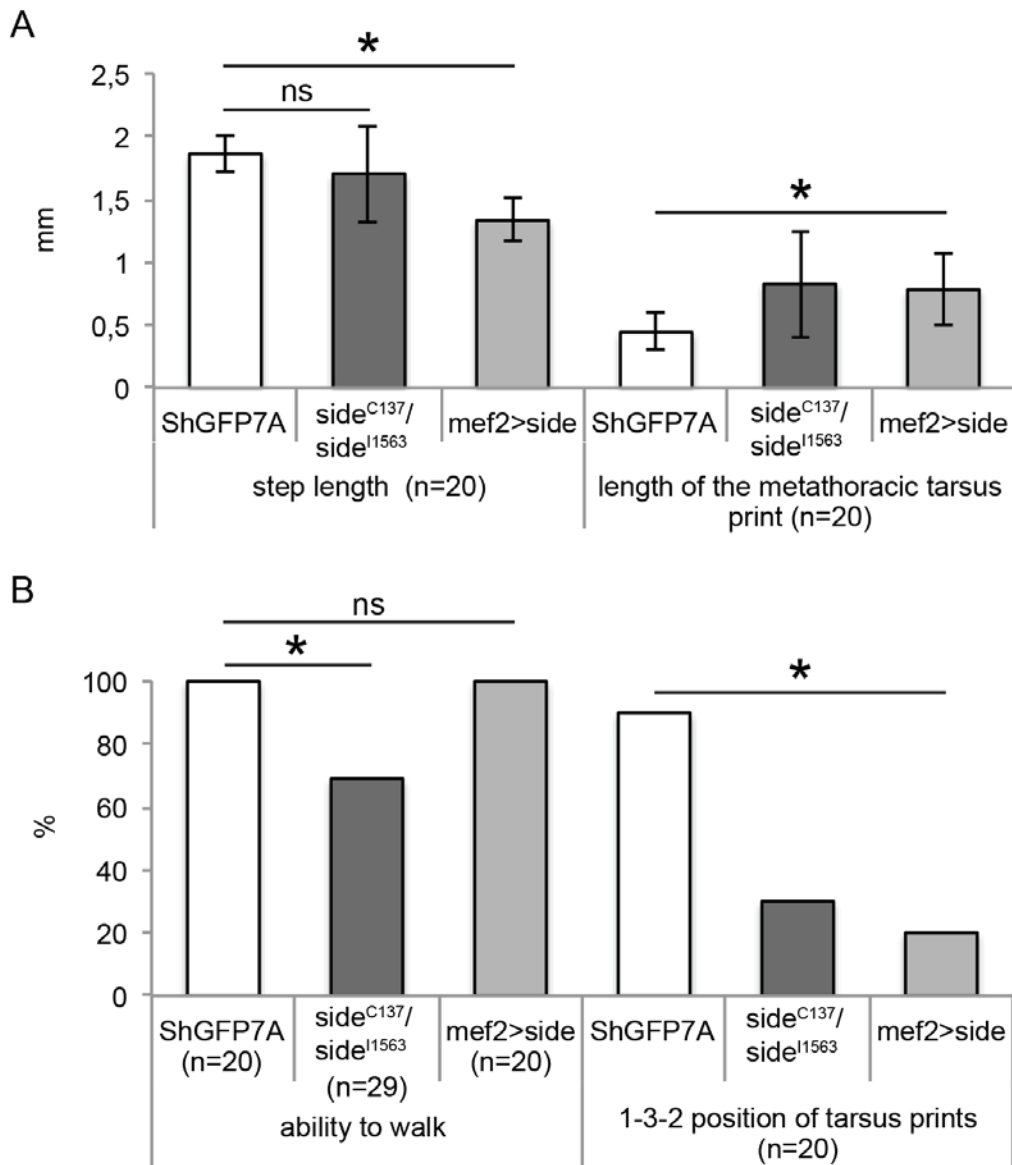


Fig 2. 73: Side loss- and gain of function flies exhibit longer tarsus prints and altered tarsus print positions.

Statistical analysis of the leg print assay. A: The step length of mutant flies is not altered compared to wild-type (p-value = 0.1 using the students t-test), but gain of function flies exhibit a shorter step length in comparison to wild-type (p-value = less than 0.001). Loss- and gain of function flies show an increased length of the third leg print (p-value = less than 0.001). B: *Side* mutants and overexpression flies show abnormal tarsus print positions compared to controls (p-value = less than 0.001 using the fisher exact test). Not all mutant flies are able to walk over the cover slide.

High-speed movies from walking mutant and gain of function flies and control flies were performed to clarify the observed motion phenotypes using the leg print assay. Control flies walk in a tripod gait using the first and third leg of one body half and the second leg of the other half. The single step starts with moving the first leg (in figure 2.74 R1 = prothoracic leg of the right body half), followed by the contralateral mesothoracic leg (L2 Fig 2.74 B) and end with the third leg (R3) (Fig 2.74 A+B). The next step starts with the prothoracic leg of the same body half as the second leg of

Results



Fig 2. 74: Side mutant flies are not able to move their pro-thoracic legs.

Temporal series of high-speed movies of walking of wild-type, Side loss- and gain of function flies. A-F: The control fly carries out one step with three legs at the same time (tripodal), moving the first and third legs of one body half and the second leg of the other body half almost simultaneously. G-L: The Side loss of function fly has big problems to walk forward based on an inability to move the prothoracic legs normally. In contrast, the other legs show a normal walking behaviour. M-R: The overexpression fly shows a normal walking behaviour similar to the control flies, but the fly sticks out its right wing during walking.

Results

the first step (L1) and proceeds further in the same way as the first step (Fig 2.74 C-E). In this way the controls walk straight forward over the microscopy slide, which was used for recording the walking behaviour.

Mutant flies are not able to walk coordinately over the microscopy slide (Fig 2.74 G-L). They often cross their prothoracic legs and are not able to move these legs correctly resulting in tumbling from one side of the performing tunnel to the other. In contrast, the movement of the meso- and metathoracic legs is not altered compared to control walking.

The overexpression flies walk in the normal tripod pattern over the microscopy slides moving three legs simultaneously (Fig 2.74 M-R). Remarkably, approximately 80% of gain of function flies stick out one or both wings during walking (n= 110).

In summary, mutations in the *side* locus causes wiring errors in adult legs resulting in the inability to climb and to move the pro-thoracic legs. Side gain of function flies show milder phenotypes compared to mutant flies analysing the walking behaviour.

2.3.2 Side loss- and gain of function flies are not able to groom themselves

Another important motion behaviour among flying and walking for a fly is the ability to groom oneself and to remove dust from the body especially from the eyes and the wings. To assess if Side loss- and gain of function flies are able to clean their bodies, flies were uniformly coated with the azo dye reactive yellow 86 and afterwards recorded for one hour (Seeds et al., 2014). ShGFP serve as control again.

Controls can relieve the dust from their eyes during the first 4 minutes and after 30 minutes the whole head is cleaned (Fig 2.75 B+C). After one hour, control flies are almost completely relieved from the azo dye. Only some remaining dye on top of the thorax is visible (Fig 2.75 D).

Loss of function flies are also able to clean their eyes during the first 4 minutes (Fig 2.75 F), but during the remaining time they are not able to clean further parts of their body. Therefore, after one hour the head, wings, abdomen and the thorax are still covered by dust (Fig 2.76 H).

Gain of function flies need 20 minutes to clean their eyes (Fig 2.75 K). However, they are able to remove the complete dust from the head during one hour. But similar to

Results

the mutants and in contrast to the controls, there is still a lot of remaining reactive yellow on top of the wings and thorax (Fig 2.75 L).

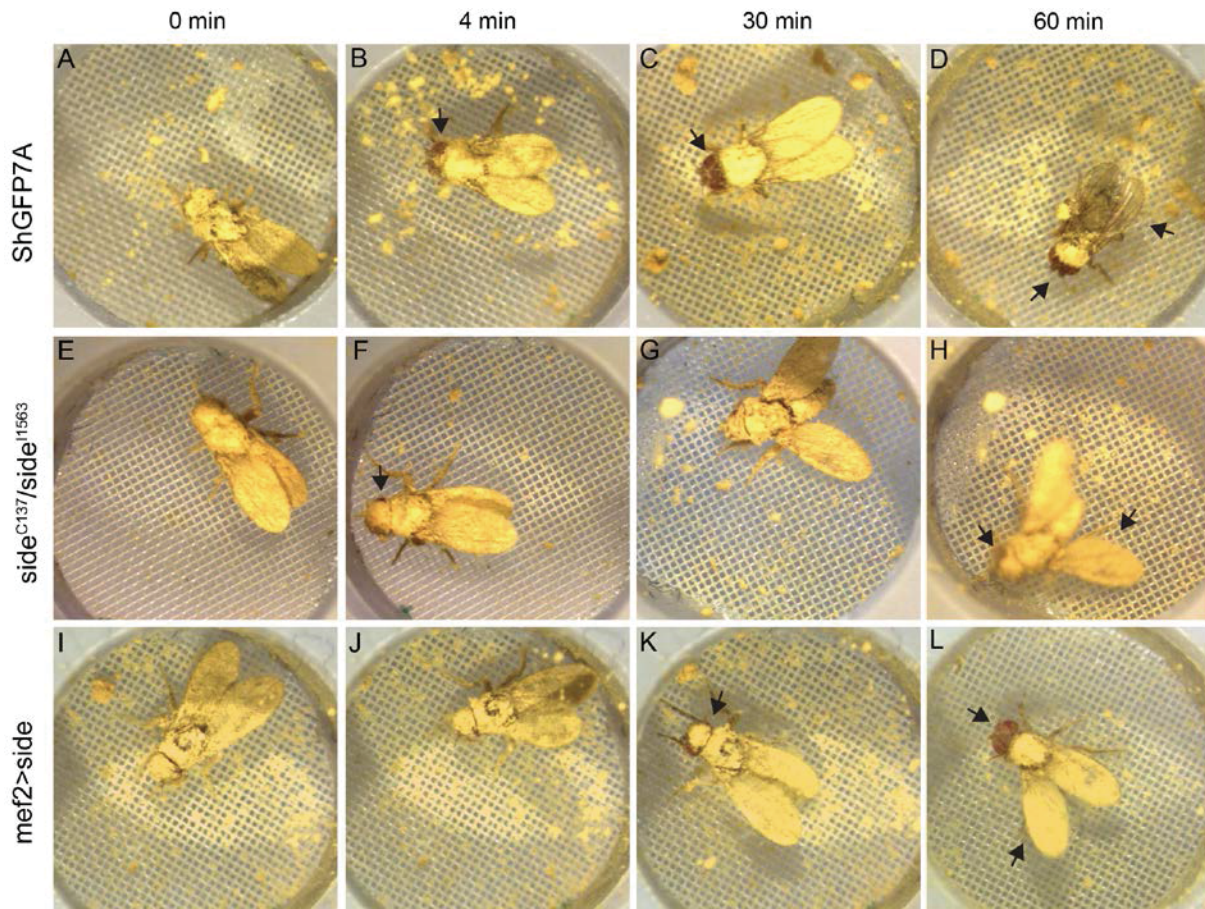


Fig 2. 75: Side gain- and loss of function flies are not able to groom themselves.

Time series of the grooming behaviour of wild-type, *side* mutant and overexpressing flies. A-D: Control flies have cleaned their eyes after four minutes and their head after twenty minutes (arrows). After one hour, flies have removed almost all dust from their body (arrows). E-H: Loss of function flies are only able to clean their eyes, but not the remaining body parts (arrows). I-L: Gain of function flies need 20 minutes to clean their eyes, but in contrast to the mutant flies they are able to clean their whole head during one hour (arrows).

2.3.3 *Side* homozygous males are sterile

The ability to reproduce is another essential behaviour to survive or for the survival of a species. To investigate if flies lacking *Side* are able to reproduce different crossing experiments were performed. As summarized in table 2.5, homozygous mutant flies among themselves are not able to reproduce, but the crossing of homozygous loss of function virgins with ShGFP males leads to progeny. In contrast, the crossing the other way around, using ShGFP virgins and homozygous mutant males, leads to no progeny.

Results

Tab 2. 5: Fertility crossings.

- = no progeny; + = progeny

| X | | males | |
|---------|---|---|-------|
| | | side ^{C137} /side ^{I1563} | ShGFP |
| virgins | side ^{C137} /side ^{I1563} | - | + |
| | ShGFP | - | + |

To test if the homozygous males are infertile testis tubes and seminal glands of ShGFP and mutant males were prepared (Fig 2.76). The testis tubes of Side loss of function flies do not show any difference to the controls. All developmental stages of the spermatozoon are detectable. Additionally, the seminal gland is filled with moving spermatozoon (Fig 2.76 D). These observations suggest that *side* mutant males are fertile and therefore, the inability of reproduction is not based on sterility.

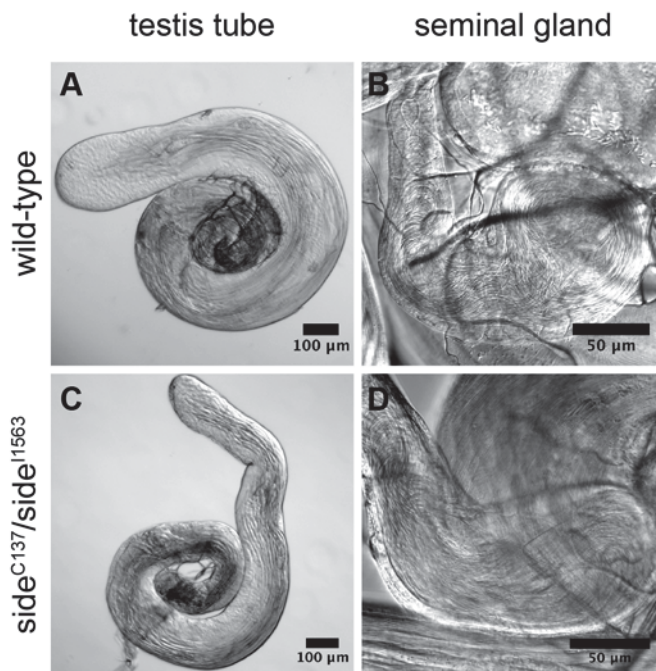


Fig 2. 76: In *side* mutant males development of spermatozoa is not altered.

Testis tubes and seminal glands of wild-type and Side loss of function males. A: Testis tube of a wild-type male shows all developmental stages of the spermatozoon. B: Filled seminal gland of a wild-type male. C+D: Side mutant male shows no defect in the spermatogenesis and exhibit also a seminal gland filled with mature spermatozoon.

3. Discussion

3.1 Gene regulation of *sidestep*

3.1.1 Side guides motor axons via two intermediate targets

The member of the immunoglobulin superfamily Sidestep is essential for axon guidance during embryogenesis in *Drosophila*. It is expressed dynamically during this process. During stages 10-11, Side protein is detected exclusively in cells along the ventral midline in the CNS. At stage 12-13 this pattern changes to a triangular pattern. Simultaneously, external sensory neurons start to express Side. From stage 15 onward, expression of Side in sensory neurons is hardly detectable (Siebert et al., 2009). *Side* mRNA is expressed from stage 13 onward in the developing somatic muscles and is present on the surface of all muscles in old embryos (stage 15-17) (Sink et al., 2001). Since Side expressing cells were so far specified due to their morphology and location, it was attempted to identify the Side expressing cell types using different cell markers.

Using the antibody anti-Repo (marker for glia cells in the CNS and PNS) it was possible to identify the Side expressing cells near the midline in early embryos as longitudinal glia (Fig 2.2). Subsequently, Side is expressed in glia associated with the ISN and SN resulting in the detectable triangular pattern during stage 12-13 (Fig 2.2). In the PNS, two different cell types express Side - glia cells and sensory neurons. The glia cell specific expression is limited to two cells per hemisegment, the external glia 9 and 10. However, sensory neuron specific expression comprises two classes of sensory cells, firstly the external sensory organs (marked by anti-BarH1/2) and secondly the multidendritic (md) neurons (marked by the driver line 21-7-Gal4 activating UAS-mCD8GFP) (Figs 2.4 + 2.5).

In this thesis it was not possible to detect endogenous *side* mRNA in mid-stage as well as in old embryos in muscles (see for example Fig 2.30). In addition, immunohistochemical co-stainings using a muscles specific marker (UASmCD8GFP driven by *mef2*-Gal4) show a similar result (data not shown). Therefore, a possible late embryonic Side expression in muscles could neither be detected on mRNA- nor on protein level. These findings suggest that Side is not expressed in muscles during the embryogenesis and thus contradict the observations of Sink and colleagues.

Discussion

Taken together, the results indicate that *Side* guides motor axons via only two different intermediate targets – glia cells (in early stages in the CNS) and sensory neurons (in mid-stages). However, following these substrates, motor axons reach their target muscle fields.

3.1.2 *Side* phenotype can be partly rescued by two enhancer fragments

To understand how the dynamic expression of *side* is regulated, the expression pattern of five different genomic fragments from potential enhancer regions were analysed using a fluorescent reporter gene. One of these lines (206961-Gal4) reflects the *side* expression in sensory neurons and covers a gene fragment from the first intron to the second exon including the start codon of *side* (Figs 2.7 + 2.9). Interestingly, another line (204347-Gal4), including a genomic fragment of the first intron, shows a muscle specific expression suggesting that *side* might also be expressed in muscles (Figs 2.7 + 2.8). Both lines were used for rescue experiments. Unexpectedly, the sensory neuron specific line (206961-Gal4) does not rescue the *side* phenotype with typical strong mis-innervations and lack of NMJs in the ventral muscle field (Fig 2.12). Driving *side* cDNA with 204347-Gal4, which is expressed in muscles starting at stage 13, in a *side* mutant background reduces ventral innervation defects almost completely. However, mis-innervations in the dorsal muscle field remain (Fig 2.12). These results suggest that the sensory neuron specific expression of *Side* is not as necessary for motor axon guidance as the muscle specific expression. Remarkably, the expression of UAS-*Side* driven by a combination of both enhancer fragments (206961-Gal4 and 204347-Gal4) leads to a much-improved rescue of the dorsal innervation compared to a rescue by 204347-Gal4 alone (Fig 2.12). This result indicates that migration of motor axons along PNS axons expressing *Side* driven by 206961-Gal4 guides them towards the dorsal muscle field. However, some hemisegments (26% (n=19)) still exhibit innervation errors of the dorsal-most muscles 1 and 9.

The remaining lack of some NMJs of the dorsal-most muscles might be caused by an incorrect expression of *side* cDNA driven by the enhancer fragment 204347. From stage 16 embryos onward to first instar larvae, 204347-Gal drives GFP expression in muscles. This expression is increased in ventral muscles and lateral muscles compared to dorsal muscles (Fig 2.8). If this uneven expression also applies for the *side* cDNA, this might result in an exuberant attraction of the motor axons by *Side*

Discussion

into these two muscle fields resulting in a premature immigration of axons in the ventro-lateral region.

In summary, these results indicate that for the correct innervation of the muscles of *Drosophila* larvae it is not only important that *side* is expressed in the right tissues. The correct timepoint is also crucial. In addition, it might be inferred that the dynamic expression of *side* is regulated by more than one enhancer element. This conclusion is supported by findings of Kvon and colleagues, who suggested that each protein-coding gene expressed during embryogenesis exhibits on average four enhancers (Kvon et al., 2014). In addition, the results imply that the CNS specific *side* expression in early embryos is regulated by a further enhancer element. None of the investigated lines reflected the *side* expression in the CNS, but it has to be considered that the available lines do not cover the entire first intron. Possibly, the uncovered regions of the first intron contain the enhancer fragment that regulates early *side* expression.

The enhancer fragments 206961-Gal4 and 204347-Gal4 exhibit highly conserved regions. Ten and eleven other *Drosophila* species respectively show high sequence homology compared to the enhancer fragments in *Drosophila melanogaster*. As expected, more closely related species exhibit a higher sequence homology than species, which are phylogenetically more distant. This result suggests that regulation of *side* expression is conserved in the clade *Drosophilidae*.

3.1.3 Side expression is not regulated by Hox-genes

The dynamic expression pattern and its regulation by different enhancer fragments indicate that *side* is regulated not only by one transcription factor. Therefore, around 20 different transcription factors and determination factors that function, amongst others, in axon growth and guidance or dendrite morphogenesis were tested for their relevance in the regulation of *side*. Among these, four Hox-genes were tested. Two of them, *antennapedia* and *ultrabithorax*, were predicted in a binding site analysis of the conserved regions of the two enhancer fragments 206961 and 204347. The identified binding sites of Antennapedia and Ultrabithorax are also conserved in other *Drosophila* species (Figs 2.13 + 2.15). This result provides the assumption that the regulation of Side expression is conserved in *Drosophilidae*.

Discussion

Homozygous embryos of *antennapedia* and *senseless* mutant flies show an altered expression of Side in comparison to wild-type embryos. Staining of *antennapedia* and *senseless* mutant embryos with anti-Futsch, a marker for sensory neurons, demonstrate that the observed alteration of Side *expression* based on a defect in sensory neuron morphology, which can be explained with the function of both transcription factors during embryogenesis. Lack of Senseless causes a loss of almost all cells in the embryonic PNS. The few remaining cells are multidendritic (md) neurons (Nolo et al., 2000). Lack of Antennapedia, however, results in a loss of external sensory (es) organs in all three thoracic segments (Heuer and Kaufman, 1992). Thus, Side expression is affected only indirectly in *antennapedia* and *senseless* mutant embryos caused by the loss of sensory neurons.

Nevertheless, these results support the findings that Side is expressed in two different classes of sensory neurons. As mentioned before, lack of Senseless and Antennapedia cause the loss of different subsets of sensory neurons. However, Side is still detectable in both *senseless* and *antennapedia* homozygous embryos but in a decreased number of cells compared to wild-type. Therefore, Side is expressed in multidendritic neurons and external sensory organs.

Antibody stainings of *notch* loss of function embryos show an increased Side expression in sensory neurons. Similar to wild-type, in late stage *notch* mutant embryos Side is no longer detectable. Interestingly, western blot analysis reveals an opposite result. Embryos up to stage 14 show the same amount of Side protein as wild-type, while in late stage embryos (stage 15-17) a strongly increased Side expression is detectable. This opposite result can be partly explained by the function of Notch. Notch works as a lateral inhibitor during embryogenesis. Lack of *notch* causes the maturation of all ectodermal cells in the neurogenic region to neurons instead of to epidermal cells (Goodman and Doe, 1993). Since western blot analysis represents the relative expression of a protein, this result suggests that the increased Side expression detectable using immunohistochemistry is based on an increased number of Side expressing sensory neurons caused by the lack of *notch*. Therefore, it is probably an indirect effect.

Finally, none of the tested transcription factors influences the Side expression in the CNS and PNS directly. Possibly, a network of different transcription factors and co-factors might regulate the expression of Side in different cell-types. Therefore, loss of

one of these factors or co-factors would not result in a down-regulation of Side. But it has to be considered that some of the tested transcription factors regulate further genes such as Notch, Huckebein, Klumpfuss and the members of the Hox family.

3.1.4 Lack of Tolloid-related causes a constitutive Side expression

Another important aspect of Side-regulation is the potential down-regulation of the Side protein in sensory neurons from stage 15 onward in wild-type embryos after this tissue has been contacted by motor axons. In contrast, in *beat* mutant embryos, Side is still detectable in the PNS in late stage embryos (Siebert et al., 2009). This might hint to a posttranslational or contact-dependent degradation mechanism. Down-regulation of a protein could come about by proteolysis, endocytosis or degradation mediated by the proteasome. Since Beat is an axon guidance molecule with no known catalytic function, mutants of different genes that are functional in the degradation of proteins were analysed. In stage 15-17 loss of function embryos of the metalloprotease Tolloid-related, Side is expressed constitutively. This result is supported by western blot analysis. Lack of *tolloid-related* as well as lack of *beat* result in an increased Side expression in stage 15-17 embryos compared to wild-type, while embryos up to stage 14 show no difference in the level of Side expression (Fig 2.27). These results suggest that Tolloid-related might play a role for the degradation of Side by cleavage - probably within the extra cellular domain of Side. In *tolloid-related* mutants, Side might then not be cleaved and is thus still detectable in the PNS. This conclusion is supported by the observation that in embryos without muscles, caused by the muscle specific overexpression of activated Notch, Side is still detectable in the PNS of late stage embryos (Best, 2014). Tolloid-related is a secreted protease which is synthesised in muscles (Meyer and Aberle, 2006; Nguyen et al., 1994; Serpe and O'Connor, 2006). Therefore, without muscles Tolloid-related might not be expressed and can thus not down-regulate Side in sensory neurons.

The constitutive expression of Side in sensory neurons in late *beat* mutant embryos suggests that Side is cleaved after its interaction with Beat. Consequently, the interaction of Side with Beat might cause a transformation of the conformation of the Side protein resulting in an exposure of a cleavage site for Tolloid-related. But it has to be considered that the potential cleavage of Side by Tolloid-related was shown only indirectly by the constitutive expression of Side in *tolloid-related* mutants. A possibility to demonstrate if Tolloid-related cleaves Side directly might be the repetition of the cell aggregation assay performed by Siebert with an additional

Discussion

transfection of the S2 cells with Tolloid-related-HA. Co-transfected S2 cells with Beat-myc and Side-GFP form large cell aggregates (Siebert et al., 2009). Further transfection with Tolloid-related-HA should result in a degradation of the aggregates if it is required for the cleavage of the Side-Beat-complex.

Interestingly, Side exhibits a different localisation in late embryos of *beat* and *tolloid-related* mutants. In *beat* loss of function embryos Side is still localised in sensory neurons, while lack of *tolloid-related* causes a shift of Side localisation from sensory neurons to motor axons (Figs 2.28). It is conceivable that Tolloid-related represses the expression of Side in motor axons directly or indirectly. Therefore, lack of Tolloid-related would result in the observed expression of Side in motor axons. A similar function was shown for Tolloid, the homolog of Tolloid-related. Tolloid enhances the activity of DPP (Decapentaplegic) by cleaving its inhibitor (Short gastrulation) and therefore determines cell fates in the ectoderm (Canty et al., 2006; Marqués et al., 1997; Shimell et al., 1991).

Similar innervation defects of third instar larvae of *beat* and *tolloid-related* mutants compared to *side* mutants are another support for the conclusion that all three proteins interact in the same process and are necessary to establish a correct wiring of the larval neuromuscular system. Mutant larvae of all three genes show the strongest innervation defects in the ventral muscles field compared to wild-type larvae. The lateral and dorsal muscle fields exhibit milder phenotypes. Side loss of function larvae exhibit the strongest phenotype in all three muscle fields compared to wild-type as well as *beat* and *tolloid-related* mutants (Fig 2.32). Similar results were already described by other working groups as well as by former members of our working group (Fambrough and Goodman, 1996; De Jong et al., 2005; Serpe and O'Connor, 2006; Siebert et al., 2009; Sink et al., 2001). The observed weaker phenotypes of *tolloid-related* mutant larvae correlates with the expectations, since Side is still expressed in *tolloid-related* mutants and can be recognised by Beat expressing motor axons. In *side* mutant larvae Beat expressing motor axons do not find any pathway labelled by Side and therefore pass by the ventral muscle field (Fig 3.1). In *beat* mutants on the other hand, the pathway is constitutively labelled by Side, but cannot be recognised by the motor axons (Fig 3.1) (Siebert et al., 2009).

Contrarily, in *tolloid-related* mutants Side and probably Beat are expressed, but Side is not down-regulated in the PNS after contact with motor axons.

The observed innervation defects of *tolloid-related* loss of function larvae can possibly be explained by the non-neutralisation of the attractiveness of sensory neurons resulting in a prolonged adhesion of motor axons on sensory neurons. Without Tolloid-related, the interaction between Beat and Side is not cleaved and thus motor axons fail to defasciculate and fail to turn into their muscles fields (Fig 3.1). Therefore, it can be concluded that the down-regulation of Side in sensory neurons after interaction with Beat expressing motor axons mediated by Tolloid-related is an essential step for the correct defasciculation of motor axons.

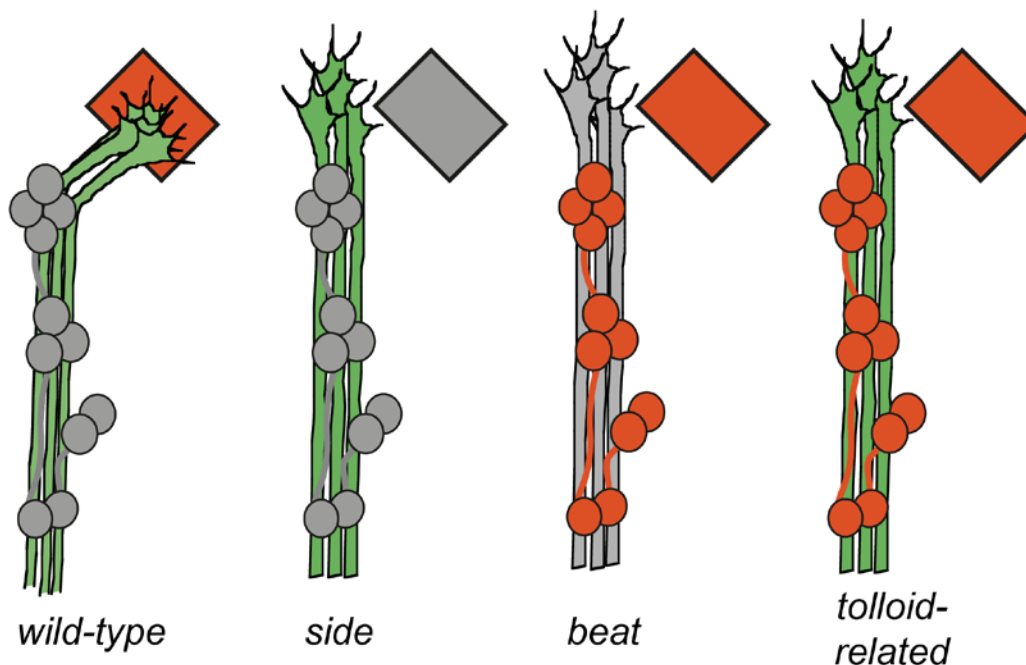


Fig 3. 1: Mis-guidance of motor axons in *side*, *beat* and *tolloid-related* (*tlr*) mutants.

In late wild-type embryos, Side expression is down-regulated in sensory neurons (grey circles) induced by motor axons (green). Up-regulation of Side in other tissues (red square) causes turning of motor axons. In *side* mutants, substrate is not labelled resulting in motor axons failing to turn into their target areas. In contrast, in *beat* mutants the pathway is constitutively labelled by Side, but cannot be recognized by the motor axons. In *tolloid-related* mutants, Side and Beat are expressed, but Side constitutively marks the pathway and axons fail to turn. Modified from Siebert et al., 2009.

Tolloid-related seems to be essential for further steps independently of Side during axon guidance and defasciculation, as *side* and *tolloid-related* double mutant larvae exhibit stronger innervation defects in comparison to single mutant larvae (Meyer and Aberle, 2006). It was further shown that Tolloid-related interacts with different TGF- β ligands. Loss of these ligands leads to similar but weaker wiring errors than the lack of Tolloid-related (Serpe and O'Connor, 2006). These results suggest together with

Discussion

the findings in this work that Tolloid-related is functional in two ways during axon guidance – Side-dependently and independent.

Analysis of *beat* and *tolloid-related* double mutant embryos using antibody staining and western blot analysis revealed that Side expression is not increased in comparison to the single mutants. This demonstrates that both genes work together in the regulation of Side expression in sensory neurons.

Interestingly, mRNA expression of *side* using qPCR is also altered in *beat* and *tolloid-related* mutant embryos (Fig 2.31). Lack of *beat* leads to a strong decrease of *side* mRNA expression in early and mid-stage (\leq stage 14) embryos and a weak, but not significant, decrease in stage 15-17 embryos. In up to stage 14 embryos of *tolloid-related* mutants a similar tendency is detectable resulting in a decreased *side* expression. These findings are contrary to the unaltered Side expression in stage 14 and the constitutive expression of Side in stage 15-17 *beat* and *tlr* mutant embryos compared to wild-type using immunohistochemical stainings. These results suggest that the lack of down-regulation of Side protein represses the expression of *side* mRNA in sensory neurons.

In summary, Side is expressed constitutively in *beat* and *tolloid-related* mutants in sensory neurons and motor axons, respectively. Side protein seems to trigger a negative feedback loop as *side* mRNA levels of different embryonic stages in mutant flies do not correlate with the levels of protein expression. It would be interesting to address open questions such as the correlation between the lack of *beat* or *tolloid-related* and the decreased expression of *side* mRNA.

3.2 Gene regulation of Beaten path Ia

The interaction partner of Side, Beaten path Ia, is expressed in a subset of motoneurons in the embryonic CNS (Fambrough and Goodman, 1996). In this thesis, one promoter fragment (40636) could be identified that reflects the expression of *beat* mRNA (Figs 2.36 + 2.37) and is able to completely rescue the *beat* mutant phenotype (Fig 2.39). This fragment exhibits one highly conserved region in the phylogenetical family of *Drosophilidae* with predicted binding sites amongst others for the transcription factor Even skipped (Eve), which are also conserved. Eve controls

the projections of dorsal motoneurons by regulating various axon guidance molecules such as *Beat* in SNa and RP2 neurons (Landgraf and Thor, 2006; Zarin et al., 2014a). These results suggest that the expression of *beat* is regulated in *Drosophila melanogaster* and other members of the clade *Drosophilidae* by one promoter element, which is activated by *Eve*.

3.3 Larval Phenotype

3.3.1 Lack and gain of *Side* cause larval wiring errors

Loss of *side* as well as overexpressing *side* in muscles cause innervation defects in larvae. Both loss- and gain of function larvae show mis-innervations in all three muscle fields. In *side* mutant larvae, the phenotype is most prominent in the ventral muscle field caused by defasciculation defects and mis-guidance of nerve branches resulting in dislocated NMJs (Fig 2.42). In larvae overexpressing *Side* the dorsal muscle field shows a nearly complete non-innervation (Fig 2.49) based on truncation of the ISN (Fig 2.51). Lack and gain of *Side* causes variable phenotypes in each larval segment. Around 80% of wild-type hemisegments exhibit 25-28 NMJs using the microscopy technique described in chapter 4.2.7: Characterisation of larval innervation (Figs 2.43 + 2.50). In contrast, *Side* loss of function larvae show a distribution between 8 and 27 NMJs per hemisegment (Fig 2.43), while *Side* gain of function larvae exhibit a distribution between 14 to 23 NMJs (Fig 2.50). These results indicate that motor axon guidance is regulated hemisegment-autonomously and not by a global regulator in the CNS.

Analysing the CNS of wild-type and *side* mutant embryos and larvae it could be shown that the *side* mutant phenotype does not base on loss of motoneurons, since no conspicuous different number of motoneurons and especially of SN neurons (in embryos) is visible. This experiment further demonstrates that motor axons grow out of the CNS to innervate the somatic muscles independently of *Side*. This result is supported by the analysis of the diameter of the ISN where it bypasses muscle 12. *Side* loss of function larvae exhibit a thicker ISN compared to wild-type (Fig 2.48), suggesting that the SNa, SNc and ISNb grow out of the CNS, but fail to defasciculate. These results indicate that *Side* is essential for the defasciculation and correct guidance into the respective muscle fields, but that *Side* is not sufficient for the development and survival of motoneurons as well as for the outgrowing itself.

Discussion

Interestingly, analysing the area of NMJs per hemisegment it became obvious that lack of *side* leads to a stronger relative decrease of NMJ area compared to NMJ number. In comparison to wild-type, *Side* loss of function larvae exhibit 37% less NMJs, but a 55% decreased synaptic area (Fig 2.43). This result suggests a second function - synaptic growth- of *Side* in the neuromuscular system of *Drosophila*. This conclusion is supported by the findings of Kaufmann and colleagues. They demonstrate that the tyrosine phosphatase LAR (leukocyte antigen-related) is essential for normal synaptic morphology besides its known function during axon guidance (Kaufmann et al., 2002; Krueger et al., 1996; Tian et al., 1991). Similar conclusions were drawn from *Side* gain of function larvae (De Jong et al., 2005). Ectopic expression of *Side* in all muscles leads to changes in synaptic morphology. Furthermore, *Side* seems to require Fasciclin II for synaptic stability, since muscle specific overexpression of *Side* cannot compensate the lack of *FasII* in *FasII* mutants, which leads to a decreased number of boutons compared to control larvae (De Jong et al., 2005). These results indicate that both overexpression and lack of *Side* result in defects in synaptic morphology.

In mammals, lack of muscle innervation induce muscular atrophy with reduction in muscle mass, strength and myofiber diameter (Cisterna et al., 2014). Lack and gain of *Side* cause similar defects. Muscles without innervation exhibit a smaller diameter compared to innervated control muscles. In addition it was shown that an increased number of NJMs in overexpression larvae conditioned by ectopic NMJs results in an increased muscle diameter compared to wild-type (Schäfer, 2015). These results suggest that non-innervation leads to muscle atrophy based probably on no or a reduced neuronal input and therefore on missing muscle contraction. An increased neuronal input conditioned by additional NMJs leads in turn to a probably stronger muscle contraction and therefore to a thicker diameter of muscles. These results further demonstrate that the observed altered muscle size is based on mis-innervation and therefore only indirectly on loss or gain of *Side* function.

Since the innervation analyses are based on the postsynaptic marker ShakerGFP, an interesting question is, if muscles without postsynapses also have no presynaptic structures. Using the presynaptic marker Synaptotagmin it is detectable that non-

Discussion

innervated muscles of both *Side* gain- and loss of function larvae exhibit still some type II boutons (Figs 2.45 + 2.53). However, in wild-type these mis-matches are also visible. These results suggest that presynapses with type II boutons do not end in postsynapses positive for ShGFP.

In summary, lack and gain of *Side* cause missing MNJs and a reduced synaptic area. In addition, not innervation of muscles results in smaller muscles diameter.

3.3.2 Mis-innervation of larval somatic muscles results in locomotion defects

Innervation defects caused by the missing or overexpression of *Side* lead to locomotion defects in crawling larvae. *Side* mutant larvae cover shorter distances compared to wild-type using the crawling assay performed on an agarose substrate (Fig 2.54) based on a longer duration of a single peristaltic wave (Fig 2.55). Using a high-speed camera for detailed analyses of locomotion, it is detectable that lack of *Side* results not only in slower crawling compared to wild-type but rather in an altered motion sequence (Figs 2.56 + 2.57). *Side* mutant larvae elevate their rear higher from the substrate to initiate the peristaltic wave in comparison to wild-type larvae. Furthermore, wild-type larvae crawl straight forward with tight contact to the agarose substrate. In contrast, *Side* loss of function larvae lose contact between the substrate and their ventral body half during the peristaltic wave wanders from the posterior to the anterior end. Similar results can be observed for gain of function larvae. They also cover smaller distances than the control larvae. However, the duration of one peristaltic wave does not show a significant difference (Figs 2.54 + 2.55). Additionally, larvae overexpressing *Side* elongate their anterior end exuberantly compared to wild-type and *side* mutants. Movies from dorsal view demonstrate a rotation of the larvae along the ventro-dorsal axis resulting in a body shape like the letter “S” during crawling.

These results suggest that mis-innervation of muscles leads to locomotion defects. Frequent lack of ventral innervation leads to stronger locomotion defects than lack of dorsal innervation as measured by the crawling distance and duration of a single peristaltic wave. Furthermore, *Side* gain- and loss of function larvae try to compensate the non-innervated muscles in different ways (e.g. elongating the anterior end).

Additionally, high-speed movies as well as the crawling assay show that lack and gain of Side result in different intensity of phenotypes. Some mutant and Side overexpression larvae exhibit no obvious defects compared to wild-type while others have big problems to crawl and to perform the normal crawling motion sequence. This different crawling behaviour possibly reflects the different observed innervation phenotypes. Therefore, larvae with strong innervation defects show strong motion defects, while weak innervation errors lead to mild crawling defects. In order to support this assumption, it would be necessary to image the innervation pattern of larvae directly after performing high-speed movies of their crawling behaviour. Thereby, it is maybe possible to draw direct conclusions between the mis-innervation of single muscles and the locomotion behaviour.

3.4 Sidestep is also functional during metamorphosis

Up to now, all analyses of Side focussed on its function during the axonal outgrowth in the embryo. As a holometabolic insect, *Drosophila* has to establish its neuromuscular system for a second time during the metamorphosis. Most of the embryonic motoneurons survive during this process, but larval NMJs retract and the motor axons have to grow out a second time to innervate their target muscles (Fernandes and Vijayraghavan, 1993; Tissot and Stocker, 2000; Truman, 1990). Thus, the question arises if Side also has an essential function during the establishment of the adult neuromuscular system or if another member of the Side family is the key-regulator of this process. Since there are seven Side paralogs encoded in the *Drosophila* genome, which are not characterised on the molecular level, it is possible that Side functions exclusively during embryogenesis, while one of its paralogs regulates the establishment of the adult neuromuscular system. Prominent examples for not identical gene families are the globulin gene families, which encode for the α -type or β -type globin chains of the haemoglobin forming a tetramer out of two α -type and two β -type chains. Each family consists of a cluster of genes, whose members are expressed at various stages of development. Thus, in mammals distinct haemoglobins are produced – firstly an embryonic one, secondly an fetal one and thirdly an adult one (Wolpert et al., 2002).

To address the question, if the lack of Side results in innervation errors of adult musculature, the innervation of adult leg and flight muscles was analysed. To

Discussion

investigate furthermore if Side is required during metamorphosis, different locomotion assays were performed with adult Side loss- and gain of function flies expecting that locomotion behaviours be not altered if Side is not functional during the remodelling of the neuromuscular system.

Lack of Side causes strong innervation errors of the femur. In control flies, one main nerve bundle projecting along a trajectory in the middle of the femur innervates the femur. Additionally, many defasciculated nerves migrate into the periphery. Lack of Side results in two principal phenotypes – decreased number of nerves innervating the periphery and a dislocalisation of the main nerve bundle. Therefore, similar to larvae, *side* mutant adults show an aberrant innervation pattern. Additionally, lack of Side leads to a thicker diameter of the main nerve in the distal part of the femur in comparison to control flies (Fig 2.70). This result suggests that the observed decreased amount of peripheral nerves is based on defasciculation defects similar to that observed in *side* mutant larvae. Furthermore, the diameter of the femur is decreased in mutants compared to wild-type (Fig 2.72). This observation might be caused by mis-innervations of the leg muscles causing muscle atrophy resulting in a thinner femur diameter. Larval somatic muscles show similar effects where non-innervation leads to a thinner diameter amongst others of muscle 12 (see chapter 2.2.1: Loss of *side* function leads to innervation defects in larvae).

Using the leg print assay to analyse the walking behaviour of adult flies, Side gain- and loss function flies show different locomotion defects. For *side* mutants three principal phenotypes are detectable (Fig 2.72). Firstly, flies representing the strong phenotype are not able to walk over the microscopy slides. Secondly, the moderate phenotype comprises flies, whose leg prints cannot be matched to a specific leg. Thirdly, flies representing the weak phenotype exhibit altered leg postures during walking and show a dragging of the metathoracic leg. These results suggest that similar to larvae, a mis-innervation of muscles leads to locomotion defects.

Gain of Side leads to a milder locomotion phenotype with a decreased step length and a longer third tarsus print (Fig 2.72). However, all overexpression flies are able to walk over the microscopy slides. Since it is not possible to overexpress *side* muscle specifically and a fluorescent dye motoneuron specifically simultaneously using the UAS-Gal4 system, it was not possible in this thesis to analyse the innervation of the

Discussion

femur of Side gain of function adults. For further experiments, a combination of the UAS-Gal4- and the LexA-LexAop system could be used to circumvent this technical problem. But the milder locomotion defects suggest that the overexpression of Side results in weaker mis-innervation errors in adult legs similar to the weaker innervation defects in larvae.

Using a high-speed camera for more detailed analysis of walking, further motion defects become obvious for both Side loss- and gain of function flies. Side mutant flies are not able to move their pro-thoracic legs resulting in a stagger of the flies during walking over the smooth microscopy slides. In contrast, Side gain of function flies have no problem to walk over the microscopy slides, but stick out one or both wings during walking.

Another essential locomotion behaviour for *Drosophila* is the ability to fly. To test if Side loss- and gain of function flies are able to fly and to take off, different locomotion assays were performed. Both genotypes show strong defects in comparison to the wild-type and analogue to larval locomotion, *side* mutant flies exhibit a stronger phenotype than the *side* overexpression flies. To investigate if the locomotion defects are based again on mis-innervation, indirect flight muscles were prepared and the innervation pattern was compared to that of control flies. Interestingly, compared to *side* mutant flies, Side gain of function flies show stronger innervation defects. Indirect flight muscles of *side* overexpression flies exhibit different phenotypes. Some muscle fibres of the indirect flight musculature show almost no innervation, while other muscle fields show a strong increase of nerve branches (Fig 2.66). In addition, the single muscles fibres are predominantly innervated on their ventral side. In *side* mutants no distinct phenotype is detectable (Fig 2.65). But it has to be considered that only four thoraxes could be analysed due to the small number of *side* mutant adults and the pulpier texture of the flight muscles compared to wild-type flies, which makes it difficult to dissect them properly.

The stronger innervation defects of flies overexpressing *side* can probably be explained by the development of the indirect flight muscles (IFMs) and their innervation. In contrast to almost all other adult muscles, the dorsal longitudinal muscles (DLMs) of the indirect flight musculature, which were analysed in this thesis, develop from larval muscles. The meso-thoracic (T2) oblique muscles 9, 10 and 19

Discussion

function as a template for the DLMs and therefore, these muscles do not emerge from adult muscle precursors (AMPs) (Fernandes et al., 1991). Innervation of adult IFMs is based on remodelling of the intersegmental and segmental nerve of the meso-thoracic segment of the larva (Fernandes and Vijayraghavan, 1993). Larvae overexpressing *side* exhibit strong mis-innervations in the dorsal muscle field that includes the muscles 9 and 10. Therefore, it is possible that the mis-guidance of the ISN persists through the metamorphosis and causes the observed strong mis-innervation of the DLMs. This in turn would mean that adult innervation defects are based on embryonic axon guidance defects and that *Side* would not necessarily be functional a second time in establishing the innervation of the DLMs. This hypothesis is supported by the *side* mutants, which show only a weak phenotype analysing the innervation of DLMs compared to the overexpression flies. In larvae, a similar result is detectable when analysing the innervation of the dorsal muscle field. Gain of function larvae exhibit on average only 2.6 NMJs, while *Side* loss of function larvae have around 4 NMJs per hemisegment in the dorsal muscle field.

The question arises why, in spite of inferior innervation defects, *side* mutants exhibit a stronger locomotion defect regarding the ability to fly and to take off compared to *side* overexpression flies. Around 2.9 fold amount of *Side* gain of function flies are able to escape by flying after dropping onto a lab bench compared to *Side* loss of function flies. Further, while around 15% of the *side* overexpression flies are able to take off from an island surrounded by water, no *side* mutant fly at all can vanish from the platform. There are two possible reasons for the inability to take off of *side* mutant flies: Firstly, the direct flight muscles, which coordinate the correct wing position, and secondly, the jump muscles, which provide the impulse for taking off.

Direct flight muscles adjust the orientation of wings, while indirect flight muscles are responsible for the flight power (Dickinson and Tu, 1997; Jähring et al., 2010). Therefore, the observed locomotion defects of *side* mutant flies might base on mis-innervation of the direct flight muscles and thus on an incorrect adjustment of the wings. This conclusion is supported by the analyses of the number of wing beats and the wing amplitude (Fig 2.64). Compared to wild-type, loss of function flies exhibit no significant different number of wing beats per second, while the amplitude of one analysed fly shows a strong decrease in comparison to a wild-type fly. These results suggest that *side* mutant flies are possibly able to generate enough power for beating

Discussion

their wings, but they are not able to adjust them correctly. This suggestion is supported by high-speed movies of fixed flies and of the take-off demonstrating that *side* mutant flies are not able to move both wings synchronously and are only able to rotate one wing in contrast to wild-type flies oscillating and rotating both wings synchronously (Figs 2.61 + 2.62).

This consideration can further confirm by the additional function of direct flight muscles in courtship and grooming (Dickinson and Tu, 1997; Ewing, 1979). *Side* mutant flies are only able groom their eyes from dust and show sterility, which is not based on defects during the spermatogenesis. Similar to flight behaviour, indirect flight muscles produce the power for the courtship song and direct muscles the timing of song pulses (Ewing, 1979). Therefore, it is possible that the sterility of the *side* mutant males is based on the inability to perform the courtship song correctly, which might be due to mis-innervation of the direct flight muscles.

The second possibility is that a mis-innervation of the two tergotrochanteral muscles (TTMs, also called jump muscles), which are associated with the mesothoracic legs, is responsible for the inability to take off. Contraction of TTMs causes an extension of the femurs of both second legs resulting in starting the take off by jumping (Nachtigall and Wilson, 1967; Trimarchi and Schneiderman, 1993). Thus, a mis-innervation of the TTM could also lead to the observed inability of *side* mutant adults to take off. This assumption is also supported by the high-speed movie of the take-off of one mutant fly (Fig 2.61). In comparison to wild-type, the *Side* loss of function fly lifts its first and third legs later based on the wing position suggesting that the fly is not able to jump with its mesothoracic legs.

Regarding adult innervation and resulting locomotion defects the question arises, if *Beaten path 1a* is, similar to its function during embryonic development, the interaction partner of *Side*. To address this question, the locomotion assays performed with *Side* loss- and gain of function flies were also performed with *Beat* loss of function flies (data not shown). Compared to *side* mutant flies, lack of *Beat* results in a milder adult phenotype. All tested flies were able to fly and around 70% of the flies can take off. Analysing the walking behaviour, *beat* mutants show an increased step length and length of the metathoracic tarsus print, but all flies are able to walk over the microscopy slides and exhibit no significantly different tarsus print

Discussion

positions. These results suggest that Beat Ia is not as important as Side for the development of the adult neuromuscular system. Therefore, it is possible that another member of the *beat* family is functional in motor axon guidance during the metamorphosis.

Taken together, mis-innervations of adult muscles lead similar to larvae to locomotion defects and Side is a possible key-regulator of axon guidance during metamorphosis. In contrast to axonal pathfinding during embryogenesis, no evidence was found that the axon guidance receptor Beat Ia is the interaction partner of Side during this process. Thus, it would be interesting to analyse if another member of the *beat* family interacts with Sidestep during the metamorphosis to establish a neuromuscular system.

4. Materials and Methods

4.1 Materials

Tab 4. 1: Chemicals and reagents

| Chemical/reagent | Manufacturer |
|--|---|
| 1kb DNA Ladder | Thermo Fisher Scientific, Oberhausen |
| Acetic acid (C ₂ H ₄ O ₂) | Sigma Aldrich Chemie GmbH, Steinheim |
| Acrylamide (37.5:1) | Carl Roth GmbH & Co. KG, Karlsruhe |
| Agar | BD (Becton, Dickinson), Sparks, USA |
| Agarose low EEO | AppliChem GmbH, Darmstadt |
| Ammonium acetate | Carl Roth GmbH & Co. KG, Karlsruhe |
| 6-Aminohexanoic acid | Carl Roth GmbH & Co. KG, Karlsruhe |
| Ammonium persulfate (APS) (NH ₄) ₂ S ₂ O ₈ | Carl Roth GmbH & Co. KG, Karlsruhe |
| Austerlitz Insect pins Minucie (⊙0.2mm, stainless steel) | Fine Sciene Tools GmbH, Heidelberg |
| BCIP/NBT liquid substrate system | Sigma Aldrich Chemie GmbH, Steinheim |
| Bromphenol blue sodium salt | Carl Roth GmbH & Co. KG, Karlsruhe |
| Chlorix (Sodiumhypochloride) | Colgate-Palmolive, Hamburg |
| Clarity™ Western ECL Substrate Peroxide solution | Bio-Rad Laboratories Inc., Hercules, USA |
| Clarity™ Western ECL Substrate Luminol/enhancer solution | Bio-Rad Laboratories Inc., Hercules, USA |
| Denhardts | Carl Roth GmbH & Co. KG, Karlsruhe |
| Dextran sulfate sodium salt | Carl Roth GmbH & Co. KG, Karlsruhe |
| DIG RNA Labeling Mix, 10x conc. | Roche Diagnostics GmbH, Mannheim |
| Disodium hydrogen phosphate (Na ₂ HPO ₄) | Grüssig GmbH, Filsum |
| dNTPs (dATP, dTTP, dGTP, dCTP) | Thermo Fisher Scientific, Schwerte |
| 1,4-Dithiothreit (DTT) (C ₄ H ₁₀ O ₂ S ₂) | Carl Roth GmbH & Co. KG, Karlsruhe |
| EGTA (C ₁₄ H ₂₄ N ₂ O ₁₀) | Carl Roth GmbH & Co. KG, Karlsruhe |
| Ethanol absolute | VWR International, Gelenaakbaakn, Belgium |
| Ethylenediaminetetraacetic acid (EDTA) | Carl Roth GmbH & Co. KG, Karlsruhe |
| Formaldehyde (37%) | AppliChem GmbH, Darmstadt |
| Formamide p.A. | AppliChem GmbH, Darmstadt |
| Glycine | Carl Roth GmbH & Co. KG, Karlsruhe |
| Glycerol | Carl Roth GmbH & Co. KG, Karlsruhe |
| Heptane | VWR International, Gelenaakbaakn, |

Material and Methods

| | |
|--|---|
| | Belgium |
| Heparin | Carl Roth GmbH & Co. KG, Karlsruhe |
| Hydrochloric acid (HCl) | VWR International, Gelenaakbaakn, Belgium |
| Immun-Blot PVDF Membrane, 0.2µm | Bio-Rad Laboratories Inc., Hercules, USA |
| Magnesium chloride (MgCl ₂) | Carl Roth GmbH & Co. KG, Karlsruhe |
| Methanol | VWR International, Gelenaakbaakn, Belgium |
| Normal Goat Serum | Jackson Immunoresearch (USA) |
| Oligo d(T) 18 mRNA Primer | New England BioLabs, Frankfurt am Main |
| Paraformaldehyde | SERVA Electrophoresis GmbH, Heidelberg |
| Potassium chloride (KCl) | AppliChem GmbH, Darmstadt |
| Potassium dihydrogenphosphate (KH ₂ PO ₄) | AppliChem GmbH, Darmstadt |
| Q5 High-Fidelity DNA Polymerase | New England BioLabs, Frankfurt am Main |
| Reactive Yellow 86 | Organic Dyes and Pigments LLC, East Providence, USA |
| Ribo Lock RNase Inhibitor | Thermo Fisher Scientific, Schwerte |
| RNase Inhibitor, Murine (M0314S) | New England BioLabs, Frankfurt am Main |
| Salmon sperm DNA | Invitrogen, Darmstadt |
| Sodium chloride (NaCl) | VWR International, Gelenaakbaakn, Belgium |
| Sodium dodecyl sulfate (SDS) | Carl Roth GmbH & Co. KG, Karlsruhe |
| Sodium dihydrogen phosphate (NaH ₂ PO ₄) | Grüssig GmbH, Filsum |
| Sodium hydroxide - Pellets (HNaO) | AppliChem GmbH, Darmstadt |
| SSC | Carl Roth GmbH & Co. KG, Karlsruhe |
| T3 RNA polymerase | Thermo Fisher Scientific, Schwerte |
| T7 RNA polymerase | Thermo Fisher Scientific, Schwerte |
| TEMED | Carl Roth GmbH & Co. KG, Karlsruhe |
| TRIS | Carl Roth GmbH & Co. KG, Karlsruhe |
| TRIS blotting-grade | Carl Roth GmbH & Co. KG, Karlsruhe |
| TRIS-hypochloride | Carl Roth GmbH & Co. KG, Karlsruhe |
| TritonX-100 | Carl Roth GmbH & Co. KG, Karlsruhe |
| Tween 20 | Carl Roth GmbH & Co. KG, Karlsruhe |
| Whatman™ Chromatography paper 3mm Chr | GE Healthcare GmbH, Solingen |

Material and Methods

Tab 4. 2: Buffer

| Buffer | Chemical | Concentration |
|---|---|----------------|
| 10x PBS, pH7,4 | NaCl | 1.37M |
| | KCl | 27mM |
| | Na ₂ HPO ₄ | 100mM |
| | KH ₂ PO ₄ | 20mM |
| 1x PTX | TritonX-100 | 0.1% in 1x PBS |
| 1x PBT | Tween 20 | 0.1% in 1x PBS |
| 1x TE | Tris-HCl (pH7.6) | 10mM |
| | EDTA (pH8.0) | 1mM |
| 50x TAE (pH8.2 with 100% acetic acid) | Tris | 2M |
| | EDTA (pH8.0) | 50mM |
| Chloride bleach | Sodiumhypochloride | 1.7% |
| Probe puffer (<i>in vitro</i> transcription) | Formamide | 50% |
| | TE (pH7) | 50% |
| | Tween 20 | 0.1% |
| AP buffer (<i>in situ</i> hybridisation) | Tris (pH9.5) | 100mM |
| | NaCl | 100mM |
| | MgCl ₂ | 100mM |
| | Tween 20 | 0.1% |
| Hybridisation buffer (<i>in situ</i> hybridisation) | Formamide | 50% |
| | 20x SSC | 4x |
| | 50x Denhardts | 1x |
| | Boiled salmon sperm DNA | 250µg/ml |
| | Heparin | 50µg/ml |
| | Dextran sulfate | 5% |
| | Tween20 | 0.1% |
| Washing buffer (<i>in situ</i> hybridisation) | Formamide | 50% |
| | 20xSSC | 2x |
| | Tween 20 | 0.1% |
| Relaxing solution (preparation flight musculature) | Phosphate buffer (pH7) | 20mM |
| | MgCl ₂ | 5mM |
| | EGTA | 5mM |
| Phosphate buffer pH7 (preparation flight musculature) | Na ₂ HPO ₄ | 0.1M |
| | NaH ₂ PO ₄ | 0.1M |
| | the pH of the fist solution will be adjusted with the second solution | |
| 2x sample buffer (western blot) | Tris-HCl (pH6.8) | 62.5mM |
| | DTT | 10mM |
| | SDS | 2% |
| | Glycerol | 10% |
| | Bromphenolblue | 0.001% |

Material and Methods

| | | |
|--|-------------------------------------|-------------------------|
| Running buffer (western blot) | Tris-HCl (pH8.3) Glycine SDS | 192mM 1.9M 34.7mM |
| Anode Puffer I (API) pH9.4 (western blot) | Tris | 300mM |
| Anode Puffer II (APII) pH9.4 (western blot) | Tris | 30mM |
| KP buffer pH9.4 (western blot) | Tris 6-Aminohexanoic acid SDS | 30mM 40mM 0.1% |
| 10x TBST (western blot) | Tris-HCl (pH7.4) NaCl Tween20 | 100mM 1.5M 0.1% |

Tab 4. 3: Media

| Medium | Chemical | Volume |
|--------------------------------------|---------------------|--------|
| Applejuice agar | Purified (VE) water | 3l |
| | Applejuice | 1l |
| | Sucrose | 100g |
| | Agar | 70g |
| Standard <i>Drosophila</i> medium | VE water | 10l |
| | Agar | 50g |
| | Yeast extract | 168g |
| | Malt extract | 450g |
| | Soy flour | 95g |
| | Corn grits | 712g |
| | Treacle | 400g |
| | Propionic acid | 45ml |
| Nipagin | 15g | |
| LB medium (pH 7.0) | NaCl | 10g |
| | Trypton | 10g |
| | Yeast extract | 5g |
| | ddH ₂ O | ad 1l |

Material and Methods

Tab 4. 4: Gels

| Gel | Chemical | Concentration |
|---------------------------------------|--|-------------------------------------|
| Agarose gel | Agarose | 0,7% in 1xTAE buffer |
| Seperating gel (8%) (western blot) | Acrylamide (37.5:1) Tris (pH8.8) SDS APS TEMED | 8% 375mM 0.1% 0.1% 0.1% |
| Stacking gel (4%) (western blot) | Acrylamide Tris (pH6.8) SDS APS TEMED | 4% 125mM 0.1% 0.1% 0.1% |

Tab 4. 5: Kits

| Kit | Manufacturer |
|--|----------------------------------|
| High Pure Plasmid Isolation Kit | Roche Diagnostics GmbH, Mannheim |
| QIAquick PCR Purification Kit | QIAGEN GmbH, Hilden |
| ToTALLY RNA Kit | Ambion |
| FastStart Essential DNA Green Master | Roche Diagnostics GmbH, Mannheim |
| SuperScript™ III Reverse Transcriptase | Invitrogen |

Tab 4. 6: Antibodies

| Antigene | Species | Dilution | Resource |
|-----------------------------------|----------------|-----------------|---|
| Ankyrin-2XL | rabbit | 1:1000 | Koch et al., 2008 |
| BarH1/2 | rabbit | 1:200 | gift from K. Choi and K. Saigo, Developmental Genetics, Department of Biological Sciences, Korea Advanced Institute of Science and Technology |
| Connectin | mouse | 1:25 | DSHB (Clone C1.427-s) |
| DVGlut | rabbit | 1:800 | Mahr and Aberle, 2006 |
| Eve | mouse | 1:100 | DSHB (Clone 2B8) |
| FasII | mouse | 1:50 | DSHB (Clone 1D4) |
| Futsch | mouse | 1:100 | gift from C.S. Goodman |
| GFP | rabbit | 1:1000 | Acris Antibodies GmbH (Germany) (TP401) |
| GFP | mouse | 1:400 | Roche (mixture of Clones 7.1 and 13.1) |
| MHC | mouse | 1:100 | DSHB |
| Repo | mouse | 1:40 | DSHB (Clone 8D12) |
| Sidestep | mouse | 1:25 | DSHB (Clone 9B8) |
| Synaptotagmin | mouse | 1:40 | gift from C.S. Goodman |
| Anti-Digoxigenin-AP Fab fragments | | 1:2000 | Roche Diagnostics GmbH, Mannheim |

Material and Methods

Tab 4. 7: Secondary antibodies

| Antigene | Fluorescent dye / enzyme | Species | Dilution | Resource |
|------------|--------------------------|---------|----------|-------------------------|
| rabbit IgG | Alexa 488 | goat | 1:500 | Jackson Immuno research |
| rabbit IgG | Cy3 | | | |
| mouse IgG | Alexa 488 | | | |
| mouse IgG | Cy3 | | | |
| rabbit IgG | HRP | | 1:7500 | |
| mouse IgG | HRP | | | |

Tab 4. 8: Primer

| Name | Sequence |
|-----------------------|--------------------------|
| T3 | AATTAACCCTCACTAAAGGG |
| T7 | TAATACGACTCACTATAGGG |
| qPCR side 48960:48980 | CAGGGACGAGGCCAGTTCAGC |
| qPCR side 53015:53036 | GTCCTCGGACAGAATGGATTTCG |
| qPCR beat 6351:6370 | CCACGCGGTGAGGCCGAGTG |
| qPCR beat 26986:26997 | CGGATGTAGCCATTGTTACCGC |
| qPCR RpL32 453:475 | CGGATCGATATGCTAAGCTGTCTG |
| qPCR RpL32 678:697 | CCAGCTCGCGCACGTTGTGC |

Tab 4. 9: Flystocks

| Flystock | | Reference/source |
|------------------------|--|-----------------------------|
| general stocks | w ¹¹¹⁸ ;+;+ | stock collection Aberle Lab |
| | w;+;ShGFP7A (III. chromosome) | Zito et al., 1999 |
| | w;ShGFP1A;+ (II. chromosome) | |
| | w,FasII-GFP ^{Mue397} ;+;+ | Siebert et al., 2009 |
| <i>sidestep</i> stocks | W;+; <u>side^{C137},ShGFP7A</u> TM6B | Aberle et al., 2002 |
| | W;+; <u>side^{C137},ShGFP7A</u> TM3,twiGFP | |
| | W;+; <u>side^{I1563},ShGFP7A</u> TM6B | |
| | W;+; <u>side^{I1563},ShGFP7A</u> TM3,twiGFP | |
| | W;+; <u>side^{C137},UAS-side^{29A},ShGFP7A</u> TM6C | Siebert et al., 2009 |
| | W; <u>OK371-Gal4,side^{C137},ShGFP7A</u> CyO,actGFP, TM6B | |
| | W;+; <u>side^{I1563},UAS-DsRed,ShGFP7A</u> TM6C | |
| | W;+; <u>side^{I1563},UAS-CD4-tdTomato</u> TM6C | |
| | Schäfer, 2015 | |

Material and Methods

| | | | |
|---|--|---|-----------------------|
| <i>beaten path la</i> stocks | W; $\frac{\text{beat}^3, \text{ShGFP1A}, \text{fasIII}^{\text{E25}}}{\text{Cyo}, \text{twiGFP}}$;+ | Fambrough and Goodman, 1996; Siebert et al., 2009 | |
| | W; $\frac{\text{beat}^{\text{C163}}, \text{ShGFP1A}}{\text{Cyo}, \text{twiGFP}}$;+ | | |
| | W; $\frac{\text{beat}^3, \text{ShGFP1A}, \text{fasIII}^{\text{E25}}}{\text{Cyo}, \text{wingless-LacZ}}$;+ | | |
| | W; $\frac{\text{beat}^{\text{C163}}, \text{ShGFP1A}}{\text{Cyo}, \text{twiGFP}}$;UAS- <i>beat</i> ⁵ | | |
| <i>tolloid-related</i> stocks | W;+; $\frac{\text{tI}^{\text{K788}}, \text{ShGFP7A}}{\text{TM3}, \text{twiGFP}}$ | Aberle et al., 2002 | |
| | W;+; $\frac{\text{tI}^{\text{D427}}, \text{ShGFP7A}}{\text{TM3}, \text{twiGFP}}$ | | |
| | W; $\frac{\text{FasIIIGFP}^{\text{Mue397}}}{\text{FM7}, \text{actGFP}}$;+; $\frac{\text{tI}^{\text{D427}}, \text{ShGFP7A}}{\text{TM3}, \text{twiGFP}}$ | stock collection Aberle Lab | |
| <i>beaten path la; tolloid-related</i> double mutant stocks | W; $\frac{\text{beat}^3, \text{ShGFP1A}}{\text{Cyo}, \text{twiGFP}}$, $\frac{\text{tI}^{\text{D427}}, \text{ShGFP7A}}{\text{TM3}, \text{twiGFP}}$ | this work | |
| | W; $\frac{\text{beat}^{\text{C163}}, \text{ShGFP1A}}{\text{Cyo}, \text{twiGFP}}$, $\frac{\text{tI}^{\text{K788}}, \text{ShGFP7A}}{\text{TM3}, \text{twiGFP}}$ | | |
| UAS-Stocks | w,UAS- <i>side</i> ⁴⁶ ;+;+ | Sink et al., 2001 | |
| | w;+;UAS- <i>side</i> ^{29A} | | |
| | w;+;UAS-mCD8GFP | Lee and Luo, 1999 | |
| | w;+;UAS-dsRed,shGFP7A | Bloomington #6282 | |
| | w;+; $\frac{\text{UAS-CD4tdTomato}}{\text{TM6}}$ | gift from P. Soba, ZMNH University Hamburg | |
| Gal4-Stocks | w;btl-Gal4;+ | gift from M. Krasnow, Stanford University, CA | |
| | w;OK3714-Gal4,ShGFP1A;+ | Mahr and Aberle, 2006 | |
| | w;+;OK371-Gal4,ShGFP7A | | |
| | w;+;mef2-Gal4 | gift from C.S. Goodman | |
| | w;+;mef2-Gal4,ShGFP7A | stock collection Aberle Lab | |
| | w;+; $\frac{\text{repo-Gal4}}{\text{TM3}}$ | Bloomington #7415 | |
| <i>promoter stocks beat</i> | w;+;P{y[+t7.7]w[+mC]=GMR92H09-GAL4}attP2 | Bloomington #40634 | Pfeiffer et al., 2008 |
| | w;+;P{y[+t7.7]w[+mC]=GMR93A02 GAL4}attP2 | Bloomington #40635 | |
| | w;+;P{y[+t7.7]w[+mC]=GMR93A04-GAL4}attP2 | Bloomington #40636 | |
| | w;+;P{y[+t7.7]w[+mC]=GMR93A05-GAL4}attP2 | Bloomington #40637 | |
| | w;+;P{y[+t7.7]w[+mC]=GMR93A09-GAL4}attP2 | Bloomington #40638 | |
| | w;+;P{y[+t7.7]w[+mC]=GMR92H08-GAL4}attP2/TM3 | Bloomington #47210 | |
| | w;+;P{y[+t7.7]w[+mC]=GMR92H11- | Bloomington | |

Material and Methods

| | | | |
|-----------------------------------|---|---|-------------------|
| | GAL4}attP2 | #47211 | |
| | w;+;P{y[+t7.7]w[+mC]=GMR93A06-GAL4}attP2 | Bloomington #47212 | |
| | w;+;P{y[+t7.7]w[+mC]=GMR92H12-GAL4}attP2/TM3, Sb[1] | Bloomington #48633 | |
| | w;+;P{y[+t7.7]w[+mC]=GMR93A03-GAL4}attP2/TM3 | Bloomington #48634 | |
| | w;+; P{VT008208-GAL4}attP2 | VDRC #203094 | Kvon et al., 2014 |
| promoter stocks <i>side</i> | w;+; P{VT048356-GAL4}attP2 | VDRC #201045 | Kvon et al., 2014 |
| | w;+; P{VT048339-GAL4}attP2 | VDRC #204220 | |
| | w;+; P{VT048340-GAL4}attP2 | VDRC #204347 | |
| | w;+; P{VT048331-GAL4}attP2 | VDRC #205905 | |
| | w;+; P{VT048335-GAL4}attP2 | VDRC #206961 | |
| | w;+; P{VT048336-GAL4}attP2 | VDRC #213798 | |
| stocks <i>side</i> degradation | W; $\frac{\text{aph-1}^{W35}, \text{FRT40A}}{\text{CyO}, \text{actGFP}}$; + | gift from T. Klein, HHU | |
| | W; $\frac{\text{Dmon1}^{\text{mut4}}}{\text{CyO}, \text{actGFP}}$; + | gift from T. Klein, HHU | |
| | W; $\frac{\text{kuz}^{\text{e29-4}}}{\text{CyO}, \text{actGFP}}$; shGFP7A | Bloomington #5804 | |
| | W; $\frac{\text{Uba1}^{\text{H33}}, \text{FRT42D}}{\text{CyO}, \text{actGFP}}$; + | gift from T. Klein, HHU | |
| | yw;P{Epgy ² }UbcD10 ^{Ey08843} ; + | Bloomington #19938 | |
| | W;+; $\frac{\text{psn}^{\text{C1}}, \text{FRT2A}}{\text{TM3}, \text{twiGFP}}$ | gift from T. Klein, HHU | |
| | W;+; $\frac{\text{tld}^{\text{10E95}}}{\text{TM3}, \text{twiGFP}}$ | gift from C. Nüsslein-Volhard | |
| transcription factors | W; $\frac{\text{aptPA5}, \text{FRT42}}{\text{CyO}, \text{twiGFP}}$; + | gift from C. Klämbt, University Münster | |
| | $\frac{\text{yw}, \text{ct}^{\text{C145}}}{\text{FM7c}, \text{twiGFP}}$; +; + | Bloomington #6946 | |
| | yw; $\frac{\text{Mi}\{\text{MIC}\} \text{dnpn}^{\text{M100051}}}{\text{Cyo}, \text{actGFP}}$; + | Bloomington #30603 | |
| | +; +; $\frac{\text{ry}^{\text{506}}, \text{P}\{\text{PZ}\} \text{E2f1}^{\text{07172}}}{\text{TM3}, \text{twiGFP}}$ | Bloomington #11717 | |
| | W;+; $\frac{\text{exex}^{\text{KK30}}, \text{e}^{\text{S}}}{\text{TM3}, \text{twiGFP}}$ | Bloomington #9930 | |
| | +; +; $\frac{\text{ru}^{\text{1}}, \text{h}^{\text{1}}, \text{Diap1}^{\text{1}}, \text{st}^{\text{1}}, \text{grn}^{\text{7L}}, \text{cu}^{\text{1}}, \text{sr}^{\text{1}}, \text{e}^{\text{S}}, \text{ca}^{\text{1}}}{\text{TM3}, \text{twiGFP}}$ | Bloomington #3103 | |
| | +; +; $\frac{\text{hkb}^{\text{2}}, \text{p}^{\text{P}}}{\text{TM3}, \text{twiGFP}}$ | Bloomington #5457 | |

Material and Methods

| | |
|--|-------------------------|
| $W; +; \frac{klu^{R51}, FRT2A}{TM3, twiGFP}$ | gift from T. Klein, HHU |
| $W; \frac{kn^{col-1}}{Cyo, actGFP}; +$ | Kyoto# 109022 |
| $+; \frac{Lim3^1, pr^1}{Cyo, actGFP}; +$ | Bloomington #3393 |
| $+; \frac{lola^{e76}}{Cyo, actGFP}; +$ | Bloomington #28283 |
| $\frac{N^{55e11}, FRT19A}{FM7c, twiGFP}; +; +$ | gift from T. Klein, HHU |
| $+; \frac{pdm2^{E46}}{Cyo, actGFP}; +$ | Bloomington #8855 |
| $W; +; \frac{pros^{17}}{TM3, twiGFP}$ | Bloomington #5458 |
| $+; +; \frac{sens^{E58}, red^1, e^1}{TM3, twiGFP}$ | Bloomington #5312 |
| $+; \frac{dpy^{ov1}, SoxN^{NC14}, pr^1, cn^1}{Cyo, actGFP}; +$ | Bloomington #9938 |
| $W; \frac{P\{UAS-sqz.A\}7-3}{Cyo, actGFP}; +$ | Bloomington #36497 |
| $W; +; \frac{P\{PZ\}zfh1^{00865}}{TM3, twiGFP}$ | Bloomington #11515 |

Tab 4. 10: Equipment

| Equipment | | Manufacture |
|----------------|---|---|
| microscopes | Axio Imager M2 | Carl Zeiss MicroImaging GmbH, Jena |
| | Confocal Laser-Scanning-Microscope (LSM710) | |
| cameras | α57 (SLT) | Sony Mobile Communications International AG, Düsseldorf |
| | Photron Fast Cam Mini | VKT GmbH, Pfullingen |
| | discovery VMS-004 Deluxe | Veho Europe, Southampton |
| nutating mixer | | VWR International, Gelenaakbaakn, Belgium |

Tab 4. 11: Software

| Software | Company |
|----------------------------------|---|
| Word | Microsoft Corporation, Redmond (USA) |
| Excel | Microsoft Corporation, Redmond (USA) |
| Power Point | Microsoft Corporation, Redmond (USA) |
| Illustrator | Adobe Systems Incorporated, San José (USA) |
| Fiji is just ImageJ | GNU General Public License |
| MacVector | MacVector Incorporated, Apex (USA) |
| Axio Vision | Carl Zeiss AG, Oberkochen |
| Image Lab | Bio-Rad Laboratories Incorporated, Hercules (USA) |
| LightCycler® Nano Software - 1.0 | Hoffmann-La Roche AG, Basel (Schweiz) |

| | |
|---------------------|--|
| Tracker | GNU General Public License |
| Vcode | GNU General Public License |
| Vdata | GNU General Public License |
| Debut Videorekorder | NHC Software Inc., Greenwood Village (USA) |

4.2 Methods

4.2.1 *Drosophila* culture

Flies were kept in plastic tubes filled with standard *Drosophila* medium (Tab 4.3) and closed with cellulose plugs. The stock collection was kept at 18°C with a 12h day/night rhythmic and tubes were changed every fourth week.

4.2.2 Fixation of *Drosophila* embryos

Adult flies of the indicated genotype were bred at 25°C in flycages on apple juice plates. Plates were changed twice a day and the plates containing the embryos laid during day were stored at 18°C overnight to slow down development. The following day, embryos were collected from both plates thus providing embryos of all developmental stages. Embryos were transferred to a sieve using a brush and tap water and were dechorionised in 1.7% hypochlorite bleach for around 3.5 minutes. Afterwards, embryos were washed with tap water to remove the hypochlorite bleach and were transferred to a 1.5ml reaction tube filled with 500µl heptane and 500µl 3.7% formaldehyde in 1xPBS. Embryos were fixed for 20 minutes on a nutator, before the lower formaldehyde phase was removed and 500µl methanol was added. By shaking the 1.5ml reaction tubes for 1 to 2 minutes in the hand vigorously, embryos lose their vitelline membranes and stuck to the bottom, while the membranes remain in the interphase. The upper and interphase were removed and embryos were washed three times for 5 minutes with 500µl methanol. At this point embryos can be stored at -20°C for weeks.

4.2.3 Antibody staining of *Drosophila* embryos

For antibody stainings fixed embryos were utilized. All washing- and incubation steps were performed at room temperature on a nutator. Firstly, methanol was removed and embryos were washed three times with 500µl PTX for 10 minutes. In order to block unspecific binding, embryos were incubated in 5% normal goat serum (NGS) in PTX for 30 minutes. The primary antibody was then added in the specific dilution

Material and Methods

(Tab 4.6) and the reaction batch was incubated over night at 4°C. The following day, embryos were washed four times with 500µl PTX for 10 minutes. All secondary antibodies were diluted 1:500 in 5% NGS in PTX and incubated at room temperature for 1 to 2 hours in the dark. The secondary antibody is directed against the species of the first antibody and linked with a fluorescent dye (Tab 4.7). Four washing steps with 500µl PTX for 10 minutes followed. In a fifth washing step embryos were washed with 500µl 1x PBS for 10 minutes to remove the detergent. Finally, 300µl 70% glycerol in 1x PBS were added. The embryos sunk to the bottom of the tube during 2 to 4 hours prior to mounting on microscope slides for subsequent imaging.

4.2.4 *In situ* hybridisation

4.2.4.1 Miniprep of plasmid DNA using High Pure Plasmid Isolation Kit

Miniprep is a method to isolate plasmid DNA out of a bacteria culture. To obtain high concentrations of DNA without contaminations, miniprep using High Pure Plasmid Isolation Kit by Roche was performed in compliance with instruction of the manufactures.

4.2.4.2 *In situ* probe synthesis by PCR

Polymerase chain reaction (PCR) is a standard procedure to exponentially amplify specific DNA fragments. For amplification the Q5 polymerase from New England Biolabs (NEB) was used. Given that all DNA templates used in this thesis are cloned into a vector containing T7- and T3-promoter, T₇- and T₃-primer were used for the amplification of all templates. The annealing temperature was always 50°C. The length of elongation depends on the length of the template. NEB gave the other parameters.

reaction batch:

| component | final concentration |
|------------------------|---------------------|
| DNA from Miniprep | <1,000ng |
| 5x Q5 reaction buffer | 1x |
| 10mM dNTP's | 200µM |
| T ₇ -primer | 0.5µM |
| T ₃ -primer | 0.5µM |
| Q5-polymerase | 0.02U/µl |
| in nuclease-free water | |

Material and Methods

4.2.3.3 PCR product purification using QIAquick PCR Purification Kit

To purify PCR products for *in vitro* transcription the QIAquick PCR Purification Kit (Qiagen) was used. Purification was carried out according to manufactures instructions. The elution was performed with 30µl elution buffer (EB) and incubation for 1 minute.

4.2.4.4 *In vitro* transcription

The *in vitro* transcription is a possibility to amplify RNA from a DNA template. In this thesis, this method was used to synthesize a RNA probe for *in situ* hybridisation. For amplification RNA-polymerases from Invitrogen or Amplichem were used. In order to later being able to recognize the probe with an antibody, nucleotides linked with DIG (digoxigenin) were utilized. Additionally, RNase inhibitor was used to protect the reaction batch from degradation by RNases. A typical reaction batch is indicated below:

reaction batch:

10µl DNA from PCR
2µl 10x buffer
2µl DIG-nucleotides
1µl RNase-Inhibitor
2µl RNA-polymerase
3µl dH₂O

Reaction batch was incubated for 4 hours at 37°C. To precipitated the probe, 30µl dH₂O, 20µl 7.5M ammonium acetate and 75µl 96% ethanol was added and the batch was incubated over night at -20°C. Probe was collected by centrifugation at 14,000rpm and 4°C followed for 15 minutes. Supernatant was carefully removed and pellet was re-suspend in 30-50µl probe buffer.

4.2.4.4 Hybridisation

An *in situ* hybridisation was carried out in order to visualize the distribution of mRNA in whole mount embryos and thus provides information about the expression pattern of a specific gene on RNA level. Similar to antibody staining, fixed embryos were used. Embryos were fixed a second time at the beginning of the *in situ* hybridisation. Firstly, methanol was removed and embryos were incubated in a mixture of 3:1 methanol and 3.7% formaldehyde in 1x PBS for 2 minutes on nutator at room

Material and Methods

temperature as all following incubation steps. Secondly, a mixture of 1:3 methanol and 3.7% formaldehyde in 1x PBS was added and incubation for 5 minutes followed. Afterwards, refixation in 3.7% formaldehyde in 1xPBS for 10 minutes occurred. Embryos were washed three times for 10 minutes with 500µl PBT and were pre-hybridised for 30 minutes in 4x volume hybridisation buffer in a moving water-bath at 52°C to block unspecific binding sites. Finally, 1-2µl of the probe (final concentration \approx 0.25ng/µl) were added to the embryos and the reaction batch was incubated overnight in the water-bath at 52°C. The next day, 4 to 6 washing steps with 500µl preheated washing buffer (52°C) were carried out. At the beginning of the third day, embryos were briefly washed twice and a third time for 30 minutes with 500µl PBT at room temperature on nutator. Afterwards 5% NGS in PBT and anti-DIG antibody in a 1:1200 dilution were added and the batch was incubated for 2 hours. Subsequently, embryos were briefly rinsed and then washed 4 times for 20 minutes with 500µl PBT followed by briefly rinsing twice and another washing step of 5 minutes with 500µl AP buffer. For the colour reaction 100µl of the colour solution was added to each 1.5ml reaction tube. Incubation occurred in darkness. Thereby, incubation duration depends on the speed and intensity of the colour reaction. Incubation was stopped when the colour intensity had reached a sufficient level. Three washing steps in 500µl PBT and one step in 500µl 1x PBS for 5 minutes each followed. Finally 500µl 70% glycerol in 1x PBS was added.

4.2.5 Western Blot

4.2.5.1 Embryo preparation for Western blot

Embryo collection and dechorionisation was performed as described previously (4.2.1). Embryos were separated manually using either white light or a UV pair of binoculars. Wild-type embryos were separated by age using white light bioculars, while mutant embryos were separated by age and homozygosity based on GFP expressing balancer chromosomes. Afterwards, embryos were transferred into 1.5ml reaction tube filled with 50µl 2x sample buffer per 150 embryos. Lysis was carried out manually using plastic pestles. An incubation of 5 minutes at 95°C to denature the proteins and a centrifugation for 5 minutes at 14,500 rpm followed. The supernatant was transferred into a fresh 1.5ml reaction tube and can be used directly for western blot or stored at -20°C.

Material and Methods

4.2.5.2 SDS-Page

Gels for SDS-Page were prepared as mentioned in table 4.4. Each gel had two parts - the upper stacking gel had a lower concentration and was used to stack the proteins together in a straight run front, while the lower separating gel with a higher concentration was used to separate the proteins by their sizes. The concentration of the separating gel depends on the size of the expected proteins. Frozen samples were denatured again for 5 minutes at 95°C. 5µl protein ladder and 20µl of each sample were loaded onto the gel, which run in running buffer initially at 80V for 20 minutes and later on with 120V for around 1 hour.

4.2.5.3 Semi-dry blot

After separating on SDS-Page gels, proteins were transferred to a PVDF membrane using semi-dry blots, which have the advantage that only the filter papers have to be soaked with blotting buffer. In this thesis, three different blotting buffer were used (Tab 4.2) - two anode buffers and one cathode buffer. At first, one filter paper soaked with API buffer was placed on the anode followed by a second filter paper soaked with APII buffer. The third layer of the blot sandwich was the PVDF membrane activated with 100% methanol. The gel was placed onto the membrane followed by three layers of filter paper soaked in KP buffer. For a uniform transfer all air bubbles between the layers have to be removed using a blot roller. On top of the sandwich was placed the cathode and the blot was performed at 20V for 20 minutes.

4.2.5.4 Antibody staining of the membrane

After washing the membrane twice with 1xTBST, an incubated for 1 hour in 5% milk powder in 1xTBST at room temperature to block unspecific binding sites followed. Primary antibody was added in tenfold dilution compared to the dilution for antibody staining using whole mount embryos (Tab 4.6). Incubation with primary antibody was carried out over night at 4°C. Membrane was washed three times to remove the remaining antibody for 10 minutes with 1xTBST. Afterwards, the HRP-conjugated secondary antibody in a 1:7500 dilution in 5% milk powder in 1xTBST was added for 2 hours. Finally, membrane was washed 3 times again in 1xTBST for 10 minutes.

4.2.5.5 Development of membrane

For the colour reaction two different solutions were used, Clarity™ Western ECL Substrate Peroxide solution and Clarity™ Western ECL Substrate Luminol/enhancer

solution (Tab 4.1), at the ratio of 1:1. The volume depends on the size of the membrane. Membrane was placed on an overhead transparent, the mixture of both solutions was pipetted uniformly onto the membrane and a second layer of overhead transparent was placed on top. After 1 minute incubation in darkness, the excessive substrate was removed and the membrane was developed and imaged with the Bio-Rad ChemiDoc MP gel documentation.

4.2.5.6 Quantification of protein level

The statistical analysis of the images of the developed membrane was performed using Fiji. α -tubulin served as housekeeping gene and therefore as correlation value.

4.2.6 Quantitative PCR (qPCR)

4.2.6.1 RNA-Isolation from *Drosophila* embryos using ToTALLY RNA Kit (Ambion)

For embryo collection a clutch as described in 4.2.1 Fixation of *Drosophila* embryos was prepared. Embryos were collected in a sieve and dechorionised with 1.7% hypochlorite-bleach for around 3 1/2 minutes. Embryos were separated as described in 4.2.4.1. Fifty milligram of embryos were transferred in a 1.5ml reaction tube filled with 100 μ l denaturation buffer. After smashing the embryos with a pestle, the denaturation buffer was added up to 500 μ l. To reduce the viscosity, the solution was treated with a gauge needle by pipetting the solution 20 times up and down. The starting volume of the lysate was measured and the RNA isolation out of the lysate was performed in compliance with instruction of the manufactures. The pellet was re-suspended in 50 μ l elution buffer and the concentration was measured with a Nano photometer (P330 - Implen GmbH). Isolated RNA was used as template for cDNA synthesis.

4.2.6.2 cDNA Synthesis using SuperScriptTM III Reverse Transcriptase (Invitrogen)

Using a reverse transcriptase it is possible to synthesize single stranded DNA from a RNA template. Synthesis was carried out according to manufactures instructions. As primer served d(T)18 oligos and to prevent possible contamination or a degradation of the RNA by RNases, a murine RNase inhibitor was added.

Material and Methods

4.2.6.3 Quantitative PCR using FastStart Essential DNA Green Master (Roche)

Quantitative PCR is a method to quantify the expression of a specific gene on mRNA level. Ribosomal protein RpL32 served as housekeeping gene and therefore as correlation value. A typical reaction is pointed out below:

reaction batch:

10µl DNA from PCR
2µl 10x buffer
2µl DIG-nucleotides
1µl RNase-Inhibitor
2µl RNA-polymerase
3µl dH₂O

The following conditions were used for the amplification with the LightCycler® Nano (Roche):

Tab 4. 12: Program of qPCRs

| Temperature (°C) | Time (s) | Nr of cycles |
|------------------|----------|--------------|
| 95 | 600 | 1 |
| 95 | 10 | 45 |
| 60 | 10 | |
| 72 | 15 | |
| 60 to 95 | 0.1°C/s | 1 |

All probes were tested in duplicates and only duplicates with a cycle (Cq) value difference ≤ 0.5 were used for analysis. The statistical analysis was performed with the LightCycler® Nano Software - 1.0 (Roche) and Microsoft excel.

4.2.7 Characterisation of larval innervation

4.2.7.1 Mounting of whole mount larvae

Wandering L3 larvae were picked and immobilized and stretched at 60°C for about 1 second. The stretched larvae were placed on a microscope slide with 50µl 70% glycerol in 1xPBS and imaged directly on the microscope LSM710.

Material and Methods

4.2.7.2 Imaging of whole mount larvae

To be able to compare the signal intensity of the ShGFP construct in different genotypes, all larvae were imaged using the same laser settings. Hemisegments of larvae were imaged in total using the air objective 10x.

4.2.7.3 Quantification of larval innervation defects/number of NMJs

For statistical analyses Fiji and Microsoft excel were used. Per larvae, one up to four segments was analysed. To determine the area of synaptic surface, a specific analytic area was set to ensure the same size of analysed muscle surface for each segment. Each hemisegment was divided in three muscle fields. The dorsal muscle field included the muscles 1, 2, 9, 10 and 18 and the lateral muscle field consists of the muscles 3-5, 8, 11, 19, 20 and 21-24. The muscles 6, 7, 12-17 and 26-30, represent the ventral muscle field. Number of NMJs was counted manually using the multi-point tool of Fiji. As a consequence using the image technique mentioned before and attributable to the bending of the larval body, only nine different NMJs can be counted in the lateral muscle field of wild-type larvae in contrast to the expected 13 NMJs.

4.2.7.4 Dissecting and staining of third instar larvae

Wandering third instar larvae were dissected in 1xPBS and fixed for 15 minutes in 3.7% formaldehyde on sylgaard plates. Larval fillets were washed four times for 15 minutes with PTX. After blocking with 5% normal goat serum in PTX, primary antibodies were added in the specific dilution (Tab 4.6) and incubated overnight at 4°C. After washing again four times for 15 minutes with PTX, secondary antibodies labelled with a fluorescent dye (Tab 4.7) were added and incubated for one hour at room temperature. Four washing steps for 15 minutes with PTX followed. Finally, 70% glycerol in 1xPBS was added and fillets sunk to the bottom.

4.2.8 Larval locomotion assays

For all assays larvae were collected in the late third instar stage and cleaned with tap water to remove putative dirt from the cuticle.

Material and Methods

4.2.8.1 Speed assay

To analyse how far larvae are able to crawl, two larvae were placed on an 2% agar plate coloured with bromophenol blue. The larval crawling was recorded for one minute from dorsal view with the camera $\alpha 57$ (SLT) (Sony) and 25 frames per seconds. Afterwards, the larval crawling was tracked with the software Tracker. The statistical analyses were performed using Microsoft excel.

4.2.8.2 Analysis of the duration of the peristaltic wave

Movies for the analysis of the duration of the peristalsis were recorded from ventral view with 50 frames per second with the high-speed camera Photron Fast Cam Mini (VKT). Per larvae the duration of 10 peristaltic waves were measured with the software Vcode and Vdata. With Microsoft excel the average per larva and per genotype was calculated.

4.2.9 Adult locomotion assays

For all locomotion assays the different genotypes were conducted using the same conditions. Only male flies were used, which were collected on the day of hatching. The assays were carried out the next day to rule out any intoxication by carbon dioxide, which might lead to abnormal motion behaviour. For the leg print and climbing assay the wings were removed directly after collecting the flies.

4.2.9.1 Leg print assay

The leg print assay was performed with 20 males per genotype as primarily described by Maqbool and colleagues (Maqbool et al., 2006). Briefly, microscope slides were coated with carbon black and each fly was allowed to walk over two slides. Tracks were imaged using the Axio vision microscope. The step length of the mesothoracic tarsus and the length of the metathoracic tarsus prints of ten steps per male were measured with the Axio vision software and the statistical analysis was carried out using Microsoft Excel. The mean value per individual and on the basis of this the mean per genotype was determined. Furthermore, the position of the tarsus prints and the ability to walk over the microscope slides were analysed.

Material and Methods

4.2.9.2 Climbing assay

To test if flies are able to climb, the negative geotaxis assay was carried out as primarily described by Chaudhuri and colleagues (Chaudhuri et al., 2007). Ten flies were transferred in two empty tubes stick together with sticky tape. Flies were tapped to the bottom of one tube and the number of flies able to climb 7cm in 3, 7, 10 and 15 seconds was counted. Ten replications were performed for each fly set. For analysis the mean of flies passing the mark per tube and thereof the mean per genotype was calculated.

4.2.9.3 Dropping assay

The ability to fly was tested using the dropping assay as performed by Newquist and colleagues (Newquist et al., 2013). Three males were dropped at the same time from one vial onto the lab bench. Each fly that escaped by flight was counted to be able to fly.

4.2.9.4 Island assay

Using the island assay, it is possible to test if flies are able to take off. The assay was executed as described by Schmidt and colleagues (Schmidt et al., 2012). Flies were placed on an island surrounded by water and take-off was recorded for two minutes using the camera discovery VMS-004 Deluxe and the software debut Videorekorder. Vanished flies were counted manually on computer screen after 10, 20, 30 and 120 seconds.

4.2.9.5 Grooming assay

The grooming assay was performed in order to test if flies are able to clean their body from dust. Single flies were covered with reactive yellow (Seeds et al., 2014) and transferred in small cages with a sieve at the bottom. At the beginning and after 4, 10, 20, 30 and 60 minutes pictures were acquired with the stereomicroscope M80 (Leica), the camera IC80HD (Leica) and the software debut Videorekorder.

4.2.10 High-speed movies

To analyse the adult walking, take-off and flight behaviour, high-speed movies with the high-speed camera Photron Fast Cam Mini (VKT) (Cosmicar/Pentax X2;

comparative Macro Zoom 0.3x ∞ 1x 1:4.5) were performed. The time series were made using Fiji Image J.

4.2.10.1 Crawling

Larvae were recorded from dorsal and lateral view during they crawl over an agarose block coloured with bromophenol blue to get a better contrast between larvae and substrate.

4.2.10.2 Walking

For recording the walking behaviour, flies walked over a cover slide and were recorded with the Fast Cam Mini from ventral view with 125 frames per second.

4.2.10.3 Take-off

As an island surrounded by water served the lid of a 200 microliter reaction tube for PCR. Flies were anaesthetised on ice and placed on the island. They were allowed themselves to take off. The frame rate was 2000 frames per second.

4.2.10.4 Flight

Flies were fixed with nail polish on the top of the thorax to a minuten pin, which was attached to a metal frame. Movies were carried out from frontal or lateral view with 2000 to 5000 frames per second. The number of wing beats per second and the position of wings were analysed using the software Tracker.

4.2.11 Preparation and staining of adult flight musculature

Adult flight musculature were prepared and stained as described in Schnorrer et al., 2010. One-day-old adult flies were collected and the head, legs and abdomen were removed using a scalpel. Thoraxes were incubated for 10 minutes in 4% paraformaldehyde in relaxing solution on nutator at room temperature as all following incubation steps. Afterwards, thoraxes were dissected sagittal with a razor blade and incubated for 20 minutes in 3% NGS in relaxing solution. A second fixation step in 4% paraformaldehyde in relaxing solution for 10 minutes followed. Thoraxes were washed twice in 500µl PTX for 10 minutes. Subsequently, the primary antibody in the specific dilution (Tab 4.6) in 0,2% Triton-X100 in 1xPBS was added and the batch

Material and Methods

was incubated for 1 hour. After washing the thoraxes twice with 500µl PTX, the secondary antibody in a dilution of 1:500 in 0,2% Triton-X100 in 1xPBS was added (Tab 4.7). Finally, thoraxes were washed again twice in 500µl PTX for 10 minutes and stored in 70% glycerol in 1xPBS.

4.2.12 Preparation of adult legs

To image the innervation of the leg musculature, flies in late pupae stages were prepared as described by Weitkunat and Schnorrer (Weitkunat and Schnorrer, 2014). The cuticle of flies at this developmental stage is still thin and more transparent as of adult flies. Pupae were stick on double-sided sticky tape and the pupal case was removed. Flies were washed in cold 1xPBS. Legs were dissected with a scissor and transferred in 70% glycerol in 1xPBS on a microscope slide.

4.2.13 Microscopy

All confocal images were performed with the laser-scanning microscope LSM710 and processed with Fiji is just ImageJ. After copying all images to Adobe Illustrator, figures were compiled and show the maximum intensity projection of several z-sections. *In situ* hybridisations were imaged using the Axio vision microscope and were also processed with Fiji and copied to Adobe Illustrator.

4.2.14 Contributions

Results of this thesis were partly performed by bachelor students, a master student, a diploma student and a technical assistant supervised by me. The relevant sections of the results in this thesis are shown in table 4.13 under specification the receptive executor and thesis.

Material and Methods

Tab 4. 13: Contributions

| Result section | Partly performed by | Reference |
|--|--|-----------------------------|
| 2.1.1.1 Side is expressed in glia and sensory neurons | Verena Best | Best, 2014 |
| 2.1.1.2 Side expression is reflected by two different enhancer Gal4-lines | Alisa Gahlen | Gahlen, 2014 |
| 2.1.1.4 Regulation of <i>side</i> expression by transcription factors | Christine Paul, Verena Best | Best, 2014; Paul, 2016 |
| 2.2.1 Loss of <i>side</i> function leads to innervation defects | Christian Schäfer | Schäfer, 2015 |
| 2.2.2 Muscle specific overexpression of <i>side</i> leads to innervation defects in larvae | | |
| 2.2.3 Side loss- and gain of function larvae show locomotion defects | | |
| 2.3.1 <i>Side</i> mutant and overexpression flies exhibit locomotion defects | Alisa Gahlen, Christian Schäfer, Filip Skubacz, Marcel Brenner | Gahlen, 2014; Schäfer, 2015 |
| 2.3.2 Side loss- and gain of function flies are not able to groom themselves | Filip Skubacz | |

Appendix

Bibliography

- Aberle, H., Haghghi, A.P., Fetter, R.D., McCabe, B.D., Magalhães, T.R., and Goodman, C.S. (2002). Wishful thinking encodes a BMP type II receptor that regulates synaptic growth in *Drosophila*. *Neuron* **33**, 545–558.
- Abmayr, S.M., and Pavlath, G.K. (2012). Myoblast fusion: lessons from flies and mice. *Development* **139**, 641–656.
- Aguilera, M., Oliveros, M., Martínez-Padrón, M., Barbas, J. A., and Ferrús, A. (2000). Ariadne-1: A vital *Drosophila* gene is required in development and defines a new conserved family of RING-finger proteins. *Genetics* **155**, 1231–1244.
- Allan, D.W., St. Pierre, S.E., Miguel-Aliaga, I., and Thor, S. (2003). Specification of neuropeptide cell identity by the integration of retrograde BMP signaling and a combinatorial transcription factor code. *Cell* **113**, 73–86.
- Araújo, S.J., and Tear, G. (2003). Axon guidance mechanisms and molecules: lessons from invertebrates. *Nat. Rev. Neurosci.* **4**, 910–922.
- Baek, M., and Mann, R.S. (2009). Lineage and birth date specify motor neuron targeting and dendritic architecture in adult *Drosophila*. *J. Neurosci.* **29**, 6904–6916.
- Bate, M. (1990). The embryonic development of larval muscles in *Drosophila*. *Development* **110**, 791–804.
- Bate, M., Rushton, E., and Currie, D.A. (1991). Cells with persistent twist expression are the embryonic precursors of adult muscles in *Drosophila*. *Development* **113**, 79–89.
- Bazan, J.F., and Goodman, C.S. (1997). Modular structure of the *Drosophila* Beat protein. *Curr. Biol.* **7**, R338–R339.
- Bernstein, S.I., Mogami, K., Donady, J.J., and Emerson, C.P. (1983). *Drosophila* muscle myosin heavy chain encoded by a single gene in a cluster of muscle mutations. *Nature* **302**, 393–397.
- Berrigan, D., and Pepin, D.J. (1995). How maggots move: Allometry and kinematics of crawling in larval diptera. *J. Insect Physiol.* **41**, 329–337.
- Best, V. (2014). Analyse der Regulation der axonalen Wegfindungsmoleküle sidestep und beaten path la in *Drosophila melanogaster*. Diploma thesis. Heinrich Heine University.
- Beuchle, D., Schwarz, H., Langegger, M., Koch, I., and Aberle, H. (2007). *Drosophila* MICAL regulates myofilament organization and synaptic structure. *Mech. Dev.* **124**, 390–406.
- Bier, E., Vaessin, H., Younger-Shepherd, S., and Jan, L.Y. (1992). deadpan, an essential pan-neural gene in *Drosophila*, encodes a helix-loop-helix protein similar to the hairy gene product. *Genes Dev.* **6**, 2137–2151.
- Blochlinger, K., Bodmer, R., Jack, J., Jan, L.Y., and Jan, Y.N. (1988). Primary structure and expression of a product from cut, a locus involved in specifying sensory organ identity in *Drosophila*. *Nature* **333**, 629–635.
- Bodmer, R., and Jan, Y.N. (1987). Morphological differentiation of the embryonic peripheral neurons in *Drosophila*. *Roux's Arch. Dev. Biol.* **196**, 69–77.
- Bodmer, R., Barbel, S., Sheperd, S., Jack, J.W., Jan, L.Y., and Jan, Y.N. (1987). Transformation of sensory organs by mutations of the cut locus of *D. melanogaster*. *Cell* **51**, 293–307.

Appendix

- Bossing, T., Technau, G.M., and Doe, C.Q. (1996). *huckebein* is required for glial development and axon pathfinding in the neuroblast 1-1 and neuroblast 2-2 lineages in the *Drosophila* central nervous system. *Mech. Dev.* *55*, 53–64.
- Broadie, K.S., Bate, M., and Broadie, S. (1993). Development of the embryonic neuromuscular synapse of *Drosophila melanogaster*. *J. Neurosci.* *13*, 144–166.
- Buescher, M., Hing, F.S., and Chia, W. (2002). Formation of neuroblasts in the embryonic central nervous system of *Drosophila melanogaster* is controlled by SoxNeuro. *Development* *129*, 4193–4203.
- Campos-Ortega, J.A., and Hartenstein, V. (1997a). Central nervous system. In *The embryonic development of Drosophila melanogaster*. *2*, 233–269.
- Campos-Ortega, J.A., and Hartenstein, V. (1997b). Peripheral nervous system. In *The embryonic development of Drosophila melanogaster*. *2*, 177–220.
- Canty, E.G., Garrigue-Antar, L., and Kadler, K.E. (2006). A complete domain structure of *Drosophila* *tolloid* is required for cleavage of short gastrulation. *J. Biol. Chem.* *281*, 13258–13267.
- Chaudhuri, A., Bowling, K., Funderburk, C., Lawal, H., Inamdar, A., Wang, Z., and O'Donnell, J.M. (2007). Interaction of genetic and environmental factors in a *Drosophila* parkinsonism model. *J. Neurosci.* *27*, 2457–2467.
- Chu-LaGraff, Q., Schmid, A., Leidel, J., Brönner, G., Jäckle, H., and Doe, C.Q. (1995). *huckebein* specifies aspects of CNS precursor identity required for motoneuron axon pathfinding. *Neuron* *15*, 1041–1051.
- Cisterna, B.A., Cardozo, C., and Sáez, J.C. (2014). Neuronal involvement in muscular atrophy. *Front. Cell. Neurosci.* *8*, 1–11.
- Cohen, S.M. (1993). Imaginal Disc Development. In *The Development of Drosophila melanogaster*. CSH Press, 747–842.
- Crémazy, F., Berta, P., and Girard, F. (2000). SoxNeuro, a new *Drosophila* Sox gene expressed in the developing central nervous system. *Mech. Dev.* *93*, 215–219.
- Desai, C.J., Gindhart, J.G., Goldstein, L.S.B., and Zinn, K. (1996). Receptor tyrosine phosphatases are required for motor axon guidance in the *Drosophila* embryo. *Cell* *84*, 599–609.
- Dickinson, M.H., and Tu, M.S. (1997). The function of dipteran flight muscle. *Comp. Biochem. Physiol. - A Physiol.* *116*, 223–238.
- Dickson, B.J. (2002). Molecular Mechanisms of Axon Guidance. *Science* *298*, 1959–1964.
- Doe, C.Q., Smouse, D., and Goodman, C.S. (1988). Control of neuronal fate by the *Drosophila* segmentation gene *even-skipped*. *Nature* *333*, 376–378.
- Doe, C.Q., Chu-LaGraff, Q., Wright, D.M., and Scott, M.P. (1991). The *prospero* gene specifies cell fates in the *drosophila* central nervous system. *Cell* *65*, 451–464.
- Dutta, D., Anant, S., Ruiz-Gomez, M., Bate, M., and VijayRaghavan, K. (2004). Founder myoblasts and fibre number during adult myogenesis in *Drosophila*. *Development* *131*, 3761–3772.
- Ewing, A.W. (1979). The Neuromuscular Basis of Courtship Song in *Drosophila*: The role of the direct and axillary wing muscles. *J. Comp. Physiol.* *93*, 87–93.
- Fambrough, D., and Goodman, C.S. (1996). The *Drosophila* *beaten path* gene encodes a novel secreted protein that regulates defasciculation at motor axon choice points. *Cell* *87*, 1049–1058.

Appendix

- Fambrough, D., Pan, D., Rubin, G.M., and Goodman, C.S. (1996). The cell surface metalloprotease/disintegrin Kuzbanian is required for axonal extension in *Drosophila*. *Proc. Natl. Acad. Sci. U. S. A.* *93*, 13233–13238.
- Fernandes, J., and Vijayraghavan, K. (1993). The development of indirect flight muscle innervation in *Drosophila melanogaster*. *Mol. Biol.* *227*, 215–227.
- Fernandes, J., Bate, M., and Vijayraghavan, K. (1991). Development of the indirect flight muscles of *Drosophila*. *Development* *113*, 67–77.
- Figeac, N., Jagla, T., Aradhya, R., Da Ponte, J.P., and Jagla, K. (2010). *Drosophila* adult muscle precursors form a network of interconnected cells and are specified by the rhomboid-triggered EGF pathway. *Development* *137*, 1965–1973.
- Frye, M. A., and Dickinson, M.H. (2004). Closing the loop between neurobiology and flight behavior in *Drosophila*. *Curr. Opin. Neurobiol.* *14*, 729–736.
- Gahlen, A. (2014). Analyse des adulten Phänotyps und Charakterisierung regulatorischer Sequenzen des axonalen Wegfindungsmoleküls Sidestep in *Drosophila melanogaster*. Bachelor thesis. Heinrich Heine University.
- Garces, A., and Thor, S. (2006). Specification of *Drosophila* aCC motoneuron identity by a genetic cascade involving even-skipped, grain and *zfh1*. *Development* *133*, 1445–1455.
- Garces, A., Bogdanik, L., Thor, S., and Carroll, P. (2006). Expression of *Drosophila* BarH1-H2 homeoproteins in developing dopaminergic cells and segmental nerve a (SNa) motoneurons. *Eur. J. Neurosci.* *24*, 37–44.
- Ghysen, A., and Dambly-Chaudiere, C. (1989). Genesis of the *Drosophila* peripheral nervous system. *Trends Genet.* *5*, 251–255.
- Giniger, E., Tietje, K., Jan, L.Y., and Jan, Y.N. (1994). *lola* encodes a putative transcription factor required for axon growth and guidance in *Drosophila*. *Development* *120*, 1385–1398.
- Goodman, C.S., and Doe, C.Q. (1993). Embryonic development of the *Drosophila* central nervous system. In *The Development of Drosophila melanogaster*. CSH Press, 1131–1206.
- Grueber, W.B., Jan, L.Y., and Jan, Y.N. (2002). Tiling of the *Drosophila* epidermis by multidendritic sensory neurons. *Development* *129*, 2867–2878.
- Grueber, W.B., Jan, L.Y., and Jan, Y.N. (2003). Different levels of the homeodomain protein cut regulate distinct dendrite branching patterns of *Drosophila* multidendritic neurons. *Cell* *112*, 805–818.
- Heuer, J.G., and Kaufman, T.C. (1992). Homeotic genes have specific functional roles in the establishment of the *Drosophila* embryonic peripheral nervous system. *Development* *115*, 35–47.
- Higashijima, S.I., Michiue, T., Emori, Y., and Saigo, K. (1992). Subtype determination of *Drosophila* embryonic external sensory organs by redundant homeo box genes BarH1 and BarH2. *Genes Dev.* *6*, 1005–1018.
- von Hilchen, C.M., Beckervordersandforth, R.M., Rickert, C., Technau, G.M., and Altenhein, B. (2008). Identity, origin, and migration of peripheral glial cells in the *Drosophila* embryo. *Mech. Dev.* *125*, 337–352.
- Hoang, B., and Chiba, A. (2001). Single-cell analysis of *Drosophila* larval neuromuscular synapses. *Dev. Biol.* *229*, 55–70.
- Hughes, C.L., and Kaufman, T.C. (2002). Hox genes and the evolution of the arthropod body plan.

Appendix

Evol. Dev. 4, 459–499.

Iwatsubo, T. (2004). The γ -secretase complex: Machinery for intramembrane proteolysis. *Curr. Opin. Neurobiol.* 14, 379–383.

Jährling, N., Becker, K., Schönbauer, C., Schnorrer, F., and Dodt, H.-U. (2010). Three-dimensional reconstruction and segmentation of intact *Drosophila* by ultramicroscopy. *Front. Syst. Neurosci.* 4, 1–6.

Johansen, J., Halpern, M.E., and Keshishian, H. (1989a). Axonal guidance and the development of muscle fiber-specific innervation in *Drosophila* embryos. *J. Neurosci.* 9, 4318–4332.

Johansen, J., Halpern, M.E., Johansen, K.M., and Keshishian, H. (1989b). Stereotypic morphology of glutamatergic synapses on identified muscle cells of *Drosophila* larvae. *J. Neurosci.* 9, 710–725.

De Jong, S., Cavallo, J. A., Rios, C.D., Dworak, H. A., and Sink, H. (2005). Target recognition and synaptogenesis by motor axons: Responses to the sidestep protein. *Int. J. Dev. Neurosci.* 23, 397–410.

Kaplan, W.D., and Trout, W.E. (1974). Genetic manipulation of an abnormal jump response in *Drosophila*. *Genetics* 77, 721–739.

Kaufmann, N., DeProto, J., Ranjan, R., Wan, H., and Van Vactor, D. (2002). *Drosophila* liprin- α and the receptor phosphatase Dlar control synapse morphogenesis. *Neuron* 34, 27–38.

Keshishian, H., Broadie, K., Chiba, A., and Bate, M. (1996). The *drosophila* neuromuscular junction: a model system for studying synaptic development and function. *Annu. Rev. Neurosci.* 19, 545–575.

Kidd, T., Bland, K.S., and Goodman, C.S. (1999). Slit is the midline repellent for the robo receptor in *Drosophila*. *Cell* 96, 785–794.

Klämbt, C., Glazer, L., and Shilo, B.Z. (1992). *breathless*, a *Drosophila* FGF receptor homolog, is essential for migration of tracheal and specific midline glial cells. *Genes Dev.* 6, 1668–1678.

Klämbt, C., and Goodman, C.S. (1991). The diversity and pattern of glia during axon pathway formation in the *Drosophila* embryo. *Glia* 4, 205–213.

Klein, T., and Campos-Ortega, J.A. (1997). *klumpfuß*, a *Drosophila* gene encoding a member of the EGR family of transcription factors, is involved in bristle and leg development. *Development* 124, 3123–3134.

Koch, I., Schwarz, H., Beuchle, D., Goellner, B., Langeegger, M., and Aberle, H. (2008). *Drosophila* Ankyrin 2 is required for synaptic stability. *Neuron* 58, 210–222.

Krueger, N.X., Van Vactor, D., Wan, H.I., Gelbart, W.M., Goodman, C.S., and Saito, H. (1996). The transmembrane tyrosine phosphatase DLAR controls motor axon guidance in *Drosophila*. *Cell* 84, 611–622.

Kvon, E.Z., Kazmar, T., Stampfel, G., Yáñez-Cuna, J.O., Pagani, M., Schernhuber, K., Dickson, B.J., and Stark, A. (2014). Genome-scale functional characterization of *Drosophila* developmental enhancers in vivo. *Nature* 512, 91–95.

Landgraf, M., and Thor, S. (2006). Development of *Drosophila* motoneurons: Specification and morphology. *Semin. Cell Dev. Biol.* 17, 3–11.

Landgraf, M., Bossing, T., Technau, G.M., and Bate, M. (1997). The origin, location, and projections of the embryonic abdominal motoneurons of *Drosophila*. *J. Neurosci.* 17, 9642–9655.

Landgraf, M., Baylies, M., and Bate, M. (1999). Muscle founder cells regulate defasciculation and

Appendix

- targeting of motor axons in the *Drosophila* embryo. *Curr. Biol.* 9, 589–592.
- Landgraf, M., Jeffrey, V., Fujioka, M., Jaynes, J.B., and Bate, M. (2003). Embryonic origins of a motor system: Motor dendrites form a myotopic map in *Drosophila*. *PLoS Biol.* 1, 221–230.
- Layden, M.J., Odden, J.P., Schmid, A., Garces, A., Thor, S., and Doe, C.Q. (2006). *Zfh1*, a somatic motor neuron transcription factor, regulates axon exit from the CNS. *Dev. Biol.* 291, 253–263.
- Lee, T., and Luo, L. (1999). Mosaic analysis with a repressible cell marker for studies of gene function in neuronal morphogenesis. *Neuron* 22, 451–461.
- Littleton, J., Bellen, H., and Perin, M. (1993). Expression of synaptotagmin in *Drosophila* reveals transport and localization of synaptic vesicles to the synapse. *Development* 118, 1077–1088.
- Madden, K., Crowner, D., and Giniger, E. (1999). *lola* has the properties of a master regulator of axon – target interaction for SNb motor axons of *Drosophila*. *Dev. Biol.* 313, 301–313.
- Mahr, A., and Aberle, H. (2006). The expression pattern of the *Drosophila* vesicular glutamate transporter: A marker protein for motoneurons and glutamatergic centers in the brain. *Gene Expr. Patterns* 6, 299–309.
- Maqbool, T., Soler, C., Jagla, T., Daczewska, M., Lodha, N., Palliyil, S., VijayRaghavan, K., and Jagla, K. (2006). Shaping leg muscles in *Drosophila*: Role of *landybird*, a conserved regulator of appendicular myogenesis. *PLoS One* 1, 1–12.
- Marqués, G. (2005). Morphogens and synaptogenesis in *Drosophila*. *J. Neurobiol.* 64, 417–434.
- Marqués, G., Musacchio, M., Shimell, M.J., Wünnenberg-Stapleton, K., Cho, K.W.Y., and O'Connor, M.B. (1997). Production of a DPP activity gradient in the early *drosophila* embryo through the opposing actions of the SOG and TLD proteins. *Cell* 91, 417–426.
- Mendes, C.S., Bartos, I., Akay, T., Márka, S., and Mann, R.S. (2013). Quantification of gait parameters in freely walking wild type and sensory deprived *Drosophila melanogaster*. *Elife* 2013, 1–24.
- Merritt, D.J., and Whitington, P.M. (1995). Central projections of sensory neurons in the *Drosophila* embryo correlate with sensory modality, soma position, and proneural gene function. *J. Neurosci.* 15, 1755–1767.
- Meyer, F., and Aberle, H. (2006). At the next stop sign turn right: the metalloprotease *Tolloid-related 1* controls defasciculation of motor axons in *Drosophila*. *Development* 133, 4035–4044.
- Mushegian, A.R. (1997). The *Drosophila* *Beat* protein is related to adhesion proteins that contain immunoglobulin domains. *Curr. Biol.* 7, R336–R338.
- Nachtigall, W., and Wilson, D.M. (1967). Neuro-muscular control of dipteran flight. *J. Exp. Biol.* 47, 77–97.
- Newquist, G., Hogan, J., Walker, K., Lamanuzzi, M., Bowser, M., and Kidd, T. (2013). Control of Male and Female Fertility by the *Netrin* Axon Guidance Genes. *PLoS One* 8, 1–16.
- Nguyen, T., Jamal, J., Shimell, M.J., Arora, K., and O'Connor, M.B. (1994). Characterization of *tolloid-related-1*: a BMP-1-like product that is required during larval and pupal stages of *Drosophila* development. *Dev. Biol.* 166, 569–586.
- Nolo, R., Abbott, L. A., Bellen, H.J. (2000). *Senseless*, a Zn finger transcription factor, is necessary and sufficient for sensory organ development in *Drosophila*. *Cell* 102, 349–362.
- Odden, J.P., Holbrook, S., and Doe, C.Q. (2002). *Drosophila* *HB9* is expressed in a subset of

Appendix

motoneurons and interneurons, where it regulates gene expression and axon pathfinding. *J. Neurosci.* **22**, 9143–9149.

Orgogozo, V., and Grueber, W.B. (2005). FlyPNS, a database of the *Drosophila* embryonic and larval peripheral nervous system. *BMC Dev. Biol.* **5**, 4.

Parrish, J.Z., Kim, M.D., Jan, L.Y., and Jan, Y.N. (2006). Genome-wide analyses identify transcription factors required for proper morphogenesis of *Drosophila* sensory neuron dendrites. *Genes Dev.* **20**, 820–835.

Paul, C. (2016). Regulation von axonalen Wegfindungsmolekülen und deren Auswirkungen auf die Innervierung der somatischen Muskulatur in *Drosophila melanogaster*. Master thesis. Heinrich Heine University.

Paululat, a, Breuer, S., and Renkawitz-Pohl, R. (1999). Determination and development of the larval muscle pattern in *Drosophila melanogaster*. *Cell Tissue Res.* **296**, 151–160.

Pfeiffer, B.D., Jenett, A., Hammonds, A.S., Ngo, T.-T.B., Misra, S., Murphy, C., Scully, A., Carlson, J.W., Wan, K.H., Lavery, T.R., et al. (2008). Tools for neuroanatomy and neurogenetics in *Drosophila*. *Proc. Natl. Acad. Sci. U. S. A.* **105**, 9715–9720.

Pipes, G.C., Lin, Q., Riley, S.E., and Goodman, C.S. (2001). The Beat generation: a multigene family encoding IgSF proteins related to the Beat axon guidance molecule in *Drosophila*. *Development* **128**, 4545–4552.

Rothberg, J.M., Hartley, D.A., Walther, Z., and Artavanis-Tsakonas, S. (1988). slit: an EGF-homologous locus of *D. melanogaster* involved in the development of the embryonic central nervous system. *Cell* **55**, 1047–1059.

Rothberg, J.M., Roger Jacobs, J., Goodman, C.S., and Artavanis-Tsakonas, S. (1990). Slit: An extracellular protein necessary for development of midline glia and commissural axon pathways contains both EGF and LRR domains. *Genes Dev.* **4**, 2169–2187.

Schäfer, C. (2015). Funktionelle und morphologische Analyse der larvalen und adulten Innervierungsdefekte des axonalen Wegfindungsmoleküls Sidestep in *Drosophila melanogaster*. Bachelor thesis. Heinrich Heine University.

Schmidt, I., Thomas, S., Kain, P., Risse, B., Naffin, E., and Klambt, C. (2012). Kinesin heavy chain function in *Drosophila* glial cells controls neuronal activity. *J. Neurosci.* **32**, 7466–7476.

Schnorrer, F., and Dickson, B.J. (2004). Muscle building mechanisms of myotube guidance and attachment site selection. *Dev. Cell* **7**, 9–20.

Schnorrer, F., Schönbauer, C., Langer, C.C.H., Dietzl, G., Novatchkova, M., Schernhuber, K., Fellner, M., Azaryan, A., Radolf, M., Stark, A., et al. (2010). Systematic genetic analysis of muscle morphogenesis and function in *Drosophila*. *Nature* **464**, 287–291.

Schuster, C.M., Davis, G.W., Fetter, R.D., and Goodman, C.S. (1996). Genetic dissection of structural and functional components of synaptic plasticity. I. Fasciclin II controls synaptic stabilization and growth. *Neuron* **17**, 641–654.

Schweitzer, R., Zelzer, E., and Volk, T. (2010). Connecting muscles to tendons: tendons and musculoskeletal development in flies and vertebrates. *Development* **137**, 2807–2817.

Seeds, A.M., Ravbar, P., Chung, P., Hampel, S., Midgley, F.M., Mense, B.D., and Simpson, J.H. (2014). A suppression hierarchy among competing motor programs drives sequential grooming in

Appendix

Drosophila. *Elife* 3, 1–23.

Seeger, M., Tear, G., Ferres-Marco, D., and Goodman, C.S. (1993). Mutations affecting growth cone guidance in *Drosophila*: Genes necessary for guidance toward or away from the midline. *Neuron* 10, 409–426.

Sepp, K.J., Schulte, J., and Auld, V.J. (2000). Developmental dynamics of peripheral glia in *Drosophila melanogaster*. *Glia* 30, 122–133.

Serpe, M., and O'Connor, M.B. (2006). The metalloprotease tolloid-related and its TGF-beta-like substrate Dawdle regulate *Drosophila* motoneuron axon guidance. *Development* 133, 4969–4979.

Shimell, M.J., Ferguson, E.L., Childs, S.R., and O'Connor, M.B. (1991). The *Drosophila* dorsal-ventral patterning gene tolloid is related to human bone morphogenetic protein 1. *Cell* 67, 469–481.

Siebert, M., Banovic, D., Goellner, B., and Aberle, H. (2009). *Drosophila* motor axons recognize and follow a sidestep-labeled substrate pathway to reach their target fields. *Genes Dev.* 23, 1052–1062.

Sink, H., and Whitington, P.M. (1991a). Location and connectivity of abdominal motoneurons in the embryo and larva of *Drosophila melanogaster*. *J. Neurobiol.* 22, 298–311.

Sink, H., and Whitington, P.M. (1991b). Pathfinding in the central nervous system and periphery by identified embryonic *Drosophila* motor axons. *Development* 112, 307–316.

Sink, H., Rehm, E.J., Lee, R., Bulls, Y.M., and Goodman, C.S. (2001). Sidestep encodes a target-derived attractant essential for motor axon guidance in *Drosophila*. *Cell* 105, 57–67.

Soler, C., Daczewska, M., Da Ponte, J.P., Dastugue, B., and Jagla, K. (2004). Coordinated development of muscles and tendons of the *Drosophila* leg. *Development* 131, 6041–6051.

Song, W., Onishi, M., Jan, L.Y., and Jan, Y.N. (2007). Peripheral multidendritic sensory neurons are necessary for rhythmic locomotion behavior in *Drosophila* larvae. *Proc. Natl. Acad. Sci. U. S. A.* 104, 5199–5204.

Strauss, R., and Heisenberg, M. (1990). Coordination of legs during straight walking and turning in *Drosophila melanogaster*. *J. Comp. Physiol. A.* 167, 403–412.

Takasu-Ishikawa, E., Yoshihara, M., Ueda, A., Rheuben, M.B., Hotta, Y., and Kidokoro, Y. (2001). Screening for synaptic defects revealed a locus involved in presynaptic and postsynaptic functions in *Drosophila* embryos. *48*, 101–119.

Taylor, M. V. (2002). Muscle differentiation: How two cells become one. *Curr. Biol.* 12, 224–228.

Thisse, B., Stoetzel, C., Gorostiza-Thisse, C., and Perrin-Schmitt, F. (1988). Sequence of the twist gene and nuclear localization of its protein in endomesodermal cells of early *Drosophila* embryos. *EMBO J.* 7, 2175–2183.

Thor, S., Andersson, S.G., Tomlinson, A., and Thomas, J.B. (1999). A LIM-homeodomain combinatorial code for motor-neuron pathway selection. *Nature* 397, 76–80.

Tian, S.S., Tsoulfas, P., and Zinn, K. (1991). Three receptor-linked protein-tyrosine phosphatases are selectively expressed on central nervous system axons in the *Drosophila* embryo. *Cell* 67, 675–685.

Tissot, M., and Stocker, R.F. (2000). Metamorphosis in *Drosophila* and other insects: The fate of neurons throughout the stages. *Prog. Neurobiol.* 62, 89–111.

Trimarchi, J.R., and Schneiderman, A.M. (1993). Giant fiber activation of an intrinsic muscle in the mesothoracic leg of *Drosophila melanogaster*. *J. Exp. Biol.* 177, 149–167.

Truman, J.W. (1990). Metamorphosis of the central nervous system of *Drosophila*. *J. Neurobiol.* 21,

Appendix

1072–1084.

Van Vactor, D., Sink, H., Fambrough, D., Tsoo, R., and Goodman, C.S. (1993). Genes that control neuromuscular specificity in *Drosophila*. *Cell* **73**, 1137–1153.

Watts, R.J., Hoopfer, E.D., and Luo, L. (2003). Axon pruning during *Drosophila* metamorphosis: Evidence for local degeneration and requirement of the ubiquitin-proteasome system. *Neuron* **38**, 871–885.

Weitkunat, M., and Schnorrer, F. (2014). A guide to study *Drosophila* muscle biology. *Methods* **68**, 2–14.

Wolpert, L., Beddington, R., Jessell, T., Lawrence, P., Meyerowitz, E., and Smith, J. (2002). Cell Differentiation. In *Principles of Development*. Oxford Univ. Press, 293–330.

Yang, X., Bahri, S., Klein, T., and Chia, W. (1997). Klumpfuss, a putative *Drosophila* zinc finger transcription factor, acts to differentiate between the identities of two secondary precursor cells within one neuroblast lineage. *Genes Dev.* **11**, 1396–1408.

Yousefian, J., Troost, T., Grawe, F., Sasamura, T., Fortini, M., and Klein, T. (2013). Dmon1 controls recruitment of Rab7 to maturing endosomes in *Drosophila*. *J. Cell Sci.* **126**, 1583–1594.

Ypsilanti, A.R., Zagar, Y., and Chedotal, A. (2010). Moving away from the midline: new developments for Slit and Robo. *Development* **137**, 1939–1952.

Zarin, A.A., Asadzadeh, J., Hokamp, K., McCartney, D., Yang, L., Bashaw, G.J., and Labrador, J.P. (2014a). A transcription factor network coordinates attraction, repulsion, and adhesion combinatorially to control motor axon pathway selection. *Neuron* **81**, 1297–1311.

Zarin, A.A., Asadzadeh, J., and Labrador, J.P. (2014b). Transcriptional regulation of guidance at the midline and in motor circuits. *Cell. Mol. Life Sci.* **71**, 419–432.

Zinn, K. (2009). Choosing the road less traveled by: A ligand-receptor system that controls target recognition by *drosophila* motor axons. *Genes Dev.* **23**, 1042–1045.

Zito, K., Parnas, D., Fetter, R.D., Isacoff, E.Y., and Goodman, C.S. (1999). Watching a synapse grow: Noninvasive confocal imaging of synaptic growth in *Drosophila*. *Neuron* **22**, 719–729.

Appendix

Index of abbreviations

| | |
|--------------|---|
| A1-8 | abdominal segment 1-8 |
| aCC | anterior corner cell |
| AMP | adult muscle precursors |
| <i>antp</i> | <i>antennapedia</i> |
| APF | after pupae formation |
| <i>aph-1</i> | <i>anterior pharynx defective 1</i> |
| APS | ammonium persulfate |
| ASC | <i>achaete-scute</i> complex |
| ATG | start codon |
| bd | bipolar dendrites |
| <i>beat</i> | <i>beaten path la</i> |
| bp | base pair |
| <i>btl</i> | <i>breathless</i> |
| CAM | cell adhesion molecule |
| cDNA | complementary DNA |
| ch | chordotonal organ |
| CNS | central nervous system |
| da | dendritic abors |
| dbd | dorsal be-dendritic neuron |
| DIG | digoxigenin |
| dda | dorsal da neuron |
| DLM | dorsal longitudinal muscle |
| DNA | deoxyribonucleic acid |
| DVGlut | Drosophila vesicular glutamate transporter |
| DVM | dorsal-ventral muscle |
| EDTA | ethylenediaminetetraacetic acid |
| es | external sensory organ |
| <i>eve</i> | <i>even-skipped</i> |
| <i>FasII</i> | <i>fasciclinII</i> |
| FC | founder cell |
| FCM | fusion competent myoblast |
| Gbb | glass bottom boat |
| <i>gcm</i> | <i>glia cells missing</i> |
| GFP | green fluorescent protein |
| <i>grn</i> | <i>grain</i> |
| ISN | intersegmental nerve |
| kb | kilobase |
| L1 | first instar larva or first leg of the left body half |
| L2 | second instar larva or second leg of the left body half |
| L3 | third instar larva or third leg of the left body half |
| lda | lateral da neuron |
| LSN | lateral segmental neuron |
| md | multidendritic neuron |
| <i>mef2</i> | <i>myocyte enhancer factor 2</i> |

Appendix

| | |
|---------------|---|
| mef2>side | mef2-Gal4 x UAS-side |
| MHC | myosin heavy chain |
| mRNA | messenger RNA |
| NGS | normal goat serum |
| NMJ | neuromuscular junction |
| ns | not significant |
| nt | nucleotide |
| PBS | phosphate buffered saline |
| pCC | posterior corner cell |
| PCR | polymerase chain reaction |
| PNS | periphery nervous system |
| PVDF | polyvinylidene difluoride |
| qPCR | quantitative PCR |
| R1 | first leg of the right body half |
| R2 | second leg of the right body half |
| R3 | third leg of the right body half |
| <i>repo</i> | <i>reversed polarity</i> |
| RNA | ribonucleic acid |
| robo | roundabout |
| <i>RpL32</i> | <i>ribosomal protein 32</i> |
| SDS | sodium dodecyl sulfate |
| <i>side</i> | <i>sidestep</i> |
| SN | segmental nerve |
| SO | sensory organ |
| SOP | sensory organ progenitor |
| T1-3 | thoracic segment 1-3 |
| td | trachea dendrites |
| tdTomato | tandemTomato |
| tlr | tolloid-related |
| UAS | upstream activating sequence |
| <i>Uba1</i> | <i>ubiquitin-activating enzyme 1</i> |
| <i>UbcD10</i> | <i>ubiquitin-conjugating ligase D10</i> |
| <i>ubx</i> | <i>ultrabithorax</i> |
| UTR | untranslated region |
| v'ada | ventral anterior da neuron |
| VDRC | Vienna Drosophila Rnai Center |
| VIN | ventral segmental neuron |
| vs | versus |
| VUM | ventral unpaired neuron |
| <i>wit</i> | <i>wishful thinking</i> |
| <i>zfh1</i> | <i>zinc finger homeodomain 1</i> |

Appendix

Index of figures

| | |
|---|----|
| FIG 1. 1: LOCATION OF MOTONEURON DENDRITES IN THE VENTRAL NERVE CORD AND THEIR TARGET MUSCLES..... | 2 |
| FIG 1. 2: TRANSCRIPTIONAL REGULATION OF DORSAL AND VENTRAL MOTONEURONS..... | 3 |
| FIG 1. 3: OUTGROWING OF MOTOR AXONS FROM THE CNS TO THEIR TARGET MUSCLES..... | 4 |
| FIG 1. 4: SCHEME OF SENSORY NEURONS OF AN EMBRYONIC HEMISEGMENT PROJECTED ONTO THE MUSCLE PATTERN (VIEWED FROM EXTERIOR)..... | 6 |
| FIG 1. 5: STRUCTURE OF THE SIDE PROTEIN..... | 8 |
| FIG 1. 6: PROTEIN STRUCTURE OF BEAT IA..... | 9 |
| FIG 1. 7: BEAT EXPRESSING MOTOR AXONS MIGRATE ALONG SIDE-LABELLED SUBSTRATE..... | 10 |
| FIG 1. 8: SCHEMATIC SCHEME OF INNERVATION PATTERN OF SOMATIC MUSCLES OF AN ABDOMINAL HEMI-SEGMENT (VIEWED FROM EXTERIOR)..... | 11 |
| FIG 1. 9: DEVELOPMENT OF MUSCLES DURING <i>DROSOPHILA</i> EMBRYOGENESIS. ... | 12 |
| FIG 1. 10: LARVAL NEUROMUSCULAR SYSTEM OF A THIRD INSTAR LARVA (LATERAL VIEW)..... | 13 |
| FIG 1. 11: MUSCLES AND INNERVATION PATTERN OF A <i>DROSOPHILA</i> LEG..... | 15 |
| FIG 1. 12: FLIGHT MUSCULATURE OF ADULT <i>DROSOPHILA</i> FLIES..... | 17 |
| FIG 1. 13: TEMPORAL PROGRESS OF INNERVATION OF INDIRECT FLIGHT MUSCULATURE DURING PUPATION..... | 18 |
| | |
| FIG 2. 1: SIDE IS EXPRESSED DYNAMICALLY DURING EMBRYOGENESIS..... | 21 |
| FIG 2. 2: SIDE IS EXPRESSED IN A SUBSET OF GLIA CELLS IN THE CNS..... | 22 |
| FIG 2. 3: SIDE IS NOT EXPRESSED IN MOTONEURONS IN THE CNS..... | 23 |
| FIG 2. 4: SIDE IS EXPRESSED IN A SUBSET OF EXTERNAL SENSORY ORGANS..... | 24 |
| FIG 2. 5: DORSAL MULTIDENDRITIC NEURONS EXPRESS SIDE IN THE PNS..... | 25 |
| FIG 2. 6: IN THE PNS, SIDE IS EXPRESSED IN TWO GLIA CELLS PER HEMISEGMENT..... | 26 |
| FIG 2. 7: <i>SIDE</i> PROMOTER-FRAGMENT-GAL4-LINES..... | 27 |
| FIG 2. 8: GFP DRIVEN BY 204347-GAL4 IS EXPRESSED IN MUSCLES AND CHORDOTONAL ORGANS..... | 28 |
| FIG 2. 9: 206961-GAL4 ACTIVATES GFP EXPRESSION IN SENSORY NEURONS..... | 29 |
| FIG 2. 10: 204347-GAL4 ACTIVATES GFP EXPRESSION IN MUSCLE CELLS..... | 30 |
| FIG 2. 11: UAS-MCD8GFP EXPRESSION DRIVEN BY 206961-GAL4 IS LOCALISED IN SIDE-POSITIVE CELLS..... | 31 |
| FIG 2. 12: <i>SIDESTEP</i> PHENOTYPE CAN BE RESCUED PARTIALLY..... | 33 |
| FIG 2. 13: THE PROMOTER FRAGMENT 204347 EXHIBITS THREE CONSERVED REGIONS..... | 34 |
| FIG 2. 14: POSITION OF THE CONSERVED REGIONS WITHIN THE PROMOTER FRAGMENT 204347..... | 34 |
| FIG 2. 15: THE ENHANCER FRAGMENT 206961 EXHIBITS FOUR SHORT CONSERVED REGIONS..... | 35 |
| FIG 2. 16: POSITION OF THE CONSERVED REGIONS OF LINE 206961..... | 35 |
| FIG 2. 17: SIDE EXPRESSION IS ALTERED IN <i>ANTENNAPEIDIA</i> MUTANT EMBRYOS... | 37 |
| FIG 2. 18: MORPHOLOGY OF SENSORY NEURONS IS ALTERED IN <i>ANTENNAPEIDIA</i> MUTANT EMBRYOS..... | 38 |
| FIG 2. 19: SIDE EXPRESSION IS NOT ALTERED IN <i>HUCKEBEIN</i> , <i>KLUMPFUSS</i> , <i>LOLA</i> , <i>PROSPERO</i> AND <i>SOX NEURO</i> MUTANT EMBRYOS..... | 40 |
| FIG 2. 20: SIDE EXPRESSION IS INCREASED IN <i>NOTCH</i> MUTANT EMBRYOS..... | 41 |
| FIG 2. 21: INCREASED SIDE EXPRESSION IN <i>NOTCH</i> MUTANT EMBRYOS IS DETECTABLE FROM STAGE 10 TO STAGE 14..... | 42 |

Appendix

| | |
|---|----|
| FIG 2. 22: SIDE EXPRESSION IS UPREGULATED IN LATE STAGE <i>NOTCH</i> LOSS OF FUNCTION EMBRYOS..... | 42 |
| FIG 2. 23: IN <i>NOTCH</i> MUTANT EMBRYOS EXPRESSION OF <i>SIDE</i> MRNA IS ALSO UPREGULATED IN EARLY AND MID-STAGE EMBRYOS COMPARED TO WILD-TYPE..... | 43 |
| FIG 2. 24: QPCR SHOWS NO UPREGULATION OF <i>SIDE</i> EXPRESSION IN <i>NOTCH</i> MUTANT EMBRYOS..... | 44 |
| FIG 2. 25: SENSORY NEURON MORPHOLOGY IS STRONGLY ALTERED IN <i>SENSELESS</i> MUTANT EMBRYOS..... | 45 |
| FIG 2. 26: IN LATE <i>BEAT</i> AND <i>TOLLOID-RELATED</i> MUTANT EMBRYOS <i>SIDE</i> IS CONSTITUTIVELY EXPRESSED..... | 47 |
| FIG 2. 27: <i>SIDE</i> EXPRESSION IS INCREASED IN LATE <i>BEAT</i> AND <i>TOLLOID-RELATED</i> MUTANT EMBRYOS..... | 48 |
| FIG 2. 28: IN LATE <i>BEAT</i> AND <i>TOLLOID-RELATED</i> MUTANT EMBRYOS <i>SIDE</i> IS EXPRESSED IN SENSORY NEURONS AND MOTOR AXONS, RESPECTIVELY..... | 49 |
| FIG 2. 29: <i>SIDE</i> -LOCALISATION SHIFTS BETWEEN STAGE 15 AND 16 FROM SENSORY NEURONS TO MOTOR AXONS IN <i>TOLLOID-RELATED</i> MUTANTS..... | 50 |
| FIG 2. 30: EXPRESSION OF <i>SIDE</i> MRNA IS NOT ALTERED IN <i>BEAT</i> AND <i>TOLLOID-RELATED</i> MUTANT EMBRYOS..... | 51 |
| FIG 2. 31: IN EARLY <i>BEAT</i> MUTANT EMBRYOS <i>SIDE</i> EXPRESSION IS DECREASED..... | 52 |
| FIG 2. 32: THE LATERAL MUSCLE FIELD OF <i>SIDE</i> , <i>BEAT</i> AND <i>TOLLOID-RELATED</i> MUTANTS SHOW STRONG MIS-INNervation..... | 53 |
| FIG 2. 33: <i>SIDE</i> IS CONSTITUTIVELY EXPRESSED IN <i>BEAT</i> ; <i>TOLLOID-RELATED</i> DOUBLE MUTANTS..... | 54 |
| FIG 2. 34: <i>SIDE</i> EXPRESSION IS INCREASED IN LATE <i>BEAT</i> ; <i>TOLLOID-RELATED</i> MUTANT EMBRYOS..... | 55 |
| FIG 2. 35: IN STAGE 16 <i>BEAT</i> ; <i>TOLLOID-RELATED</i> DOUBLE MUTANT EMBRYOS <i>SIDE</i> IS EXPRESSED IN MOTOR AXONS..... | 55 |
| FIG 2. 36: <i>BEAT</i> PROMOTER-FRAGMENT-GAL4-LINES..... | 56 |
| FIG 2. 37: 40636-GAL4 ACTIVATES GFP EXPRESSION IN MOTONEURONS AND AXONS DURING EMBRYOGENESIS AND LARVAL DEVELOPMENT..... | 57 |
| FIG 2. 38: GFP DRIVEN BY 40636-GAL4 IS EXPRESSED IN MOTONEURONS..... | 58 |
| FIG 2. 39: COMPLETE RESCUE OF <i>BEAT</i> PHENOTYPE BY THE ENHANCER FRAGMENT 40636-GAL4..... | 59 |
| FIG 2. 40: THE PROMOTER FRAGMENT 40636 EXHIBITS ONE CONSERVED REGION..... | 60 |
| FIG 2. 41: POSITION OF THE CONSERVED REGION WITHIN THE <i>BEAT</i> PROMOTER-FRAGMENT 40636..... | 60 |
| FIG 2. 42: <i>SIDE</i> MUTANT LARVAE EXHIBIT MIS-INNervations IN VENTRAL, LATERAL AND DORSAL MUSCLE FIELDS..... | 62 |
| FIG 2. 43: <i>SIDE</i> LOSS OF FUNCTION LARVAE SHOW A DECREASED NUMBER OF NMJS..... | 63 |
| FIG 2. 44: NON-INNervation LEADS TO A SMALLER DIAMETER OF MUSCLE 12..... | 63 |
| FIG 2. 45: MUSCLES WITHOUT POST-SYNAPSES EXHIBIT ALSO NO TYPE I PRE-SYNAPTIC STRUCTURES IN <i>SIDE</i> MUTANTS..... | 64 |
| FIG 2. 46: IN <i>SIDE</i> HOMOZYGOUS EMBRYOS SNA NEURONS ARE STILL PRESENT..... | 65 |
| FIG 2. 47: MOTONEURONS SURVIVE UP TO THIRD INSTAR IN <i>SIDE</i> HOMOZYGOUS LARVA..... | 66 |
| FIG 2. 48: ISN OF <i>SIDE</i> LOSS OF FUNCTION LARVAE EXHIBIT A THICKER DIAMETER..... | 67 |
| FIG 2. 49: MUSCLE SPECIFIC OVEREXPRESSION OF <i>SIDE</i> LEADS TO INNervation DEFECTS..... | 68 |
| FIG 2. 50: <i>SIDE</i> OVEREXPRESSION LARVAE EXHIBIT LESS NMJS..... | 69 |
| FIG 2. 51: IN <i>SIDE</i> GAIN OF FUNCTION EMBRYOS MOTOR AXONS ARE ATTRACTED TOO EARLY..... | 70 |

Appendix

| | |
|---|-----|
| FIG 2. 52: NON-INNERVATED MUSCLES 9 AND 10 EXHIBIT A DECREASED DIAMETER. | 70 |
| FIG 2. 53: MUSCLES WITHOUT POST-SYNAPSES EXHIBIT ALSO NO PRE-SYNAPTIC STRUCTURES IN SIDE GAIN OF FUNCTION LARVAE. | 71 |
| FIG 2. 54: SIDE LOSS- AND GAIN OF FUNCTION LARVAE CRAWL SLOWER. | 72 |
| FIG 2. 55: SIDE LOSS OF FUNCTION LARVAE PERFORM LONGER PERISTALTIC WAVES. | 73 |
| FIG 2. 56: CONTROL LARVAE CRAWL STRAIGHT FORWARD WITH TIGHT CONTACT TO THE SUBSTRATE..... | 74 |
| FIG 2. 57: SIDE LOSS OF FUNCTION LARVAE LOSE CONTACT TO THE SUBSTRATE DURING CRAWLING..... | 75 |
| FIG 2. 58: SIDE GAIN OF FUNCTION LARVAE STRONGLY ELONGATE THEIR ANTERIOR END DURING CRAWLING..... | 77 |
| FIG 2. 59: MUTATIONS IN THE <i>SIDE</i> GENE ARE LETHAL..... | 78 |
| FIG 2. 60: SIDE GAIN- AND LOSS OF FUNCTION FLIES ARE NOT ABLE TO FLY AND TO TAKE-OFF..... | 79 |
| FIG 2. 61: <i>SIDE</i> MUTANT AND OVEREXPRESSION FLIES SHOW AN ALTERED TAKE- OFF SEQUENCE. | 80 |
| FIG 2. 62: SIDE LOSS- AND GAIN OF FUNCTION FLIES ARE NOT ABLE TO OSCILLATE THEIR WINGS SYNCHRONOUSLY..... | 82 |
| FIG 2. 63: SIDE GAIN- AND LOSS OF FUNCTION FLIES ARE NOT ABLE TO MOVE THEIR HALTERS. | 83 |
| FIG 2. 64: SIDE GAIN OF FUNCTION FLIES EXHIBIT A DECREASED NUMBER OF WING BEATS COMPARED TO WILD-TYPE. | 84 |
| FIG 2. 65: <i>SIDE</i> MUTANT FLIES SHOW MINOR DIFFERENCES OF INDIRECT FLIGHT MUSCLES INNERVATION. | 85 |
| FIG 2. 66: GAIN OF SIDE CAUSES IRREGULAR INNERVATION OF INDIRECT FLIGHT MUSCLES. | 86 |
| FIG 2. 67: IFMS OF SIDE GAIN OF FUNCTION FLIES ARE LESS INNERVATED. | 86 |
| FIG 2. 68: GAIN OF SIDE CAUSES IRREGULAR INNERVATION OF SINGLE MUSCLE FIBRES OF INDIRECT FLIGHT MUSCULATURE. | 87 |
| FIG 2. 69: SIDE LOSS OF FUNCTION FLIES SHOW MIS-INNERVATION OF FEMURS. ... | 88 |
| FIG 2. 70: SIDE LOSS OF FUNCTION FLIES EXHIBIT A THICKER LEG MAIN NERVE BUNDLE..... | 89 |
| FIG 2. 71: SIDE LOSS- AND GAIN OF FUNCTION FLIES ARE NOT ABLE TO CLIMB..... | 89 |
| FIG 2. 72: SIDE LOSS- AND GAIN OF FUNCTION FLIES EXHIBIT ALTERED LEG PRINTS. | 91 |
| FIG 2. 73: SIDE LOSS- AND GAIN OF FUNCTION FLIES EXHIBIT LONGER TARSUS PRINTS AND ALTERED TARSUS PRINT POSITIONS. | 92 |
| FIG 2. 74: <i>SIDE</i> MUTANT FLIES ARE NOT ABLE TO MOVE THEIR PRO-THORACIC LEGS..... | 93 |
| FIG 2. 75: SIDE GAIN- AND LOSS OF FUNCTION FLIES ARE NOT ABLE TO GROOM THEMSELVES. | 95 |
| FIG 2. 76: IN <i>SIDE</i> MUTANT MALES DEVELOPMENT OF SPERMATOCYTES IS NOT ALTERED..... | 96 |
| | |
| FIG 3. 1: MIS-GUIDANCE OF MOTOR AXONS IN <i>SIDE</i> , <i>BEAT</i> AND <i>TOLLOID-RELATED</i> (TLR) MUTANTS..... | 103 |

Appendix

Index of tables

| | |
|--|-----|
| TAB 2. 1: MARKERS EMPLOYED TO IDENTIFY SIDE EXPRESSING CELLS..... | 21 |
| TAB 2. 2: PREDICTED TRANSCRIPTION FACTOR BINDING SITES OF THE CONSERVED ENHANCER FRAGMENTS..... | 36 |
| TAB 2. 3: SELECTED TRANSCRIPTION AND DIFFERENTIATION FACTORS..... | 39 |
| TAB 2. 4: DEGRADATION WAYS OF A PROTEIN AND GENES AFFECTING THESE DIFFERENT WAYS..... | 46 |
| TAB 2. 5: FERTILITY CROSSINGS..... | 96 |
| | |
| TAB 4. 1: CHEMICALS AND REAGENTS..... | 114 |
| TAB 4. 2: BUFFER..... | 116 |
| TAB 4. 3: MEDIA..... | 117 |
| TAB 4. 4: GELS..... | 118 |
| TAB 4. 5: KITS..... | 118 |
| TAB 4. 6: ANTIBODIES..... | 118 |
| TAB 4. 7: SECONDARY ANTIBODIES..... | 119 |
| TAB 4. 8: PRIMER..... | 119 |
| TAB 4. 9: FLYSTOCKS..... | 119 |
| TAB 4. 10: EQUIPMENT..... | 122 |
| TAB 4. 11: SOFTWARE..... | 122 |
| TAB 4. 12: PROGRAM OF QPCRS..... | 129 |
| TAB 4. 13: CONTRIBUTIONS..... | 135 |

Appendix

Supplemental data

Tab S1: Supplemental movies

| Number | Behaviour | View | Genotype | Related figure |
|--------|-----------|---------|---|----------------|
| S1 | Crawling | lateral | ShGFP7A | 2. 57 |
| S3 | | | side ^{I1563} /side ^{C137} | 2. 58 |
| S5 | | | mef2>side | 2. 59 |
| S2 | | dorsal | ShGFP7A | 2. 57 |
| S4 | | | side ^{I1563} /side ^{C137} | 2. 58 |
| S6 | | | mef2>side | 2. 59 |
| S7 | Take-off | | ShGFP7A | 2. 62 |
| S8 | | | side ^{I1563} /side ^{C137} | 2. 62 |
| S9 | | | mef2>side | 2. 62 |
| S10 | Flying | frontal | ShGFP7A | 2. 63 |
| S11 | | | side ^{I1563} /side ^{C137} | 2. 63 |
| S12 | | | mef2>side | 2. 63 |
| S13 | | lateral | ShGFP7A | 2. 64 |
| S14 | | | side ^{I1563} /side ^{C137} | 2. 64 |
| S15 | | | mef2>side | 2. 64 |
| S16 | Walking | | ShGFP7A | 2. 76 |
| S17 | | | side ^{I1563} /side ^{C137} | 2. 76 |
| S18 | | | ShGFP7A | 2. 76 |

Eidesstattliche Versicherung

Ich versichere an Eides statt, dass die Dissertation von mir selbstständig und ohne unzulässige fremde Hilfe unter Beachtung der „Grundsätze zur Sicherung guter wissenschaftlicher Praxis an der Heinrich-Heine-Universität Düsseldorf“ erstellt worden ist.

Des Weiteren erkläre ich hiermit, dass die Dissertation bisher noch nicht an einer anderen Fakultät eingereicht worden ist und es somit noch keinen bisherigen Promotionsversuch gegeben hat.

Düsseldorf, den _____ 2016

Danksagung

Diese Arbeit wurde am Institut für funktionelle Zellmorphologie unter der Leitung von Herrn Professor Hermann Aberle angefertigt. Somit bedanke ich mich zuerst bei Hermann für die Themenstellung und die Möglichkeit diese Arbeit an seinem Institut zu erstellen. Auch dem Teilen des umfangreichen Wissens innerhalb und außerhalb der Wissenschaft, den anregenden Diskussionen und den wirklich schönen Weihnachtsfeiern gilt mein Dank.

Herrn Prof. Dr. Eckhard Lammert danke ich für die Bereitschaft diese Arbeit als Zweitgutachter zu bewerten, die Anregungen während der Institutsmeetings und die freundliche Aufnahme als Teil der beiden Institutsflure.

Des Weiteren danke ich allen aktuellen und ehemaligen Mitgliedern der Ag Aberle. Ein ganz besonderes Dankeschön geht hierbei an meine Doktorschwester Caro. Danke für deine viele Hilfe gerade am Anfang und Ende dieser Arbeit, deine super ordentlichen Protokolle und unsere Freundschaft, die hoffentlich weit über unsere gemeinsame Zeit an der HHU hinaus gehen wird.

Marcel, du gute Seele der Abteilung, vielen Dank für deinen Bastlersinn, die Fähigkeit alles zu besorgen was gebraucht wird und deinem gewissen Humor mit den Dingen umzugehen.

Thomas danke ich für sein stetig offenes Ohr und die Sicht auf die Dinge aus einer anderen Perspektive.

Nicht zu vergessen meine lieben Studenten, Verena, Christine, Alisa, Christian und Filip. Vielen Dank für euren engagierten Einsatz während eurer Abschlussarbeiten, wodurch ihr einen erheblichen Teil zu dieser Arbeit beigetragen habt. Mit jedem von euch war es wirklich eine schöne Zeit.

Allen aktuellen und ehemaligen Mitgliedern der AG Lammert danke ich für eine tolle Arbeitsatmosphäre und die legendären Altweiberfrühstücks. Ein besonderer Dank geht hierbei an Jan und Tobias. Jan, ohne dich würde ich vermutlich heute noch nicht wissen, wie Fiji und Illustrator funktioniert. Tobi, danke, dass du selbst dem miesesten Tag was Lustiges abgewinnen kannst.

Natürlich gilt mein Dank auch meinen Freunden außerhalb der Uni. Eure „Durchhalte-Parolen“ gerade zum Ende hin waren eine unglaubliche Unterstützung.

Zu guter Letzt bedanke ich mich bei meiner Familie, der diese Arbeit gewidmet ist. Ihr habt mich immer auf meinem Weg unterstützt und mir stets das Gefühl gegeben, alles erreichen zu können. Maja, dir danke ich dafür, dass es plötzlich nur noch wichtig ist, ob alle Balus am richtigen Ort sind und alles andere egal ist.

Ich kann es kaum glauben, aber ich bin tatsächlich fertig!!!

PS: Lieber Werner, jetzt dauert es nicht mehr lang und aus dem „Fräulein Doktor“ wird endlich eine „Frau Doktor“ ;-)